



**CATARINA ISABEL
ALMEIDA FERREIRA**

**PRODUÇÃO DE ADSORVENTES A PARTIR DE
RESÍDUOS PARA A REMOÇÃO DE ANESTÉSICOS
VETERINÁRIOS EM SISTEMAS DE RECIRCULAÇÃO
EM AQUACULTURA**

**PRODUCTION AND APPLICATION OF BIOWASTE-
BASED ADSORBENTS FOR THE REMOVAL OF FISH
ANAESTHETICS IN RECIRCULATING
AQUACULTURE SYSTEMS**



**CATARINA ISABEL
ALMEIDA FERREIRA**

**PRODUÇÃO DE ADSORVENTES A PARTIR DE
RESÍDUOS PARA A REMOÇÃO DE ANESTÉSICOS
VETERINÁRIOS EM SISTEMAS DE RECIRCULAÇÃO
EM AQUACULTURA**

**PRODUCTION AND APPLICATION OF BIOWASTE-
BASED ADSORBENTS FOR THE REMOVAL OF FISH
ANAESTHETICS IN RECIRCULATING
AQUACULTURE SYSTEMS**

Tese apresentada à Universidade de Aveiro para cumprimento dos requisitos necessários à obtenção do grau de Doutor em Ciências e Engenharia do Ambiente, realizada sob a orientação científica do Doutor Valdemar Inocêncio Esteves, Professor Auxiliar do Departamento de Química da Universidade de Aveiro e da Doutora Maria Helena Gomes de Almeida Gonçalves Nadais, Professora Auxiliar do Departamento de Ambiente e Ordenamento da Universidade de Aveiro.



À minha família e aos meus amores, André e Vicente.

o júri

presidente

Doutora Ana Isabel Couto Neto da Silva Miranda
professora catedrática da Universidade de Aveiro

Doutora Maria Arminda Costa Alves
professora catedrática da Faculdade de Engenharia da Universidade do Porto

Doutora Angelina Lopes Simões Pena
professora associada da Faculdade de Farmácia da Universidade de Coimbra

Doutora Maria Manuela Lopes Ribeiro Carrott
professora associada da Universidade de Évora

Doutora Helena Maria Rodrigues Vasconcelos Pinheiro
professora auxiliar do Instituto Superior Técnico, Universidade de Lisboa

Doutora Maria Eduarda Bastos Henriques dos Santos
professora auxiliar da Universidade de Aveiro

Doutor Valdemar Inocêncio Esteves
professor auxiliar da Universidade de Aveiro

agradecimentos

Quero agradecer sincera e profundamente a todas as pessoas e instituições que me acompanharam ao longo destes quatro anos e que tornaram possível a realização deste trabalho.

Ao meu orientador, Professor Valdemar Esteves, que me recebeu no seu laboratório de braços abertos, pela sua orientação, o seu incansável apoio, motivação e total disponibilidade para me ouvir sempre que precisei.

À minha co-orientadora, Professora Maria Helena Nadais, por ter aceitado o desafio de me acompanhar nesta jornada e por ter estado sempre disponível para ajudar.

À Fundação para a Ciência e a Tecnologia (FCT) pelo apoio financeiro sob a forma de bolsa de Doutoramento (SFRH/BD/88965/2012) e ao projeto RemPharm (PTDC/AAG-TEC/1762/2014), financiado pelo FEDER através do COMPETE 2020 e por fundos nacionais através da FCT. Agradecimentos são devidos pelo apoio financeiro ao CESAM (UID/AMB/50017), por parte da FCT/MEC através de fundos nacionais, e pelo cofinanciamento pelo FEDER, no âmbito do Acordo de Parceria PT2020, e COMPETE 2020.

Ao Eng^o Pedro Sarmento e Eng^o António Mendes de Sousa do Instituto de Investigação da Floresta e do Papel (RAIZ) e à Eng^a Renata Serradeiro, ex-diretora da Aquacria Piscícolas, pela prestimosa colaboração.

Ao Doutor Eduardo Cuerda-Correa e ao Doutor Sérgio Santos pela colaboração prestada na realização de análises físicas e químicas dos materiais.

À Doutora Marta Otero, um enorme agradecimento pela tão estreita colaboração, que mesmo longe esteve sempre perto para ajudar, por todos os conselhos dados, pelos conhecimentos científicos transmitidos e por toda a força que me deu para continuar. Devo muito deste trabalho a ti!

Às melhores colegas de laboratório que eu poderia desejar e que rapidamente se tornaram mais do que colegas, Vânia Calisto (chefe), Patrícia Silva (Patite), Diana Lima (Di) e Guilaine Jaria (Gui), pelos momentos extraordinários passados no laboratório e fora dele, pela boa disposição mesmo quando tudo parece correr mal e por todo o apoio e força ao longo destes anos. Acima de tudo, obrigada pela vossa amizade!

À minha “chefe” Vânia quero ainda deixar um agradecimento especial por me ter acompanhado em cada passo, por todas as conversas e todos os conselhos dados, pessoais e profissionais. Aprendi e continuo a aprender muito contigo e tenho-te como exemplo em tudo. Por tudo isto e muito, muito mais, dedico esta tese a ti!

Às minhas amigas e confidentes de longa data, Ana Duarte e Cátia, por todos os momentos de desabafo e descontração que tanto me ajudaram ao longo destes quatro anos.

À minha família, pai, mãe, irmão, cunhada e sobrinhos, por toda a força e confiança depositadas em mim ao longo não só desta etapa mas ao longo destes meus 29 anos. O que sou hoje devo a vocês!

Por fim, um agradecimento muito especial ao homem da minha vida, André, por toda a sua paciência, força e ânimo nos dias menos bons, por me ouvires e por tentares sempre ajudar, por fazeres-me feliz todos os dias. Obrigada por partilhares a vida comigo!

palavras-chave

Aquacultura intensiva; anestésicos veterinários; tratamento e reutilização de água; ambiente; bioresíduos agrícolas; lamas da indústria papeleira; pirólise; energia; biocarvão; adsorção; reator em coluna de leito fixo; redimensionamento; regeneração de adsorventes.

resumo

A partir de 1960 a atividade aquícola aumentou abruptamente, tornando-se o setor de produção de alimentos de maior crescimento. A implementação de sistemas de aquacultura intensiva contribuiu para esse acentuado desenvolvimento; contudo, a sua prática impõe elevados riscos relativos ao bem-estar dos peixes, tornando-os vulneráveis a doenças, *stress* e a condições ambientais adversas. Para o controlo do *stress* são utilizados anestésicos, sendo os mais comuns a triclaína, benzocaína e 2-fenoxietanol. Estes fármacos são administrados solubilizando-os na água dos tanques e, conseqüentemente, contaminando-a. Atualmente, as instalações de criação intensiva estão equipadas com sistemas de recirculação em aquacultura (SRA) onde a água é tratada e reciclada. Os SRAs típicos são eficazes na remoção de sólidos suspensos e no controlo do nível de carbono orgânico dissolvido e amónia mas não estão preparados para eliminar fármacos. O processo de adsorção, utilizando carvões ativados, é uma tecnologia bem documentada e eficaz na remoção de contaminantes orgânicos, incluindo fármacos, e tem sido proposta como processo de tratamento terciário em SRA; no entanto, os carvões ativados são dispendiosos.

O projeto desta tese visa a produção de adsorventes alternativos, usando bioresíduos agrícolas e industriais como precursores, capazes de competir com os carvões ativados comerciais, recorrendo a técnicas simples, baratas e amigas do ambiente. O principal objetivo consiste na aplicação dos adsorventes produzidos na remoção de anestésicos veterinários em SRA. Relativamente à valorização dos resíduos testados, os resultados mostraram que os bioresíduos agrícolas (casca de Eucalipto, sementes de uva, caroços de pêssego, cascas de nozes, resíduos de azeitona e cascas de amendoim) podem competir com os carvões fósseis em aplicações de combustão (por exemplo, produção de combustível e energia). Por outro lado, os biocarvões produzidos por pirólise dos bioresíduos industriais (lamas primárias e biológicas da indústria papeleira) são adsorventes promissores, uma vez que os resultados revelaram elevadas capacidades de adsorção com bom desempenho em sistemas fechado e contínuo. Os adsorventes produzidos a partir das lamas biológicas podem ser aplicados no tratamento de águas de aquacultura intensiva com o mesmo desempenho independentemente das condições da água (temperatura, salinidade e presença de matéria orgânica e inorgânica). Sendo as lamas produzidas em larga escala, o custo associado aos precursores destes adsorventes é nulo, com a vantagem de eliminar os esforços de gestão destes resíduos. Além disso, contrariamente aos carvões ativados comerciais, o método de produção usado evita o uso de agentes químicos e permite a recuperação de energia, sendo considerado um processo amigo do ambiente. Estes factos aliados aos bons resultados obtidos na remoção de anestésicos veterinários indicam que o uso de adsorventes a partir de lamas da indústria papeleira poderá ser uma alternativa a aplicar em SRA.

keywords

Intensive aquaculture; fish anaesthetics; water treatment and recycling; environment; agricultural biowastes; paper mill sludge; pyrolysis; energy; biochar; adsorption; fixed-bed column reactor; scale-up; adsorbents regeneration.

abstract

The aquaculture activity has steeply increased since the 1960's, being the fastest growing food production industry. The implementation of intensive aquaculture systems has contributed to this impressive development in the world food fish production; however, this practice imposes high risks on the welfare of fish, making them vulnerable to adverse impacts from disease, stress and also from environmental conditions. For the fishes' stress control, anaesthetics are administered and the most commonly used are tricaine, benzocaine and 2-phenoxyethanol. These pharmaceuticals are administered by solubilization in the fish tank's water, which, therefore, becomes contaminated. Nowadays, intensive aquaculture facilities are equipped with a recirculating aquaculture system (RAS) where the water is treated and remains in a closed circuit. A typical RAS is planned to remove suspended solids and to control dissolved organic carbon and ammonia levels but the processes used are not prepared to eliminate pharmaceuticals. The adsorption process, using activated carbons, is a well-established technology for the removal of organic contaminants, including pharmaceuticals, and it has been proposed as tertiary treatment in RASs; however, activated carbons are very expensive.

The project of this thesis aims at the production of alternative adsorbents, using agricultural or industrial biowastes as precursors, by means of a simple, inexpensive and environmentally friendly production technique and capable to compete with the commercial activated carbons. The objective is the application of the produced adsorbents for the removal of fish anaesthetics from water in the RASs. A first evaluation about the valorisation of such residues showed that the agricultural biowastes (*Eucalyptus* bark, grape seeds, peach stones, walnut shells, olive waste and peanut shells) can compete with fossil coals in combustion applications (e.g., fuel and power generation). On the other hand, the biochars produced by the pyrolysis of the industrial biowastes (primary and biological paper mill sludge) have favourable properties to be used as adsorbents. The adsorption results revealed highest adsorption capacities using paper mill sludge-based adsorbents with good performance in both batch and continuous (fixed-bed column) systems. Also, it was observed that the biological sludge-based adsorbent can be employed in intensive aquaculture wastewater treatment with the same performance independently of the water characteristics (temperature, salinity and presence of organic and inorganic matter). Overall, these sludges are produced in large scale, therefore the cost associated with the precursor of these alternative adsorbents is null with the additional benefit of eliminating managing costs of such residues. Moreover, contrarily to commercial activated carbons, the production process used avoids the utilization of activating chemicals and allows the recovery of energy from these residues, so it may be considered an environmentally friendly process. For these reasons, and allied to the good results obtained for the removal of fish anaesthetics, the use of paper mill sludge-based adsorbents may be an alternative choice to be applied in RASs.

Table of Contents

	Page
<i>1 Introduction</i>	33
1.1 Motivation and relevance.....	35
1.2 Objectives and outline	36
1.3 References.....	39
<i>2 Literature review</i>	41
2.1 Use of medicines in aquaculture.....	43
2.1.1 Aquaculture medicines in the environment	45
2.2 Anaesthetics in aquaculture	47
2.2.1 Anaesthesia and legislation	47
2.2.2 Anaesthesia by inhalation.....	49
2.2.2.1 Tricaine methanesulfonate (MS-222).....	51
2.2.2.2 Benzocaine	52
2.2.2.3 2-Phenoxyethanol (2-PE)	53
2.2.2.4 Clove oil, Eugenol.....	54
2.2.2.5 Quinaldine, Quinaldine sulphate	55
2.2.2.6 Other drugs	61
2.2.3 Presence of fish anaesthetics in the environment	61
2.3 Aquaculture wastewater treatment and recycling	63
2.3.1 Recirculating aquaculture systems (RASs)	64
2.3.1.1 Mechanical filtration	64
2.3.1.2 Biological filtration	65
2.3.1.3 Aeration and stripping.....	65
2.3.1.4 Oxygenation	65
2.3.1.5 Tertiary treatment	66
2.3.2 Removal of fish anaesthetics from water.....	67
2.4 Adsorption process for the removal of organic pollutants	68
2.4.1 Activated carbons	69
2.4.2 Alternative adsorbents	71
2.4.3 Adsorption in batch system	80
2.4.3.1 Adsorption kinetic	81
2.4.3.2 Equilibrium of adsorption	82
2.4.3.3 Thermodynamics of adsorption.....	84
2.4.4 Adsorption in continuous system – Fixed-bed columns.....	85
2.4.4.1 Fixed-bed column modelling.....	86
2.4.4.2 Scale-up of fixed-bed columns.....	90
2.4.5 Adsorbent regeneration.....	91
2.4.5.1 Thermal regeneration	92
2.4.5.2 Chemical regeneration.....	93
2.5 Conclusions.....	94
2.6 References.....	96
<i>3 Comparative valorisation of agricultural and industrial biowastes by combustion and pyrolysis</i>	111
3.1 Contextualization.....	113
3.2 Materials and methods.....	114
3.2.1 Wastes: sampling and preparation.....	114

3.2.1.1	Agricultural wastes	114
3.2.1.2	Industrial wastes	114
3.2.1.3	Wastes preparation	115
3.2.2	Materials characterization.....	115
3.2.2.1	Proximate analysis.....	115
3.2.2.2	Elemental analysis	115
3.2.2.3	Heat of combustion.....	116
3.2.2.4	Thermogravimetric analysis coupled with mass spectrometry (TG-MS).....	116
3.3	Results and discussion	119
3.3.1	Materials characterization.....	119
3.3.2	Heat of combustion.....	122
3.3.3	TG-MS results	124
3.4	Conclusions.....	130
3.5	References.....	130
4	<i>Application of pyrolysed agricultural biowastes as adsorbents for MS-222 removal from water.....</i>	<i>135</i>
4.1	Contextualization	137
4.2	Materials and methods	138
4.2.1	Adsorbent materials	138
4.2.1.1	Production of agricultural biowaste-based adsorbents	138
4.2.1.2	Commercial activated carbon	139
4.2.2	Materials characterization.....	139
4.2.2.1	Thermogravimetric analysis (TGA)	139
4.2.2.2	Proximate analysis.....	140
4.2.2.3	Elemental analysis	140
4.2.2.4	Total organic carbon (TOC)	140
4.2.2.5	Fourier Transform Infra-red spectroscopy (FTIR)	140
4.2.2.6	¹³ C CP-MAS NMR and ¹ H MAS NMR	140
4.2.2.7	Physical Characterization	140
4.2.3	Fish anaesthetic.....	141
4.2.4	Determination of the MS-222 concentration in water by micellar electrokinetic chromatography (MEKC)	141
4.2.5	Adsorption experiments.....	141
4.3	Results and discussion	142
4.3.1	Agricultural biowastes pyrolysis	142
4.3.2	Adsorbents characterization.....	143
4.3.3	Adsorption results.....	154
4.4	Conclusions.....	161
4.5	References.....	161
5	<i>Application of pyrolysed paper mill sludge as adsorbents for fish anaesthetics removal from water.....</i>	<i>163</i>
5.1	Contextualization	165
5.2	Materials and methods	166
5.2.1	Adsorbent materials	166
5.2.1.1	Production of paper mill sludge-based adsorbents	166
5.2.1.2	Commercial activated carbon	167
5.2.2	Materials characterization.....	167
5.2.2.1	Characterization of paper mill sludge before and after pyrolysis	167
5.2.2.2	Characterization of pyrolysed and washed paper mill sludge and PAC.....	168
5.2.3	Fish anaesthetics	169
5.2.4	Determination of the anaesthetics concentration in water by MEKC.....	170

5.2.5	Adsorption experiments.....	170
5.3	Results and discussion	171
5.3.1	Paper mill sludge pyrolysis.....	171
5.3.2	Characterization of paper mill sludge before and after pyrolysis	172
5.3.3	Characterization of pyrolysed and washed paper mill sludge and PAC.....	181
5.3.4	Adsorption results.....	184
5.4	Conclusions.....	190
5.5	References.....	191
6	<i>Study of the influence of operational conditions on the adsorption of MS-222 onto biological paper mill sludge-based adsorbent</i>	193
6.1	Contextualization	195
6.2	Materials and methods	196
6.2.1	Adsorbent materials	196
6.2.2	Fish anaesthetics	196
6.2.3	Determination of the MS-222 concentration in water by MEKC.....	196
6.2.4	Adsorption experiments.....	196
6.2.4.1	Influence of the adsorbent particle size	197
6.2.4.2	Influence of the temperature.....	197
6.2.4.3	Influence of the salinity	197
6.2.4.4	Aquaculture wastewater	198
6.3	Results and discussion	199
6.3.1	Influence of particle size.....	199
6.3.2	Influence of the temperature.....	201
6.3.3	Influence of the salinity	203
6.3.4	Aquaculture wastewater	203
6.4	Conclusions.....	207
6.5	References.....	207
7	<i>Fixed-bed adsorption of MS-222 and 2-phenoxyethanol onto biological paper mill sludge-based adsorbent</i>	211
7.1	Contextualization	213
7.2	Materials and methods	213
7.2.1	Adsorbent materials	213
7.2.2	Fish anaesthetics	214
7.2.3	Determination of the MS-222 and 2-PE concentrations in water by MEKC	214
7.2.4	Fixed-bed column adsorption experiments.....	214
7.2.4.1	Fixed-bed column data analysis and modelling	215
7.3	Results and discussion	216
7.3.1	Fixed-bed adsorption of MS-222.....	216
7.3.1.1	Effect of the flow rate, influent concentration and bed depth	216
7.3.1.2	Breakthrough curves data modelling.....	219
7.3.1.3	Aquaculture wastewater	220
7.3.1.4	Scale-up	223
7.3.2	Fixed-bed adsorption of 2-PE.....	225
7.3.2.1	Effect of the flow rate, influent concentration and bed depth	225
7.3.2.2	Breakthrough curves data modelling.....	228
7.3.2.3	Scale-up	231
7.4	Conclusions.....	233
7.5	References.....	233
8	<i>Chemical and thermal regeneration of biological paper mill sludge-based adsorbent</i>	235
8.1	Contextualization	237

8.2	Materials and methods	238
8.2.1	Adsorbent materials	238
8.2.2	Fish anaesthetics	238
8.2.3	Determination of the MS-222 concentration	238
8.2.3.1	In water matrix	238
8.2.3.2	In NaOH matrix	238
8.2.3.3	In HCl matrix	238
8.2.4	Chemical regeneration	239
8.2.5	Thermal regeneration	240
8.3	Results and discussion	241
8.3.1	Chemical regeneration	241
8.3.2	Thermal regeneration	242
8.4	Conclusions	244
8.5	References	244
9	<i>Final remarks</i>	247
9.1	Conclusions	249
9.2	Future work	252
A	Anaesthetics properties	257
A.1	Absorbance spectra	257
B	Preliminary adsorption experiments	259
B.1	Effect of the pyrolysis residence time on the adsorption capacity	259
C	Capillary electrophoresis (CE)	261
C.1	CE calibration curves	261
C.1.1	Quantification of MS-222	262
C.1.1.1	in water	262
C.1.1.2	in NaOH	263
C.1.1.3	in HCl	264
C.1.2	Benzocaine	265
C.1.3	2-phenoxyethanol	266
C.2	References	267

List of Figures

	Page
Figure 2.1 - World capture fisheries and aquaculture production (adapted from FAO (2016) [3]).	44
Figure 2.2 - Possible pathways for veterinary medicines into the environment (adapted from Boxall et al. (2003) [13]).	46
Figure 2.3 - Representation of a RAS (adapted from Bregnballe (2015) [148]).	64
Figure 2.4 - Conditions, products, yields and properties of biochars resultant from biomass thermochemical conversion processes (adapted from Inyang et al. (2015) [262]).	80
Figure 2.5 - Concentration profile during single-solute adsorption in a fixed-bed column.	85
Figure 2.6 - Material balance around a differential volume element of a fixed-bed column.	87
Figure 3.1 - Graphical representation of O/C ratio versus HHV_{exp} for the studied agricultural and industrial wastes (— linear regression using all materials; --- linear regression excluding GS and BS).	120
Figure 3.2 - Calculated and measured HHV for each material. UL - upper limit ($HHV_{exp}+10\%$); LL - lower limit ($HHV_{exp}-10\%$). Note that y-axis scale is not the same in all graphs to allow a better visualization of the results. Correlations No. 1-15 are listed in Table 3.1.	123
Figure 3.3 - Thermogravimetric (— TG) and derivative thermogravimetric (—•— DTG) curves corresponding to the pyrolysis of each material.	125
Figure 3.4 - Evolution curves of the gaseous products during pyrolysis process.	128
Figure 4.1 - Thermogravimetric (— TG) and derivative thermogravimetric (—•— DTG) curves corresponding to the pyrolysis of agricultural wastes.	143
Figure 4.2 - FTIR spectra of starting biowaste materials (—), and their respective biochars (-- --).	146
Figure 4.3 - ^{13}C CPMAS solid state NMR of starting materials (—) and respective biochar (-- --).	148
Figure 4.4 - ^1H MAS solid state NMR of starting materials (—) and respective biochar (----).	149
Figure 4.5 - Mercury intrusion curves (left) and corresponding pore size distributions (right) of biochars and PAC.	150
Figure 4.6 - SEM micrographs of starting and pyrolysed materials at 2 500 \times , 10 000 \times and 30 000 \times magnification (from left to right).	152
Figure 4.7 - Experimental and predicted kinetic curves for the adsorption of MS-222 in water using produced biochars and PAC. The experimental data (o) were fitted to pseudo-first order (---), pseudo-second order (---) and double exponential (---) kinetic models. Each experimental point (\pm standard deviation) is the average of three replicates. Note that x and y-axis scales are not the same in all graphs to allow a better visualization of the result.	155
Figure 4.8 - Adsorption rate profile for the external diffusion step (— r_e) and intraparticle diffusion step (--- r_i) from double exponential kinetic model. Vertical line indicates the prevalent step change.	157
Figure 4.9 - Experimental and predicted isotherms for the adsorption of MS-222 in water using biochars and PAC. The experimental data (o) were fitted to Langmuir (---), Freundlich (---) and Langmuir-Freundlich (---) equilibrium models. Each experimental point (\pm standard deviation) is the average of three replicates. Note that x and y-axis scales are not the same in all graphs to allow a better visualization of the results.	159
Figure 5.1 - Thermogravimetric (— TG) and derivative thermogravimetric (—•— DTG) curves for PS and BS.	172
Figure 5.2 - FTIR spectra of a.) primary sludge (PS) and b.) biological sludge (BS) before and after pyrolysis at different temperatures and residence times.	176

Figure 5.3 - ^{13}C CPMAS and ^1H MAS solid state NMR of primary sludge (a.) and c.), respectively) and biological sludge (b.) and d.), respectively) before and after pyrolysis.	177
Figure 5.4 - SEM micrographs of PS, PS800-10, PS800-150, BS and BS800-10 (from top to bottom) at 3 000, 10 000 and 30 000 \times magnifications (from left to right).....	180
Figure 5.5 - FTIR spectra of PS, BS and pyrolysed and washed sludge (a.) and b.), respectively).	182
Figure 5.6 - Experimental data and predicted kinetic curves for the adsorption of three fish anaesthetics in water using the produced adsorbents and PAC. The experimental data (o) of PAC, PSC and BSC-b were fitted to pseudo-first order (---), pseudo-second order (---) and double exponential (---) kinetic models. Each experimental point (\pm standard deviation) is the average of three replicates. Note that x and y -axis scales are not the same in all graphs to allow a better visualization of the results.....	185
Figure 5.7 - Experimental and predicted isotherms for the adsorption of the MS-222, benzocaine and 2-PE in water using produced biochars and PAC. The experimental data of PAC (o), PSC (\square) and BSC-b (Δ) were fitted to Langmuir (---), Freundlich (---) and Langmuir-Freundlich (---) equilibrium models. Each experimental point (\pm standard deviation) is the average of three replicates. Note that y -axis scales are not the same in all graphs to allow a better visualization of the results.....	188
Figure 6.1 - Experimental kinetic curves for the adsorption of MS-222 in aqueous solution testing the effect of a.) BSC particle size; b.) temperature (BSC-b), and c.) salinity (BSC-b) on adsorption capacity. The experimental data were fitted to pseudo-first order (—) and pseudo-second order (---) kinetic models. Each experimental point (\pm standard deviation) is the average of three replicates.	200
Figure 6.2 - a.) Experimental isotherms for the adsorption of MS-222 in aqueous solution at different temperatures and the fitting of the Langmuir model to the experimental data; b.) Variation of $\ln K_L$ with temperature for the adsorption of MS-222 onto BSC-b (Van't Hoff plot).....	202
Figure 6.3 - Experimental and predicted kinetic curves for the adsorption of MS-222 in aquaculture wastewater matrix using BSC-b (left) and DARCO 12 \times 20 (right). The experimental data were fitted to pseudo-first order (---) and pseudo-second order (---) kinetic models. Each experimental point (\pm standard deviation) is the average of three replicates. Note that x and y -axis scales are not the same in both graphs to allow a better visualization of the results.	205
Figure 6.4 - Experimental and predicted isotherms for the adsorption of MS-222 in aquaculture wastewater matrix using BSC-b (left) and DARCO 12 \times 20 (right). The experimental data were fitted to Langmuir (---), Freundlich (---) and Langmuir-Freundlich (---) equilibrium models. Each experimental point (\pm standard deviation) is the average of three replicates. Note that x and y -axis scales are not the same in both graphs to allow a better visualization of the results.	206
Figure 7.1 - Schematic diagram of the experimental setup for fixed-bed column experiments.....	215
Figure 7.2 - Breakthrough curves for MS-222 adsorption onto BSC-b at different a.) flow rate ($C_i=250 \text{ mg L}^{-1}$ and $Z=4.5 \text{ cm}$); b.) influent concentration ($Q=4.4 \text{ mL min}^{-1}$ and $Z=4.5 \text{ cm}$), and c.) bed depth ($Q=4.4 \text{ mL min}^{-1}$ and $C_i=250 \text{ mg L}^{-1}$). The experimental data were fitted to Thomas, Clark, Yoon-Nelson and Dose-Response models.....	217
Figure 7.3 - Breakthrough curves for adsorption of MS-222 onto BSC-b a.) in ultra-pure water and aquaculture wastewater, b.) in aquaculture wastewater fitted to Thomas, Clark, Yoon-Nelson and Dose-Response models ($Q=4.4 \text{ mL min}^{-1}$; $C_i=250 \text{ mg L}^{-1}$; $Z=4.5 \text{ cm}$).	222
Figure 7.4 - MS-222 iso-concentration lines for breakthrough points of 10, 50 and 90% and for bed depths of 4.5, 9 and 13 cm ($C_i=250 \text{ mg L}^{-1}$; $Q=4.4 \text{ mL min}^{-1}$; $v=5.6 \text{ cm min}^{-1}$).	224
Figure 7.5 - BDST model predicted and experimental breakthrough curves of MS-222 fixed-bed column scale-up experiment ($C_i=250 \text{ mg L}^{-1}$; $Z=35 \text{ cm}$; $Q=12 \text{ mL min}^{-1}$; $v=2.4 \text{ cm min}^{-1}$).	225

Figure 7.6 - Breakthrough curves for 2-PE adsorption onto BSC-b at different a.) flow rate ($C_i=0.3 \text{ cm}^3 \text{ L}^{-1}$ and $Z=4.5 \text{ cm}$); b.) influent concentration ($Q=4.4 \text{ mL min}^{-1}$ and $Z=4.5 \text{ cm}$), and c.) bed depth ($Q=4.4 \text{ mL min}^{-1}$ and $C_i=0.3 \text{ cm}^3 \text{ L}^{-1}$). The experimental data were fitted to Thomas, Clark, Yoon-Nelson and Dose-Response models.....	227
Figure 7.7 - 2-PE iso-concentration lines for breakthrough points of 10, 50 and 90% and for bed depths of 4.5, 9 and 13 cm ($C_i=0.3 \text{ cm}^3 \text{ L}^{-1}$; $Q=4.4 \text{ mL min}^{-1}$; $v=5.6 \text{ cm min}^{-1}$).....	231
Figure 7.8 - BDST model predicted and experimental breakthrough curves of 2-PE fixed-bed column scale-up experiment ($C_i=0.3 \text{ cm}^3 \text{ L}^{-1}$; $Z=35 \text{ cm}$; $Q=12 \text{ mL min}^{-1}$; $v=2.4 \text{ cm min}^{-1}$).	232
Figure 8.1 - Thermogravimetric (— TG) and derivative thermogravimetric (—•— DTG) curves of MS-222.	240
Figure 8.2 – MS-222 desorption kinetic curves using different chemical agents of regeneration and respective recovery efficiency.	242
Figure 8.3 - Breakthrough curves for saturation of BSC-b with MS-222 and subsequent cycles of regeneration-adsorption ($Q=4.4 \text{ mL min}^{-1}$; $C_i=250 \text{ mg L}^{-1}$; $Z=13 \text{ cm}$).....	243
Figure A.1 - Absorbance spectrum of MS-222 ($C=5 \text{ mg L}^{-1}$).....	257
Figure A.2 - Absorbance spectrum of benzocaine ($C=2.5 \text{ mg L}^{-1}$).....	257
Figure A.3 - Absorbance spectrum of 2-PE ($C=0.2 \text{ cm}^3 \text{ L}^{-1}$).....	258
Figure B.1 - Adsorption percentages for biochars pyrolysed during 10 and 120 min.	259
Figure C.1 - CE calibration curve for MS-222 in water solution. Each point (\pm standard deviation) is the average of three replicates.	262
Figure C.2 - CE calibration curve for MS-222 in NaOH solution. Each point (\pm standard deviation) is the average of three replicates.	263
Figure C.3 - CE calibration curve for MS-222 in HCl solution. Each point (\pm standard deviation) is the average of three replicates.	264
Figure C.4 - CE calibration curve for benzocaine. Each point (\pm standard deviation) is the average of three replicates.	265
Figure C.5 - CE calibration curve for 2-phenoxyethanol. Each point (\pm standard deviation) is the average of three replicates.	266

List of Tables

	Page
Table 2.1 - Physical and chemical properties of the mostly used anaesthetics in aquaculture by inhalation.....	50
Table 2.2 - Anaesthetics dosage for different stages of anaesthesia (IT-induction time; RT-recovery time).....	57
Table 2.3 - Alternative adsorbents for the removal of pharmaceuticals from water (S_{BET} -specific surface area; t_e -equilibrium time; q -adsorption capacity).....	74
Table 3.1 - Correlations for calculation of HHV.....	117
Table 3.2 - Proximate analysis, elemental analysis and calorific values determined for the studied agricultural and industrial wastes.....	121
Table 3.3 - Characteristic parameters obtained from the TG and DTG curves corresponding to the agricultural and industrial wastes.....	126
Table 3.4 - Integrated peak areas of the gaseous compounds evolved during temperature programmed pyrolysis of each material.....	129
Table 4.1 - Conditions of adsorbents production.....	139
Table 4.2 - Chemical characterization of all starting and pyrolysed materials.....	145
Table 4.3 - Textural characterization of the biochars.....	150
Table 4.4 - Fitting parameters of pseudo-first order and pseudo-second order and double exponential kinetic models to the experimental data.....	156
Table 4.5 - Fitting parameters of Langmuir, Freundlich and Langmuir-Freundlich equilibrium models to the experimental data.....	160
Table 5.1 - Conditions of adsorbents production (T -pyrolysis temperature; τ_p -pyrolysis residence time).....	167
Table 5.2 - Dosage of each adsorbent used in adsorption experiments.....	170
Table 5.3 - Chemical characterization of PS, BS and pyrolysed sludge.....	174
Table 5.4 - Physical characterization of the pyrolysed sludge.....	178
Table 5.5 - Proximate and elemental analyses of PSC, BSC and PAC.....	182
Table 5.6 - Physico-chemical properties of pyrolysed and washed materials.....	184
Table 5.7 - Fitting parameters of pseudo-first and pseudo-second order kinetic models and double exponential model to the experimental data.....	186
Table 5.8 - Fitting parameters of Langmuir, Freundlich and Langmuir-Freundlich equilibrium models to the experimental data.....	189
Table 6.1 - Fitting parameters of pseudo-first order and pseudo-second order kinetic models to the experimental data for different particle size of BSC.....	201
Table 6.2 - Fitting parameters of pseudo-first and pseudo-second order kinetic models to the experimental data for different temperatures for BSC-b.....	202
Table 6.3 - Fitting parameters of Langmuir model and thermodynamic parameters for the adsorption of MS-222 onto BSC-b.....	202
Table 6.4 - Fitting parameters of pseudo-first order and pseudo-second order kinetic models to the experimental data for different solution salinities for BSC-b.....	203
Table 6.5 - Fitting parameters of pseudo-first and pseudo-second order kinetic models and of Langmuir, Freundlich and Langmuir-Freundlich equilibrium models to the experimental data.....	205
Table 7.1 - Data from breakthrough curves for the fixed-bed adsorption of MS-222 (solutions in ultra-pure water) onto BSC-b at different flow rates, Q ($C_i=250 \text{ mg L}^{-1}$ and $Z=4.5 \text{ cm}$); influent concentrations, C_i ($Q=4.4 \text{ mL min}^{-1}$ and $Z=4.5 \text{ cm}$); bed depths, Z ($Q=4.4 \text{ mL min}^{-1}$ and $C_i=250 \text{ mg L}^{-1}$); and also using aquaculture wastewater as matrix ($Q=4.4 \text{ mL min}^{-1}$; $C_i=250 \text{ mg L}^{-1}$; $Z=4.5 \text{ cm}$).....	219

Table 7.2 - Thomas, Clark, Yoon-Nelson and Dose-Response model parameters at different flow rate ($C_i=250 \text{ mg L}^{-1}$ and $Z=4.5 \text{ cm}$), influent concentrations ($Q=4.4 \text{ mL min}^{-1}$ and $Z=4.5 \text{ cm}$) and bed depths ($Q=4.4 \text{ mL min}^{-1}$ and $C_i=250 \text{ mg L}^{-1}$) to MS-222 fixed-bed column adsorption	221
Table 7.3 - Thomas, Clark, Yoon-Nelson and Dose-Response model parameters for different matrices.....	223
Table 7.4 - Predicted parameters for the BDST model at $Q=4.4 \text{ mL min}^{-1}$ to MS-222 fixed-bed column scale-up.....	224
Table 7.5 - Predicted breakthrough times based on the BDST model parameters for MS-222 fixed-bed column scale-up at $v=2.4 \text{ cm min}^{-1}$	225
Table 7.6 - Column data from breakthrough curves for the fixed-bed adsorption of 2-PE (solutions in ultra-pure water) onto BSC-b at different flow rates ($C_i=0.3 \text{ cm}^3 \text{ L}^{-1}$ and $Z=4.5 \text{ cm}$), influent concentrations ($Q=4.4 \text{ mL min}^{-1}$ and $Z=4.5 \text{ cm}$) and bed depths ($Q=4.4 \text{ mL min}^{-1}$ and $C_i=0.3 \text{ cm}^3 \text{ L}^{-1}$)	228
Table 7.7 - Thomas, Clark, Yoon-Nelson and Dose-Response model parameters at different flow rate ($C_i=0.3 \text{ cm}^3 \text{ L}^{-1}$ and $Z=4.5 \text{ cm}$), influent concentrations ($Q=4.4 \text{ mL min}^{-1}$ and $Z=4.5 \text{ cm}$) and bed depths ($Q=4.4 \text{ mL min}^{-1}$ and $C_i=0.3 \text{ cm}^3 \text{ L}^{-1}$) to 2-PE fixed-bed column adsorption	230
Table 7.8 - Predicted parameters for the BDST model at $Q=4.4 \text{ mL min}^{-1}$ to 2-PE fixed-bed column scale-up.....	231
Table 7.9 - Predicted breakthrough times based on the BDST model parameters for 2-PE fixed-bed column scale-up at $v=2.4 \text{ cm min}^{-1}$	232
Table 8.1 - Column data obtained from BSC-b saturation and subsequent regeneration-adsorption cycles ($Q=4.4 \text{ mL min}^{-1}$; $C_i=250 \text{ mg L}^{-1}$; $Z=13 \text{ cm}$).....	243
Table 8.2 - Physical and chemical properties of BSC-b before and after saturation and after regeneration	243
Table C.1 - Calibration parameters of MS-222 calibration curves in different matrices	265
Table C.2 - Calibration parameters of benzocaine calibration curve	266
Table C.3 - Calibration parameters of 2-phenoxyethanol calibration curve	267

Notation

List of acronyms

AC	Activated carbon
AOP	Advanced oxidation process
ATR	Attenuated total reflectance
CEPI	Confederation of European Paper Industries
CVMP	Committee for Veterinary Medicinal Products
CZE	Capillary zone electrophoresis
BDST	Bed depth service time
BET	Brunauer-Emmett-Teller
BOD	Biochemical oxygen demand
BS	Biological paper mill sludge
BSC	Biological sludge-based carbon
DEM	Double exponential model
DOC	Dissolved organic carbon
DOM	Dissolved organic matter
DTGA	Derivative thermogravimetric analysis
EB	<i>Eucalyptus</i> bark
ECD	Elemental chlorine free
EGE	Ethylene glycol ethers
EHS	Environment, Health & Safety
EMA	European Medicines Agency
EPA	U.S. Environmental Protection Agency
EU	European Union
FAO	United Nations Food and Agriculture Organization
FC	Fixed carbon content
FDA	U.S. Food and Drug Administration
FTIR	Fourier Transform Infra-red spectroscopy
FWS	U.S. Fish and Wildlife Service
GRAS	Generally recognized as safe
GAC	Granulated activated carbon
GS	Grape seeds
HHV	Higher heating value
IC	Inorganic carbon

IS	Internal standard
IT	Induction time
LCA	Life cycle assessment
LL	Lower limit
LOD	Limit of detection
LOQ	Limit of quantification
MA	Marketing authorization
MEKC	Micellar electrokinetic chromatography
MRL	Maximum residue limit
MS-222	Tricaine methanesulfonate
MTZ	Mass transfer zone
NMR	Nuclear magnetic resonance
NTP	U.S. National Toxicology Program
OW	Olive waste
PAC	Powdered activated carbon
PeS	Peach stones
PNS	Peanut shells
PS	Primary paper mill sludge
PSC	Primary sludge-based carbon
PZC	Point of zero charge
RAS	Recirculating aquaculture system
RT	Recovery time
SDS	Sodium dodecylsulphate
SEM	Scanning electron microscopy
TC	Total carbon
TGA	Thermogravimetric analysis
TG-MS	Thermogravimetry coupled with mass spectrometry
TOC	Total organic carbon
TSS	Total suspended solids
UL	Upper limit
USA	United States of America
UV	Ultraviolet
VM	Volatile matter content
VOC	Volatile organic compound
WHO	World Health Organization

WS	Walnut shells
WWTP	Wastewater treatment plant
^{13}C CP-MAS	Cross-Polarization Magic Angle Spinning Carbon-13
^1H MAS	Magic Angle Spinning Hydrogen-1
2-PE	2-phenoxyethanol

List of Symbols

Latin Symbols

A_a	Area above the curve (min)
A_R	Cross-sectional area (cm^2)
A_u	Area under the curve (mg min L^{-1})
a	Slope of the BDST model linear regression (min cm^{-1})
B_0	Strength of the magnet (T)
b	y-intercept of the BDST model linear regression (min)
C	Solute concentration (mg L^{-1})
C_b	Solute concentration at breakthrough time (mg L^{-1})
C_e	Solute concentration in solution at equilibrium (mg L^{-1})
C_i	Initial or influent solute concentration (mg L^{-1})
C_s	Solute concentration at saturation time (mg L^{-1})
D	Distribution coefficient
D_e	DEM adsorption rate of external diffusion step (mg L^{-1})
D_i	DEM adsorption rate of intraparticle diffusion step (mg L^{-1})
D_p	Average pore diameter (nm)
DTG_{max}	Maximum weight loss rate ($\% \text{ min}^{-1}$)
D_z	Axial dispersion coefficient ($\text{cm}^2 \text{ min}^{-1}$)
K_F	Freundlich adsorption constant ($\text{mg g}^{-1} (\text{mg L}^{-1})^{-1/NF}$)
K_L	Affinity coefficient of Langmuir model (L mg^{-1})
K_{LF}	Langmuir-Freundlich adsorption constant ($\text{mg g}^{-1} (\text{mg L}^{-1})^{-1/NLF}$)
K_{oc}	Soil organic carbon-water partitioning coefficient
k_1	Pseudo-first order rate constant (min^{-1})
k_2	Pseudo-second order rate constant ($\text{g mg}^{-1} \text{ min}^{-1}$)
k_{BDST}	BDST adsorption rate constant ($\text{L mg}^{-1} \text{ min}^{-1}$)
k_C	Clark adsorption rate constant (min^{-1})
k_e	DEM diffusion rate of external diffusion step (min^{-1})

k_i	DEM diffusion rate of intraparticle diffusion step (min^{-1})
k_{Th}	Thomas adsorption rate constant ($\text{mL mg}^{-1} \text{min}^{-1}$)
k_{YN}	Yoon-Nelson adsorption rate constant (min^{-1})
L	Average micropore width (nm)
M	Adsorbent amount in solution (g L^{-1})
M_w	Molecular weight (g mol^{-1})
m	Dry weight of adsorbent (g)
$m_{adsorbed}$	Mass of solute adsorbed (mg)
$m_{desorbed}$	Mass of solute desorbed (mg)
N_0	Dynamic bed adsorption capacity (mg g^{-1})
$\dot{N}_{accumulation}$	Change of the amount of adsorbate during accumulation ($\text{mg L}^{-1} \text{min}^{-1}$)
$\dot{N}_{adsorption}$	Change of the amount of adsorbate during adsorption ($\text{mg L}^{-1} \text{min}^{-1}$)
$\dot{N}_{advection}$	Difference on the amount of adsorbate between input and output caused by advection ($\text{mg L}^{-1} \text{min}^{-1}$)
$\dot{N}_{dispersion}$	Difference on the amount of adsorbate between input and output caused by axial dispersion ($\text{mg L}^{-1} \text{min}^{-1}$)
N_F	Degree of non-linearity related with Freundlich model
N_{LF}	Degree of non-linearity related with Langmuir-Freundlich model
P	Partition coefficient
pKa	Acid dissociation constant
Q	Flow rate (mL min^{-1})
Q_v	Volumetric flow rate ($\text{cm}^3 \text{min}^{-1}$)
q	Adsorption capacity (mg g^{-1})
q_e	Adsorption capacity at equilibrium (mg g^{-1})
$q_{max,L}$	Langmuir maximum adsorption capacity (mg g^{-1})
$q_{max,LF}$	Langmuir-Freundlich maximum adsorption capacity (mg g^{-1})
q_s	Bed adsorption capacity at the saturation time (mg g^{-1})
q_t	Adsorption capacity at time t (mg g^{-1})
q_{Th}	Thomas maximum adsorption capacity (mg g^{-1})
R	Universal gas constant ($8.314 \text{ J mol}^{-1} \text{ K}^{-1}$)
RE	Solute recovery efficiency (%)
r	DEM overall adsorption rate ($\text{mg min}^{-1} \text{g}^{-1}$)
$r_{ash,free}$	Ash free pyrolysis yield (%)
$r_{e,t}$	DEM external diffusion rate at time t ($\text{mg min}^{-1} \text{g}^{-1}$)
$r_{i,t}$	DEM intraparticle diffusion rate at time t ($\text{mg min}^{-1} \text{g}^{-1}$)

r_p	Pyrolysis yield (%)
S_{BET}	Specific surface area ($\text{m}^2 \text{g}^{-1}$)
S_w	Solubility in water (g L^{-1})
T	Temperature ($^{\circ}\text{C}$ or K)
T_f	Final pyrolysis temperature ($^{\circ}\text{C}$)
T_i	Initial thermal decomposition temperature ($^{\circ}\text{C}$)
T_{max}	Temperature of maximum rate of weight loss ($^{\circ}\text{C}$)
t	Contact or operation time (min)
t_b	Breakthrough time (min)
t_e	Equilibrium time (min)
t_f	Final time (min)
$t_{i\%}$	Time required for retaining i % of the initial solute concentration (min)
t_s	Saturation time (min)
V	Volume (L or mL)
V_b	Volume of effluent treated at breakthrough time (mL)
V_{ma}	Macropore volume ($\text{cm}^3 \text{g}^{-1}$)
V_{me}	Mesopore volume ($\text{cm}^3 \text{g}^{-1}$)
V_p	Total pore volume ($\text{cm}^3 \text{g}^{-1}$)
W_0	Total micropore volume ($\text{cm}^3 \text{g}^{-1}$)
Z	Bed depth (cm)
z	Axial coordinate (cm)

Greek Symbols

α	Constant of the Dose-Response model
ΔG°	Gibbs energy (kJ mol^{-1})
ΔH°	Enthalpy (kJ mol^{-1})
ΔS°	Entropy ($\text{kJ mol}^{-1} \text{K}^{-1}$)
ε	Bed porosity
ρ_{app}	Apparent density (g cm^{-3})
ρ_b	Bed density (g cm^{-3})
τ	Tortuosity
τ_p	Pyrolysis residence time (min)
v	Fluid velocity (cm min^{-1})

Part I

Chapter 1

Introduction

Chapter 2

Literature review

1 Introduction

This first chapter presents the motivation and relevance of the work described and discussed in this thesis and clearly states the objectives. The way that this document is organized is also presented.

1.1 Motivation and relevance

The significant increase of the world population since the 20th century leads to the necessity of food production. Aquaculture is the fastest growing food production industry since the 1960's, which is consequence of improving the water quality, control of diseases, nutritionally complete feeds and the development of improved stocks [1]. The implementation of intensive aquaculture systems of many fish species has contributed to the impressive development of the world food fish production. This system depends on nutritionally complete diets added into the tanks, either fresh, wild, marine or freshwater fish, or on formulated diets, usually in dry pelleted form [2,3]. However, the intensive aquaculture practice also imposes high risks on the welfare of fish, making them vulnerable to adverse impacts from disease, stress and environmental conditions, such as water pollution, which can contribute to the increase of the mortality rate of farmed fish. For disease control and also to control growth, reproduction and stress, organic chemical therapeutants are usually administered to farmed fish in intensive aquaculture systems [1,4]. Nowadays, there are efficient and safe techniques for the disease prevention on fish, such as vaccination and immunization [5], and broad spectrum antibiotics designed to kill pathogenic bacteria and inhibit their growth [6]. On the other hand, for stress control, mainly during handling and confinement operations, anaesthetics are administered mostly by inhalation [7]. The anaesthetic active ingredients most frequently used in aquaculture are tricaine methanesulfonate (MS-222), benzocaine, 2-phenoxyethanol (2-PE), clove oil or eugenol and quinaldine or quinaldine sulphate [7-9]. Apart from the desired stage of anaesthesia, there are factors that determine the dosage of the anaesthetic agent and its efficacy, such as environmental factors (temperature, pH, oxygen content, hardness and salinity of water) and biological factors (fish species, age, gender, size, weight, lipid content and density of biomass) [7]. These drugs enter the fish's body via gill uptake and are eliminated by branchial and/or renal excretion in their original form or metabolites [10-14]. Even considering the low oral acute toxicity of these pharmaceuticals, fish are not recommended to be taken for human consumption during or immediately after treatment and, also, it is necessary to strictly observe safety regulations. Furthermore, taking into account the toxicological effects of long-exposure to this class of drugs for both fish and human, it is imperative to ensure the water quality for recycling and/or for discharge into the environment.

Nowadays, intensive aquaculture facilities are equipped with a water recirculation system where the water remains in a closed circuit, named recirculating aquaculture system (RAS). Recirculation can be carried out at different intensities depending on the degree of recirculated or reused water (*e.g.*, intensive systems use 1 m³ or less of new water per kg of fish produced per year) [15]. Recirculation aquaculture can be considered the most environmentally friendly way of

producing fish and the limited use of water gives a great benefit to the production, once that external factors (such as water temperature, cleanliness of the water, oxygen levels, salinity, solids or weed and leaves drifting downstream and blocking the inlet screens) are controlled. Also, in a RAS it is necessary to continuously treat the water to remove the waste products excreted by the fish, uneaten feed and/or medicines, and to add oxygen to keep the fish welfare. The typical RAS was initially designed to remove suspended solids and to control dissolved organic carbon and ammonia levels which are efficiently removed by mechanical and biological filtration [16]. However, these filters are not designed to remove organic therapeutants, such as the anaesthetic's class, and the shock loading of pharmaceuticals on filters may destroy the nitrifying bacteria. So, water treatment processes should be implemented in order to prevent the release of these pollutants into the environment.

The adsorption process using activated carbons is a well-established technology for the removal of organic contaminants, such as pharmaceuticals [17-19]. This process has been proposed in addition to biological filters as tertiary treatment or polishing stage in RASs to remove ozone and, also, persistent non-biodegradable organic compounds [20]. So, it has been tested for the removal of several contaminants presented in aquaculture wastewater, *e.g.*, ammonia [21], phosphorus [22] and organic micropollutants, such as the fungicides malachite green [23-26] and formaldehyde [24,25,27], the antibacterial agents chloramine-T [24,25] and oxytetracycline [24], and the fish anaesthetics MS-222 and benzocaine [28,29]. However, despite its easy implementation and high efficiency, the main drawback of activated carbons is their high price [30-32]. Consequently, in aquaculture facilities, activated carbon filters have been incorporated only as an auxiliary filter to support biofiltration in RASs [33]. In this sense, several studies have been performed in order to find alternative low-cost adsorbents to be applied in the treatment of water contaminated with human and veterinary pharmaceuticals [34-38]. At the best of our knowledge, there is no study regarding the production of new low-cost adsorbents aiming at the removal of fish anaesthetics for the possible application in RASs.

1.2 Objectives and outline

The main goal of this work is the production of alternative adsorbents, using as precursors agricultural or industrial biowastes, recurring to a simple and environmentally friendly production technique and capable to compete with the commercial activated carbons. The objective is the application of the produced adsorbents for the removal of fish anaesthetics from water in the recirculating aquaculture systems. To accomplish the main goal, the following points must be addressed:

- i.* Use of residues as raw materials in order to, firstly, reduce the waste disposal and, secondly, transform the waste into a new resource by using it for the production of both solid and gaseous added-value products;
- ii.* Perform a complete chemical and physical characterization of the produced adsorbents;
- iii.* Evaluate the performance of the most promising produced adsorbent on different operational conditions (temperature, salinity and presence of organic and inorganic matter using an aquaculture effluent) in batch adsorption system;
- iv.* Evaluate the performance of the most promising produced adsorbent in continuous system using a lab-scale fixed-bed column at different operational conditions (flow rate, influent concentration and bed depth) and perform a scale-up to a semi-pilot scale;
- v.* Describe the adsorption mechanisms by the application of mathematical models;
- vi.* Test the regeneration of the produced adsorbent by chemical and thermal methods.

The work presented in this thesis is divided into five parts: *Part I* corresponds to the contextualization of the work; *Part II* presents the comparative valorisation of two types of wastes; *Part III* reports the production and characterization of the adsorbents and their application in the adsorption of fish anaesthetics in batch system; *Part IV* presents the adsorption of two fish anaesthetics in continuous system, using fixed-bed columns packed with the selected adsorbent and its performance after chemical and thermal regeneration; and *Part V* shows the main conclusions of this work and future work. Within those five parts are included a total of nine chapters organized as follows:

Part I

Chapter 1 *Introduction*

Chapter 2 *Literature review*

The second chapter presents an overview of the state-of-the-art concerning the aquaculture activity with focus on the use of pharmaceuticals, mainly fish anaesthetics. The pharmacology, pharmacokinetics and toxicology of the most used inhalation anaesthetics in farmed fish are described and, also, the effects of their possible presence in the environment are reported, based on the available literature data. The methodologies of aquaculture wastewater treatment implemented in the recirculating aquaculture systems are also presented in this chapter. Finally, the adsorption process aiming at the removal of organic contaminants, such as human and veterinary pharmaceuticals, is herein detailed as well as the recent developments in the search for new low-cost adsorbents for this objective.

Part II

Chapter 3 *Comparative valorisation of agricultural and industrial biowastes by combustion and pyrolysis*

Chapter 3 compares the valorisation of two types of lignocellulosic biowastes (agricultural and industrial residues) by two thermochemical conversion processes (combustion and pyrolysis).

Part III

Chapter 4 *Application of pyrolysed agricultural biowastes as adsorbents for MS-222 removal from water*

The fourth chapter describes the production of adsorbents by pyrolysis of six different agricultural biowastes and their chemical and physical characterization. Also, the results of the adsorptive performance of these agricultural biowaste-based adsorbents for the removal of the fish anaesthetic tricaine methanesulfonate (MS-222), in batch system, are shown in this chapter.

Chapter 5 *Application of pyrolysed paper mill sludge as adsorbents for fish anaesthetics removal from water*

Chapter 5 describes the production of adsorbents by pyrolysis of primary and biological paper mill sludge and their chemical and physical characterization. These two industrial biowaste-based adsorbents were applied for the removal of the three most used fish anaesthetics (MS-222, benzocaine and 2-phenoxyethanol), in batch system, from water and the results are presented in this chapter.

Chapter 6 *Study of the influence of operational conditions on the adsorption of MS-222 onto biological paper mill sludge-based adsorbent*

The sixth chapter presents the results of the adsorptive performance of biological paper mill sludge-based adsorbent, in batch system, under extreme operational conditions, simulating those corresponding to different farmed fish species: temperature, salinity and presence of organic and inorganic matter in the aquaculture wastewater.

Part IV

Chapter 7 Fixed-bed adsorption of MS-222 and 2-phenoxyethanol onto biological paper mill sludge-based adsorbent

Chapter 7 reports the removal of MS-222 and 2-phenoxyethanol from water in a fixed-bed column packed with biological paper mill sludge-based adsorbent for application in recirculating aquaculture systems. Laboratory-scale and scale-up to semi-pilot scale experiments were performed and are presented in this chapter.

Chapter 8 Chemical and thermal regeneration of biological paper mill sludge-based adsorbent

Chapter 8 describes and compares the regeneration of biological paper mill sludge-based carbon saturated with MS-222 by chemical and thermal methods.

Part V

Chapter 9 Final remarks

Chapter 9 is dedicated to present the main conclusions and suggestions for future work.

1.3 References

- [1] Sapkota, A., Sapkota, A.R., Kucharski, M., Burke, J., McKenzie, S., Walker, P. and Lawrence, R., 2008, *Environment International*, 34 (8), 1215-1226.
- [2] EC, http://ec.europa.eu/fisheries/cfp/aquaculture/aquaculture_methods/index_en.htm, last accessed in July 2016.
- [3] FAO, <http://www.fao.org/fishery/technology/aquaculture/en>, last accessed in July 2016.
- [4] Shao, Z.J., 2001, *Advanced Drug Delivery Reviews*, 50 (3), 229-243.
- [5] Harikrishnan, R., Balasundaram, C. and Heo, M.-S., 2011, *Aquaculture*, 320 (1–2), 1-21.
- [6] Burrige, L., Weis, J.S., Cabello, F., Pizarro, J. and Bostick, K., 2010, *Aquaculture*, 306 (1–4), 7-23.
- [7] Ross, L.G. and Ross, B., 2008, *Anaesthetic and Sedative Techniques for Aquatic Animals*, Blackwell Publishing Ltd, Oxford, UK.
- [8] Zahl, I., Samuelsen, O. and Kiessling, A., 2012, *Fish Physiology and Biochemistry*, 38 (1), 201-218.
- [9] Daniel, P., 2009, *The use of veterinary drugs and vaccines in Mediterranean aquaculture*, Zaragoza: CIHEAM, 197-205.
- [10] Stenger, V.G. and Maren, T.H., 1974, *Comparative and General Pharmacology*, 5 (1), 23-35.
- [11] Meinertz, J., Stehly, G. and Gingerich, W., 1999, *Xenobiotics in Fish*, Springer US, Chapter 14, 189-200.
- [12] Schmuck, G., Steffens, W. and Bomhard, E., 2000, *Archives of Toxicology*, 74 (4), 281-283.
- [13] Guénette, S.A., Uhland, F.C., Hélie, P., Beaudry, F. and Vachon, P., 2007, *Aquaculture*, 266 (1–4), 262-265.

- [14] Hunn, J.B. and Allen, J.L., 1974, *The Progressive Fish-Culturist*, 36 (3), 157-159.
- [15] Bregnballe, J., 2015, A Guide to Recirculation Aquaculture, *FAO and EUROFISH International Organisation*.
- [16] Martins, C.I.M., Eding, E.H., Verdegem, M.C.J., Heinsbroek, L.T.N., Schneider, O., Blancheton, J.P., d'Orbcastel, E.R. and Verreth, J.A.J., 2010, *Aquacultural Engineering*, 43 (3), 83-93.
- [17] Ternes, T.A., Meisenheimer, M., McDowell, D., Sacher, F., Brauch, H.-J., Haist-Gulde, B., Preuss, G., Wilme, U. and Zulei-Seibert, N., 2002, *Environmental Science & Technology*, 36 (17), 3855-3863.
- [18] Sheng, C., Nnanna, A.G.A., Liu, Y. and Vargo, J.D., 2016, *Science of The Total Environment*, 550, 1075-1083.
- [19] Snyder, S.A., Adham, S., Redding, A.M., Cannon, F.S., DeCarolis, J., Oppenheimer, J., Wert, E.C. and Yoon, Y., 2007, *Desalination*, 202 (1), 156-181.
- [20] Lawson, T.B., 1995, *Fundamentals of aquacultural engineering*, 1st ed., *Chapman & Hall*, New York, USA.
- [21] Sichula, J., Makasa, M.L., Nkonde, G.K., Kefi, A.S. and Katongo, C., 2011, *Malawi Journal of Aquaculture and Fisheries*, 1 (2), 10-15.
- [22] Oladoja, N.A., Adelagun, R.O.A., Ahmad, A.L. and Ololade, I.A., 2015, *Process Safety and Environmental Protection*, 98, 296-308.
- [23] Nethaji, S., Sivasamy, A., Thennarasu, G. and Saravanan, S., 2010, *Journal of Hazardous Materials*, 181 (1-3), 271-280.
- [24] Aitcheson, S.J., Arnett, J., Murray, K.R. and Zhang, J., 2000, *Aquaculture*, 183 (3-4), 269-284.
- [25] Aitcheson, S.J., Arnett, J., Murray, K.R. and Zhang, J., 2001, *Aquaculture*, 192 (2-4), 249-264.
- [26] Guo, Y., Yang, S., Fu, W., Qi, J., Li, R., Wang, Z. and Xu, H., 2003, *Dyes and Pigments*, 56 (3), 219-229.
- [27] Agarwal, M., Dave, M. and Upadhayaya, S., 2011, *Current World Environment*, 6 (1), 53-59.
- [28] Dawson, V.K., Marking, L.L. and Bills, T.D., 1976, *Transactions of the American Fisheries Society*, 105 (1), 119-123.
- [29] Howe, G.E., Bills, T.D. and Marking, L.L., 1990, *The Progressive Fish-Culturist*, 52 (1), 32-35.
- [30] Keller, A.A., Sandall, O.C., Rinker, R.G., Mitani, M.M., Bierwagen, B.G. and Snodgrass, M.J., 1998, *Health and environmental assessment of MTBE*, 4.
- [31] Stavropoulos, G.G. and Zabaniotou, A.A., 2009, *Fuel Processing Technology*, 90 (7-8), 952-957.
- [32] Alade, A.O., Amuda, O.S., Afolabi, A.O. and Adelowo, F.E., 2012, *Journal of Environmental Science and Technology*, 5, 192-209.
- [33] Helfrich, L.A. and Libey, G., 2011, *Fish Farming in Recirculating Aquaculture Systems*, *Department of Fisheries and Wildlife Sciences; Virginia Tech*.
- [34] Akar, E., Altinişik, A. and Seki, Y., 2013, *Ecological Engineering*, 52, 19-27.
- [35] Tzeng, T.-W., Liu, Y.-T., Deng, Y., Hsieh, Y.-C., Tan, C.-C., Wang, S.-L., Huang, S.-T. and Tzou, Y.-M., 2016, *International Journal of Environmental Science and Technology*, 13 (3), 973-984.
- [36] Liu, P., Liu, W.-J., Jiang, H., Chen, J.-J., Li, W.-W. and Yu, H.-Q., 2012, *Bioresource Technology*, 121 (0), 235-240.
- [37] Kyzas, G.Z., Fu, J., Lazaridis, N.K., Bikiaris, D.N. and Matis, K.A., 2015, *Journal of Molecular Liquids*, 209, 87-93.
- [38] Baccar, R., Sarrà, M., Bouzid, J., Feki, M. and Blánquez, P., 2012, *Chemical Engineering Journal*, 211-212, 310-317.

2 *Literature review*

This chapter aims to present an overview of the state of aquaculture activity and its challenges. The focus is given to the use of therapeutic agents in intensive aquaculture systems, mainly to the problematic of the administration of fish anaesthetics. The pharmacology, pharmacokinetics and toxicology of the most used inhalation anaesthetics in farmed fish are herein described. An overview of the methodologies of aquaculture wastewater treatment implemented in the recirculating aquaculture systems are also presented. The adsorption process aiming at the removal of organic contaminants, such as pharmaceuticals, is herein detailed as well as the recent developments in the search for new low-cost adsorbents for this purpose.

2.1 Use of medicines in aquaculture

As defined by the United Nations Food and Agriculture Organization (FAO), aquaculture is an activity focused on aquatic organism farm, including fish, molluscs, crustaceans and plants. This sector of activity develops on coastal and continental areas [1]. Although the origin of aquaculture was not clearly defined, evidences of this practice were found in Egypt and China, dating back to the years 2500 BC and 1100 BC, respectively [2]. The increase of the world population since 20th century urges food production and, for this reason, global fish production has increased dramatically since the 1960's, with food fish supply increasing at an average annual rate of 3.2% in the period 1961-2013 [3]. This is a consequence of improvements in the water quality, control of diseases, nutritionally complete feeds and the development of improved stocks [4]. In the period 2000–2012, world food fish production by aquaculture expanded at an average annual rate of 6.2%, being the fastest growing food production industry [5]. On the other hand, the capture fishery production has remained constant since the late 1980's, as can be seen in Figure 2.1. Aquaculture systems can be broadly classified into three groups: extensive, semi-intensive and intensive systems. The extensive system consists of trapping wild aquatic animals in lagoons, ponds or small shallow lakes and water management is totally dependent on tidal fluctuation. Lagoons, ponds or lakes are maintained in such a way to promote the development of aquatic fauna at a greater yield than the one found in the natural ecosystem; therefore, utilizes natural photosynthetic production of food to feed the fish. This system plays an important and positive role in the landscape, water management and biodiversity; however, the density of fish production is low and may lead to the destruction of the natural habitat by eutrophication of water bodies and/or introduction of invasive species in the ecosystems. Semi-intensive aquaculture occurs in ponds or lagoons and depends largely on natural food which is increased over baseline levels by fertilisation and/or use of supplementary feed to complement natural food. An intensive indoor aquaculture system is generally composed of several rectangular or circular concrete tanks of different sizes and depths suited to the different stages of growth of the fish. The intensive system depends on nutritionally complete diets added into the tanks, either fresh, wild, marine or freshwater fish, or on formulated diets, usually in dry pelleted form. Nowadays, an intensive aquaculture facility has a water recirculation system where the water remains in a closed circuit, named recirculating aquaculture system (RAS) [6,7].

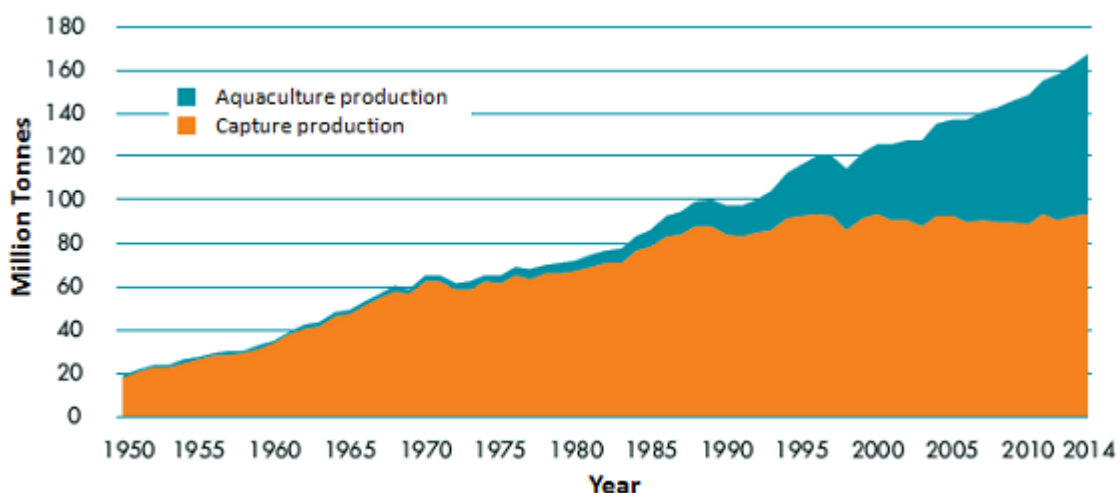


Figure 2.1 - World capture fisheries and aquaculture production (adapted from FAO (2016) [3]).

The implementation of systems for the indoor rearing (intensive aquaculture systems) of many species of fish has contributed to the impressive development of the world food fish production by aquaculture. However, the intensive aquaculture practice also imposes high risks on the welfare of fish, making them vulnerable to adverse impacts of disease and environmental conditions. Factors such as stress, water pollution and disease caused by bacteria, fungi, parasites and virus, contribute for the mortality rate of farmed fish. The feed, medication and reproduction control are needed to gain an improved and effective production [4,8]. For the disease prevention and also for growth control, therapeutic agents are administered to farmed fish. Presently, there are efficient and safe techniques for the disease prevention on fish such as vaccination and immunization [9]. Broad spectrum antibiotics are designed to kill pathogenic bacteria and inhibit their growth [10]. However, the use of antibiotics in farmed fish has been a concern due to the direct toxicity of the compounds to non-target organisms, the emergence of bacterial-resistance, the prophylactic use of this therapeutic agents and the resistance and persistence of the remain active ingredients in the environment [4,11-16]. Moreover, parasiticides and disinfectants are also used in aquaculture to treat bacterial infestations [10].

Albeit their vulnerability to diseases caused by organisms, farmed fish are also subjected to handling and confinement operations, such as netting, weighing, sorting, vaccination, transport and slaughter [17,18]. In some cases, mainly for research purposes, even invasive procedures, such as small incisions, are performed on fish [19]. All of these situations compromise the farmed fish welfare causing stress and anxiety and, consequently, damaging the normal work of the aquaculture activity. Thus, it becomes necessary to immobilize or anesthetize the fish using approved veterinary anaesthetics. There are three main ways of sedation and anaesthesia of fish: the use of drugs and gases (administered by injection or inhalation); induction of hypothermia; and exposure

to electric current. The main features of an anaesthetic agent are: the easiness of administration; effectiveness at low dose or exposure and prompt induction of the desired state; easiness and rapidness to reverse the process; wide safety margin and low-cost method, without compromising the safety of the operator, the treated animal, the consumer and the environment [20]. To control and understand the potential hazard, legislation regarding veterinary pharmaceuticals has been evolved towards important restrictions in the use of medicines to treat food producing animals. In the United States of America (USA), drugs for use in food animals, whether they are for direct medication or for addition to feed, generally must be approved, conditionally approved or index listed by U. S. Food and Drug Administration (FDA) [21]. In Europe, approved pharmacologically active substances and their classification regarding maximum residue limits in foodstuffs of animal origin are listed by European Commission, Department of Health and Food Safety [22,23]. Although varying widely worldwide, the legislation has numerous common features, especially in Europe, North America, Australia and New Zealand, which will be covered in section 2.2.1.

2.1.1 Aquaculture medicines in the environment

Recently, veterinary medicines have been detected worldwide in soils, surface waters and groundwater [15,24]. These veterinary drugs can reach the environment via several pathways, as shown in Figure 2.2. Emissions during the manufacture, formulation and treatment processes, inappropriate disposal of used containers and unused medicines are some ways of soil and water contamination. However, the most important routes are the direct discharge of aquaculture products, the excretion of substances in urine and faeces of livestock animals, and the wash off of topical treatments from these animals [13,14]. Although pharmaceutical industry and intensive aquaculture systems have their own wastewater treatment plants (WWTPs) and RASs, respectively, the ineffectiveness to eliminate organic compounds such as pharmaceuticals is well documented [14,25-27] and, consequently, the discharge of these contaminated effluents into the environment is pointed out as the main source of pharmaceutically active ingredients.

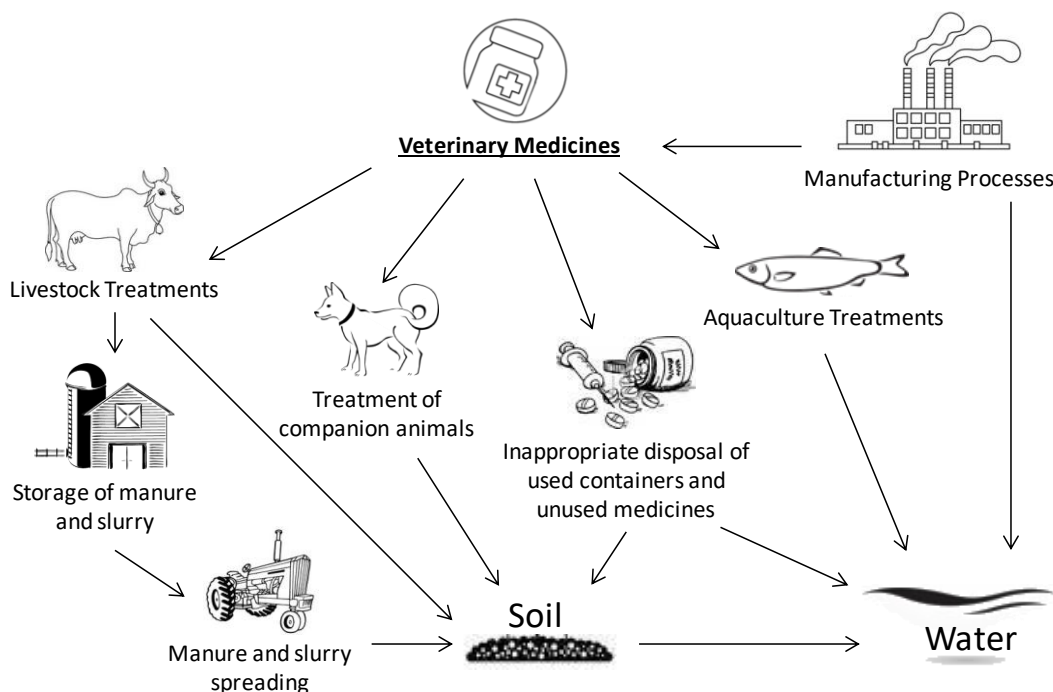


Figure 2.2 - Possible pathways for veterinary medicines into the environment (adapted from Boxall et al. (2003) [13]).

Once in the environment, veterinary drugs and their metabolites are transported and distributed mainly to water, soil or sediment through different processes which highly depend on their physico-chemical properties (*e.g.*, water solubility, volatility, the extent of the degradation in manure, slurry, soil or water, propensity to partition to soil and sediment, and characteristics of the receiving environment). The pharmaceuticals sorption onto soil or sediments is closely related with their hydrophobicity, *i.e.*, with the octanol-water partition coefficient ($\log P$) or distribution coefficient ($\log D$) [14]. Therefore, hydrophobic pharmaceuticals (high values of $\log P$) tend to be sorbed onto soil or sediment matrices. Other mechanisms, such as cation exchange, cation bridging at clay surfaces, surface complexation, and hydrogen bonding may also play a role in the sorption of veterinary pharmaceuticals to soils and sediments [28]. The sorbed pharmaceuticals in soil may suffer aerobic biodegradation and when combined with manure, their persistence period, which is dependent on the manure type, may vary from days to months. Eventually, drugs and/or their biotransformation products may reach surface water from runoff during rainfall episodes [15,27]. On the other hand, hydrophilic pharmaceuticals are quickly transported to surface water, easily reaching the groundwater. Once in the aquatic environment, the pharmaceuticals may be degraded abiotically via photodegradation and/or hydrolysis or biotically by aerobic or anaerobic organisms [14].

While the application of drugs in intensively reared livestock represents the main route of entry in terrestrial environment, the aquaculture therapy has a high potential to reach aquatic

environment (Figure 2.2) [13]. Once in the environment, medicines used in aquaculture are also of great concern, mostly due to the direct toxicity of these compounds to non-target organisms, the emergence of bacterial-resistance and the resistance and persistence of the remaining active ingredient in the environment [4,29]. Some antibiotics usually used in aquaculture were already found in the environment: Pereira et al. (2015) [30] found enrofloxacin and oxytetracycline in most samples collected from portuguese aquaculture surroundings, both with an overall average of 4.4 ng L^{-1} and 5.5 ng L^{-1} , respectively; Terzić et al. (2008) [31] also found enrofloxacin ($< 20 \text{ ng L}^{-1}$) in Western Balkan Region; Lalumera et al. (2004) [32] detected, near the River Oglio, Italy, the presence of oxytetracycline and flumequine in sediments (246 and $579 \mu\text{g kg}^{-1} \text{ d.w.}$, respectively) from a trout and sea-bass farms; oxytetracycline, flumequine and other antibiotics, such as amoxicillin, oxolinic acid and combination of trimethoprim and sulfadiazine, were also found in several aquaculture-producing countries (India, Japan, Philippines, Indonesia, South Korea, Bangladesh, Thailand, Chile, Norway, Vietnam, Taiwan and USA) [4]. Besides the low concentrations found, a potential accumulation of drug residues in the aquatic food chain may occur, leading to direct or indirect exposure of biota around farm sites and representing another hidden threat. Little information may be found regarding the occurrence, persistence and toxicity of other medicines applied in aquaculture activity, such as anaesthetics, in the environment.

2.2 Anaesthetics in aquaculture

The anaesthesia by inhalation is the most used approach that consists of the direct immersion of the fish in a suitable concentration of the anaesthetic drug so that spontaneous ventilation is maintained. The anaesthetic active ingredients most frequently used in aquaculture are tricaine methanesulfonate (MS-222), benzocaine, 2-phenoxyethanol (2-PE), clove oil or eugenol and quinaldine or quinaldine sulphate [18,20,33]. There are four stages of anaesthesia in fish, comprising light and deep sedation; light and deep anaesthesia; surgical anaesthesia and medullar collapse. Thus, the concentration of drug administered to farmed fish depends on the desire stage of anaesthesia. Moreover, there is a series of biological and environmental factors which can alter or mediate the efficacy of the anaesthesia in fish.

2.2.1 Anaesthesia and legislation

Legislation regarding veterinary pharmaceuticals used in aquaculture varies worldwide. In USA, legal use of therapeutic aquaculture drugs and anaesthetics depends on approval by the FDA. Before approval, drugs must be characterized in order to ensure their rate of depletion from edible

tissues. This characterization allows FDA to establish withdrawal times for exposed fish and to ensure that residue concentrations are lower than the permitted before fish are made available for human consumption. Concerning the use of anaesthetics in aquaculture, until now, FDA approved the MS-222 (commercially named by Tricaine-S[®]) for use to temporary immobilization of fish, amphibians and other aquatic-blooded animals, with a 21-days withdrawal time; calcium chloride (CaCl₂) for holding and transportation of fish, and carbon dioxide (CO₂) and sodium bicarbonate (NaHCO₃) for anaesthetic purposes in fish. The last three drugs were considered “low regulatory aquaculture drugs” by FDA [21]. Benzocaine has been mentioned by several authors as an approved drug by FDA; however this drug does not appear in the last guidance of FDA-approved aquaculture drugs [21]. In fact, it has been encouraged the approval of both BENZOAK[®] (20% Benzocaine) and AQUI-S[®]20E (10% Eugenol) as fish anaesthetics by the U.S. Fish and Wildlife Service (FWS) once the preliminary evaluation was promising, presumed safe and, contrary to MS-222, BENZOAK[®] was considered the best approach for a zero withdrawal time anaesthetic [34-37].

In the European Union (EU), the equivalent authority is the European Medicines Agency (EMA) for Europe-wide authorization or the Member State’s regulatory authority if individual country authorization is required. All pharmaceuticals may be subject to three forms of assessment: a maximum residue limit (MRL); a marketing authorization (MA) and, in some cases, an authorization for discharge into the environment [38]. Requests for the last two authorizations for aquaculture medicines are usually submitted to national authorities of EU member states for assessment and that is why this licensing process varies significantly between countries [39]. Regarding the MRL, Annexes I, II and III in Council Regulation (EEC) N° 2377/90 lay down a community procedure for the establishment of maximum residue limit of veterinary medicinal products in foodstuffs of animal origin [40]. According to the last update of these annexes, the use benzocaine (only for salmonids) and MS-222 are considered safe and no MRL is required [23]. On the other hand, 2-phenoxyethanol is a common anaesthetic used in fish farming in Portugal, Iceland and Czech Republic but it is not included in Annexes I, II or III in Council Regulation (EEC) N° 2377/90 [22,39]; however, its approval as active substance for biocidals is now under review [41]. Aside from USA and EU, MS-222 and benzocaine are also permitted in Australia and New Zealand, together with eugenol, while quinaldine sulphate is permitted in Philippines [20].

There are four stages of anaesthesia in fish [42,43]:

- Stage I – comprehends light sedation with normal respiratory rate but slight loss of reactivity to visual and tactile stimuli and deep sedation with decrease of respiratory rate;

- Stage II – includes light and deep narcosis with an increase in respiratory rate and total loss of equilibrium, respectively, and light anaesthesia;
- Stage III – corresponds to surgical anaesthesia with total loss of reactivity;
- Stage IV – comprehends the medullar collapse with total loss of gill movement followed by cardiac arrest and eventual death.

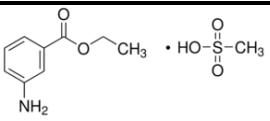
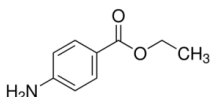
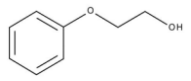
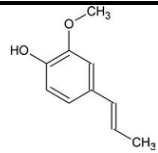
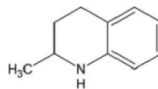
Apart from the desired stage of anaesthesia, there are other factors that determine the dosage of the anaesthetic agent and its efficacy, such as environmental factors, *i.e.*, temperature, pH, oxygen content, hardness and salinity of water, and biological factors like fish species, age, gender, size, weight, lipid content and density of biomass.

2.2.2 Anaesthesia by inhalation

As mentioned above, anaesthesia by inhalation is the most widely used technique. The simplest way to achieve fish anaesthesia by inhalation is to prepare the recommended drug concentration in a container and to transfer the fish into the container. The fish capture must be gentle to avoid skin abrasion. After being weighed, measured and/or marked, fish should be transferred to well-aerated clean water [20].

There is an extensive range of drugs for fish anaesthesia to be administered by inhalation. The following subsections provide a detailed description of the most commonly anaesthetics used. Physico-chemical properties of these anaesthetics are listed in Table 2.1. Anaesthetic dosage and induction (IT) and recovery times (RT) of these drugs for a range of different fish species rearing in Europe by semi-intensive and intensive aquaculture systems are summarized in Table 2.2; pharmacology, pharmacokinetics and toxicology studies of each drug are also surveyed in the following subsections.

Table 2.1 - Physical and chemical properties of the mostly used anaesthetics in aquaculture by inhalation

	MS-222	Benzocaine	2-phenoxyethanol	Eugenol	Quinaldine
Structure					
Molecular Formula	C ₁₀ H ₁₅ NO ₅ S	C ₉ H ₁₁ NO ₂	C ₈ H ₁₀ O ₂	C ₁₀ H ₁₂ O ₂	C ₁₀ H ₉ N
CAS	886-86-2	94-09-7	122-99-6	97-53-0	91-63-4
M_w (g mol⁻¹)	261.29	165.19	138.16	164.22	143.19
S_w (g L⁻¹)	100 (20 °C)	2.5 (20 °C) ^b	26.7 (20 °C)	2.5 (25 °C)	0.5 (25 °C)
pKa	3.6 (25 °C) ^c	2.5 (25 °C)	15.1 (25 °C)	10.2 (25 °C)	5.7 (22 °C)
ACD/logD^a (pH 7.4)	1.54	1.95	1.25	2.2	1.99
ACD/Koc^a (pH 7.4)	165	272	114	376	558

Source: ChemIDplus, U.S. National Library of Medicine.

^aValues from Advanced Chemistry Development/Labs Software.

^bValue from Yalkowsky (2003) [44].

^cValue from Dubé et al. (1986) [45].

2.2.2.1 Tricaine methanesulfonate (MS-222)

MS-222 is the most used anaesthetic in the world for a wide range of operations, such as, fish selection, weight measurements, transportation, broodstock anaesthesia, gamete collection, blood and urine sampling, vaccination and surgical procedures [17-19,46,47]. The base molecule of MS-222 is ethyl-3-aminobenzoate and presents itself as a white and crystalline powder. However, MS-222 has a sulphonated side-chain which makes it acidic but more soluble in water than ethyl-3-aminobenzoate. It is the most soluble anaesthetic, 100 g L^{-1} (see Table 2.1) and it can be dissolved in freshwater or seawater without resorting to organic solvents. The MS-222 working solution is acidic and, consequently, it may be irritant to fish [20]. So, in order to minimize or prevent this effect, some procedures indicate that this anaesthetic should be buffered with sodium bicarbonate (NaHCO_3) at pH 7-7.5 [20,48]. On the other hand, Carter et al. (2011) [49] reported that saltwater and freshwater with higher alkalinities contain a sufficient buffering capacity to maintain an acceptable pH.

Table 2.2 shows the effective dosage of MS-222 administered to some fish species reared by intensive and semi-intensive aquaculture in Europe. The dosages are significantly different among species, so the exposure times may vary between seconds or few minutes for high concentrations and up to hours for low concentrations. Fish recovery takes place after 2 to >60 min and during this period fish should be observed. The anaesthesia by MS-222 acts impeding neuronal signal transmission peripherally to the central nervous system, *i.e.*, inhibits the initiation and propagation of action potentials by blocking voltage-sensitive sodium channels [50]. A well-documented list of physiological consequences in anaesthetized fish with MS-222, including elevated hematocrit, erythrocyte swelling, hypoxia, hypercapnia, hyperglycemia, changes in blood electrolytes, hormones, cholesterol, urea, lactate and inter-renal ascorbic acid may be found elsewhere [20,42,46,50]. Prolonged exposure of farmed fish to MS-222 may be fatal [51].

Since MS-222 administration is by inhalation, both absorption and elimination of the drug occurs by diffusion across the gill membranes. Pharmacokinetic studies were performed by Stenger et al. (1974) [52] in *Squalus acanthias* and, more recently, Kolanczyk et al. (2003) [53] reported the biotransformation of MS-222 in rainbow trout. The results suggest two types of MS-222 transformation: in the first, hydrolysis of the ethyl group of MS-222 occurs producing *m*-aminobenzoic acid followed by acetylation of the amine group to yield *m*-acetylaminobenzoic acid; the second biotransformation involves the acetylation of the amine group to produce ethyl-*m*-acetylaminobenzoate followed by hydrolysis of the acetyl group yielding *m*-acetylaminobenzoic acid as the end product. The total urinary excretion of all four components is about 5% of the administered dose. The most lipid-soluble, *i.e.* non-polar substances, ethyl-*m*-aminobenzoate (MS-

222) and ethyl-*m*-acetylaminobenzoate were rapidly excreted by diffusion across the gill. The remaining metabolites, mostly lipid-insoluble, were excreted by renal secretion [52]. In rainbow trout, renal excretion accounts for 15 to 21% of an injected anaesthetic dose and acetyl-derivatives account for 77 to 96% of the urinary products [54].

MS-222 is considered of low oral acute toxicity, but animals are not recommended to be taken for human consumption during or immediately after treatment [55], so the withdrawal time required by the FDA for animals anaesthetized with MS-222 in the food chain is 21 days. Moreover, the long-exposure of skin to MS-222 causes retinal toxicity, *i.e.*, causes the decrease of vision, photophobia and photopsia [56]. For this reason, many sources advise the use of chemical resistant gloves, dust mask and goggles to individuals with occupational exposure to MS-222 in order to prevent the systemic absorption of this retinotoxic agent [56-59].

2.2.2.2 Benzocaine

Benzocaine (ethyl 4-aminobenzoate) is a local anaesthetic of the ester class, chemically similar to MS-222, with poor solubility in water, as can be seen in Table 2.1. The standard approach is to prepare a stock solution in ethanol or acetone (usually 100 g L⁻¹) which may be kept for more than a year when sealed in a dark bottle. In contrast with MS-222, benzocaine is neutral in solution and therefore causes less hyperactivity and initial stress reaction than the unbuffered MS-222 [20], *e.g.*, striped bass (*Morone saxatilis*) are very sensitive to MS-222, but are effectively anaesthetized using benzocaine solutions (55 to 80 mg L⁻¹). Moreover, water hardness or pH does not affect benzocaine efficacy; however, as with MS-222, benzocaine is fat-soluble and recovery times can be delayed in older or pregnant animals [20,60]. Dosage range administration for some fish species are listed in Table 2.2. The dose could be from 20 up to 200 mg L⁻¹ depending on the species and the desired anaesthesia stage. Similarly to MS-222, benzocaine enters the body via gill uptake and produces anaesthesia by impeding neuronal signal transmission peripherally to the central nervous system, preventing the generation and conduction of the nerve impulse [50,61]. Pharmacokinetic data published by Meinertz et al. (1991) [62] indicates that benzocaine is rapidly distributed and eliminated from the fish plasma. Branchial elimination is the first and the major excretory route for benzocaine residues whilst renal excretion is a minor and slower route (within 3 h only 2.7% of the dose is excreted by kidneys and 9% at 24 h). Likewise MS-222, biotransformation of benzocaine occurs in rainbow trout by acetylation and hydrolysis of the ethyl ether group of the benzocaine to yield acetylbenzocaine, *p*-aminobenzoic acid and *p*-acetaminobenzoic acid [52,62,63]. Despite the absence of the need to establish an MRL for benzocaine, the Committee for Veterinary Medicinal Products (CVMP) recommended the application of a withdrawal period [64].

Besides its efficiency as anaesthetic, many studies reported one potential complication concerning the use of benzocaine: the induction of methemoglobin, *i.e.*, the oxidation of the ferrous iron (Fe^{2+}) in hemoglobin to the ferric state (Fe^{3+}), which results in the inability of hemoglobin to bind oxygen [65]. The majority of these reports described benzocaine-induced methemoglobinemia in humans, as a consequence of the use of benzocaine in the clinic as a topical anaesthetic [66-69]; however, there is no information about the absorption of benzocaine in the digestive tract after consumption of foods by humans, such as edible tissue from benzocaine-treated fish. In this sense, Von Tungeln et al. (2011) [70] estimated the potential impact of benzocaine residues in fish on the human consumer using a rat model to determine if acute oral exposure to benzocaine could cause methemoglobinemia. This study suggests that the consumption of fish treated with benzocaine will not cause methemoglobinemia in humans based upon the dose-response data in rats. However, some of benzocaine metabolites, in particular *p*-aminobenzoic acid, have the potential to induce methemoglobin [71]; others metabolites, such as acetylbenzocaine, have a longer persistence in edible fish tissue than the parent drug [63].

2.2.2.3 2-Phenoxyethanol (2-PE)

The 2-PE is an oily, liquid compound of the glycol ether family that contains a potentially reactive phenol. This is used as an antibacterial and antifungal agent in various consumer goods [72,73], a preservative in vaccines [74,75], a fish anaesthetic [18,20] among other applications. For farmed fish, it is widely used as inhalation anaesthetic and, because its antibacterial and antifungal action, 2-PE is useful during surgical procedures [20]. Besides its lipophilic properties, 2-PE is miscible in water (see Table 2.1) and the drug remains effective in solution for at least 3 days. Another advantage is that it causes no pH change when added to seawater. The precise mode of action of this anaesthetic in fish is unknown, but it has been suggested that an expansion of neural cell membranes is involved [76] and, therefore, it may suppress activity in the central nervous system. The efficacy of 2-PE has been documented for many fish species and the administration dosage varies as shown in Table 2.2. Zahl et al. (2012) [18] reported some adverse effects in fish treated with 2-PE, including reduced ventilation, heart rate and blood pressure. After inhalation, 2-PE is rapidly metabolized to 2-phenoxyacetic acid and their conjugates. More than 90% of all the metabolites are rapidly eliminated via urine, so only small amounts of 2-PE and its metabolites are to be found in organs and tissues [77,78]. Withdrawal time has not been established yet for this agent since it is not registered nor approved as a fish anaesthetic. Moreover, there is no information about the oral acute toxicity resulting from the consumption of treated fish during or immediately after treatment.

Many case reports have been published about the toxicity of the 2-PE in humans in consequence of the use of cosmetics and pharmaceuticals containing this compound [79]: Burka et al. (1997) [76] reported a 24-year-old Asian woman that suffered an episode of acute urticaria after taking a shower and applying a body lotion containing phenoxyethanol 1%; Vogt et al. (1998) [80] published a case of an 18-month-old boy who developed generalized eczema within 24 h after administration of a DPT (diphtheria, pertussis, tetanus) vaccine due to the presence of 2-PE 2% in the vaccine. More recently, Regulska et al. (2010) [81] studied the effect of some ethylene glycol ethers (EGEs), including 2-PE, on the cell viability in the human neuroblastoma cells. The results demonstrated that among the studied EGEs, 2-PE showed the most consistent cytotoxic effect on neurons in *in vitro* conditions and the increase of the hydrogen peroxide-induced damage in the human neuroblastoma and, for this reason, it might be responsible for initiation or exacerbation of neuronal cell damage. Geier et al. (2010) [82] also discourage the use of 2-PE as preservative in licensed vaccine/biological preparations due to its levels of cytotoxicity in humans.

Considering that 2-PE is toxic and dangerous for humans, it is necessary to strictly observe safety regulations, especially for aquaculture workers and in poorly ventilated rooms. Besides the described effects on the central nervous system, it may cause fatigue, drowsiness and irritation of the skin and eyes [79,83,84]. In order to prevent these effects, the use of face shield and safety glasses, complete suit protecting against chemicals, gloves to avoid skin contact and, principally, appropriate air-purifying respirators is recommended [85].

2.2.2.4 Clove oil, Eugenol

Clove oil results from the distillation of the flowers, stalks and leaves of *Syzygium aromaticum* and eugenol is the principal constituent of this oil (70–90% by weight) [20]. Eugenol has been used as a topical anaesthetic since antiquity and nowadays its potential application to treat periodontal disease as antibacterial, anti-inflammatory, antioxidant, antifungal, antiviral, analgesic and anaesthetic has been studied [86-91]. Although eugenol does not appear in FDA-approved aquaculture drugs list, AQUI-S®20E (10% Eugenol) is widely used as a fish anaesthetic under the U.S. Fish and Wildlife Service's Investigational New Animal Drug exemption [92]. AQUI-S®20E is a clear viscous yellow liquid which is dispersible in freshwater and seawater and can be mixed directly within the treatment water, under vigorous agitation, to attain the final concentration (see Table 2.2) [20]. It can be used for all fish husbandry and transport applications and is effective at low concentrations [93]. Eugenol acts on fish, firstly by inhibition of the cerebral cortex (period of tactile loss), secondly by the basal ganglion and cerebellum (excitation period), and finally by the spinal cord (narcosis stage) [94,95]. Renault et al. (2011) [96] and Iversen et al. (2003) [97] reported that anaesthesia with eugenol strongly reduces the plasma cortisol levels of European eels

(*Anguilla Anguilla* L.) and Atlantic salmon (*Salma salar* L.), respectively, acting as a stress-reducing sedative. Guénette et al. (2007) [98-100] performed pharmacokinetic studies of eugenol in some species and found an eugenol half-life in blood of 18 h for rats, 4 h for frogs and 12 h for rainbow trout; however, in case of repeated eugenol administrations, a wash out period of approximately 128 h for rats, 28 h for frogs and 85 h for rainbow trout would have to be respected to allow total elimination of the drug. Kildea et al. (2004) [101] found a total clearance of eugenol in silver perch after 48 h of withdrawal time. As reported by Munerato et al. (2005) [102], there are two eugenol metabolization pathways: one is the epoxidation leading to 2',3'-epoxyeugenol, characterized as an *in vitro* mutagenic agent and as an *in vivo* carcinogenic compound [103]; another one is the hydroxylation that generates the metabolite 1'-hydroxyeugenol, quickly transformed into a methide quinone. This last metabolite is able to induce DNA damage through single strand breaks related to its action as an inducer of active oxygen species [104].

The FDA categorizes clove oil as “generally recognized as safe” (GRAS) for use in dental disease, but neither clove oil nor any of its components are rated as GRAS to use as anaesthetic for fish due to concerns regarding its toxicity to fish and to fish-consuming humans [105]; also, both FDA and U.S. Environmental Protection Agency (EPA) indicate that clove oil contains 5-15 % methyleugenol which is determined as “Reasonably Anticipated to be a Human Carcinogen” by the U.S. National Toxicology Program (NTP) due to its carcinogenicity in rodents [106]. Concerning the primary compound of clove oil (eugenol), in 1983 NTP evaluated its carcinogenesis in rats and mice and there was no evidence of carcinogenicity [107]; in 2006, FAO and World Health Organization (WHO) tested eugenol and related hydroxyallylbenzene derivatives toxicity in humans and concluded that eugenol undergoes rapid first-pass conjugation and rapid elimination and that the short residence time of eugenol in the body might explain the absence of toxic effects [108].

2.2.2.5 Quinaldine, Quinaldine sulphate

Quinaldine (2-methylquinoline) is a yellowish oily liquid that must be dissolved in acetone or alcohol prior to mixing in water. It belongs to the quinoline family which has antiseptic and antipyretic properties and it is used as precursor to drugs, especially anti-malarial medicines [109,110]. On the other hand, quinaldine sulphate is a water-soluble powder and strongly acidic, and thus must be buffered with bicarbonate. The precise mechanism of action is unknown, but it has been suggested that quinaldine and quinaldine sulphate enter the fish body through the gills membranes and, like MS-222 and most inhalants, depress the central nervous system sensory centers [60]. Brown et al. (1972) [111] reported that, due to high lipid solubility, quinaldine tends to accumulate in the brain tissues more than quinaldine sulphate and this might result in a deeper anaesthesia, which also makes it less safe when compared with quinaldine sulphate [20,112]. As

result of the anaesthesia, Ortuño et al. (2002) [113] and Cuesta et al. (2004) [114] observed a significant increase of blood glucose and serum IgM levels, respectively, in the gilthead seabream anaesthetized with quinaldine sulphate; moreover, Davis et al. (2004) [115] reported that the increase of glucose concentration and plasma cortisol in sunshine bass anaesthetized with quinaldine was higher than in those anaesthetized with clove oil and quinaldine sulphate. Increase of fish heart rate, followed by bradycardia and impaired respiratory function were other responses observed by Lochowitz et al. (1974) [116] in rainbow trout anaesthetized with quinaldine. Hunn et al. (1975) [117] observed that the elimination of quinaldine from fish's plasma and muscle was rapid, but slower from bile. Contrarily to the other inhalants, quinaldine is not biotransformed and is totally eliminated by urine and faeces within about 24 h after fish returned to freshwater [117,118].

Although not approved by FDA for use in USA, quinaldine has been used to anaesthetize fish for many years mostly because of its low price, and also because of its effectiveness at very low concentrations (see Table 2.2), purported low toxicity and wide safety margin, and short fish recovery time [119]. However, it is an unpleasant material to work with, being irritant to the human eyes and skin [120]. Moreover, according to Ross et al. (2008) [20] quinaldine has caused corneal damage in salmonids and when exposed to quinaldine or quinaldine sulphate alone fish retain a strong reflexive response to touch, even when deeply anaesthetized, *i.e.*, these compounds have potentially lack of analgesia, making them inappropriate for transportation, handling and noxious procedures [119]. In order to reduce toxicity and, at the same time, increase efficacy and analgesia, some researchers have been studying the combination of anaesthetics: Schoettger et al. (1970) [121] and Gilderhus et al. (1973) [122] evaluated the synergistic effects of MS-222 and quinaldine combination in several fish species and found that this mixture resulted in an effective anaesthesia with lower dosages than when each drug was used alone; however, Dawson et al. (1973) [123] found that not only the efficacy but also the toxicity increased when these drugs were administered in combination. To reduce toxicity, Yanar et al. (2001) [124] tested the combination of quinaldine sulphate with the benzodiazepine diazepam in sea bass juveniles (doses shown in Table 2.2) resulting in a decrease in the excitement and hyperactivity of the fish without leading to mortality, suitable to light and deep anaesthesia stages.

Table 2.2 - Anaesthetics dosage for different stages of anaesthesia (IT-induction time; RT-recovery time)

Anaesthetic	Species	Dose	Weight/Age	T(°C)	Comments	Ref.
MS-222	<i>Anguilla rostrata</i> (American eel)	75 mg L ⁻¹ 100-230 mg L ⁻¹	-	-	Sedation Light anaesthesia (22-30 min IT)	[60] [20,42]
	<i>Centrarchidae</i>	260-330 mg L ⁻¹	-	10-27	Light anaesthesia for spawning, marking, measuring, and some surgical operations (3-5 min IT; 7-11 min RT)	[58]
	<i>Ctenopharyngodon</i> <i>idella</i> (Grass carp)	100 mg L ⁻¹ induction 75 mg L ⁻¹ maintenance	1.6-3.7 kg	31	Anaesthesia for surgical procedures (5 min IT; 5-25 min RT)	[125]
	<i>Cyprinus carpio</i> (Common carp)	25-100 mg L ⁻¹	-	-	Sedation, transport (3.7-4.9 min IT)	[20,126]
	<i>Dicentrarchus labrax</i> (Sea bass)	70 mg L ⁻¹	30 mg	-	Sorting	[127]
	<i>Gadus morhua</i> (Atlantic cod)	75 mg L ⁻¹	84 ± 5 g	8.4	Anaesthesia (4 min IT; 3.7-7.1 min RT)	[128]
	<i>Hippoglossus</i> <i>hippoglossus</i> (Atlantic halibut)	250-480 mg L ⁻¹	-	-	Deep anaesthesia (< 5 min IT; 10 min RT)	[129]
	<i>Ictalurus punctatu</i> (Channel catfish)	100 mg L ⁻¹	Adult (1.1±0.04kg)	14.5	Anaesthesia (4.5 min IT; 1.7 min RT)	[130]
	<i>Oncorhynchus mykiss</i> (Rainbow trout)	60-150 mg L ⁻¹	-	-	Light to deep anaesthesia	[42]
	<i>Salmo salar</i> (Atlantic salmon)	50-100 mg L ⁻¹	-	-	Light to deep anaesthesia	[20,112]
<i>Sparus aurata</i> (Gilthead seabream)	25-50 mg L ⁻¹	150 ± 16 g	20	Deep anaesthesia. Considered useful for transport (1 min IT; > 60 min RT).	[113]	

Table 2.2 (continuation) - Anaesthetics dosage for different stages of anaesthesia (IT-induction time; RT-recovery time)

Anaesthetic	Species	Dose	Weight/Age	T(°C)	Comments	Ref.
Benzocaine	<i>Cyprinus carpio</i> (Common carp)	50 mg L ⁻¹	5.1 ± 0.1 g	27-29	Benzocaine dissolved in 95% ethanol at 1:10 ratio. Anaesthesia (3 min IT; 5 min RT)	[131]
	<i>Gadus morhua</i> (Atlantic cod)	40 mg L ⁻¹	101 ± 6 g	9.5	Benzocaine dissolved in ethanol. Anaesthesia (3 min IT; 3.9-10.8 min RT)	[128]
	<i>Oncorhynchus mykiss</i> (Rainbow trout)	20 mg L ⁻¹	100-500 g	10	Sedation (30 s IT)	[132]
		25-40 mg L ⁻¹	Juveniles (2-500 g)	7-17	Light to heavy sedation (1.25-5.5 min IT; 4-16 min RT)	[60]
		30-45 mg L ⁻¹	Adults (0.68-2.04 kg)		Light to heavy sedation (2.25-4.5 min IT; 5.5-13.5 min RT)	
	<i>Prochilodus lineatus</i>	100-200 mg L ⁻¹	6-27 g	20-25	Total loss of reactivity	[20,133]
	<i>Salmo salar</i> (Atlantic salmon)	30-100 mg L ⁻¹	45 g	5.4	BENZOAK® (20% benzocaine) Anaesthesia	[97]
	<i>Salmo trutta</i> (Sea trout)	50 mg L ⁻¹	100-500 g	10	Sedation (30 s IT)	[132]
<i>Sparus aurata</i> (Gilthead seabream)	22.5 µL L ⁻¹	220 ± 15 g	24	Benzocaine dissolved in 100% ethanol (1:20). Used for diagnostic sampling (8 min IT; 90 s RT)	[134]	

Table 2.2 (continuation) - Anaesthetics dosage for different stages of anaesthesia (IT-induction time; RT-recovery time)

Anaesthetic	Species	Dose	Weight/Age	T(°C)	Comments	Ref.
2-PE	<i>Argyrosomus regius</i> (Meagre)	0.3 mL L ⁻¹	1.3 ± 0.03 g	20	Anaesthesia	[135]
	<i>Carassius auratus</i> (Goldfish)	0.25-0.35 mL L ⁻¹ 0.45 mL L ⁻¹	4 ± 2 g	24	Light sedation Anaesthesia with loss of equilibrium	[60]
	<i>Ctenopharyngodon</i> <i>idella</i> (Grass carp)	0.2 mL L ⁻¹ 0.4 mL L ⁻¹	Broodstock 3-12 kg	25	Light sedation (2-3 min IT) Anaesthesia (5-10 min IT)	[136]
	<i>Cyprinus carpio</i> (Common carp)	0.8-1.2 mL L ⁻¹	5.2 ± 0.1 g	27-29	2-PE mixed with pure ethyl alcohol. Anaesthesia; total loss of equilibrium (0.5-6 min IT; 2- 9 min RT)	[137]
	<i>Dicentrarchus labrax</i> (Sea bass)	0.3-0.45 cm ³ L ⁻¹	2.7 ± 0.03 g	19	Anaesthesia	[138]
		0.32 cm ³ L ⁻¹	0.9 ± 0.1 g	18		[139]
		350 mg L ⁻¹	33 ± 1 g	25	Deep Anaesthesia (< 3 min IT;	[140]
		300 mg L ⁻¹	44.6 ± 0.1 g	15	< 10 min RT)	
	<i>Hypophthalmichthys</i> <i>molitrix</i> (Silver carp)	0.2 cm ³ L ⁻¹ 0.4 cm ³ L ⁻¹	Broodstock 3-12 kg	25	Light sedation (2-3 min IT) Anaesthesia (5-10 min IT)	[136]
	<i>Mugil cephalus</i> (Grey mullet)	400 mg L ⁻¹	38 ± 4 g	31	Provided total loss of equilibrium.	[60]
<i>Oncorhynchus mykiss</i> (Rainbow trout)	0.3 cm ³ L ⁻¹	Broodstock	-	Anaesthesia	[141]	
<i>Sparus aurata</i> (Gilthead seabream)	300 mg L ⁻¹	42 ± 3 g	25	Deep Anaesthesia (< 3 min IT;	[140]	
	450 mg L ⁻¹	72 ± 1 g	15	< 10 min RT)		

Table 2.2 (continuation) - Anaesthetics dosage for different stages of anaesthesia (IT-induction time; RT-recovery time)

Anaesthetic	Species	Dose	Weight/Age	T(°C)	Comments	Ref.
Eugenol	<i>Anguilla Anguilla</i> (European eel)	3.37 mL L ⁻¹	81 ± 9 g	-	Total loss of reflex reactivity (3 min IT)	[142]
	<i>Cyprinus carpio</i> (Common carp)	50-100 mg L ⁻¹	700-750 g	20	Anaesthesia; loss of reflex activity (12-21 min IT; 15 min RT)	[143]
Clove Oil	<i>Dicentrarchus labrax</i> (Sea bass)	40 mg L ⁻¹	33 ± 1 g	25	Deep Anaesthesia (< 3 min IT; < 10 min RT)	[140]
		30 mg L ⁻¹	44.6 ± 0.1 g	15		
	<i>Ictalurus punctatu</i> (Channel catfish)	100 mg L ⁻¹	19 ± 4 g	-	Total loss of equilibrium	[144]
	<i>Salmo salar</i> (Atlantic salmon)	5 mg L ⁻¹	31-44 g	15	Clove oil dissolved in 95% ethanol at 1:10 ratio. Sedation for 6 h without loss of equilibrium. Considered useful for transport.	[145]
	<i>Sparus aurata</i> (Gilthead seabream)	40 mg L ⁻¹	42 ± 3 g	25	Deep Anaesthesia (< 3 min IT; < 10 min RT)	[140]
		55 mg L ⁻¹	72 ± 1 g	15		
Quinaldine	<i>Ctenopharyngodon idella</i> (Grass carp)	50 mg L ⁻¹	1.6-3.7 kg	22	Anaesthesia for surgical procedures	[125]
	<i>Cyprinus carpio</i> (Common carp)	10-50 mg L ⁻¹	-	-	Anaesthesia	[112]
Quinaldine sulphate with diazepam	<i>Dicentrarchus labrax</i> (Sea bass)	5 mg L ⁻¹	Juveniles	24-25	Light anaesthesia suitable for transportation (1-2 min IT; 3-5 min RT)	[124]
		2 mg L ⁻¹	(8-9 g)			
		7.5 mg L ⁻¹	Juveniles	24-25	Deep anaesthesia suitable for marking, surgery and handling (1-2 min IT; 4-6 min RT)	[124]
		2 mg L ⁻¹	(8-9 g)			
Quinaldine sulphate	<i>Sparus aurata</i> (Gilthead seabream)	10 mg L ⁻¹	Juveniles 6-7 g	25-26	Light anaesthesia (0-1 min IT; 3-5 min RT)	[119]

2.2.2.6 *Other drugs*

Other drugs have been used for anaesthesia by inhalation in aquaculture activity, such as metomidate, etomidate, and other even less used, as barbiturates, choral hydrate, chlorbutanol, chloroform, diethyl ether, lidocaine, methyl pentynol, piscaine, propanidid, tertiary amyl alcohol, tribromoethanol and urethane. These drugs, in some cases, are quite effective but have not been adopted by fish biologists or veterinarians for several reasons: some of them have unwanted side effects, others are unpleasant to work with and/or there is lack of knowledge of their precise physiological effects [20].

This work is focused on the fish anaesthetics MS-222, benzocaine and 2-PE, which are the mostly used in worldwide aquaculture activity.

2.2.3 **Presence of fish anaesthetics in the environment**

In case of fish anaesthetics, there are no studies related with their presence in the environment, wastewaters and sewage sludge or sediments; however, considering the fact that these pharmaceuticals need to be solubilised before administration, water from the fish tanks becomes contaminated. In semi-intensive aquaculture, the anaesthetic drug is released directly in a pond or lagoon without further water treatment, which means a direct contamination of the environment. In intensive aquaculture systems, anaesthetic contaminated water passes through the RAS, the contaminant is eliminated or not, and part of the treated water returns to fish's tank. Depending on the characteristics of each anaesthetic used, it may be sorbed by sewage sludge, which has been applied as fertilizer by many aquaculture-producers [146-148], entering then in terrestrial environment. Also, low volumes of anaesthetic solutions prepared for procedures, such as netting, weighing, sorting, vaccination, transport and/or slaughter, eventually may reach the environment. Notwithstanding the scarcity of information about the occurrence, persistence and toxicity of this class of compounds in the environment, some reports suggest special care in their handling and disposal. Many sources indicate that MS-222 is biodegradable but is not recommended to discard it in the environment [57-59]. Moreover, according to the Environment, Health & Safety (EHS), the unused powders or solutions of MS-222 should be disposed of as a hazardous material [149]. Once in the environment, based on MS-222 properties (S_w , ACD/Koc and ACD/logD) shown in Table 2.1, it is expected that MS-222 has presence in the aquatic environment (high solubility in water), with high mobility in soil and low possibility of adsorption to suspended solids and sediments (low values of ACD/Koc and ACD/logD).

In the same way, benzocaine production and use as anaesthetic may result in its release to the environment through several waste streams: if released to air, benzocaine may be degraded in the atmosphere by reaction with photochemically-produced hydroxyl radicals and the half-life for this reaction is estimated to be 11 h; if released to soil, it is expected to have moderate mobility and non-volatilization of benzocaine from moist soil surfaces; if released in aquatic environment, benzocaine has an estimated half-life of 91 h (at pH 7), which is classified as biodegradable, and is not expected to be adsorbed onto suspended solids and sediments [79]. This is expected information which indicates that benzocaine is more persistent in the aquatic environment. It is not advisable to discharge benzocaine solutions into the environment and it is highly recommended the contact with a licensed professional waste disposal service to treat them [79,150]. At the best of our knowledge, there is no information regarding MS-222 and benzocaine concentrations in water and/or soil or sediments.

The 2-PE compound may enter the environment during its production, its use as fish anaesthetic and, also, from human disposal. When present in terrestrial environment, 2-PE is expected to have very high mobility in soil, due to its low value of ACD/Koc (Table 2.1), and the theoretical 2-PE biochemical oxygen demand (BOD) of 50% at 20-day indicates that biodegradation may be an important environmental process in soil [79]. In aquatic environment, 2-PE is not expected to undergo hydrolysis due to the lack of functional groups that hydrolyze under environmental conditions [151]. Finally, when present in the atmosphere, vapour-phase 2-PE is degraded and its half-life in air is estimated to be 11.8 h [152]. However, it is not expected that 2-PE suffers direct photolysis by sunlight, since it does not absorb at wavelengths > 290 nm (see Figure A.3 from Appendix A). Additionally, Poliakova et al. (2000) [153] studied the effect of the possible deposition of organic contaminants due to atmospheric transport and results show that 2-PE can be removed from the atmosphere via precipitation such as snow, reaching the terrestrial and aquatic environment. Volatilization of 2-PE from moist soil and water surfaces is not expected to be an important fate process [79]. Some authors already found the occurrence of 2-PE compound in drinking water, river water and wastewater: it was qualitatively detected in drinking water concentrates collected in Cincinnati, Ohio, in 1978 [154]; Rivera et al. (1985) [155] found 2-PE concentrations of less than 5 mg L⁻¹ in groundwater from Llobregat river, Spain, located near to pesticide and surfactants industries; more recently, Kimura et al. (2014) [156] detected 2-PE at a maximum concentration of 14 mg L⁻¹ in Japanese rivers; Piperidou et al. (2000) [157] found 2-PE in influent from olive oil mill and reported the incomplete removal of this compound after biological treatment; Gulyas et al. (2000) [158] monitored some organic constituents in oil reclaiming wastewater, before and after precipitation/flocculation/sedimentation processes and after contacting with activated sludge: 2-PE was detected at concentrations of 14.6 and 14.3 mg L⁻¹

before the three processes and after a short contact with activated sludge, respectively, and, in another sample, 67.9 and 60.7 mg L⁻¹ before and after precipitation/flocculation/sedimentation, respectively.

In general, BurrIDGE et al. (2010) [10] state that the use of anaesthetics is considered to be of low risk to the environment; however Grigorakis et al. (2011) [29] suggests that additional work is urgently needed to gain a thorough understanding of the possible presence of anaesthetic compounds in water and/or sediments near fish farms and their possible bioaccumulation in the environment. Moreover, taking into account the toxicological effects at long-exposure to these kind of compounds described in section 2.2.2, for both fish and human, it is important to ensure the water quality for recycling, through RASs, and/or for discharge in the environment.

2.3 Aquaculture wastewater treatment and recycling

Aquaculture activity depends strongly on water resources and the volume of consumed water (sea or freshwater) may differ significantly, depending on cultured specie and the type of farm system and its water recycling capacity. EU water management directive (directive 2000/60/EC) calls for sound environmental friendly aquaculture production systems [159]. In this sense, the implementation of RASs provides the opportunity to reduce water consumption, to promote waste management and nutrient recycling and, at the same time, to control biological pollution for a better hygiene and disease management and to avoid the discharge of waste, especially organic pollutants, in the environment. It has been well documented that minerals, drug residues, hazardous feed compounds and metabolites may accumulate in the system and affect the health, quality and safety of the farmed animals [160-164].

Recirculation can be carried out at different intensities depending on the degree of recirculated or reused water: intensive systems, installed inside a closed insulated building, use 1 m³ or less of new water per kg of fish produced per year, which corresponds to more than 98% of recycled water one time per hour; semi-intensive systems, that have been rebuilt into recirculated systems, use around 3 m³ of new water per kg of fish produced per year, corresponding to 96% of recycled water one time per hour; while extensive systems (flow-through systems) use around 30 m³ of new water per kg of fish produced per year, *i.e.*, no water is recycled [148]. Although recirculating in aquaculture can be considered the most environmentally friendly way of producing fish, the limited use of water is a great benefit to the production, since the external factors (such as, water temperature, cleanliness of the water, oxygen levels, salinity, solids or weed and leaves

drifting downstream and blocking the inlet screens) are controlled, either completely or partially depending on the degree of recirculation, contrasting with traditional flow-through system.

Thereby, in a RAS it is necessary to treat the water continuously to remove the waste products excreted by the fish, uneaten feed and/or medicines, and to add oxygen to keep the fish welfare.

2.3.1 Recirculating aquaculture systems (RASs)

In a typical RAS, the water flows from the outlet of the fish tanks to a mechanical filter (primary treatment) and then to a biological filter (secondary or biological treatment) before it is aerated and stripped of carbon dioxide and returned to the fish tanks. Some facilities may also have oxygenation process with pure oxygen and tertiary treatment processes, such as ultraviolet radiation, activated carbon filtration or ozonation [148]. Figure 2.3 presents a scheme of a RAS and each process herein illustrated is detailed in the following subsections.

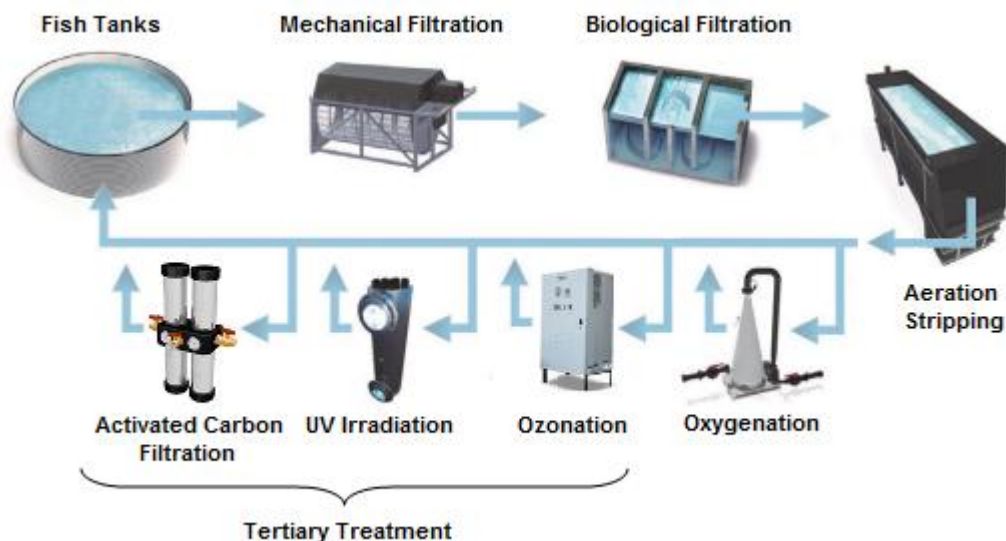


Figure 2.3 - Representation of a RAS (adapted from Bregnballe (2015) [148]).

2.3.1.1 Mechanical filtration

Particulate waste from faeces, feed fines and uneaten feed is the main source of carbonaceous oxygen demand and nutrient input into the water tank. Mechanical filtration is the primary phase of aquaculture wastewater treatment and it has proven to be a practical solution for the removal of the organic waste particles [148]. Microscreen filters are commonly used in RASs because they are able to remove a large proportion of the solids produced during each pass. Depending on the size of the microscreen mesh, the filter hydraulic capacity, total solids removal,

sludge production rate and concentration and filter wash frequency can be affected; microscreen filters with small openings remove more total suspended solids (TSS) but also require more frequent washings than filters with larger openings [165]. This process has the advantage of reducing the organic load in aquaculture water and, simultaneously, improving conditions for the biofilter.

2.3.1.2 Biological filtration

The mechanical filtration does not remove all the organic matter; the finest particles may pass through, together with toxic dissolved compounds, such as phosphate and nitrogen in the form of free ammonia (NH_3), nitrite and nitrate. To breakdown the organic matter and transform ammonia in harmless nitrate, a biological process carried out by bacteria is required: heterotrophic bacteria oxidise the organic matter by consuming oxygen and producing carbon dioxide, ammonia and sludge; on the other hand, nitrifying bacteria convert ammonia into nitrite and ultimately to nitrate. The efficiency of the biological treatment depends mainly on the water temperature and pH level in the system [148,166].

In RASs, the biological wastewater treatment is often carried out in fixed bed filters or moving bed filters. In the fixed bed filter, the bacteria support (generally plastic media) is fixed and the water runs through the media as a laminar flow to make contact with the bacterial film. Also, fixed bed filter acts as a fine mechanical filtration unit, removing fine organic particles by adherence to the bacterial film. In the moving bed filter, the bacteria support is moving around in the water inside the biofilter by a current created by pumping in air [148,165,167].

2.3.1.3 Aeration and stripping

During all the fish rearing and water treatment processes, the accumulation of gases in the fish tanks, namely CO_2 and N_2 , is detrimental to the fish. The degassing of the water is carried out by an aeration/stripping process, *i.e.*, pumping air into the water, whereby the turbulent contact between the air bubbles and the water drives out the toxic gases. The trickling filter system, also called degasser, has also been used in RASs for the removal of gases. This technique consists of stripping off gases by physical contact between the water and plastic media stacked in a column; the water is routed to the top of the filter and flushed down through the plastic media to maximize turbulence and contact, making this system more efficient than the aeration system [148].

2.3.1.4 Oxygenation

The oxygen content decreases from 100 to 70% when the water passes through the fish tanks and it is further reduced in the biofilter. Aeration/stripping process may bring the saturation

level of the oxygen in the water up to around 90% and, in some systems, 100% may be reached. Oxygen saturation level higher than 100% in the inlet water to the fish tanks is often preferred in order to have sufficient oxygen available for a high and stable fish growth, and for this the use of pure oxygen is necessary. There are several techniques to super-saturate water with oxygen levels of 200-300%: the technique typically used is the high pressure oxygen cone system or low head oxygen system based on oxygen platforms. Both techniques have the same principle, *i.e.*, water and pure oxygen are mixed under pressure so that the oxygen is forced into the water. In an oxygen cone system, the pressure is accomplished with a pump in order to create a high pressure in the cone (around 1.4 bar). In this case, only a part of the circulating water is used for oxygen enrichment. In the oxygen platform system, the pressure is lower and the water is simply pumped through the box, mixing water and oxygen. This last system is used for the main recirculation flow often in combination with the overall pumping of water round in the system [148].

2.3.1.5 Tertiary treatment

The application of tertiary treatment in RASs is mainly for water disinfection and/or removal of organic pollutants before the water runs back into the fish tanks. In this sense, advanced oxidation processes (AOPs) such as ozonation and ultraviolet (UV) radiation have been employed separately or in combination [148,165,168-170]. The use of ozone (O₃) is particularly well suited to aquaculture since it is a strong disinfectant by the heavy oxidation of organic matter, nitrogen compounds and fine suspended particles and it causes the destruction of pathogenic organisms with a rapid reaction rate [165]. However, the ozonation in fish farming has been criticised because over-dosing and ozonation by-products can be harmful to the fish [148]. This process requires ozone generation, ozone transfer into solution, contact time for ozone to react and also ozone destruction to ensure that no residual ozone remains in the fish tanks [165]. In this context, Summerfelt (1996) [165] listed three methods to eliminate ozone from aquaculture water: use of larger contact times, stripping the ozone into air or passing the flow through a biofilter or bed of activated carbon. Alternatively, Bregnballe (2015) [148] suggests the UV radiation treatment as a good and safe substitute for ozone and Summerfelt et al. (2009) [170] propose the use of ozonation followed by UV radiation before water returns to the fish tanks to improve biosecurity. UV radiation destroys DNA of microorganisms causing their death or lost of function, and also destroys ozone residuals; yet, it depends on the wavelength of the UV light source and the quantity of energy transmitted. The wavelengths for the destruction of ozone residuals range from 250 to 260 nm and the most effective wavelength for microorganisms inactivation is 254 nm. So, low pressure UV bulb systems supply monochromatic radiation at 254 nm, which is almost an industrial standard to RASs application [169].

The adsorption process, using activated carbon filters, has been also proposed in addition to biological filters, as tertiary treatment or polishing stage, to remove not only ozone but also persistent nonbiodegradable organic compounds [171]. This process has been tested for the removal of ammonia [172], phosphorus [173] and organic micropollutants, such as the fungicides malachite green [174-177] and formaldehyde [175,176,178], the antibacterial agents chloramine-T [175,176] and oxytetracycline [175], and the fish anaesthetics MS-222 and benzocaine [179,180].

The typical RAS was initially planned to remove suspended solids and to control dissolved organic carbon (DOC) and ammonia levels which are efficiently removed by mechanical and biological filtration. However, these filters are not designed to remove organic therapeutants and the shock loading of pharmaceuticals on filters may destroy the nitrifying bacteria. For that reason, it is common to administer the drugs in separated tanks which are not connected with the RAS or simply purge recycle aquaculture systems since pharmaceuticals have been administered; the normal effluent treatment and recirculation resumes when pharmaceuticals are released from the fish's body. Water treatment processes should be implemented in order to prevent the release of these pollutants into the environment whether as a purge from an intensive aquaculture system or any land-based operations for disease treatment, particularly if there is concern and doubt about their fate in the ecosystem, which is the case of the anaesthetic's class.

2.3.2 Removal of fish anaesthetics from water

Regarding the treatment of wastewaters contaminated with fish anaesthetics, few studies were performed until now. Dawson et al. (1976) [179] tested the adsorption of the fish anaesthetics MS-222 and benzocaine and other fish toxicants in a filter of activated carbon. The authors performed continuous adsorption experiments in a glass column packed with a granulated activated carbon (DARCO[®], particle size 0.42-0.85 mm, produced by Atlas Chemical Industries, Inc.) and the total adsorption capacities obtained were 63.4 and 63.2 mg g⁻¹ for MS-22 and benzocaine, respectively. Later, Howe et al. (1990) [180] evaluated the performance of three types of activated carbon for the removal of benzocaine from water (30 mg L⁻¹), also using a packed glass column. Adsorption capacities of 76.1, 31.9 and 1.0 mg g⁻¹ were obtained using 36 g of Filtrasorb 400, 300 and 816, from Calgon Carbon Corporation, respectively (particle sizes of 0.55-0.75, 0.8-1.0 and 1.2-1.3 mm, respectively), when 30% of adsorbent saturation is reached. The authors concluded that smaller particle size resulted in an increase of adsorption capacity; however, powdered carbon also impeded column flow. Ross et al. (2008) [20] affirmed that the adsorption process has not been widely explored for the removal of this kind of compounds, but its application may be a consideration to obtain approval for other veterinary drugs in the future.

Concerning the removal of 2-PE from aquaculture wastewater, there are no studies reported; however, studies aiming at the removal of 2-PE, used as an antibacterial and antifungal agent in various consumer goods, from water have been performed: Puyol et al. (2011) [181] investigated the efficiency of an upflow anaerobic sludge blanket reactor for the treatment of cosmetic wastewater and, after 154 days, the 2-PE removal efficiency was 96.4%. Real et al. (2012) [182] studied the elimination of emerging contaminants, including 2-PE, in ultrapure water and secondary effluents by UV radiation and UV/H₂O₂, Fenton's reagent, Fenton-like and photo-Fenton systems. The photo-Fenton system reached the highest removal of 2-PE from ultrapure water, with about 62% in 1.5 min. The photodegradation percentage of 2-PE from real water matrices decreased about 3 times. The identification of undesired by-products was not performed in this study, which is usually the main drawback of AOPs, together with its expensive application.

2.4 Adsorption process for the removal of organic pollutants

Adsorption is a specific or non-specific process that arises from the interaction between the solid (adsorbent) and the molecules present in liquid or gas phases (adsorptive). This interaction results from the unsaturated and unbalanced molecular forces that occur on every solid surface; so, when the adsorbent is brought into contact with a liquid or gas, there is an interaction between force fields of the solid surface and that of the liquid or gas. Adsorption involves physical forces (dipole moments, polarization forces, dispersive forces or short-range repulsive interactions) and chemical forces (valence forces arising from the redistribution of electrons between the adsorbent and the adsorbed atoms) and, depending upon the nature of the forces, the adsorption may be physical (physisorption) or chemical (chemisorption) [183]. Briefly, in the case of physisorption, the adsorbate is bound to the adsorbent by relatively weak van der Waals forces (similar to the molecular forces of cohesion), whereas chemisorption involves exchange and sharing of electrons between the adsorbate and adsorbent. In this last case, the adsorbate-adsorbent interaction is essentially a chemical bond and the enthalpy of adsorption is generally of the order of 100-400 kJ mol⁻¹, which is much higher than in the physisorption (20-40 kJ mol⁻¹). In this sense, physical adsorption is generally considered non-specific and occurs between any adsorbate-adsorbent system, while chemical adsorption is a specific process [183-186]. The type of adsorption depends on the nature of the adsorbate, of the adsorbent (surface reactivity, surface area and porosity) and on temperature and pressure. Furthermore, there are other parameters which can strongly influence the whole adsorption process: solution pH, contact time, initial adsorbate concentration, mixing speed, volume of adsorbate solution, ionic strength of the solution and adsorbent dosage [183,185].

The physical and chemical properties of the adsorbent play an important role in the adsorption process. The porous structure determines the adsorption capacity; the chemical structure influences the interaction with the adsorbates (polar or nonpolar) and the active sites, dislocations and discontinuities determine the chemical reactions with other atoms. The porous structure can be classified into three major groups, according to the pore width: micropores (< 2 nm), mesopores (2–50 nm) and macropores (> 50 nm). So, the concept of porosity is usually defined as the ratio of the volume of pores to the volume occupied by the solid. Micropores and mesopores are especially important in the context of adsorption [187]. Another significant physical characteristic of an adsorbent is the specific surface area, defined as the area available for adsorption per gram of adsorbent and which depends on the extent of surface roughness and porosity [184]. Specific surface area is determined commonly by adsorption methods and the mostly used method was developed by Brunauer and Emmett in 1938, named Brunauer-Emmett-Teller (BET) theory. In this method, N₂ is generally used as the adsorbate at 77 K [188,189]. Moreover, the presence or absence of surface groups that may bond themselves to the solid atoms gives adsorbents with different chemical properties.

2.4.1 Activated carbons

Activated carbons are known as excellent and versatile adsorbents with numerous applications in several areas such as purification of drinking water and treatment of industrial wastewater, purification of industrial chemicals, and in a variety of gas-phase applications [183,187,190,191]. They are also known as a highly porous material (mainly microporous) produced from a carbon-rich precursor by some form of chemical or physical activation. The raw materials for activated carbons are usually carbonaceous resources such as coal, petroleum coke, bones, wood, peat, coconut shell and fruit nuts; however, anthracite and bituminous coals have been the major sources [192]. The activated carbons production process involves two main steps: the pyrolysis (or carbonization) of the carbonaceous raw material at temperatures usually below 800 °C in an inert atmosphere (*e.g.*, N₂, Ar, He) and the activation, which can be performed after or during the pyrolysis step [183,192]. During the pyrolysis process, most of the non-carbon elements (oxygen, hydrogen and nitrogen) are eliminated as volatile matter by pyrolytic decomposition of the starting material, resulting in the so-called char or biochar. The char is mainly composed by residual elementary carbon atoms that group themselves into stacks of flat, aromatic sheets cross-linked in a random manner. These aromatic sheets are irregularly arranged, leaving interstices which give rise to pores. However, during pyrolysis process these pores could be filled with the products of decomposition, essentially inorganic matter, or blocked partially by disorganized carbon [183]. The activation step aims to develop and enhance the pore structure by converting the

char into a form that contains the highest possible number of randomly distributed pores of various sizes and shapes and giving rise to an extremely high surface area [184]. The physical activation of the char is usually carried out in an atmosphere of air, carbon dioxide (CO₂) or steam at temperatures ranging from 700 to 1100 °C [183]. On the other hand, chemical activation is frequently used for preparation of activated carbons in one-step, *i.e.*, pyrolysis and activation occur simultaneously. Different chemical activating agents can be used (*e.g.*, zinc chloride (ZnCl₂), phosphoric acid (H₃PO₄), potassium hydroxide (KOH), potassium carbonate (K₂CO₃), sodium hydroxide (NaOH) and sulphuric acid (H₂SO₄)) to develop porosity, by means of dehydration and degradation; the mixture of the chemical and the precursor is then pyrolysed at a maximum of 800 °C [191-194]. There are a wide variety of ways to activate a material physically or chemically, depending on the precursor [191,192]. As a result of the activation process, a typical activated carbon has been found to be mainly carbon (above 80% C) with low content of hydrogen, nitrogen and sulphur (about 0.5% H, 0.5% N and 1% S) and oxygen content around 6-7%, according to the source of the raw material and the conditions of the activation process [183]. The inorganic matter contained in activated carbons is measured as ash content and generally ranging between 2 and 10% [192]. These materials have a microcrystalline structure, highly microporous, with a large specific surface area (S_{BET}), which in some cases may be as high as 2500 m² g⁻¹. The porous structure is perhaps the main physical property that characterizes activated carbons [183,184,191,192].

The use of activated carbons as adsorbents is a well-established process for the removal of organic contaminants from water and wastewater systems [190,195-197] and different process variants and reactor types could be used. The options are essentially related to the particle size of the applied adsorbent: stirred tank reactors (in batch or continuous system) are used for powdered activated carbon (PAC), whereas fixed-bed reactors are applied for granulated activated carbon (GAC) [198]. From the kinetic point of view, higher adsorption rates is the advantage of PAC and, consequently, the equilibrium is attained within a short contact time; however, its use in fixed-bed reactors is not possible due to the flow resistance that increases with the decrease of particle size. Stirred tank reactors with PAC are often used in cases where an adsorption step within the treatment plant is not continuously needed, *e.g.*, when the effluent quality varies over time [199]. However, in this type of reactors an additional separation step is necessary to remove the loaded adsorbent particles from the water and the adsorbent consumption to achieve a given treatment goal is usually higher. In this context, the use of fixed-bed reactors is more advantageous since no additional separation step is necessary and the adsorbent consumption is lower in comparison to stirred tank reactors; moreover, contrarily to PAC which cannot be efficiently regenerated, GAC can be regenerated or reactivated and used repeatedly [199,200].

In the particular case of aquaculture activity, specific activated carbons produced from wood, coal, lignite and coconut shell have been commercialized mainly for the removal of ozone, halogens (chlorine and bromide), colours, pesticides, odours and metabolic by-products in RASs [201]. Also, as mentioned in section 2.3.1.5, activated carbons were tested to remove fungicides, antibiotics and fish anaesthetics [174-180]. Fixed-bed columns packed with activated carbons may be used as a polishing stage to remove persistent nonbiodegradable organic pollutants [171]. However, despite their easy implementation and high efficiency, the main drawback of activated carbons is their high price (due to its precursor and production process) [202-204]. For this reason, activated carbon filters have been incorporated only as an auxiliary filter to support biofiltration in RASs, since this form of filtration requires large amount of relatively costly activated carbon [205]. In this sense, in the last decades, studies have been conducted to find alternative adsorbents, equally efficient but cheaper, and with the possibility of regeneration for re-use.

2.4.2 Alternative adsorbents

Several studies have been performed in order to find alternative low-cost adsorbents to be applied in the treatment of waters contaminated with organic pollutants. Many reviews have been published about the use of alternative adsorbents mostly aiming at the removal of dyes from water [206-213] and the removal of both organic (dyes, pharmaceuticals and personal care products, pesticides and phenolic compounds) and inorganic contaminants (mostly heavy metals) in general [214-221]. Recently, several studies have been focused on the search for alternative adsorbents to remove human and veterinary pharmaceuticals from water and wastewater, as shown in Table 2.3. There is a relation between the properties of the adsorbent and its effectiveness (*i.e.*, maximum adsorption capacity) in eliminating organic pollutants from water. Three major approaches have been used to produce such kind of alternative adsorbents: the use of natural adsorbents, *i.e.*, without thermal, chemical or physical treatment; the use of different raw materials for the production of new activated carbons (mainly, agricultural, industrial and/or municipal residues or by-products); and the use of simpler methods to produce new adsorbents (mostly by thermochemical conversion processes, such as pyrolysis) [193,221-223].

The use of agricultural residues (*e.g.*, nuts shells, fruit stones or seeds, diverse type of wood and agricultural biomass) as adsorbents or as precursors for the production of adsorbents (activated or non-activated carbons) has been considered more attractive due to their world wide availability and low or null economic value [193,208,209,224]. For example, only in the south of Europe, between 4.5 and 10 Mt of olive mill solids; between 1.3 and 2.8 Mt of grape waste from winery industry and between 0.1 and 0.2 Mt of tomato solid residues were produced in 2012 [225].

Also, their physical and chemical properties make them attractive for such application. These are lignocellulosic materials which contain three main structural components, hemicelluloses, cellulose and lignin, with high molecular weights resulting in high yields in the production of adsorbents. Lignocellulosic materials also contain extractives, *i.e.*, compounds with small molecular size, but in lower quantity [209]. So, agricultural wastes are a rich source for adsorbents production due to their high organic carbon content, low ash content and reasonable hardness [193]. As can be seen in Table 2.3, some authors tested natural agricultural biomass as adsorbents to remove antibiotics and paracetamol; however, low adsorption capacities were obtained as consequence of the low specific surface area of these natural adsorbents. In order to increase the adsorption capacity, the so-called activation processes, physical or chemical activation mentioned in section 2.4.1, are usually performed to develop the pore network of the biowastes. In Table 2.3, it is possible to observe that, depending on the type of activation and raw agricultural waste, S_{BET} may increase up to three orders of magnitude, thus increasing the adsorption capacity.

In the last years, the use of industrial residues for the production of adsorbents has aroused great interest which is a consequence of an environmental legislation increasingly stringent concerning the disposal of such residues. The landfilling practice has been discouraged and limited to the necessary minimum and, when waste needs to be landfilled, it must be sent to landfills which comply with the requirements of European Landfill Directive 1999/31/EC [226]. Also, incineration of industrial wastes has been discouraged by the application of operational conditions, technical requirements and emission limit values within the EU. Directive 2000/76/EC sets limit values and monitoring requirements for emission of pollutants to air, such as dust, nitrogen oxides (NO_x), sulphur dioxide (SO_2), hydrogen chloride (HCl), hydrogen fluoride (HF), heavy metals and dioxins and furans [227]. The objective of these directives is to prevent or reduce negative effects on the environment, in particular on surface water, groundwater, soil, air and on human health. In this sense, Waste Framework Directive 2008/98/EC lays down some basic waste management principles prioritizing waste recycling over incineration and landfilling [228]. This drives the need of developing better sustainable practices that involve the wastes' valorisation through their reutilization as raw materials for distinct purposes, which is also part of the EU action plan for the Circular Economy. The production of adsorbents for water remediation has been one of the applications of industrial residues. As shown in Table 2.3, ashes from different industrial processes, granulated and powdered wastes produced over industrial processes, sludge from WWTPs and manure have been used as precursors for the production of activated and/or non-activated adsorbents aiming at the removal of pharmaceuticals from contaminated waters. Depending on the type of residue and the process it has undergone, different materials with distinct properties can be obtained. For example, Mall et al. (2005) [229] have used bagasse fly ash collected from the

sugarcane bagasse-fired boilers, without any additional treatment, as an adsorbent for the removal of malachite green (an anti-fungal, anti-bacterial and anti-parasitical agent used in fish farming) from water and, comparing with two commercial activated carbons, this alternative adsorbent presented higher adsorption capacity in a shorter time of equilibrium. On the other hand, Gupta et al. (2004) [230] and Mittal et al. (2005) [231] studied the adsorption of malachite green onto bottom ash from thermal station and de-oiled soya, respectively, treated with hydrogen peroxide in order to oxidize the adhering organic material, but the results were not encouraging. Studies conducted by Mestre et al. (2007, 2014) [232, 233] showed that the physical or chemical activation of cork powder waste and granulates of expanded corkboard resulted in adsorbents with good properties, capable to compete with the commercial ones. These authors produced powdered and granulated activated carbons with high S_{BET} (between 750 and 1060 $\text{m}^2 \text{g}^{-1}$), with high capacities of adsorption for ibuprofen, between 143 and 378 mg g^{-1} (Table 2.3).

The production of alternative adsorbents from agricultural and/or industrial wastes eliminates the cost associated to the precursor with the additional benefit of eliminating managing costs of such residues. However, the use of activation agents, mainly in chemical activation process, has been reported as environmentally unfriendly. Hjalila et al. (2013) [234] investigated the environmental impacts of the production of activated carbon from olive-waste cakes chemically activated with H_3PO_4 , at laboratorial scale, by using life cycle assessment (LCA) methodology. Their results showed that the impregnation step presented the highest environmental impact regarding the eutrophication potential (96.31%), terrestrial ecotoxicology (92.47%), fresh water aquatic ecotoxicology (90.02%), human toxicity (63.99%), acidification potential (62.32%) and ozone layer depletion potential (44.31%). The pyrolysis and cooling steps obtained the high relative photochemical oxidation potential and this is, mainly, due to the C_2H_4 emissions during the pyrolysis of the olive-waste cakes. Also, CH_4 and CO_2 emissions contributed for greenhouse effect. The main factor responsible for this impact was the high amount of methane released when natural gas is used to produce the electricity needed in the pyrolysis and drying steps. However, although Hjalila et al. (2013) [234] did not included it in their study, the reuse of the gases produced during the pyrolysis step as energy source could be beneficial since it allows reducing the use of electrical energy.

Table 2.3 - Alternative adsorbents for the removal of pharmaceuticals from water (S_{BET} -specific surface area; t_e -equilibrium time; q -adsorption capacity)

Precursor	Treatment	S_{BET} ($\text{m}^2 \text{g}^{-1}$)	Contaminant	t_e (min)	q (mg g^{-1})	Conditions	Ref.
<i>Agricultural wastes</i>							
Mushroom substrate	-	-	Sulfamethyldiazine Sulfamethazine Sulfathiazole Sulfamethoxazole	150-170 120-150 150-180 120-150	2.11 1.81 2.30 2.21	Particle size: 0.1-0.3 mm Adsorption conditions: 15 °C, pH=3.0; 100 rpm; 2 g L ⁻¹ of adsorbent; C _{pharm} =0.5-10 mg L ⁻¹	[235]
Grape stalk	-	-	Paracetamol	16-24 h	2.18	Adsorbent particle size: 0.63-0.75 mm Adsorption conditions: 20 °C, pH=6.0; 30 rpm; 3-33 g L ⁻¹ of adsorbent; C _{pharm} =20 mg L ⁻¹	[236]
Walnut shell	-	13.1	Sulfamethoxazole	-	0.47	Adsorbent particle size: 0.25-0.5 mm Adsorption conditions: 20 °C, pH=7.0, 10 g L ⁻¹ of adsorbent; C _{pharm} =0.5-5.0 mg L ⁻¹	[237]
Mugwort leaves	Chemical activation with 60% (v/v) H ₂ SO ₄ (8-12 h) and pyrolysis at 450 °C (30 min) under N ₂ flow	358	Ibuprofen	240-300	16.9	Adsorbent particle size: 2-3 mm Adsorption conditions: 25 °C, pH=2; 200 rpm; 2 g L ⁻¹ of adsorbent; C _{pharm} =10-50 mg L ⁻¹	[238]
Peach stones	Chemical activation with 12 M H ₃ PO ₄ and carbonization at 400 °C (4 h) under air flow	1521	Ibuprofen Tetracycline	48 h 24 h	111 1106	Adsorbent particle size: 0.25-0.355 mm Adsorption conditions: 30 °C; 250 rpm; 0.3-20 g L ⁻¹ of adsorbent; C _{pharm} =100 mg L ⁻¹	[239]
Rice husk	Chemical activation with 12 M H ₃ PO ₄ and carbonization at 400 °C (4 h) under air flow	278	Ibuprofen Tetracycline	24 h 48-72 h	110 56000	Adsorbent particle size: 0.25-0.355 mm Adsorption conditions: 30 °C; 250 rpm; 0.3-20 g L ⁻¹ of adsorbent; C _{pharm} =100 mg L ⁻¹	[239]

Table 2.3 (continuation) - Alternative adsorbents for the removal of pharmaceuticals from water (S_{BET} -specific surface area; t_e -equilibrium time; q -adsorption capacity)

Precursor	Treatment	S_{BET} ($m^2 g^{-1}$)	Contaminant	t_e (min)	q ($mg g^{-1}$)	Conditions	Ref.
Potato peels	Hydrothermal treatment and chemical activation (2 M KOH)	-	Pramipexole Dorzolamide	-	66 60	AC oxidation with 70 % (v/v) HNO ₃ during 4 h at room temperature	[240]
	Chemical activation with 2 M KOH and pyrolysis at 600 °C (2 h) under N ₂ flow	-	Pramipexole Dorzolamide	-	56 52	Adsorption conditions: 25 °C; pH=2.0; 160 rpm; 1 g L ⁻¹ of adsorbent; C _{pharm} =0-200 mg L ⁻¹	
Olive stones	Physical activation using CO ₂ at 800 °C	1055	Ibuprofen Amoxicillin	250 2500	178 159	Particle size: 0.212-0.710 mm Adsorption conditions: 25 °C; pH=4.3; 100 rpm; 0.3 g L ⁻¹ of adsorbent; C _{pharm} =5-	[241]
	Physical activation using CO ₂ at 800 °C; wet oxidation	903	Ibuprofen Amoxicillin	600 250	160 128	100 mg L ⁻¹	
	Chemical activation with H ₃ PO ₄ (1:3)	1106	Ibuprofen Amoxicillin	750 1500	313 217		
Industrial wastes							
Bagasse fly ash	-	169	Malachite green	30-60	170	Particle size: < 0.85 mm Adsorption conditions: 30 °C, pH=7; 145 rpm; 1 g L ⁻¹ of adsorbent; C _{pharm} = 10-250 mg L ⁻¹	[229]
Biochar from fast pyrolysis of rice husk at 450-500 °C	-	34.4	Tetracycline	120 h	16.95	Adsorption conditions:30 °C; 5 g L ⁻¹ of adsorbent	[242]
	Washing with 10% H ₂ SO ₄ (v/v)	46.8		160 h	23.26		
	Washing with 3 M KOH	117.8		75 h	58.82		

Table 2.3 (continuation) - Alternative adsorbents for the removal of pharmaceuticals from water (S_{BET} -specific surface area; t_e -equilibrium time; q -adsorption capacity)

Precursor	Treatment	S_{BET} ($\text{m}^2 \text{g}^{-1}$)	Contaminant	t_e (min)	q (mg g^{-1})	Conditions	Ref.
Bottom ash from thermal power station	Treatment with H_2O_2	0.087	Malachite green	60-120	6.2	Particle size: < 0.08 mm Adsorption conditions: 50 °C, pH=5; 4 g L^{-1} of adsorbent; $C_{\text{pharm}} = 1.0 \times 10^{-5}$ - 1.0×10^{-4} M	[230]
De-oiled soya	Treatment with H_2O_2	-	Malachite green	120-180	12.9	Particle size: 0.3 mm Adsorption conditions: 50 °C, pH=5; 2 g L^{-1} of adsorbent; $C_{\text{pharm}} = 1.0 \times 10^{-5}$ - 1.0×10^{-4} M	[231]
Olive-waste cake	Chemical activation with H_3PO_4 and pyrolysis at 450 °C (2 h) under N_2 flow	793	Naproxen Ketoprofen Diclofenac Ibuprofen	5-24 h	39.5 24.7 56.2 12.6	Particle size: 0.10-0.16 mm Adsorption conditions: 25 °C, pH=4.1; 200 rpm; 0.3-1.5 g L^{-1} of adsorbent; $C_{\text{pharm}} = 19.78; 19.28; 14.80;$ 10.04 mg L^{-1} (respectively)	[243]
Spent tea leaves	Chemical activation with 4 % NaOH and pyrolysis at 450 °C (1 h) under N_2 flow	134	Malachite green	20	256	Particle size: < 0.21 mm Adsorption conditions: 45 °C, pH=10; 150 rpm; 0.8 g L^{-1} of adsorbent	[244]
Cork powder waste	Chemical activation with K_2CO_3 (1:1) and pyrolysis at 700 °C (1 h) under N_2 flow	891	Ibuprofen	60-120	145	Particle size: < 0.297 mm Adsorption conditions: 30 °C; 700 rpm; 0.67 g L^{-1} of adsorbent; $C_{\text{pharm}} = 20-120 \text{ mg L}^{-1}$	[232]
	Physical activation with steam using N_2 as carrier flow at 750 °C (1 h)	1060	Ibuprofen	60-120	378		

Table 2.3 (continuation) - Alternative adsorbents for the removal of pharmaceuticals from water (S_{BET} -specific surface area; t_e -equilibrium time; q -adsorption capacity)

Precursor	Treatment	S_{BET} ($\text{m}^2 \text{g}^{-1}$)	Contaminant	t_e (min)	q (mg g^{-1})	Conditions	Ref.
Primary paper mill sludge	Pyrolysis at 800 °C (10 min) under N ₂ flow	121	Citalopram	30-60	8.5	Powdered biochar Adsorption conditions: 25 °C, pH=9.5; 50 rpm; 0.1-2.5 g L ⁻¹ of adsorbent; C _{pharm} =5 mg L ⁻¹	[245]
			Fluoxetine	240	120	Powdered biochar Adsorption conditions: 25 °C, pH=9.5; 80 rpm; 0.025–0.900 g L ⁻¹ of adsorbent; C _{pharm} =10 mg L ⁻¹	[246]
	Pyrolysis at 800 °C (150 min) under N ₂ flow	209	Citalopram	10	19.6	Powdered biochar Adsorption conditions: 25 °C; 50 rpm; 0.1-2.5 g L ⁻¹ of adsorbent; C _{pharm} =5 mg L ⁻¹	[245]
			Diclofenac	100/100	23.4/26.7	Powdered biochar q : wastewater/ultrapure water Adsorption conditions: 25 °C, pH=7.6; 250 rpm; 0.1-2.5 g L ⁻¹ of adsorbent; C _{pharm} =100 mg L ⁻¹	[247]
			Salicylic acid	200/200	15.1/12.1		
			Ibuprofen	200/200	12.9/12.7		
			Acetaminophen	500/500	15.5/12.3		
			Carbamazepine	5	12.6	Powdered biochar Adsorption conditions: 25 °C, pH=10.5; 80 rpm; 0.02–0.12 g L ⁻¹ of adsorbent; C _{pharm} =5 mg L ⁻¹	[248]
			Oxazepam	5	7.8		
			Sulfamethoxazole	15-30	1.69		
Piroxicam	5	5.82					
Cetirizine	5	8.2					
Venlafaxine	15-30	8.5					
Paroxetine	5	38					

Table 2.3 (continuation) - Alternative adsorbents for the removal of pharmaceuticals from water (S_{BET} -specific surface area; t_e -equilibrium time; q -adsorption capacity)

Precursor	Treatment	S_{BET} ($m^2 g^{-1}$)	Contaminant	t_e (min)	q ($mg g^{-1}$)	Conditions	Ref.
Primary paper mill sludge	Chemical activation with KOH 1:1 (w/w)	115	Fluoxetine	120-240	192	Powdered activated carbon Adsorption conditions: 25 °C, pH=9.5; 80 rpm; 0.025–0.900 g L ⁻¹ of adsorbent; C _{pharm} =10 mg L ⁻¹	[246]
	Chemical activation with NaOH 1:1 (w/w)	60	Fluoxetine	240-360	137	Powdered activated carbon Adsorption conditions: 25 °C, pH=9.5; 80 rpm; 0.025–0.900 g L ⁻¹ of adsorbent; C _{pharm} =10 mg L ⁻¹	[246]
	Chemical activation with ZnCl ₂ 1:1 (w/w) and washing with 1 M HCl	592	Fluoxetine	360-480	29.8	Powdered activated carbon Adsorption conditions: 25 °C, pH=4; ; 80 rpm; 0.100–0.400 g L ⁻¹ of adsorbent; C _{pharm} =10 mg L ⁻¹	[246]
Biological paper mill sludge	Pyrolysis at 800 °C (10 min) under N ₂ flow	10.8	Citalopram	120	4	Particle size: 0.18-0.5 mm Adsorption conditions: 25 °C; 50 rpm; 0.5-50 g L ⁻¹ of adsorbent; C _{pharm} =5 mg L ⁻¹	[245]
Cow manure	Pyrolysis at 800 °C under N ₂ flow and washing with 3 M HCl	115	Sulfamethazine	8-12 h	142	Particle size: < 0.25 mm Adsorption conditions: 25 °C; pH= 3; 1 g L ⁻¹ of adsorbent; C _{pharm} =5-100 mg L ⁻¹	[249]

Recently, many authors have suggested the application of biochars for the remediation of organic and inorganic contaminants in water [242,250-259]. The International Biochar Initiative defines biochar as “*a solid material obtained from the thermochemical conversion of biomass in an oxygen-limited environment*” [260]. The thermochemical conversion processes used to produce biochars are slow pyrolysis, fast pyrolysis or gasification [260-263]. In the scheme from Figure 2.4 the conditions, products, yields and characteristics of biochars from these biomass thermochemical conversion processes are summarized. Slow pyrolysis produces biochar by heating biomass in the absence of oxygen (O_2) at moderate temperatures (350-800 °C), low heating rate ($\leq 10 \text{ }^\circ\text{C min}^{-1}$), and for a relatively long residence time, ranging from minutes to days. Slow pyrolysis maximizes biochar production and, due to increased burn off of fixed carbon mass during pyrolysis, the surface areas and pore volumes of biochar generally increase with increasing temperatures and residence times [261]. On the other hand, fast pyrolysis produces biochar also in the absence of O_2 but at high heating rates ($> 100 \text{ }^\circ\text{C min}^{-1}$), temperatures between 400 and 650 °C and short residence times ($< 2 \text{ s}$). The resulting biochar may be low in surface area and pore volume and, due to their short residence times, fast pyrolysis-biochars may retain more O-containing groups, such as phenolic, aromatic ether and carbonyl groups [261,264]. The main difference between these two pyrolysis processes are the yields of biochar and bio-oil, *i.e.*, fast pyrolysis favours high yield of bio-oil while slow pyrolysis favours high yield of biochar [261,263]. Gasification process, also known as a physical activation process, is typically used to increase the porosity and surface area of biochar. During gasification, biomass is combusted in the presence of oxygen at temperatures above 800 °C and residence times within seconds to hours [261]. The gasification atmosphere can be oxygen, air, steam or mixtures of these gases. Gasification-biochars, in most instances, have a higher S_{BET} than slow or fast pyrolysis-biochars and, therefore, gasification is applied after pyrolysis as a physical activation. However, depending on the feedstock, gasified biochars can exhibit significantly high mineral content, which is reflected in a high percentage of ash (up to 73%) [261,263]. The high ash content may limit the adsorption of organic compounds, so biochars must be de-ashed using acid/alkaline and/or water rinses prior to applying them in water treatment [265,266]. Table 2.3 shows some studies performed on the removal of pharmaceuticals using biochars as adsorbent. For example, Liu et al. (2012) [242] used biochar from fast pyrolysis of rice husk ($S_{BET}=34.4 \text{ m}^2 \text{ g}^{-1}$) to adsorb tetracycline from water and obtained an adsorption capacity of around 17 mg g^{-1} ; after washing with H_2SO_4 and KOH , S_{BET} increased to 46.8 and $117.8 \text{ m}^2 \text{ g}^{-1}$, respectively, increasing the adsorption capacities. Also, biochars produced by pyrolysis of primary and biological paper mill sludge were successfully applied to the removal of several classes of pharmaceuticals from water [245-248].

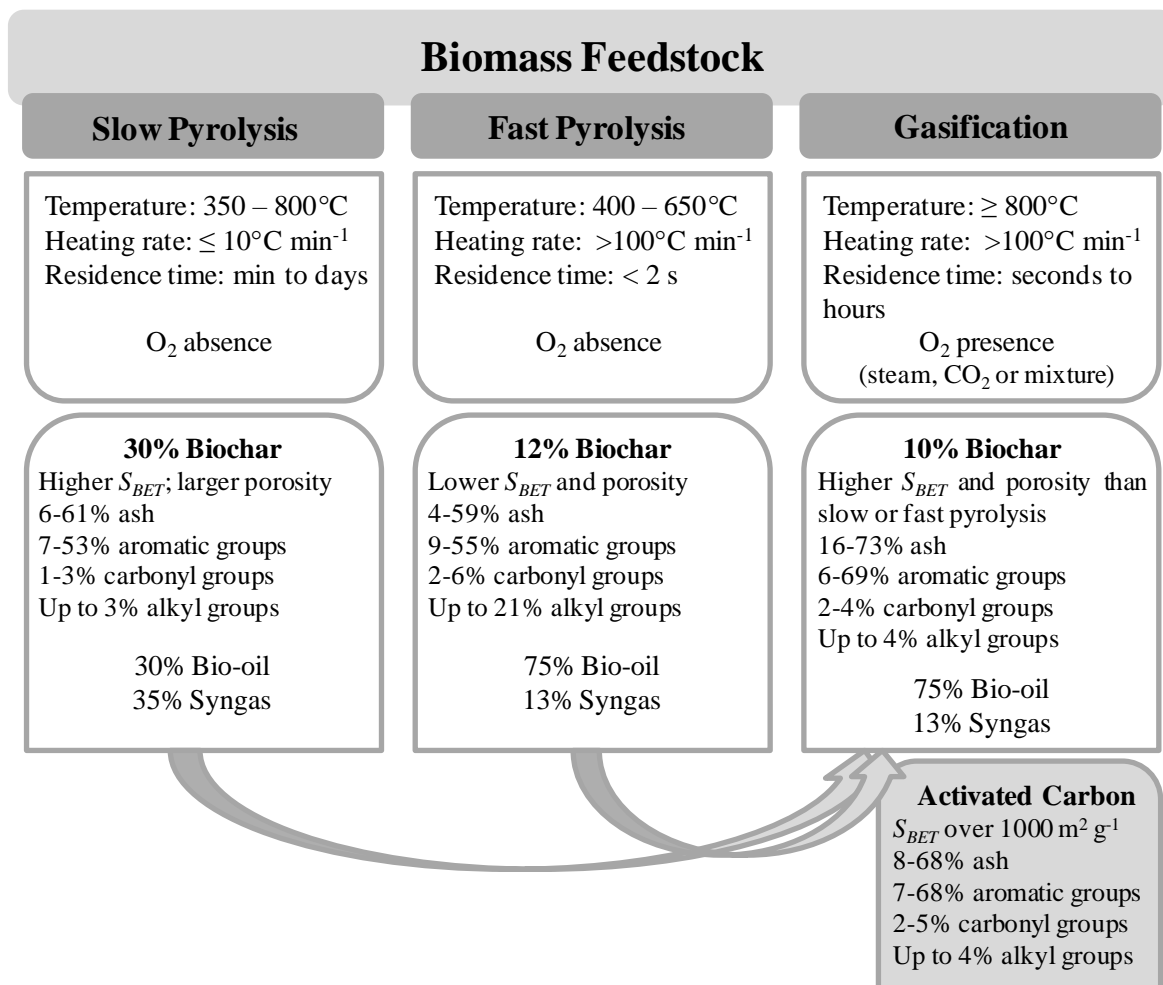


Figure 2.4 - Conditions, products, yields and properties of biochars resultant from biomass thermochemical conversion processes (adapted from Inyang et al. (2015) [262]).

2.4.3 Adsorption in batch system

Batch stirred tank reactors are usually applied for powdered adsorbents and are limited to the treatment of small volumes of effluent. In batch system, the adsorbent is in contact with the adsorbate solution until the equilibrium is reached and, after that, an additional separation step is necessary to remove the loaded adsorbent particles from the water [199,200]. Contrarily, the use of continuous reactors is favoured; it is more versatile and offers more advantages, as described in section 2.4.1; however, its design typically requires considerations about the adsorption kinetic and equilibrium. So, in any case, the study of a particular adsorption process requires the knowledge of adsorption kinetics and equilibrium data performed in batch system.

2.4.3.1 Adsorption kinetic

The kinetic study has the important practical meaning of determining the adsorption rate for a given adsorbent-adsorbate system. This is probably the most important factor in adsorption system design, as the adsorbate residence time and the reactor dimensions are controlled by the system kinetics [267]. Kinetics data are usually represented by plotting the concentration of solute in the aqueous phase, C (mg L^{-1}), or the adsorption capacity, q (mg g^{-1}), over time. The adsorption capacity, q , is the amount of solute adsorbed per gram of adsorbent (mg g^{-1}) and is determined according to Eq. 2.1:

$$q = \frac{(C_i - C)V}{m} \quad 2.1$$

where C_i (mg L^{-1}) is the initial concentration of the solute, V (L) is the volume of the solution and m (g) is the dry weight of adsorbent.

Different models are used to fit the kinetic curves in order to define the adsorption rate parameters and explain the mechanism of mass transfer. There are essentially two types of models that have been commonly used to represent the kinetics: the first corresponds to a diffusion-controlled process and the second assumes that adsorption is controlled by reaction in liquid/solid interface [268]. Lagergren (1898) [269] suggested the first-order equation for describing liquid-solid adsorption of oxalic acid and malonic acid onto charcoal. This is the earliest known model describing the adsorption rate based on the adsorption capacity; so, in order to distinguish a kinetic equation based on the adsorption capacity of a solid from the ones based on the concentration of a solution, Lagergren's first-order rate equation has been called pseudo-first order [270-272]. Nowadays, it is widely applied and it has been well suited for explaining adsorption kinetics of organic [273-275] and inorganic [276-278] pollutants from wastewaters. Lagergren's pseudo-first order kinetic can be given by:

$$q_t = q_e \left(1 - e^{-k_1 t}\right) \quad 2.2$$

where t (min) represents the contact time, q_e and q_t (mg g^{-1}) the adsorption capacity at equilibrium and at time t , respectively, and k_1 (min^{-1}) the pseudo-first order rate constant.

On the other hand, Ho (1995) [279] described a kinetic process of the adsorption of divalent metal ions onto peat and assumed that the adsorption might be second-order and the rate limiting step might be chemical adsorption, involving valence forces through sharing or exchanging of electrons. Similarly to Lagergren's expression, the second-order rate equation has been called pseudo-second order kinetic and it is also based on the adsorption capacity [280,281]. This equation has been successfully applied not only to adsorption of metal ions [282-285] but also

of organic substances, such as pharmaceuticals [286,287], dyes [288,289], pesticides [274,290] and oils [291,292] from aqueous solutions. The pseudo-second order kinetic model is represented as Eq. 2.3:

$$q_t = \frac{q_e^2 k_2 t}{1 + q_e k_2 t} \quad 2.3$$

with k_2 ($\text{g mg}^{-1} \text{min}^{-1}$) representing the pseudo-second order rate constant and the other variables are described as in Eq. 2.2.

Additionally, Wilczak et al. (1993) [293] applied a double-exponential function to correlate the two-step kinetics of the adsorption of lead and copper onto activated carbon: the first step of which corresponds to a rapid step involving external diffusion and the second to a slower step concerning intraparticle diffusion. Since then, this correlation, named double exponential model (DEM), has been applied with good agreement in the adsorption of other metal ions and organic pollutants from aqueous solution, and volatile organic compounds (VOCs) from gaseous phase [294]. DEM is described as follows [295]:

$$q_t = q_e - \frac{D_e}{M} e^{-k_e t} - \frac{D_i}{M} e^{-k_i t} \quad 2.4$$

where M represents the adsorbent amount in solution (g L^{-1}); D_e (mg L^{-1}) and k_e (min^{-1}) represent adsorption rate and diffusion rate parameters of the external diffusion step, respectively, and similarly D_i and k_i represent the parameters of the intraparticle diffusion step. Thus, the first derivative of the previous equation leads to Eq. 2.5, which allows the determination of the overall adsorption rate r ($\text{mg min}^{-1} \text{g}^{-1}$) at time t :

$$r = \frac{dq_t}{dt} = r_{e,t} + r_{i,t} = \frac{D_e}{M} k_e e^{-k_e t} + \frac{D_i}{M} k_i e^{-k_i t} \quad 2.5$$

where $r_{e,t}$ and $r_{i,t}$ ($\text{mg min}^{-1} \text{g}^{-1}$) are the external and intraparticle diffusion rates at time t , respectively. For the initial conditions, at $t = 0$:

$$r_{t=0} = r_{e,0} + r_{i,0} = \frac{D_e}{M} k_e + \frac{D_i}{M} k_i \quad 2.6$$

2.4.3.2 Equilibrium of adsorption

The equilibrium of adsorption is a dynamic balance between the concentration of adsorbate in the bulk solution and the adsorbate in the liquid-solid interface established after the necessary contact time between the adsorbate and the adsorbent [296]. This time is known as equilibrium time and is determined by the adsorption kinetics. The equilibrium data are obtained from adsorption isotherms which indicate the relation between the adsorption capacity (q_e , mg g^{-1}) and the solute concentration in the bulk phase (C_e , mg L^{-1}) in equilibrium, at constant temperature.

Isotherms are essentially used to evaluate the maximum capacity of the adsorbent to adsorb a particular molecule. This parameter is generally considered the most adequate tool to discriminate among different adsorbent materials and thereby to choose the most appropriate one for a particular application.

The most commonly applied adsorption isotherm models are the Langmuir, the Freundlich, the BET and the Dubinin equations. Langmuir and Freundlich isotherms are very important both for describing physisorption and chemisorption theories. The BET and Dubinin equations are more appropriate for analysis of the physical adsorption of gases and vapours on porous carbons [183].

Langmuir (1918) [297] developed the first theoretically adsorption isotherm model and its concept is the base for many other equations proposed later. This model is based on the following assumptions [297]:

- The adsorbed molecules of the adsorbate are attached to the surface at specific localized sites;
- Homogeneous monolayer adsorption, *i.e.*, each site accommodates only one adsorbed molecule;
- The energy state of each adsorbed molecule is the same at all sites on the surface independent of the presence or absence of other adsorbed molecules at neighbouring sites.

Langmuir model is given as follows in Eq. 2.7:

$$q_e = \frac{q_{max,L} K_L C_e}{1 + K_L C_e} \quad 2.7$$

where $q_{max,L}$ (mg g^{-1}) is the Langmuir maximum adsorption capacity and K_L (L mg^{-1}) the affinity coefficient of the Langmuir model.

The Freundlich isotherm is a limiting form of the Langmuir isotherm given that it is applicable only in the middle ranges of concentrations [183]. This empirical model describes the non-ideal and reversible adsorption, not restricted to the formation of a monolayer, and it is adequate to describe heterogeneous adsorption of the solute onto the adsorbent surface [298]. The Freundlich equation is presented in Eq. 2.8 [299]:

$$q_e = K_F C_e^{1/N_F} \quad 2.8$$

where K_F ($\text{mg g}^{-1} (\text{mg L}^{-1})^{-1/N_F}$) is the Freundlich adsorption constant and N_F is the Freundlich constant related with the degree of non-linearity of the equation (for $N_F < 1$, non-favourable adsorption; $N_F = 1$, linear adsorption; $N_F > 1$, favourable adsorption).

Sips (1948) [300] suggested a combined form of Langmuir and Freundlich expressions for predicting the heterogeneous adsorption systems and in order to circumvent the limitations associated with Freundlich isotherm model [300,301]. Thus, at low solute concentrations, it reduces to Freundlich isotherm; at high concentrations, it predicts a monolayer adsorption capacity characteristic of the Langmuir isotherm [298]. Sips model, also known as Langmuir-Freundlich model, is presented in Eq. 2.9:

$$q_e = \frac{q_{\max,LF} K_{LF} C_e^{1/N_{LF}}}{1 + K_{LF} C_e^{1/N_{LF}}} \quad 2.9$$

with $q_{\max,LF}$ (mg g^{-1}) representing the Langmuir-Freundlich maximum adsorption capacity, K_{LF} ($\text{mg g}^{-1} (\text{mg L}^{-1})^{-1/N_{LF}}$) the affinity coefficient of Langmuir-Freundlich model and N_{LF} the degree of non-linearity.

2.4.3.3 Thermodynamics of adsorption

Adsorption is a spontaneous process and thus it is accompanied by a decrease in the free energy of the system which results in a decrease in entropy during adsorption. Eq. 2.10 correlates the Gibbs energy, ΔG° (kJ mol^{-1}), enthalpy, ΔH° (kJ mol^{-1}), and the entropy, ΔS° ($\text{kJ mol}^{-1} \text{K}^{-1}$), of adsorption at constant temperature, T (K):

$$\Delta G^\circ = \Delta H^\circ - T\Delta S^\circ \quad 2.10$$

The enthalpy, or heat of adsorption, is generally negative indicating that adsorption is an exothermic process, according to the nature of the forces involved. However, a few adsorption cases have been reported to be endothermic, consequence of an increase in the entropy of the adsorbate due to the dissociation of the molecule during the adsorption process or to an increase in the entropy of the adsorbent [183].

The Gibbs energy of adsorption is related to the equilibrium constant (K_L from Langmuir isotherm model) by the classic Van't Hoff equation:

$$\Delta G^\circ = -RT \ln K_L \quad 2.11$$

Combining Eq. 2.10 and 2.11, this equation can be rewritten:

$$\ln K_L = \frac{-\Delta G^\circ}{RT} = \frac{\Delta S^\circ}{R} - \frac{\Delta H^\circ}{RT} \quad 2.12$$

where R is the universal gas constant ($8.314 \text{ J mol}^{-1} \text{K}^{-1}$). Thus, ΔS° and ΔH° can be obtained from the intercept and from the slope of the linear Van't Hoff plot, respectively, *i.e.*, plotting $\ln K_L$ as a function of $\frac{1}{T}$.

2.4.4 Adsorption in continuous system – Fixed-bed columns

Fixed-bed adsorption process using GAC is commonly applied in WWTPs as tertiary treatment. Adsorption in fixed-bed columns is a time and distance-dependent process, in which each adsorbent particle in the bed accumulates the adsorbate molecules from the percolating solution as long as the state of equilibrium is reached. This equilibration process proceeds successively, layer by layer, from the column inlet to outlet; so, the equilibrium takes place in a more or less broad zone of the adsorbent bed, referred as the mass transfer zone (MTZ). As it is shown in Figure 2.5, at a given time, t , a distinction can be made between three different zones within the adsorbent bed.

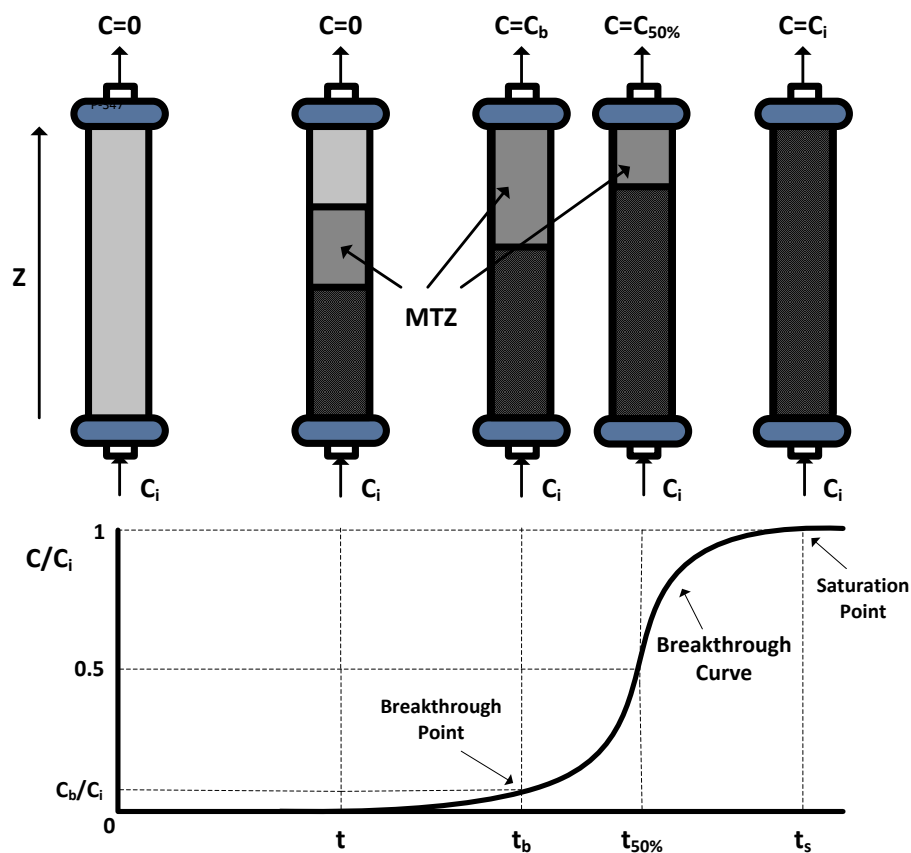


Figure 2.5 - Concentration profile during single-solute adsorption in a fixed-bed column.

In the first zone, between the column inlet and the MTZ, the adsorbent is already loaded; so, in this zone the maximum adsorption capacity was already attained and no more mass transfer from aqueous phase to the adsorbent particles takes place. Therefore, the effluent concentration (concentration of solute in the aqueous phase, C) of this first zone is constant and equals the inlet solute concentration, C_i . In the MTZ, the mass transfer from the aqueous phase to the adsorbent takes place, *i.e.*, adsorption occurs and the solute concentration in this zone decreases from $C=C_i$ to

$C=0$ and, consequently, the adsorbed amount increases. At last, in the third zone, the adsorbent is still free of adsorbate and the solute concentration in aqueous phase is $C=0$. During the adsorption process, the MTZ passes through the column with a velocity that is much slower than the water velocity. The higher the difference between the MTZ velocity and the water velocity, more effective is the adsorption, and MTZ takes longer to reach the column outlet. When the entire MTZ has passed through the column, it “breaks through”, *i.e.*, the effluent concentration equals the influent concentration, $C=C_i=C_s$, which means that the fixed-bed attained its saturation. The related time is referred to as saturation time, t_s . The shape and length of the MTZ depend on the adsorption rate, the shape of the adsorption isotherm (equilibrium curve) and the diffusion characteristics. The shape of the MTZ must be determined experimentally by means of breakthrough curve design (Figure 2.5). The curve front may change shape as it moves through the bed, and the MTZ may broaden or shorten. For example, unfavourable and linear isotherms tend to broaden (less steep breakthrough curve); while favourable Langmuir and Freundlich isotherms may broaden at first, but quickly achieve a constant pattern front, an asymptotic shape [200]. From a practical point of view, when the effluent concentration reaches the maximum acceptable emission limit, adsorption must be stopped and the adsorbent should be replaced or regenerated. This point is named breakthrough point and allows determining the time of the process (t_b) and, essentially, the volume of treated effluent (V_b). In the particular case of wastewater treatment, this point is settled according to the target quality of the final effluent [191,198].

Fixed-bed columns can be operated as single or multiple units, in series or parallel; however, each bed can be replaced as a complete, separate unit. A single-column system could be considered when: (i) the breakthrough curves are steep; (ii) the adsorbent will last so long at the desired processing conditions that the cost of replacing or regenerating it represents only a minor part of the operating costs; (iii) the capital cost of additional columns cannot be justified because savings in the adsorbent cost in a multiple column system are not enough to pay for the additional equipment needed [198,199]. Also, the fixed-bed columns can operate by upflow or downflow: in upflow operation, special pipes and pumps are required, while downflow system could have gravity feed, however, pumps could also be required to handle a significant pressure drop [198, 199].

2.4.4.1 Fixed-bed column modelling

In order to evaluate the continuous adsorption of a particular adsorbate in a packed column under different operating conditions, breakthrough curves are obtained by expressing C/C_i as a function of operation time (t , in min) or volume (V , in mL), as represented in Figure 2.5. Breakthrough curves allow the assessment of important parameters of fixed-bed adsorption, including the adsorbent usage, volume of solution treated and also the bed capacity. This last

parameter is the mass of solute adsorbed by the adsorbent at time t , q_t (mg g^{-1}), and it can be calculated using the following expression:

$$q_t = \frac{Q}{1000} \frac{C_i A_a}{m} = \frac{Q}{1000} \frac{C_i}{m} \int_{t=0}^{t=t} \left(1 - \frac{C}{C_i}\right) dt \quad 2.13$$

Thus, the total bed capacity, q_s , is determined at saturation time, t_s :

$$q_s = \frac{Q}{1000} \frac{C_i}{m} \int_{t=0}^{t=t_s} \left(1 - \frac{C}{C_i}\right) dt \quad 2.14$$

where Q (mL min^{-1}) is the flow rate and A_a (min) is the area above the breakthrough curve.

To model a liquid-solid dynamic column adsorption, it is necessary to take into account four basic steps:

1. adsorption/desorption reaction;
2. intraparticle mass transfer involving pore diffusion and surface diffusion;
3. liquid phase mass transfer including convective mass transfer and molecular diffusion;
4. interface diffusion between liquid phase and the exterior surface of the adsorbent – film diffusion.

Taking into consideration a differential volume element, $dV = A_R dz$, of a fixed-bed column with the cross-sectional area A_R , to establish a differential material balance it is assumed that the amount of adsorbate that is adsorbed onto the adsorbent ($\dot{N}_{adsorption}$, $\text{mg L}^{-1} \text{min}^{-1}$) or accumulated in the void fraction of the volume element ($\dot{N}_{accumulation}$, $\text{mg L}^{-1} \text{min}^{-1}$) must be equal to the difference between the input and the output of the volume element (Figure 2.6). Input and output occur by axial dispersion ($\dot{N}_{dispersion}$, $\text{mg L}^{-1} \text{min}^{-1}$) and advection ($\dot{N}_{advection}$, $\text{mg L}^{-1} \text{min}^{-1}$) [200].

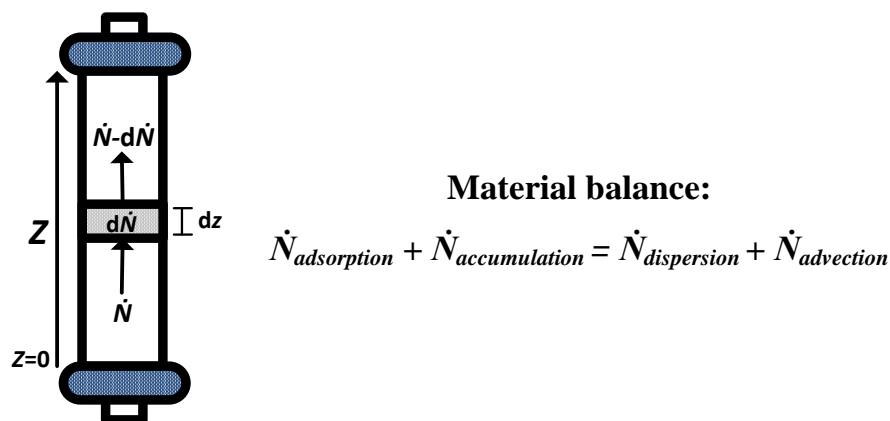


Figure 2.6 - Material balance around a differential volume element of a fixed-bed column.

So, the overall mass balance for liquid-solid column adsorption is given by [187,200,302,303]:

$$\rho_b \frac{\partial q}{\partial t} + \varepsilon \frac{\partial C}{\partial t} = D_z \frac{\partial^2 C}{\partial z^2} - v \frac{\partial C}{\partial z} \quad 2.15$$

where ρ_b (g cm^{-3}) the bed density; ε the bed porosity; D_z ($\text{cm}^2 \text{min}^{-1}$) the axial dispersion coefficient; v (cm min^{-1}) is the fluid velocity in the empty column and z (cm) the axial coordinate. The first two terms of the Eq. 2.15 correspond to the change of the amount of adsorbate with time during adsorption and accumulation, respectively; the third term represents the difference on the amount of adsorbate between input and output caused by axial dispersion and the last one corresponds to the difference on the amount of adsorbate between input and output caused by advection (Figure 2.6). In many cases, the axial dispersion is ignored and Eq. 2.15 would be reduced to [303]:

$$v \frac{\partial C}{\partial z} + \rho_b \frac{\partial q}{\partial t} + \varepsilon \frac{\partial C}{\partial t} = 0 \quad 2.16$$

The last two equations are based on the following assumptions:

- the system is in a steady state, *i.e.*, the influent concentration is constant;
- the radial dispersion is negligible;
- the process is isothermal;
- the column is packed with spherical particles;
- the flow rate is constant (plug-flow model).

Based on the overall mass balance, several simple mathematical models have been proposed to predict the dynamic behaviour of fixed-bed columns and estimate the kinetic coefficients. The most used models were developed by Thomas [304], Clark [305], Yoon-Nelson [306] and Dose-Response [307]. A short description of each model is presented below.

Thomas Model

Thomas model [304] is one of the most generally used in column performance theory, based on the assumption of adsorption-desorption with extremely small external and internal diffusion resistances and following the second-order reversible reaction kinetic and the Langmuir isotherm. The total adsorption capacity of the adsorbent, q_{Th} (mg g^{-1}), and the adsorption rate constant, k_{Th} ($\text{mL min}^{-1} \text{mg}^{-1}$), could be calculated by fitting this model, as follows:

$$\frac{C}{C_i} = \frac{1}{1 + e^{\left(\frac{k_{Th}}{Q}\right)(m q_{Th} - C_i V)}} = \frac{1}{1 + e^{\left(\frac{k_{Th} m q_{Th}}{Q} - k_{Th} C_i t\right)}} \quad 2.17$$

Clark Model

Clark (1987) [305] developed a model to predict the performance of a fixed-bed column packed with GAC to adsorb organic compounds. This model presupposes that length of the MTZ is constant; all the adsorbate molecules are removed at the end of the column, and that the adsorbate-adsorbent system obeys to the Freundlich isotherm. So, Clark model correlates the mass-transfer rate with the Freundlich isotherm as follows:

$$\frac{C}{C_i} = \frac{1}{1 + Ae^{-k_c t}} \quad \text{with} \quad A = \left(\frac{C_i^{N_F-1}}{C_b^{N_F-1}} - 1 \right) e^{k_c t_b} \quad 2.18$$

where N_F is the Freundlich constant predicted by Freundlich isotherm model and k_C (min^{-1}) is the adsorption rate constant.

Yoon-Nelson Model

Yoon-Nelson model [306] is based on the assumption that the rate of the decrease in the probability of adsorption for each solute molecule is proportional to the probability of solute adsorption and the probability of solute breakthrough on the adsorbent. Eq. 2.19 represents this model:

$$\frac{C}{C_i} = \frac{e^{(k_{YN}t - k_{YN}t_{50\%})}}{1 + e^{(k_{YN}t - k_{YN}t_{50\%})}} \quad 2.19$$

where k_{YN} (min^{-1}) is the adsorption rate constant and $t_{50\%}$ (min) the time required for retaining 50 % of the initial solute concentration ($C/C_i=0.5$).

Dose-Response Model

The Dose-Response model [307], commonly used in pharmacology to describe different types of processes, is currently being applied to describe fixed-bed biosorption. This model basically diminishes the error resulting from the use of the Thomas model, particularly at the lowest and highest times of the breakthrough curve. The mathematical expression of the model is represented as:

$$\frac{C}{C_i} = \frac{C_s}{C_i} - \frac{\frac{C_s}{C_i}}{1 + \left(\frac{v}{v_{50\%}}\right)^\alpha} = \frac{C_s}{C_i} - \frac{\frac{C_s}{C_i}}{1 + \left(\frac{t}{t_{50\%}}\right)^\alpha} \quad 2.20$$

where C_s is the solute concentration at t_s and α is the constant of the Dose-Response model.

2.4.4.2 Scale-up of fixed-bed columns

The scale-up of fixed-bed columns requires the determination of breakthrough curves in laboratory-scale as basis for the prediction of the breakthrough behaviour in full-scale columns. In this context, the bed depth service time (BDST) model is extensively used by the water industry and can be applied to other industrial situations [308]. The BDST model [309], assumes that the adsorption rate is controlled by the surface reaction between the solute and the void spaces of the adsorbent and establishes a relationship between the bed depth, Z (cm), and the operation time, t , according to:

$$t = \frac{N_0}{C_i v} Z - \frac{1}{k_{BDST} C_i} \ln \left(\frac{C_i}{C} - 1 \right) \quad 2.21$$

where N_0 (mg L^{-1}) is the dynamic bed adsorption capacity; v (cm min^{-1}) is the linear fluid velocity, which is defined as the ratio between the volumetric flow, Q_v ($\text{cm}^3 \text{min}^{-1}$), and the cross-sectional area of the bed, A_R (cm^2); and k_{BDST} ($\text{L mg}^{-1} \text{min}^{-1}$) is the adsorption rate constant. N_0 and k_{BDST} can be determined from the slope and intercept of the plot of t vs. Z . A simplified form of the BDST model is expressed by Eq. 2.22:

$$t = aZ - b \quad 2.22$$

$$\text{with: } a = \frac{N_0}{C_i v} \quad 2.23$$

$$\text{and } b = \frac{1}{k_{BDST} C_i} \ln \left(\frac{C_i}{C} - 1 \right) \quad 2.24$$

By varying the column bed depth (Z), a and b have the same values; however, applying Eq. 2.21, a new operation time is obtained. If there is a change in the initial solute concentration C_i to a new value C_i' , the new values of a and b can be, respectively, obtained from the slope and the intercept according to the relations proposed by Hutchins (1973) [309]:

$$a' = a \frac{C_i}{C_i'} \quad 2.25$$

$$b' = b \frac{C_i}{C_i'} \frac{\ln \left(\frac{C_i'}{C} - 1 \right)}{\ln \left(\frac{C_i}{C} - 1 \right)} \quad 2.26$$

Also, when the linear flow rate is changed from v to v' , the new value of the slope (a) is obtained by:

$$a' = a \frac{v}{v'} \quad 2.27$$

However, the intercept (b) remains unchanged because it depends on the inlet solute concentration C_i .

2.4.5 Adsorbent regeneration

During the adsorption process, the adsorbent material becomes progressively saturated and, once it is completely exhausted, the adsorbent must be replaced by a new one or regenerated. When it is replaced, the saturated adsorbent is commonly incinerated or disposed in landfills, but these operations entail important environmental and economic inconveniences. Alternatively, the saturated materials can be reused after an appropriate regeneration step. For example, in the case of activated carbons, regeneration is preferred due to their high production cost. The main goal of regeneration is to remove the adsorbed molecules and recover the original adsorption capacity of the adsorbent without modifying its porosity or causing adsorbent mass losses [310,311]. Moreover, adsorbent regeneration process is not only important from the viewpoint of restoring their adsorption capacity, but also because in many cases the recovery of the adsorbate is important [191]. By this way, regeneration can result in valuable products, avoiding the contamination that the disposal of saturated adsorbent would cause. So, the technological and economic viability of an adsorbent also depends on its regeneration and reuse potential for many cycles of operation [192].

The ideal regeneration process involves the desorption of the pollutant's molecules concentrated in the adsorbent without any modification of its initial textural properties. So, regeneration of an adsorbent is based on the principle that the adsorbent is a stable material that can withstand changes in temperature and it is resistant to acidic and basic media. That's why the regeneration is normally carried out only on granular adsorbents [191]. Common regeneration techniques of GAC beds in industrial applications are based on thermal (CO₂, steam and/or inert atmosphere) and chemical methods (pH-switch or extraction with solvents) [310,312-314]. Alternatively to these conventional techniques, several other regeneration processes have been reported in the past few decades, such as biological regeneration [315,316], electrochemical regeneration [317,318], extraction with supercritical fluids [319,320] and microwave-assisted regeneration [321,322], applied to adsorbents loaded with organic contaminants. However, these last techniques have showed some disadvantages and limitations. For example, many studies described lower efficiencies and longer times of recovery using biological regeneration of activated carbons saturated with organic adsorbates when compared with conventional methods [315,323]. Narbaitz et al. (2012) [317] reported that the electrochemical regeneration efficiency is not as high as that of the thermal regeneration and that it is unable to treat large amounts of saturated adsorbent, *i.e.*, the direct contact between the adsorbent particles and the electrodes is essential and, for that, the bed depth must be limited. On the other hand, Charinpanitkul et al. (2011) [324] observed that supercritical water oxidation regeneration of activated carbons saturated with pyridine or phenol increased the regeneration efficiency but oppositely decreased the yield of AC

remaining after regeneration. Çalışkan et al. (2012) [325] also observed that microwave-assisted regeneration did not lead to better results than those obtained under conventional electric heating in the regeneration of activated carbon saturated with the pharmaceutical promethazine. In this section, the most common regeneration techniques, thermal and chemical, applied to adsorbents loaded with organic compounds, are detailed.

2.4.5.1 Thermal regeneration

Due to the simplicity and high efficiency, thermal regeneration is the most widely used regeneration method and consists of heating the exhausted adsorbent, in an inert and/or oxidizing atmosphere, which results in the destruction of the retained adsorbate. Thermal regeneration generally follows three processing steps: (1) drying at around 105 °C, (2) pyrolysis under inert atmosphere and (3) gasification of residual organics by an oxidizing gas [326,327]. The pyrolytic step (2) usually occurs at relatively low temperatures (up to 800 °C) and aims at the desorption of the volatile compounds adsorbed in the adsorbent pores, including residual moisture and the thermal decomposition of other less-volatile compounds. If the adsorbate molecules are not desorbed in their original form, they could be decomposed on the adsorbent surface via thermal cracking. In this case, the charred residue could be stored in the adsorbent pores and becomes part of its structure. The amount of residue depends on the nature of the adsorbate [327]. The oxidative step (3) involves the controlled gasification of the pyrolysed carbon at temperatures ≥ 800 °C, in the presence of a mildly oxidizing atmosphere, such as steam, CO₂ or a mixture of both. In this step, the oxidizing agent at high temperature reacts with the residual carbonated compounds resulting in their degradation. This last step of the regeneration is also called reactivation of the adsorbent. After this process, it is expected that the adsorbents restore the original structure and adsorption capacity [310,327]. If the S_{BET} is larger after regeneration, it means that a proper reactivation has taken place, consequently reducing the bulk density [191]. The oxidative stage on the thermal regeneration process is an essential step in the industrial reactivation of commercial activated carbons, obtaining more than 97% of regeneration efficiency [328,329].

Despite the high efficiency of thermal regeneration, it also has a number of disadvantages: in many cases, the exhausted adsorbent has to be handled and transported to a regeneration centre (*ex situ* operation) and transported back to the in-process plant; it may introduce changes in the adsorbent properties; significant weight losses of the adsorbent by attrition and/or burnoff might occur (10-20% by weight); and high energy costs are required to achieve the regeneration temperature [313]. These problems could have a cumulative high impact especially when the number of regeneration cycles increase.

2.4.5.2 Chemical regeneration

Chemical regeneration is another widely studied and applied regeneration technique. It consists of the desorption of adsorbed molecules by elution, using small volume of a solvent or a solution that modifies the adsorption equilibrium and with high affinity for the adsorbate(s) (*e.g.*, HCl, NaOH or surfactants). In both cases, desorption or extraction of adsorbate molecules is a simple and inexpensive method and, contrarily to thermal regeneration, it could be performed by passing the eluent solution through the adsorbent bed (*in situ* operation) and the adsorbent loss is smaller than in thermal regenerative processes [330]. Several solvents have been tested in the regeneration of activated carbons exhausted with organic compounds. Cooney et al. (1983) [331] studied the desorption of phenol from activated carbon using nineteen solvents in batch tests and found three of the best solvents (acetone, dimethylformamide and methanol) which also possessed complete miscibility with water. The authors also tested regeneration in continuous mode and restored 88% of the fixed-bed capacity (7.5 g of granulated activated carbon) for phenol using 300 mL of methanol. Martin et al. (1984, 1985) [332, 333] tested a wide range of organic and inorganic solvents as regeneration agents of activated carbon exhausted with 5 organic compounds (2-naphthol, 2-methoxyphenol, 2-chlorophenol, o-cresol and 2-nitrophenol). The authors observed that there is a correlation between decreasing molecular weight of adsorbate and decreasing value of regeneration efficiency, *i.e.*, the smaller the adsorbate, the deeper it could penetrate into the micropores of the carbon, resisting to the regeneration process. In this sense, they reported that the regeneration agent should be smaller than the smallest adsorbate, in order to penetrate into the micropores of the carbon and displace the adsorbate. Besides the interesting conclusions, the regeneration efficiencies did not exceed 84%. Although the use of solvents as regeneration agent is more advantageous than thermal regeneration in some aspects (mainly, there is no mass loss, no damage to the porous structure and adsorbates are easily recovered), it has disadvantages: organic solvents are expensive, are pollutants and usually highly toxic and, thus, chemical regeneration is not considered an environmentally friendly method [311]. In order to reuse the solvent, a more expensive purification step has to be performed. So, this kind of regeneration is recommended only when the adsorbate is a high-value product [313].

Alternatively, surfactant solutions, such as di-octyl sodium sulfosuccinate, sodium dodecyl sulfate, cetyltrimethyl ammonium bromide and dodecylbenzenesulfonic acid have also been tested as regeneration agents. Those agents contain micelles that enhance the dissolution of organic compounds, as congo red dye, phenol or aniline [330,334,335]. However, in all these cited studies, the regeneration efficiencies did not exceed 65%. On the other hand, it has been proved that, depending on the properties of the adsorbate, regeneration can effectively occur through a pH change in the medium containing the adsorbent. Activated carbons exhausted with certain

adsorbates can be regenerated by NaOH solutions. The removal of species that react with NaOH depends on the products of the reactions: for example, adsorbates that produce soluble salts are easily removable (such as phenol or benzoic acid) and result in higher regeneration efficiency than those that after adsorption generate stable compounds not degradable by chemical reaction (such as benzaldehyde) [332,333]. On the other hand, there are adsorbates that do not react with NaOH (such as aniline, benzyl alcohol or dyes) but they are removed when the pH of the adsorbent surface changes [336]. In case of activated carbons that are negatively charged due to the high pH of the medium, the intensification of repulsive forces between anionic molecules adsorbed and the carbon surface breaks the adsorbent-adsorbate bonds [311]. NaOH concentration and NaOH solution volume-adsorbent mass ratio are the most important parameters, *i.e.*, in general, the increase of these parameters facilitates the regeneration [337,338]. Nevertheless, a very high NaOH concentration can cause the retention of OH⁻ groups on the active sites and hinders the subsequent adsorption step [332]; so, NaOH regeneration step must be followed by a washing treatment to remove remaining OH⁻ groups. This pH-switch method is an attractive alternative to other thermal and chemical regenerations because it employs mild regeneration conditions and does not use expensive chemical reagents; however, the regeneration efficiencies are generally lower than 80% [311,336,339].

2.5 Conclusions

The necessity of food production, namely in the aquaculture industry, urges with the significant increase of the world population since the 20th century. The implementation of intensive aquaculture systems has contributed to this impressive development; however, the intensive aquaculture practice also imposes high risks on the welfare of fish, making them vulnerable to adverse impacts from disease and environmental conditions. For disease control and also to control growth, reproduction and stress, therapeutants are usually administered to farmed fish in intensive systems. Anaesthetics are used to control stress during handling and confinement operations and the most worldwide used are tricaine methanesulfonate, benzocaine and 2-phenoxyethanol. These drugs are considered of low oral acute toxicity but fish are not recommended to be taken for human consumption during or immediately after treatment and, thus, it is necessary to strictly observe safety regulations. Moreover, taking into account their toxicological effects at long-exposure, for both fish and human, it is important to ensure the water quality for recycling and/or for discharge in the environment.

The typical recirculating aquaculture system (RAS) was initially designed to remove suspended solids and to control dissolved organic carbon and ammonia levels which are efficiently

removed by mechanical and biological filtration. However, these filters are not designed to remove organic therapeutants, such as the anaesthetic's class; so, water treatment processes should be implemented in order to prevent the release of these pollutants in the environment. The adsorption process using activated carbons is a well-established technology for the removal of organic contaminants from water and wastewater systems with high efficiencies and easy implementation. In aquaculture facilities, activated carbon filters have been incorporated only as an auxiliary filter to support biofiltration in RASs, since this form of filtration requires large amount of activated carbon which is expensive. In this context, several studies have been performed in order to find alternative low-cost adsorbents to be applied in the treatment of waters contaminated with organic pollutants. The use of agricultural and industrial residues or by-products, with low or null economic value, as adsorbent or as precursor for the production of adsorbents has been an attractive alternative. The principal approaches include the use of these residues as natural adsorbents (without chemical or physical treatment or activation), as precursors to produce new activated carbons, or using simple methods to produce new adsorbents (mostly by thermochemical conversion processes, such as pyrolysis and/or gasification). The physical and chemical properties of the adsorbent play an important role in the adsorption process: the porous structure and specific surface area determine the adsorption capacity and, thus, micropores and mesopores are especially important in this context; the chemical structure influences the interaction with the adsorbates (polar or nonpolar) and the active sites. In order to assess the performance of an adsorbent to the target adsorbate, adsorption experiments in batch mode should be performed. Adsorption kinetic tests determine the rate at which adsorption takes place for a given adsorbent-adsorbate system, while adsorption equilibrium tests evaluate the maximum capacity of the adsorbent to adsorb a particular molecule. This parameter is generally considered the most adequate tool to discriminate among different adsorbent materials and thereby to choose the most appropriate one for a particular application. Within the continuous adsorption processes, fixed-bed adsorption columns packed with GAC are the most used in WWTPs as tertiary treatment. Fixed-bed adsorption columns have several advantages when compared with the continuous stirred tank reactors using PAC: no additional loaded-adsorbent separation step is necessary and the adsorbent consumption is lower in comparison to stirred tank reactors; moreover, contrarily to PAC which cannot be efficiently regenerated, GAC can be regenerated or reactivated and used repeatedly. So, the technological and economic viability of an adsorbent also depends on its regeneration and reuse potential for many cycles of operation.

2.6 References

- [1] FAO, <http://www.fao.org/fishery/cwp/handbook/j/en>, last accessed in August 2016.
- [2] Landau, M., 1992, Introduction to Aquaculture, *John Wiley & Sons*, New York, USA.
- [3] FAO, 2016, The State of World Fisheries and Aquaculture, *Food and Agriculture Organization of the United Nation*; Fisheries Department; Rome.
- [4] Sapkota, A., Sapkota, A.R., Kucharski, M., Burke, J., McKenzie, S., Walker, P. and Lawrence, R., 2008, *Environment International*, 34 (8), 1215-1226.
- [5] FAO, 2014, The State of World Fisheries and Aquaculture, *Food and Agriculture Organization of the United Nation*; Fisheries Department; Rome.
- [6] EC, http://ec.europa.eu/fisheries/cfp/aquaculture/aquaculture_methods/index_en.htm, last accessed in July 2016.
- [7] FAO, <http://www.fao.org/fishery/technology/aquaculture/en>, last accessed in July 2016.
- [8] Shao, Z.J., 2001, *Advanced Drug Delivery Reviews*, 50 (3), 229-243.
- [9] Harikrishnan, R., Balasundaram, C. and Heo, M.-S., 2011, *Aquaculture*, 320 (1–2), 1-21.
- [10] Burridge, L., Weis, J.S., Cabello, F., Pizarro, J. and Bostick, K., 2010, *Aquaculture*, 306 (1–4), 7-23.
- [11] Defoirdt, T., Sorgeloos, P. and Bossier, P., 2011, *Current Opinion in Microbiology*, 14 (3), 251-258.
- [12] Read, P. and Fernandes, T., 2003, *Aquaculture*, 226 (1–4), 139-163.
- [13] Boxall, A.B.A., Kolpin, D.W., Halling-Sørensen, B. and Tolls, J., 2003, *Environmental Science & Technology*, 37 (15), 286A-294A.
- [14] Boxall, A.B.A., Fogg, L.A., Blackwell, P.A., Blackwell, P., Kay, P., Pemberton, E.J. and Croxford, A., 2004, Reviews of Environmental Contamination and Toxicology, Springer New York, USA, 1-91.
- [15] Bártíková, H., Podlipná, R. and Skálová, L., 2016, *Chemosphere*, 144, 2290-2301.
- [16] Kołodziejska, M., Maszkowska, J., Białk-Bielińska, A., Steudte, S., Kumirska, J., Stepnowski, P. and Stolte, S., 2013, *Chemosphere*, 92 (9), 1253-1259.
- [17] Ashley, P.J., 2007, *Applied Animal Behaviour Science*, 104 (3–4), 199-235.
- [18] Zahl, I., Samuelsen, O. and Kiessling, A., 2012, *Fish Physiology and Biochemistry*, 38 (1), 201-218.
- [19] Stoskopf, M. and Posner, L.P., 2008, Anesthesia and Analgesia in Laboratory Animals, 2nd ed., Academic Press, San Diego, 519-534.
- [20] Ross, L.G. and Ross, B., 2008, Anaesthetic and Sedative Techniques for Aquatic Animals, *Blackwell Publishing Ltd*, Oxford, UK.
- [21] FDA, 2011, Fish and Fishery Products Hazards and Controls Guidance, *U.S. Department of Health and Human Services; Food and Drug Administration; Center for Food Safety and Applied Nutrition*.
- [22] EFSA, 2008, *European Food Safety Authority Journal*, 844, 1-21.
- [23] EC, 2009, Pharmacologically active substances and their classification regarding maximum residue limits in foodstuffs of animal origin, *Commission Regulation (EU) No 37/2010*.
- [24] Wei, R., Ge, F., Zhang, L., Hou, X., Cao, Y., Gong, L., Chen, M., Wang, R. and Bao, E., 2016, *Chemosphere*, 144, 2377-2383.
- [25] EAHC, 2013, Study on the environmental risks of medicinal products, *Final Report prepared for Executive Agency for Health and Consumers*.
- [26] Jelic, A., Gros, M., Ginebreda, A., Cespedes-Sánchez, R., Ventura, F., Petrovic, M. and Barcelo, D., 2011, *Water Research*, 45 (3), 1165-1176.
- [27] Kümmerer, K., 2010, *Annual Review of Environment and Resources*, 35 (1), 57-75.
- [28] Tolls, J., 2001, *Environmental Science & Technology*, 35 (17), 3397-3406.
- [29] Grigorakis, K. and Rigos, G., 2011, *Chemosphere*, 85 (6), 899-919.
- [30] Pereira, A.M.P.T., Silva, L.J.G., Meisel, L.M. and Pena, A., 2015, *Journal of Toxicology and Environmental Health, Part A*, 78 (15), 959-975.

- [31] Terzić, S., Senta, I., Ahel, M., Gros, M., Petrović, M., Barcelo, D., Müller, J., Knepper, T., Martí, I., Ventura, F., Jovančić, P. and Jabučar, D., 2008, *Science of The Total Environment*, 399 (1–3), 66-77.
- [32] Lalumera, G.M., Calamari, D., Galli, P., Castiglioni, S., Crosa, G. and Fanelli, R., 2004, *Chemosphere*, 54 (5), 661-668.
- [33] Daniel, P., 2009, The use of veterinary drugs and vaccines in Mediterranean aquaculture, Zaragoza: CIHEAM, 197-205.
- [34] Bowker, J., Carty, D. and Wandelaar, N., 2013, *Drug Research Information Bulletin, AADAP*, 32.
- [35] Carty, D., Bowker, J., Wandelaar, N. and Bowman, M.P., 2013, *Drug Research Information Bulletin, AADAP*, 35.
- [36] FWS, <https://www.fws.gov/fisheries/aadap/inads-available/sedatives/aqui-s/index.html>, last accessed in March 2016.
- [37] Bowker, J., 2007, Potential Zero-Withdrawal Anesthetics for Use in Fisheries and Aquaculture, *USFWS, AADAP Program*.
- [38] EMA, <http://www.ema.europa.eu/ema/>, last accessed in July 2016.
- [39] Costello, Grant, Davies, Cecchini, Papoutsoglou, Quigley and Saroglia, 2001, *Journal of Applied Ichthyology*, 17 (4), 173-180.
- [40] EC, 1990, Council directive 1999/31/EC of 26 April 1999 on the landfill of waste, *Council Regulation (EEC) No 2377/90*.
- [41] ECHA, <http://echa.europa.eu/information-on-chemicals/biocidal-active-substances>, last accessed in July 2016.
- [42] Topic Popovic, N., Strunjak-Perovic, I., Coz-Rakovac, R., Barisic, J., Jadan, M., Persin Berakovic, A. and Sauerborn Klobucar, R., 2012, *Journal of Applied Ichthyology*, 28 (4), 553-564.
- [43] Coyle, S.D., Durborow, R.M. and Tidwell, J.H., 2004, *SRAC Publication*, 3900, 1-6.
- [44] Yalkowsky, S.H., 2003, Handbook of Aqueous Solubility Data, *CRC Press*.
- [45] Dubé, F. and Epel, D., 1986, *Experimental Cell Research*, 162 (1), 191-204.
- [46] Weber, R.A., Pérez-Maceira, J.J., Peleteiro, J.B., García-Martín, L. and Aldegunde, M., 2011, *Aquaculture*, 321 (1–2), 108-112.
- [47] Wagner, E., Arndt, R. and Hilton, B., 2002, *Aquaculture*, 211 (1–4), 353-366.
- [48] Davis, M.W., Stephenson, J. and Noga, E.J., 2008, *Journal of Aquatic Animal Health*, 20 (2), 86-95.
- [49] Carter, K.M., Woodley, C.M. and Brown, R.S., 2011, *Reviews in Fish Biology and Fisheries*, 21 (1), 51-59.
- [50] Sneddon, L.U., 2012, *Journal of Exotic Pet Medicine*, 21 (1), 32-43.
- [51] Marking, L.L., 1967, Toxicity of MS-222 to Selected Fishes, *U.S. Department of Interior, Fish and Wildlife Service*.
- [52] Stenger, V.G. and Maren, T.H., 1974, *Comparative and General Pharmacology*, 5 (1), 23-35.
- [53] Kolanczyk, R.C., Fitzsimmons, P.N., McKim Sr, J.M., Erickson, R.J. and Schmieder, P.K., 2003, *Aquatic Toxicology*, 64 (2), 177-184.
- [54] Hunn, J.B., Schoettger, R.A. and Willford, W.A., 1968, *Journal of the Fisheries Research Board of Canada*, 25 (1), 25-31.
- [55] EMEA, 1999, Tricaine mesilate summary report, *Committee for Veterinary Medicinal Products*, UK.
- [56] Bernstein, P.S., Digre, K.B. and Creel, D.J., *American Journal of Ophthalmology*, 124 (6), 843-844.
- [57] Pharmaq, 2010, MS-222: Material health and safety data sheet, Pharmaq Ltd., Fordingbridge, UK.
- [58] Drugs.com, <http://www.drugs.com/vet/tricaine-s.html>, last accessed in July 2016.
- [59] ACUC, 2015, Guideline & Standard Operating Procedure for MS-222, Animal Care and Use Procedure.

- [60] Neiffer, D.L., West, G., Heard, D. and Caulkett, N., 2008, *Zoo Animal and Wildlife Immobilization and Anesthesia*, Blackwell Publishing Ltd, p. 159-196.
- [61] EMEA, 1997, Benzocaine summary report 1, *Committee for Veterinary Medicinal Products*, UK.
- [62] Meinertz, J.R., Gingerich, W.H. and Allen, J.L., 1991, *Xenobiotica*, 21 (4), 525-533.
- [63] Stehly, G.R., Meinertz, J.R. and Gingerich, W.H., 2000, *Food Additives & Contaminants*, 17 (5), 387-392.
- [64] EMEA, 2001, Benzocaine summary report 2, *Committee for Veterinary Medicinal Products*, UK.
- [65] Moos, D.D. and Cuddeford, J.D., 2007, *Gastroenterology Nursing*, 30 (5), 342-345.
- [66] Lehr, J., Masters, A. and Pollack, B., 2012, *Journal of Pediatric Nursing*, 27 (5), 583-588.
- [67] Chung, N.-Y., Batra, R., Itzkevitch, M., Boruchov, D. and Baldauf, M., 2010, *The Journal of Emergency Medicine*, 38 (5), 601-606.
- [68] Dahshan, A. and Donovan, G.K., 2006, *Pediatrics*, 117 (4), e806–e809.
- [69] Sachdeva, R., Pugada, J.G., Casale, L.R., Meizlish, J.L. and Zarich, S.W., 2003, *Texas Heart Institute Journal*, 30 (4), 308-310.
- [70] Von Tungeln, L.S., Zhou, T., Woodling, K.A., Doerge, D.R., Greenlees, K.J. and Beland, F.A., 2011, *Food and Chemical Toxicology*, 49 (10), 2530-2535.
- [71] Davis, J.A., Greenfield, J.E. and Brewer, T.G., 1993, *American Journal of Veterinary Research*, 54 (8), 1322-1326.
- [72] Rowe, R.C., Sheskey, P.J., Quinn, M.E. and Association, A.P., 2009, *Handbook of Pharmaceutical Excipients*, *Pharmaceutical Press*.
- [73] Andersen, F.A., 2011, *International Journal of Toxicology*, 30 (Supplement 2), 73S-127S.
- [74] Meyer, B.K., Ni, A., Hu, B. and Shi, L., 2007, *Journal of Pharmaceutical Sciences*, 96 (12), 3155-3167.
- [75] Lowe, I. and Southern, J., 1994, *Letters in Applied Microbiology*, 18 (2), 115-116.
- [76] Burka, J.F., Hammell, K.L., Horsberg, T.E., Johnson, G.R., Rainnie, D.J. and Speare, D.J., 1997, *Journal of Veterinary Pharmacology and Therapeutics*, 20 (5), 333-349.
- [77] Belsito, D., Bickers, D., Bruze, M., Calow, P., Dagi, M.L., Fryer, A.D., Greim, H., Miyachi, Y., Saurat, J.H. and Sipes, I.G., 2012, *Food and Chemical Toxicology*, 50, Supplement 2, S52-S99.
- [78] Schmuck, G., Steffens, W. and Bomhard, E., 2000, *Archives of Toxicology*, 74 (4), 281-283.
- [79] NIH, <http://toxnet.nlm.nih.gov/>, last accessed in July 2016.
- [80] Vogt, T., Landthaler, M. and Stolz, W., 1998, *Contact Dermatitis*, 38 (1), 50-51.
- [81] Regulska, M., Pomierny, B., Basta-Kaim, A., Starek, A., Filip, M., Lason, W. and Budziszewska, B., 2010, *Pharmacological Reports*, 62, 1243-1249.
- [82] Geier, D.A., Jordan, S.K. and Geier, M.R., 2010, *Medical Science Monitor*, 16 (5), SR21-27.
- [83] Mácová, S., Doleželová, P., Pištěková, V., Svobodová, Z., Bedáňová, I. and Voslářová, E., 2008, *Neuroendocrinology Letters*, 29 (5), 680-684.
- [84] Vrskova, D. and Modra, H., 2012, *Veterinarni Medicina*, 57 (5), 245-250.
- [85] SigmaAldrich, 2012, 2-phenoxyethanol: Safety Data Sheet, Sigma Aldrich.
- [86] Pramod, K., Aji Alex, M.R., Singh, M., Dang, S., Ansari, S.H. and Ali, J., 2016, *Journal of Drug Targeting*, 24 (1), 24-33.
- [87] Pulikottil, S. and Nath, S., 2015, *South African Dental Journal*, 70, 108-115.
- [88] d' Avila Farias, M., Oliveira, P.S., Dutra, F.S.P., Fernandes, T.J., de Pereira, C.M.P., de Oliveira, S.Q., Stefanello, F.M., Lencina, C.L. and Barschak, A.G., 2014, *Journal of Pharmacy and Pharmacology*, 66 (5), 733-746.
- [89] Bachiega, T.F., de Sousa, J.P.B., Bastos, J.K. and Sforcin, J.M., 2012, *Journal of Pharmacy and Pharmacology*, 64 (4), 610-616.
- [90] Garg, A. and Singh, S., 2011, *Colloids and Surfaces B: Biointerfaces*, 87 (2), 280-288.

- [91] Cortés-Rojas, D.F., de Souza, C.R.F. and Oliveira, W.P., 2014, *Asian Pacific Journal of Tropical Biomedicine*, 4 (2), 90-96.
- [92] Bowker, J. and Trushenski, J., 2013, *Fisheries*, 38 (12), 549-552.
- [93] AQUI-S, <http://www.aqui-s.com/index.php/aqui-s-20e>, last accessed in July 2016.
- [94] Kong, X., Liu, X., Li, J. and Yang, Y., 2014, *Curr Opin Complement Alternat Med*, 1 (1), 8-11.
- [95] Fish, R., Danneman, P.J., Brown, M. and Karas, A., 2011, *Anesthesia and Analgesia in Laboratory Animals*, Elsevier Science.
- [96] Renault, S., Daverat, F., Pierron, F., Gonzalez, P., Dufour, S., Lancelleur, L., Schäfer, J. and Baudrimont, M., 2011, *Ecotoxicology and Environmental Safety*, 74 (6), 1573-1577.
- [97] Iversen, M., Finstad, B., McKinley, R.S. and Eliassen, R.A., 2003, *Aquaculture*, 221 (1-4), 549-566.
- [98] Guénette, S.A., Ross, A., Marier, J.-F., Beaudry, F. and Vachon, P., 2007, *European Journal of Pharmacology*, 562 (1-2), 60-67.
- [99] Guénette, S.A., Hélie, P., Beaudry, F. and Vachon, P., 2007, *Veterinary Anaesthesia and Analgesia*, 34 (3), 164-170.
- [100] Guénette, S.A., Uhland, F.C., Hélie, P., Beaudry, F. and Vachon, P., 2007, *Aquaculture*, 266 (1-4), 262-265.
- [101] Kildea, M.A., Allan, G.L. and Kearney, R.E., 2004, *Aquaculture*, 232 (1-4), 265-277.
- [102] Munerato, M.C., Sinigaglia, M., Reguly, M.L. and de Andrade, H.H.R., 2005, *Mutation Research/Genetic Toxicology and Environmental Mutagenesis*, 582 (1-2), 87-94.
- [103] Delaforge, M., Janiaud, P., Dorange, J., Morizot, J.P. and Padieu, P., 1977, *Comptes Rendus des Séances de la Société de Biologie*, 171, 100-107.
- [104] Mizutani, T., Satoh, K. and Nomura, H., 1991, *Research communications in chemical pathology and pharmacology*, 73, 87-95.
- [105] FDA, 2007, Guidance for Industry: Concerns Related to the Use of Clove Oil as an Anesthetic for Fish, *Guideline No.150, US FDA Center for Veterinary Medicine*.
- [106] NTP, 2000, Toxicology and carcinogenesis studies of methyleugenol, *NTP technical report 491*.
- [107] NTP, 1983, Carcinogenesis studies of eugenol, *NTP technical report 223*.
- [108] FAO/WHO, 2006, Evaluation of certain food additives, *WHO Technical Report 934*.
- [109] Bentzinger, G., De Souza, W., Mullié, C., Agnamey, P., Dassonville-Klimpt, A. and Sonnet, P., 2016, *Tetrahedron: Asymmetry*, 27 (1), 1-11.
- [110] Vandekerckhove, S. and D'hooghe, M., 2015, *Bioorganic & Medicinal Chemistry*, 23 (16), 5098-5119.
- [111] Brown, E.A.B., Franklin, J.E., Pratt, E. and Trams, E.G., 1972, *Comparative Biochemistry and Physiology Part A: Physiology*, 42 (1), 223-231.
- [112] Neiffer D. L. , S.M.A., 2009, *ILAR Journal*, 50.
- [113] Ortuño, J., Esteban, M.A. and Meseguer, J., 2002, *Fish & Shellfish Immunology*, 12 (1), 49-59.
- [114] Cuesta, A., Meseguer, J. and Esteban, M.A., 2004, *Veterinary Immunology and Immunopathology*, 101 (3-4), 203-210.
- [115] Davis, K.B. and Griffin, B.R., 2004, *Aquaculture*, 233 (1-4), 531-548.
- [116] Lochowitz, R.T., Miles, H.M. and Hafemann, D.R., 1974, *Comparative and General Pharmacology*, 5 (3-4), 217-224.
- [117] Hunn, J.B. and Allen, J.L., 1975, *General Pharmacology: The Vascular System*, 6 (1), 15-18.
- [118] Hunn, J.B. and Allen, J.L., 1974, *The Progressive Fish-Culturist*, 36 (3), 157-159.
- [119] Kumlu, M. and Yanar, M., 1999, *Israeli Journal of Aquaculture*, 51, 143-147.
- [120] ECHA, <http://echa.europa.eu/substance-information/-/substanceinfo/100.004.173>, last accessed in July 2016.
- [121] Schoettger, R.A. and Steucke, E.W., 1970, *The Progressive Fish-Culturist*, 32 (4), 202-205.

- [122] Gilderhus, P.A., Berger, B.L., Sills, J.B. and Harman, P.D., 1973, *Investigations in Fish Control, United States Department of the Interior*, 54.
- [123] Dawson, V.K., Marking, L.L., Fisheries, U.S.B.o.S. and Wildlife, 1973, Toxicity of Mixtures of Quinaldine Sulfate and MS-222 to Fish, *U.S. Department of Interior, Fish and Wildlife Service*.
- [124] Yanar, M. and Kumlu, M., 2001, *Turkish Journal of Veterinary and Animal Science*, 25, 185–189.
- [125] Schramm, H.L. and Black, D.J., 1984, *The Progressive Fish-Culturist*, 46 (3), 185-190.
- [126] Dziaman, R., Klyszejko, B. and Hajek, G., 2005, *Acta Ichthyologica et Piscatoria*, 35, 125-131.
- [127] Chatain, B. and Corrao, D., 1992, *Aquaculture*, 107 (1), 81-88.
- [128] Mattson, N.S. and Ripley, T.H., 1989, *Aquaculture*, 83 (1–2), 89-94.
- [129] Iwama, G.K. and Ackerman, P.A., 1994, *Biochemistry and Molecular Biology of Fishes*, Elsevier, 1-15.
- [130] Small, B.C. and Chatakondi, N., 2005, *North American Journal of Aquaculture*, 67 (1), 72-78.
- [131] Mohamed, S.J., 1999, *Acta Ichthyologica et Piscatoria*, 29 (2), 91-97.
- [132] Oswald, R.L., 1978, *Comparative Biochemistry and Physiology Part C: Comparative Pharmacology*, 60 (1), 19-26.
- [133] Croux, M.J.P.d., 1990, *Journal of Applied Ichthyology*, 6 (3), 189-192.
- [134] Bressler, K. and Ron, B., 2004, *Israeli Journal of Aquaculture*, 56, 5-13.
- [135] Serezli, R., Basaran, F., Gungor Muhtaroglu, C. and Kaymakci Basaran, A., 2012, *Journal of Applied Ichthyology*, 28 (1), 87-90.
- [136] McCarter, N., 1992, *The Progressive Fish-Culturist*, 54 (4), 263-265.
- [137] Altun, T. and Danabas, D., 2006, *Israeli Journal of Aquaculture*, 58, 178-182.
- [138] Basaran, F., Şen, H. and Karabulut, Ş., 2007, *Aquaculture Research*, 38 (9), 933-939.
- [139] Maršić-Lučić, J., Mladineo, I. and Tudor, M., 2005, *Aquaculture International*, 13 (6), 543-553.
- [140] Mylonas, C.C., Cardinaletti, G., Sigelaki, I. and Polzonetti-Magni, A., 2005, *Aquaculture*, 246 (1–4), 467-481.
- [141] Velíšek, J., Z. Svobodová. , 2004, *ACTA VET. BRNO*, 73, 379-384.
- [142] Altun, T., Hunt, A.Ö. and Usta, F., 2006, *Journal of Applied Animal Research*, 30 (2), 171-176.
- [143] Hikasa, Y., Takase, K., Ogasawara, T. and Ogasawara, S., 1986, *The Japanese Journal of Veterinary Science*, 48 (2), 341-351.
- [144] Waterstrat, P.R., 1999, *Journal of the World Aquaculture Society*, 30 (2), 250-255.
- [145] Hoskonen, P. and Pirhonen, J., 2004, *Aquaculture Research*, 35 (10), 1002-1005.
- [146] Hosetti, B.B. and Frost, S., 1995, *Ecological Engineering*, 5 (4), 421-431.
- [147] Campo, L.M., Ibarra, P., Gutiérrez, X. and Takle, H., 2010, *Norfima Marin AS*, Report 9/2010.
- [148] Bregnballe, J., 2015, A Guide to Recirculation Aquaculture, *FAO and EUROFISH International Organisation*.
- [149] EHS, <https://ehs.unc.edu/files/2015/09/ms-222.pdf>, last accessed in July 2016.
- [150] SigmaAldrich, 2012, Benzocaine: Safety Data Sheet, Sigma Aldrich.
- [151] Lyman, W.J., Reehl, W.F. and Rosenblatt, D.H., 1990, Handbook of chemical property estimation methods: environmental behavior of organic compounds, *American Chemical Society*.
- [152] Meylan, W.M. and Howard, P.H., 1993, *Chemosphere*, 26 (12), 2293-2299.
- [153] Poliakov, O.V., Lebedev, A.T. and Hänninen, O., 2000, *Toxicological & Environmental Chemistry*, 75 (3-4), 181-194.
- [154] Howard, P.H., 1993, Handbook of Environmental Fate and Exposure Data for Organic Chemicals, *Taylor & Francis*.
- [155] Rivera, J., Caixach, J., Ventura, F. and Espadaler, I., 1985, *Chemosphere*, 14 (5), 395-402.

- [156] Kimura, K., Kameda, Y., Yamamoto, H., Nakada, N., Tamura, I., Miyazaki, M. and Masunaga, S., 2014, *Chemosphere*, 107, 393-399.
- [157] Piperidou, C.I., Chaidou, C.I., Stalikas, C.D., Soulti, K., Pilidis, G.A. and Balis, C., 2000, *Journal of Agricultural and Food Chemistry*, 48 (5), 1941-1948.
- [158] Gulyas, H. and Reich, M., 2000, *Journal of Environmental Science and Health, Part A*, 35 (4), 435-464.
- [159] EC, 2000, EU Water Framework Directive, *Directive 2000/60/EC*.
- [160] Martins, C.I.M., Pistrin, M.G., Ende, S.S.W., Eding, E.H. and Verreth, J.A.J., 2009, *Aquaculture*, 291 (1-2), 65-73.
- [161] Martins, C.I.M., Ochola, D., Ende, S.S.W., Eding, E.H. and Verreth, J.A.J., 2009, *Aquaculture*, 298 (1-2), 43-50.
- [162] Davidson, J., Good, C., Welsh, C. and Summerfelt, S.T., 2014, *Aquacultural Engineering*, 59, 30-40.
- [163] Mota, V.C., Martins, C.I.M., Eding, E.H., Canário, A.V.M. and Verreth, J.A.J., 2014, *Aquacultural Engineering*, 62, 9-16.
- [164] Martins, C.I.M., Eding, E.H. and Verreth, J.A.J., 2011, *Food Chemistry*, 126 (3), 1001-1005.
- [165] Summerfelt, S.T., 1996, Engineering design of a water reuse system, *NCRAC Culture Series 101*, 277-309.
- [166] Martins, C.I.M., Eding, E.H., Verdegem, M.C.J., Heinsbroek, L.T.N., Schneider, O., Blancheton, J.P., d'Orbcastel, E.R. and Verreth, J.A.J., 2010, *Aquacultural Engineering*, 43 (3), 83-93.
- [167] Wik, T.E.L., Lindén, B.T. and Wramner, P.I., 2009, *Aquaculture*, 287 (3-4), 361-370.
- [168] Summerfelt, S., Bebak-Williams, J. and Tsukuda, S., 2001, Controlled Systems: Water Reuse and Recirculation, *American Fisheries Society*, 285-395.
- [169] Summerfelt, S.T., 2003, *Aquacultural Engineering*, 28 (1-2), 21-36.
- [170] Summerfelt, S.T., Sharrer, M.J., Tsukuda, S.M. and Gearheart, M., 2009, *Aquacultural Engineering*, 40 (1), 17-27.
- [171] Lawson, T.B., 1995, Fundamentals of aquacultural engineering, 1st ed., *Chapman & Hall*, New York, USA.
- [172] Sichula, J., Makasa, M.L., Nkonde, G.K., Kefi, A.S. and Katongo, C., 2011, *Malawi Journal of Aquaculture and Fisheries*, 1 (2), 10-15.
- [173] Oladoja, N.A., Adelagun, R.O.A., Ahmad, A.L. and Ololade, I.A., 2015, *Process Safety and Environmental Protection*, 98, 296-308.
- [174] Nethaji, S., Sivasamy, A., Thennarasu, G. and Saravanan, S., 2010, *Journal of Hazardous Materials*, 181 (1-3), 271-280.
- [175] Aitchison, S.J., Arnett, J., Murray, K.R. and Zhang, J., 2000, *Aquaculture*, 183 (3-4), 269-284.
- [176] Aitchison, S.J., Arnett, J., Murray, K.R. and Zhang, J., 2001, *Aquaculture*, 192 (2-4), 249-264.
- [177] Guo, Y., Yang, S., Fu, W., Qi, J., Li, R., Wang, Z. and Xu, H., 2003, *Dyes and Pigments*, 56 (3), 219-229.
- [178] Agarwal, M., Dave, M. and Upadhyaya, S., 2011, *Current World Environment*, 6 (1), 53-59.
- [179] Dawson, V.K., Marking, L.L. and Bills, T.D., 1976, *Transactions of the American Fisheries Society*, 105 (1), 119-123.
- [180] Howe, G.E., Bills, T.D. and Marking, L.L., 1990, *The Progressive Fish-Culturist*, 52 (1), 32-35.
- [181] Puyol, D., Monsalvo, V.M., Mohedano, A.F., Sanz, J.L. and Rodriguez, J.J., 2011, *Journal of Hazardous Materials*, 185 (2-3), 1059-1065.
- [182] Real, F.J., Benitez, F.J., Acero, J.L., Roldan, G. and Casas, F., 2012, *Industrial & Engineering Chemistry Research*, 51 (50), 16209-16215.
- [183] Bansal, R.C. and Goyal, M., 2005, Activated Carbon Adsorption, *CRC Press*, U.S.A.

- [184] Rouquerol, J., Rouquerol, F., Llewellyn, P., Maurin, G. and Sing, K.S.W., 2014, Adsorption by Powders and Porous Solids: Principles, Methodology and Applications, 2nd ed., *Academic Press*, Oxford.
- [185] Bottani, E.J. and Tascón, J.M.D., 2008, Adsorption by Carbons, *Elsevier Science*.
- [186] Butt, H.-J., Graf, K. and Kappl, M., 2004, Physics and Chemistry of Interfaces, *Wiley-VCH Verlag GmbH & Co. KGaA*, 177-205.
- [187] Bandosz, T.J., 2006, Activated Carbon Surfaces in Environmental Remediation, *Academic Press*.
- [188] ASTM C1274-12, Standard Test Method for Advanced Ceramic Specific Surface Area by Physical Adsorption, *ASTM International*, West Conshohocken, PA, 2012, www.astm.org.
- [189] ISO, 9277:2010 (E), Determination of the specific surface area of solids by gas adsorption – BET method, 2010.
- [190] Ternes, T.A., Meisenheimer, M., McDowell, D., Sacher, F., Brauch, H.-J., Haist-Gulde, B., Preuss, G., Wilme, U. and Zulei-Seibert, N., 2002, *Environmental Science & Technology*, 36 (17), 3855-3863.
- [191] Marsh, H. and Reinoso, F.R., 2006, Activated Carbon, *Elsevier Science*.
- [192] Yang, R.T., 2003, Adsorbents: Fundamentals and Applications, *John Wiley & Sons, Inc*.
- [193] Dias, J.M., Alvim-Ferraz, M.C.M., Almeida, M.F., Rivera-Utrilla, J. and Sánchez-Polo, M., 2007, *Journal of Environmental Management*, 85 (4), 833-846.
- [194] Ali, I., Asim, M. and Khan, T.A., 2012, *Journal of Environmental Management*, 113 (0), 170-183.
- [195] Sheng, C., Nnanna, A.G.A., Liu, Y. and Vargo, J.D., 2016, *Science of The Total Environment*, 550, 1075-1083.
- [196] Snyder, S.A., Adham, S., Redding, A.M., Cannon, F.S., DeCarolis, J., Oppenheimer, J., Wert, E.C. and Yoon, Y., 2007, *Desalination*, 202 (1–3), 156-181.
- [197] Yu, Z., Peldszus, S. and Huck, P.M., 2008, *Water Research*, 42 (12), 2873-2882.
- [198] Tchobanoglous, G., Burton, F.L. and Stensel, H.D., 2003, Wastewater Engineering: Treatment and Reuse, *McGraw-Hill Education*.
- [199] McKay, G., 1995, Use of Adsorbents for the Removal of Pollutants from Wastewater, 1st ed., *CRC Press*, New York, USA.
- [200] Worch, E., 2012, Adsorption Technology in Water Treatment, Fundamentals, Processes, and Modeling, 1st ed., *Walter de Gruyter GmbH & Co. KG*, Berlin, Germany.
- [201] PENTAIR, <http://pentairaes.com/learn-about-aquaculture/technical-talks/activated-carbon-in-aquaculture-tt42>, last accessed in June 2016.
- [202] Keller, A.A., Sandall, O.C., Rinker, R.G., Mitani, M.M., Bierwagen, B.G. and Snodgrass, M.J., 1998, *Health and environmental assessment of MTBE*, 4.
- [203] Stavropoulos, G.G. and Zabaniotou, A.A., 2009, *Fuel Processing Technology*, 90 (7–8), 952-957.
- [204] Alade, A.O., Amuda, O.S., Afolabi, A.O. and Adelowo, F.E., 2012, *Journal of Environmental Science and Technology*, 5, 192-209.
- [205] Helfrich, L.A. and Libey, G., 2011, Fish Farming in Recirculating Aquaculture Systems, *Department of Fisheries and Wildlife Sciences; Virginia Tech*.
- [206] Adegoke, K.A. and Bello, O.S., 2015, *Water Resources and Industry*, 12, 8-24.
- [207] Bharathi, K.S. and Ramesh, S.T., 2013, *Applied Water Science*, 3 (4), 773-790.
- [208] Dawood, S. and Sen, T.K., 2014, *Journal of Chemical and Process Engineering*, 1, 1-7.
- [209] Demirbas, A., 2009, *Journal of Hazardous Materials*, 167 (1–3), 1-9.
- [210] Rafatullah, M., Sulaiman, O., Hashim, R. and Ahmad, A., 2010, *Journal of Hazardous Materials*, 177 (1–3), 70-80.
- [211] Yagub, M.T., Sen, T.K., Afroze, S. and Ang, H.M., 2014, *Advances in Colloid and Interface Science*, 209, 172-184.
- [212] Anastopoulos, I. and Kyzas, G.Z., 2014, *Journal of Molecular Liquids*, 200, Part B, 381-389.

- [213] Rangabhashiyam, S., Anu, N. and Selvaraju, N., 2013, *Journal of Environmental Chemical Engineering*, 1 (4), 629-641.
- [214] Mohan, D., Sarswat, A., Ok, Y.S. and Pittman Jr, C.U., 2014, *Bioresource Technology*, 160, 191-202.
- [215] Tan, X., Liu, Y., Zeng, G., Wang, X., Hu, X., Gu, Y. and Yang, Z., 2015, *Chemosphere*, 125 (0), 70-85.
- [216] Bhatnagar, A., Sillanpää, M. and Witek-Krowiak, A., 2015, *Chemical Engineering Journal*, 270, 244-271.
- [217] Çifçi, D.İ. and Meriç, S., 2016, *Desalination and Water Treatment*, 57 (39), 18131-18143.
- [218] Foo, K.Y. and Hameed, B.H., 2009, *Advances in Colloid and Interface Science*, 152 (1-2), 39-47.
- [219] Gisi, S.D., Lofrano, G., Grassi, M. and Notarnicola, M., 2016, *Sustainable Materials and Technologies*, in press.
- [220] Ahmaruzzaman, M., 2008, *Advances in Colloid and Interface Science*, 143 (1-2), 48-67.
- [221] Kyzas, G. and Kostoglou, M., 2014, *Materials*, 7 (1), 333.
- [222] Xie, T., Reddy, K.R., Wang, C., Yargicoglu, E. and Spokas, K., 2015, *Critical Reviews in Environmental Science and Technology*, 45 (9), 939-969.
- [223] Bhatnagar, A. and Sillanpää, M., 2010, *Chemical Engineering Journal*, 157 (2-3), 277-296.
- [224] Crini, G. and Badot, P.M., 2011, Sorption processes and pollution: Conventional and non-conventional sorbents for pollutant removal from wastewaters, *Presses universitaires de Franche-Comté*.
- [225] Scoma, A., Rebecchi, S., Bertin, L. and Fava, F., 2016, *Critical Reviews in Biotechnology*, 36 (1), 175-189.
- [226] EC, 1999, Council directive 1999/31/EC of 26 April 1999 on the landfill of waste, Directive 1999/31/EC, *Official Journal of the European Communities*.
- [227] EC, 2000, Directive 2000/76/EC of European Parliament and of the Council of 4 December 2000 on the incineration of waste, *Official Journal of the European Communities*.
- [228] EC, 2008, Directive 2008/98/EC of European Parliament and of the Council of 19 November 2008 on waste and repealing certain Directives, *Official Journal of the European Union*.
- [229] Mall, I.D., Srivastava, V.C., Agarwal, N.K. and Mishra, I.M., 2005, *Colloids and Surfaces A: Physicochemical and Engineering Aspects*, 264 (1-3), 17-28.
- [230] Gupta, V.K., Mittal, A., Krishnan, L. and Gajbe, V., 2004, *Separation and Purification Technology*, 40 (1), 87-96.
- [231] Mittal, A., Krishnan, L. and Gupta, V.K., 2005, *Separation and Purification Technology*, 43 (2), 125-133.
- [232] Mestre, A.S., Pires, J., Nogueira, J.M.F. and Carvalho, A.P., 2007, *Carbon*, 45 (10), 1979-1988.
- [233] Mestre, A.S., Pires, R.A., Aroso, I., Fernandes, E.M., Pinto, M.L., Reis, R.L., Andrade, M.A., Pires, J., Silva, S.P. and Carvalho, A.P., 2014, *Chemical Engineering Journal*, 253, 408-417.
- [234] Hjaila, K., Baccar, R., Sarrà, M., Gasol, C.M. and Blázquez, P., 2013, *Journal of Environmental Management*, 130, 242-247.
- [235] Zhou, A., Zhang, Y., Li, R., Su, X. and Zhang, L., 2016, *Desalination and Water Treatment*, 57 (1), 388-397.
- [236] Villaescusa, I., Fiol, N., Poch, J., Bianchi, A. and Bazzicalupi, C., 2011, *Desalination*, 270 (1-3), 135-142.
- [237] Teixeira, S., Delerue-Matos, C. and Santos, L., 2012, *Environmental Science and Pollution Research*, 19 (8), 3096-3106.
- [238] Dubey, S.P., Dwivedi, A.D., Sillanpää, M. and Gopal, K., 2010, *Chemical Engineering Journal*, 165 (2), 537-544.

- [239] Álvarez-Torrellas, S., Rodríguez, A., Ovejero, G. and García, J., 2016, *Chemical Engineering Journal*, 283, 936-947.
- [240] Kyzas, G.Z. and Deliyanni, E.A., 2015, *Chemical Engineering Research and Design*, 97, 135-144.
- [241] Mansouri, H., Carmona, R.J., Gomis-Berenguer, A., Souissi-Najar, S., Ouederni, A. and Ania, C.O., 2015, *Journal of Colloid and Interface Science*, 449, 252-260.
- [242] Liu, P., Liu, W.-J., Jiang, H., Chen, J.-J., Li, W.-W. and Yu, H.-Q., 2012, *Bioresource Technology*, 121 (0), 235-240.
- [243] Baccar, R., Sarrà, M., Bouzid, J., Feki, M. and Blánquez, P., 2012, *Chemical Engineering Journal*, 211–212, 310-317.
- [244] Akar, E., Altinışik, A. and Seki, Y., 2013, *Ecological Engineering*, 52, 19-27.
- [245] Calisto, V., Ferreira, C.I.A., Santos, S.M., Gil, M.V., Otero, M. and Esteves, V.I., 2014, *Bioresource Technology*, 166 (0), 335-344.
- [246] Jaria, G., Calisto, V., Gil, M.V., Otero, M. and Esteves, V.I., 2015, *Journal of Colloid and Interface Science*, 448 (0), 32-40.
- [247] Coimbra, R.N., Calisto, V., Ferreira, C.I.A., Esteves, V.I. and Otero, M., 2015, *Arabian Journal of Chemistry*.
- [248] Calisto, V., Ferreira, C.I.A., Oliveira, J.A.B.P., Otero, M. and Esteves, V.I., 2015, *Journal of Environmental Management*, 152 (0), 83-90.
- [249] Tzeng, T.-W., Liu, Y.-T., Deng, Y., Hsieh, Y.-C., Tan, C.-C., Wang, S.-L., Huang, S.-T. and Tzou, Y.-M., 2016, *International Journal of Environmental Science and Technology*, 13 (3), 973-984.
- [250] Zheng, H., Wang, Z., Zhao, J., Herbert, S. and Xing, B., 2013, *Environmental Pollution*, 181, 60-67.
- [251] Xie, M., Chen, W., Xu, Z., Zheng, S. and Zhu, D., 2014, *Environmental Pollution*, 186, 187-194.
- [252] Chen, C., Zhou, W. and Lin, D., 2015, *Bioresource Technology*, 179, 359-366.
- [253] Jung, C., Park, J., Lim, K.H., Park, S., Heo, J., Her, N., Oh, J., Yun, S. and Yoon, Y., 2013, *Journal of Hazardous Materials*, 263, Part 2, 702-710.
- [254] Kearns, J.P., Wellborn, L.S., Summers, R.S. and Knappe, D.R.U., 2014, *Water Research*, 62, 20-28.
- [255] Reddy, K.R., Xie, T. and Dastgheibi, S., 2014, *Journal of Environmental Engineering*, 140 (12), 04014043,1-10.
- [256] Inyang, M., Gao, B., Zimmerman, A., Zhou, Y. and Cao, X., 2015, *Environmental Science and Pollution Research*, 22 (3), 1868-1876.
- [257] Inyang, M., Gao, B., Zimmerman, A., Zhang, M. and Chen, H., 2014, *Chemical Engineering Journal*, 236, 39-46.
- [258] Chen, T., Zhang, Y., Wang, H., Lu, W., Zhou, Z., Zhang, Y. and Ren, L., 2014, *Bioresource Technology*, 164 (0), 47-54.
- [259] Kupryianchyk, D., Hale, S., Zimmerman, A.R., Harvey, O., Rutherford, D., Abiven, S., Knicker, H., Schmidt, H.-P., Rumpel, C. and Cornelissen, G., 2016, *Chemosphere*, 144, 879-887.
- [260] IBI, <http://www.biochar-international.org/about>, last accessed in July 2016.
- [261] Pecha, B. and Garcia-Perez, M., 2015, *Bioenergy*, Academic Press, Boston, p. 413-442.
- [262] Inyang, M. and Dickenson, E., 2015, *Chemosphere*, 134, 232-240.
- [263] Qian, K., Kumar, A., Zhang, H., Bellmer, D. and Huhnke, R., 2015, *Renewable and Sustainable Energy Reviews*, 42, 1055-1064.
- [264] Brewer, C.E., Unger, R., Schmidt-Rohr, K. and Brown, R.C., 2011, *BioEnergy Research*, 4 (4), 312-323.
- [265] Sun, K., Kang, M., Zhang, Z., Jin, J., Wang, Z., Pan, Z., Xu, D., Wu, F. and Xing, B., 2013, *Environmental Science & Technology*, 47 (20), 11473-11481.
- [266] Zhang, P., Sun, H., Yu, L. and Sun, T., 2013, *Journal of Hazardous Materials*, 244–245, 217-224.

- [267] Qiu, H., Lv, L., Pan, B.-c., Zhang, Q.-j., Zhang, W.-m. and Zhang, Q.-x., 2009, *Journal of Zhejiang University SCIENCE A*, 10 (5), 716-724.
- [268] Simonin, J.-P., 2016, *Chemical Engineering Journal*, 300, 254-263.
- [269] Lagergren, S.Y., 1898, *Kungliga Svenska Vetenskapsakademiens*, 24 (4), 1-39.
- [270] Ho, Y.S. and McKay, G., 1998, *Process Safety and Environmental Protection*, 76 (4), 332-340.
- [271] Ho, Y.S. and McKay, G., 1998, *Chemical Engineering Journal*, 70 (2), 115-124.
- [272] Ho, Y.S. and McKay, G., 1998, *Process Safety and Environmental Protection*, 76 (2), 183-191.
- [273] Robati, D., Rajabi, M., Moradi, O., Najafi, F., Tyagi, I., Agarwal, S. and Gupta, V.K., 2016, *Journal of Molecular Liquids*, 214, 259-263.
- [274] Vithanage, M., Mayakaduwa, S.S., Herath, I., Ok, Y.S. and Mohan, D., 2016, *Chemosphere*, 150, 781-789.
- [275] Acosta, R., Fierro, V., Martinez de Yuso, A., Nabarlantz, D. and Celzard, A., 2016, *Chemosphere*, 149, 168-176.
- [276] Mihara, Y., Sikder, M.T., Yamagishi, H., Sasaki, T., Kurasaki, M., Itoh, S. and Tanaka, S., 2016, *Journal of Water Process Engineering*, 10, 9-19.
- [277] Yari, M., Rajabi, M., Moradi, O., Yari, A., Asif, M., Agarwal, S. and Gupta, V.K., 2015, *Journal of Molecular Liquids*, 209, 50-57.
- [278] Yi, Z.-j., Yao, J., Kuang, Y.-f., Chen, H.-l., Wang, F. and Yuan, Z.-m., 2015, *Water Science and Technology*, 72 (6), 983-989.
- [279] Ho, Y.S., 1995, Adsorption of Heavy Metals from Waste Streams by Peat, PhD Thesis, University of Birmingham.
- [280] Ho, Y.-S., 2006, *Journal of Hazardous Materials*, 136 (3), 681-689.
- [281] Ho, Y.S. and McKay, G., 1999, *Process Biochemistry*, 34 (5), 451-465.
- [282] Hafeznezami, S., Zimmer-Faust, A.G., Dunne, A., Tran, T., Yang, C., Lam, J.R., Reynolds, M.D., Davis, J.A. and Jay, J.A., 2016, *Environmental Pollution*, 215, 290-301.
- [283] Ali, R.M., Hamad, H.A., Hussein, M.M. and Malash, G.F., 2016, *Ecological Engineering*, 91, 317-332.
- [284] Sadeek, S.A., Negm, N.A., Hefni, H.H.H. and Wahab, M.M.A., 2015, *International Journal of Biological Macromolecules*, 81, 400-409.
- [285] Zarghami, Z., Akbari, A., Latifi, A.M. and Amani, M.A., 2016, *Bioresource Technology*, 205, 230-238.
- [286] Shin, H.S. and Kim, J.-H., 2016, *Process Biochemistry*, 51 (7), 917-924.
- [287] Liu, X., Wang, F. and Bai, S., 2015, *Water Science and Technology*, 72 (12), 2229-2235.
- [288] Heibati, B., Rodriguez-Couto, S., Al-Ghouti, M.A., Asif, M., Tyagi, I., Agarwal, S. and Gupta, V.K., 2015, *Journal of Molecular Liquids*, 208, 99-105.
- [289] Subbaiah, M.V. and Kim, D.-S., 2016, *Ecotoxicology and Environmental Safety*, 128, 109-117.
- [290] Kameda, T., Uchiyama, T. and Yoshioka, T., 2016, *Journal of Alloys and Compounds*, 670, 322-328.
- [291] Ilgen, O. and Dulger, H.S., 2016, *Industrial Crops and Products*, 81, 66-71.
- [292] Ilgen, O., 2014, *Fuel Processing Technology*, 118, 69-74.
- [293] Wilczak, A. and Keinath, T.M., 1993, *Water Environment Research*, 65 (3), 238-244.
- [294] Tosun, İ., 2012, *International Journal of Environmental Research and Public Health*, 9 (3), 970.
- [295] Chiron, N., Guilet, R. and Deydier, E., 2003, *Water Research*, 37 (13), 3079-3086.
- [296] Limousin, G., Gaudet, J.P., Charlet, L., Szenknect, S., Barthès, V. and Krimissa, M., 2007, *Applied Geochemistry*, 22 (2), 249-275.
- [297] Langmuir, I., 1918, *Journal of the American Chemical Society*, 40 (9), 1361-1403.
- [298] Foo, K.Y. and Hameed, B.H., 2010, *Chemical Engineering Journal*, 156 (1), 2-10.
- [299] Freundlich, H., 1906, *Zeitschrift für Physikalische Chemie*, 57, 385-470.
- [300] Sips, R., 1948, *The Journal of Chemical Physics*, 16 (5), 490-495.

- [301] Sips, R., 1950, *The Journal of Chemical Physics*, 18 (8), 1024-1026.
- [302] Tien, C., 1994, *Adsorption Calculations and Modeling*, Butterworth-Heinemann, USA.
- [303] Xu, Z., Cai, J.-g. and Pan, B.-c., 2013, *Journal of Zhejiang University SCIENCE A*, 14 (3), 155-176.
- [304] Thomas, H.C., 1944, *Journal of the American Chemical Society*, 66 (10), 1664-1666.
- [305] Clark, R.M., 1987, *Environmental Science & Technology*, 21 (6), 573-580.
- [306] Yoon, Y.H. and Nelson, J.H., 1984, *American Industrial Hygiene Association Journal*, 45 (8), 509-516.
- [307] Yan, G., Viraraghavan, Viraraghavan, T. and Chen, M., 2001, *Adsorption Science & Technology*, 19 (1), 25-43.
- [308] Thomas, W.J. and Crittenden, B.D., 1998, *Adsorption Technology and Design*, Butterworth-Heinemann, USA.
- [309] Hutchins, R.A., 1973, *Chemical Engineering Journal*, 20, 133-138.
- [310] Salvador, F., Martin-Sanchez, N., Sanchez-Hernandez, R., Sanchez-Montero, M.J. and Izquierdo, C., 2015, *Microporous and Mesoporous Materials*, 202, 259-276.
- [311] Salvador, F., Martin-Sanchez, N., Sanchez-Hernandez, R., Sanchez-Montero, M.J. and Izquierdo, C., 2015, *Microporous and Mesoporous Materials*, 202, 277-296.
- [312] Ledesma, B., Román, S., Álvarez-Murillo, A., Sabio, E. and González, J.F., 2014, *Journal of Analytical and Applied Pyrolysis*, 106, 112-117.
- [313] Berenguer, R., Marco-Lozar, J.P., Quijada, C., Cazorla-Amorós, D. and Morallón, E., 2010, *Energy & Fuels*, 24 (6), 3366-3372.
- [314] Bhagawan, D., Poodari, S., Ravi kumar, G., Golla, S., Anand, C., Banda, K.S., Himabindu, V. and Vidyavathi, S., 2015, *Journal of Material Cycles and Waste Management*, 17 (1), 185-193.
- [315] Coelho, C., Oliveira, A.S., Pereira, M.F.R. and Nunes, O.C., 2006, *Journal of Hazardous Materials*, 138 (2), 343-349.
- [316] Toh, R.-H., Lim, P.-E., Seng, C.-E. and Adnan, R., 2013, *Bioresource Technology*, 143, 265-274.
- [317] Narbaitz, R.M. and Karimi-Jashni, A., 2012, *Chemical Engineering Journal*, 197, 414-423.
- [318] Asghar, H.M.A., Hussain, S.N., Roberts, E.P.L. and Brown, N.W., 2013, *Korean Journal of Chemical Engineering*, 30 (7), 1415-1422.
- [319] Salvador, F., Martin-Sanchez, N., Sanchez-Montero, M.J., Montero, J. and Izquierdo, C., 2013, *The Journal of Supercritical Fluids*, 74, 1-7.
- [320] Carmona, M., Garcia, M.T., Carnicer, Á., Madrid, M. and Rodríguez, J.F., 2014, *Journal of Chemical Technology & Biotechnology*, 89 (11), 1660-1667.
- [321] Pan, R.R., Fan, F.L., Li, Y. and Jin, X.J., 2016, *RSC Advances*, 6 (39), 32960-32966.
- [322] Mao, H., Zhou, D., Hashisho, Z., Wang, S., Chen, H. and Wang, H., 2015, *Journal of Industrial and Engineering Chemistry*, 21, 516-525.
- [323] Silva, M., Fernandes, A., Mendes, A., Manaia, C.M. and Nunes, O.C., 2004, *Water Research*, 38 (11), 2677-2684.
- [324] Charinpanitkul, T. and Tanthapanichakoon, W., 2011, *Journal of Industrial and Engineering Chemistry*, 17 (3), 570-574.
- [325] Çalışkan, E., Bermúdez, J.M., Parra, J.B., Menéndez, J.A., Mahramanlioğlu, M. and Ania, C.O., 2012, *Journal of Environmental Management*, 102, 134-140.
- [326] Van Deventer, J.S.J. and Camby, B.S., 1988, *Thermochimica Acta*, 136, 179-189.
- [327] Suzuki, M., Misic, D.M., Koyama, O. and Kawazoe, K., 1978, *Chemical Engineering Science*, 33 (3), 271-279.
- [328] CalgonCarbon, <http://www.calgoncarbon.com/reactivation-services/>, last accessed in August 2016.
- [329] Carbot, <http://www.cabotcorp.com/solutions/products-plus/activated-carbon/reactivation-services>, last accessed in August 2016.
- [330] Guo, D., Shi, Q., He, B. and Yuan, X., 2011, *Journal of Hazardous Materials*, 186 (2-3), 1788-1793.

- [331] Cooney, D.O., Nagerl, A. and Hines, A.L., 1983, *Water Research*, 17 (4), 403-410.
- [332] Martin, R.J. and Ng, W.J., 1984, *Water Research*, 18 (1), 59-73.
- [333] Martin, R.J. and Ng, W.J., 1985, *Water Research*, 19 (12), 1527-1535.
- [334] Purkait, M.K., Maiti, A., DasGupta, S. and De, S., 2007, *Journal of Hazardous Materials*, 145 (1-2), 287-295.
- [335] Leng, C.-C. and Pinto, N.G., 1996, *Industrial & Engineering Chemistry Research*, 35 (6), 2024-2031.
- [336] Lu, P.-J., Lin, H.-C., Yu, W.-T. and Chern, J.-M., 2011, *Journal of the Taiwan Institute of Chemical Engineers*, 42 (2), 305-311.
- [337] Özkaya, B., 2006, *Journal of Hazardous Materials*, 129 (1-3), 158-163.
- [338] Rinkus, K., Reed, B.E. and Lin, W., 1997, *Separation Science and Technology*, 32 (14), 2367-2384.
- [339] Kuo, C.-Y., 2008, *Journal of Hazardous Materials*, 152 (3), 949-954.

Part II

Chapter 3

Comparative valorisation of agricultural and industrial biowastes by combustion and pyrolysis

3 Comparative valorisation of agricultural and industrial biowastes by combustion and pyrolysis

In this chapter, combustion and pyrolysis processes were assessed and compared for two types of lignocellulosic biowastes: agricultural (Eucalyptus bark, grape seeds, peach stones, walnut shells, olive waste and peanut shells) and industrial (primary and biological paper mill sludge). They were characterized by elemental, proximate and thermal analyses; the pyrolysis behaviour was studied by thermogravimetric analysis and the gases produced were identified using mass spectrometry. Agricultural biowastes showed the highest calorific values, close to the fossil fuel values (20–30 MJ kg⁻¹) and, in general, for these wastes, the emission of gases containing carbon (CH₄, C₂H₂, CO and CO₂) was higher than for the tested industrial biowastes, making the agricultural biowastes highly competitive for combustion applications such as gas fuel. Also, the solid product which resulted from the pyrolysis of industrial biowastes is a material with large specific surface area, which is a promising characteristic for applications as adsorbent for water remediation.

The work presented and discussed in this chapter resulted in the following publication:

[1] Ferreira, C.I.A., Calisto, V., Cuerda-Correa, E.M., Otero, M., Nadais, H. and Esteves, V.I. (2016) Comparative valorisation of agricultural and industrial biowastes by combustion and pyrolysis. *Bioresource Technology*, 218, 918-925. DOI: 10.1016/j.biortech.2016.07.047

3.1 Contextualization

The European Union (EU) has clear objectives to fulfil regarding the energy and climate policies for 2030. The EU main goals include the reduction of greenhouse gas emissions by 40%, the increase of renewable energy share by around 30% and the enhancement of the energy system (which will impact the energy prices) [2]. Besides the energy from wind, water and solar power, it is expected, both in the EU and globally, an increase in the use of biowastes to produce energy [2], and also to minimize the waste disposal. The European Commission has launched a public consultation about developing a sustainability plan for biowastes, where the end-use efficiency of converting them to heat and electricity or, as an alternative, producing solid, liquid and gaseous fuels as a way of waste management is a central issue [3]. In this sense, biowastes may be converted into desirable, high added-value products mainly by biochemical (using enzymes and/or microorganisms) and thermochemical (using heat energy with or without chemical catalysts) processes. The thermochemical conversion technology consists of combustion, gasification, pyrolysis, and liquefaction and has several advantages such as applicability to a wide range of feedstock, conversion of both carbohydrate and lignin into high added-value products, faster reaction rates, and the ability to produce diverse fuels [4]. This chapter is focus on the combustion and pyrolysis of two types of lignocellulosic biowastes widely produced in EU: agricultural and industrial biowastes from pulp and paper industry.

Combustion is an exothermic oxidation reaction in which carbon is oxidized to carbon dioxide and hydrogen is oxidized to water producing energy, in the form of heat, and ashes as a main residue. Biomass offers important advantages as a combustion feedstock due to its high volatility and reactivity. However, in comparison with solid fossil fuels, biomass contains much less carbon, more oxygen and has a low heating value [5]. On the other hand, pyrolysis involves the heating of biomass in the absence of oxygen and thus the organic fraction thermally decomposes releasing gases and a residual solid (biochar), whose relative proportions depend on the biomass composition, heating rate and pyrolysis temperature [6], as mentioned in Chapter 2. By cooling the pyrolysis vapour, polar and high molecular weight compounds condense into a liquid (bio-oil) while low-molecular-weight volatile compounds remain in the gas phase. These low-molecular-weight volatile compounds are usually combusted to produce heat to drive the pyrolysis process, and bio-oil is further upgraded to biodiesel and petrochemicals [7]. Compared to biomass combustion, pyrolysis holds several attractive features such as relative low temperature requirements, adaptability to a wide variety of feedstock and the possibility to result in several interesting/usable products from typical waste streams. Therefore, the pyrolysis of biowastes

constitutes a practical, effective, and environmentally sustainable way of producing large quantities of renewable bio-energy while simultaneously reducing emissions of greenhouse gases and other pollutants [8]. A main advantage of the pyrolysis of biomass is the generation of biochar, which, due to its specific properties, including high carbon content, large specific surface area and porous structure, has been applied as soil amendment, enhancing soil fertility through improving nutrient retention due to cation adsorption, reduction in nitrous oxide (NO) and methane (CH₄), along with CO₂ emissions [9], and, also, as an alternative adsorbent for the removal of contaminants from water, as already mentioned in Chapter 2, section 2.4.2.

The work presented in this chapter aims to assess and compare the valorisation of agricultural and industrial biowastes by their combustion and pyrolysis, in order to, firstly, reduce the waste disposal and, secondly, transform the waste into a new raw material by using it for the production of both solid and gaseous added-value products, which is part of the EU action plan for the Circular Economy. The agricultural biowastes here used were *Eucalyptus* bark, grape seeds, peach stones, walnut shells, olive waste and peanut shells and the industrial biowastes were primary and biological paper mill sludge. Estimated and experimental heats of combustion corresponding to all agricultural and industrial biowastes were evaluated. The pyrolysis of these biowastes and the gases evolved during the process were determined by thermogravimetry coupled with mass spectrometry (TG-MS) and their potential to energy generation was evaluated.

3.2 Materials and methods

3.2.1 Wastes: sampling and preparation

3.2.1.1 Agricultural wastes

The agricultural wastes used in this work consisted of *Eucalyptus* bark (EB), grape seeds (GS), walnut shells (WS), peanut shells (PNS) and olive waste, which includes olive pomace and stone (OW) and were provided by local producers. The peach stones (PeS) were provided by a Portuguese food and beverages company.

3.2.1.2 Industrial wastes

Primary (PS) and biological paper mill sludge (BS) were provided by a mill which employs the kraft ECD (elemental chlorine free) pulp production process. The mill has more than 6 decades of existence and was the first one, worldwide, to produce paper pulp from eucalyptus wood (*Eucalyptus globulus*) by the kraft process. Its production reaches the order of 320,000 tons of bleached pulp per year. On average, PS and BS are produced at a rate of 20 and 10 kg per ton of

air dried pulp, respectively. The PS results from fibers rejected after the cooking/digestion pulping step and losses of fibers and other solids which occur when liquid effluents are involved (for example, washing and bleaching); the composition of the PS is very similar to the pulp, consisting essentially of organic matter (fibers). After primary treatment, the effluent is submitted to biological treatment: the BS is essentially biomass (after dehydration) that results from the action of microorganisms, under aerobic conditions, which are meant to reduce the organic matter content of the effluent.

3.2.1.3 Wastes preparation

After collection, all these materials were dried at room temperature for several days, followed by a 24 h period at 105 °C in an oven. Afterwards, EB, GS, PNS, OW and PS were ground with a blade mill in order to obtain a powder material (particle diameter < 0.2 mm). Due to their, WS, PeS and BS were ground with a hammer mill (particle diameter < 0.2 mm).

3.2.2 Materials characterization

3.2.2.1 Proximate analysis

The proximate analyses were performed using a Setaram SETSYS Evolution-1750 thermal analyser and an experimental procedure previously proposed by Valenzuela et al. (1985) [10]. Briefly, 20-25 mg of sample was placed in an alumina crucible and heated (80 °C min⁻¹) from room temperature up to 950 °C under an inert gas flow (helium, 200 mL min⁻¹). The sample was kept at this temperature for 7 min. Next, the carrier gas was automatically switched to air (200 mL min⁻¹) and the sample was maintained at 950 °C until total stabilization of the weight. The mass loss observed around 100 °C is attributed to moisture. The mass loss registered from the end of this first step up to the switching of the carrier gas corresponds to the volatile matter. The mass loss comprised between the introduction of the air flow and the stabilization of the weight is attributed to the fixed carbon content. The final residue corresponds to the ash content of the sample.

3.2.2.2 Elemental analysis

The determination of the sample content in C, H, N and S was performed in a LECO CHNS-932 elemental analyser. Standard methods were employed to determine the content in C, H, N [11] and S [12], while the oxygen content was calculated by difference. Elemental analyses were performed in triplicate. The results were corrected considering the water content of the samples (presented at a dry basis).

3.2.2.3 Heat of combustion

The determination of the experimental higher heating value (HHV_{exp}) was carried out by means of an isoperibol oxygen bomb calorimeter LECO AC-600 according to the procedure UNE-EN 14918:2011 [13].

One can find several correlations in the literature for the calculation of HHV based on elemental, proximate and both elemental and proximate composition [14]. In this work, some of the most used and cited correlations were considered; these are listed in Table 3.1 together with their corresponding basis and assumptions/applications. The HHVs obtained from these correlations were then compared with the experimental ones.

3.2.2.4 Thermogravimetric analysis coupled with mass spectrometry (TG-MS)

Thermogravimetric analysis was carried out in a Setaram SETSYS Evolution-1750. Temperature programmed experiments were the same used for the proximate analysis of samples, previously described in section 3.2.2.1, following the procedure by Valenzuela et al. (1985) [10]. Simultaneously, gases evolved during pyrolysis experiments were monitored and analysed on-line with the aid of a quadrupole mass spectrometer (Pfeiffer Omnistar) coupled to the gas off-take of the TG equipment.

The TG-MS data were normalized, *i.e.*, the maximum value of the total intensity registered in the MS was used as the normalisation factor. It is important to note that each compound (m/z) detected by MS has its own response factor, so, only the intensities of the same compound, for different samples, can be compared. Contrarily, only the shape and the characteristic temperatures of the peak can be compared between the different m/z signals.

Table 3.1 - Correlations for calculation of HHV

No.	Reference	Correlation	Application
<i>Based on Elemental Analysis</i>			
1	Tillman (1978) [15]	$\text{HHV}(\text{MJ kg}^{-1}) = 0.4373[\text{C}] - 1.6701$	Whole range of biomass materials for which HHV is a very strong function of its carbon content
2	Jenkins (1980) [16]	$\text{HHV}(\text{MJ kg}^{-1}) = 0.4791[\text{C}] + 0.6676[\text{H}] + 0.589[\text{O}] + 1.2077[\text{S}] - 8.42$	Residue-derived fuels
3	Jenkins et al. (1985) [17]	$\text{HHV}(\text{MJ kg}^{-1}) = -0.763 + 0.301[\text{C}] + 0.525[\text{H}] + 0.064[\text{O}]$	All types of biomass
4	Sheng et al. (2005) [18]	$\text{HHV}(\text{MJ kg}^{-1}) = -1.3675 + 0.3137[\text{C}] + 0.7009[\text{H}] + 0.0318[\text{O}]$	Wide range of biomass materials
5	Yin (2011) [19]	$\text{HHV}(\text{MJ kg}^{-1}) = 0.2949[\text{C}] + 0.8250[\text{H}]$	Wide range of lignocellulosic materials (agricultural by-products and wood)
6	Callejón-Ferre et al. (2011) [20]	$\text{HHV}(\text{MJ kg}^{-1}) = -3.440 + 0.517([\text{C}] + [\text{N}]) - 0.433([\text{H}] + [\text{N}])$	Greenhouse crop residues
<i>Based on Proximate Analysis</i>			
7	Jenkins et al. (1985) [17]	$\text{HHV}(\text{MJ kg}^{-1}) = 26.601 - 0.304[\text{Ash}] - 0.082[\text{VM}]$	All biomass
8	Jiménez et al. (1991) [21]	$\text{HHV}(\text{MJ kg}^{-1}) = -10.81408 + 0.3133([\text{VM}] + [\text{FC}])$	Lignocellulosic residues
9	Sheng et al. (2005) [18]	$\text{HHV}(\text{MJ kg}^{-1}) = -3.0368 + 0.2218[\text{VM}] + 0.2601[\text{FC}]$	Wide range of biomass materials
10	Yin (2011) [19]	$\text{HHV}(\text{MJ kg}^{-1}) = 0.1905[\text{VM}] + 0.2521[\text{FC}]$	Wide range of lignocellulosic materials (agricultural by-products and wood)
11	Callejón-Ferre et al. (2011) [20]	$\text{HHV}(\text{MJ kg}^{-1}) = -2.057 - 0.092[\text{Ash}] + 0.279[\text{VM}]$	Greenhouse crop residues

Table 3.1 (continuation) - Correlations for calculation of HHV

No.	Reference	Correlation	Assumptions
<i>Based on Elemental and Proximate Analyses</i>			
12	IGT [22]	$\text{HHV}(\text{MJ kg}^{-1}) = 0.341[\text{C}] + 1.323[\text{H}] + 0.068[\text{S}] - 0.0153[\text{Ash}] - 0.1194([\text{O}] - [\text{N}])$	Derived from the properties of more than 700 coal samples
13	Grabosky et al. (1981) [23]	$\text{HHV}(\text{MJ kg}^{-1}) = 0.328[\text{C}] + 1.4306[\text{H}] - 0.0237[\text{N}] + 0.0929[\text{S}] - (1 - [\text{Ash}]/100)(40.11 [\text{H}]/[\text{C}])$	For biomass materials it is based on the pertinent reactions of C, H, S and N to CO ₂ , H ₂ O, SO ₂ and NO ₂
14	Channiwala et al. (2002) [14]	$\text{HHV}(\text{MJ kg}^{-1}) = 0.3491[\text{C}] + 1.1783[\text{H}] + 0.1005[\text{S}] - 0.1034[\text{O}] - 0.0151[\text{N}] - 0.0211[\text{Ash}]$	Solid, liquid and gaseous fuels
15	Callejón-Ferre et al. (2011) [20]	$\text{HHV}(\text{MJ kg}^{-1}) = 9.756 - 309.454[\text{VM}]^{-1} + 6.164[\text{H}]^{-1} + 0.006[\text{C}]^2$	Greenhouse crop residues
Note: [C]-carbon content; [H]-hydrogen content; [N]-nitrogen content; [S]-sulphur content; [O]-oxygen content; [FC]-fixed carbon content; [VM]-volatile matter content; [Ash]-ash content, expressed in wt% on dry basis.			

3.3 Results and discussion

3.3.1 Materials characterization

The proximate and elemental analyses of the biowastes herein considered are presented in Table 3.2. From the proximate analysis it can be observed that all samples have moisture contents below 7%, which favours an easy ignition and prevents reduction of the heating value due to the energy needed to evaporate the additional moisture. Regarding the ash content, in the case of agricultural biomass, all values are below 4%, in contrast with the industrial biowastes which showed significantly higher ash contents (above 37%). High percentages of ash could affect the pyrolysis process due to clinkering and slagging problems that may cause blockages during the industrial process. Regarding the volatile matter content, agricultural biomass samples reached over 70%, whereas the primary and biological paper mill sludge had 44% and 58%, respectively. The energy value that can be obtained from each material is closely related to the elemental composition, *i.e.*, high ratios of H/C and O/C reduce the energy value of the fuel. As can be observed in Table 3.2, the H/C ratios are very similar between the agricultural and industrial biowastes here considered. On the other hand, it was observed that high O/C ratios result in lower HHVs, with the exception of GS and BS. As shown in Figure 3.1 there is a linear relation between HHV_{exp} and O/C ratio ($r^2=0.794$); however, GS and BS did not have the same trend and a higher coefficient of determination was obtained when these materials were excluded from the linear regression ($r^2=0.952$). Regarding the content of S, both agricultural and industrial biowastes showed low or null values when compared with conventional fuels (0.7-4.9%) [24], which reduces the probability of releasing sulphur compounds during combustion or pyrolysis, such as H₂S and SO₂, that negatively affect the environment (*e.g.* contribute to acidification of soil and water), and the human health (*e.g.* its inhalation can cause respiratory diseases and premature deaths from cardiopulmonary diseases) [25].

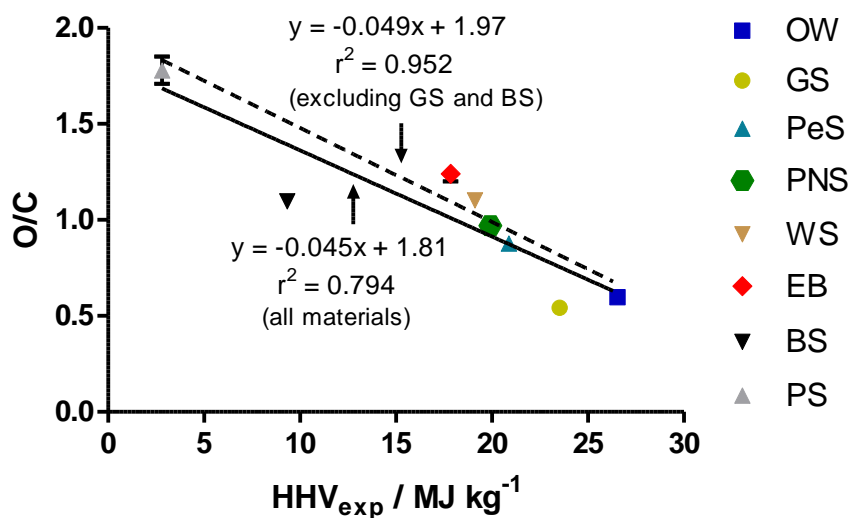


Figure 3.1 - Graphical representation of O/C ratio versus HHV_{exp} for the studied agricultural and industrial wastes (— linear regression using all materials; ---- linear regression excluding GS and BS).

A complete physicochemical characterization of these agricultural and industrial biowastes, before and after pyrolysis, may be found in the next Chapters 4 and 5. Briefly, Fourier transform infra-red spectroscopy (FTIR) analysis of the agricultural materials showed typical bands corresponding to cellulose and/or aliphatic chains, aromatic linkages from lignin, hemicelluloses and also phenols, alcohols and carboxylic groups. PS and BS FTIR analysis indicated the presence of typical bands of cellulose and possible carbonyl groups of hemicelluloses, likewise the agricultural biowastes. However, the industrial biowastes also showed characteristic bands of carbonates in its composition. The presence of carbonates in the industrial biowastes could be the reason for such high values of ash content observed in proximate analysis (Table 3.2). After pyrolysis, due to the cellulose and hemicelluloses thermal decomposition, the aliphatic groups disappeared and some aromatic groups remain for both agricultural and industrial biowastes. Nevertheless, after pyrolysis, PS still presented the peaks corresponding to carbonates. Regarding the physical characterization, biochars produced by agricultural biowastes and by BS revealed low specific surface area (S_{BET} ranging from 2 up to $11 \text{ m}^2 \text{ g}^{-1}$) with a negligible microporous development. In contrast, biochar from PS presented a relatively high specific surface area when pyrolysed at $800 \text{ }^\circ\text{C}$ during 10 min ($121 \text{ m}^2 \text{ g}^{-1}$) and there was a steep increase with the increase of pyrolysis residence time from 10 to 150 min, reaching $209 \text{ m}^2 \text{ g}^{-1}$. Consequently, micropore volume was also much higher for pyrolysed PS ($0.078 \text{ cm}^3 \text{ g}^{-1}$) and pore radius was much lower (0.63 nm).

Table 3.2 - Proximate analysis, elemental analysis and calorific values determined for the studied agricultural and industrial wastes

Sample	Agricultural Residues						Industrial Residues		
	EB	PNS	WS	PeS	GS	OW	PS	BS	
Proximate analysis (%) ^a	Moisture content	1.1	0.4	1.6	6.3	1.2	1.1	1.6	5.5
	Volatile Matter (VM)	80	73	81	76	76	82	44	58
	Fixed Carbon (FC)	20	23	19	23	21	16	0.56	5.6
	Ash	0.8	3.7	0.5	1.2	3.3	1.9	55	37
Elemental analysis (%) ^a	C	42.0 ± 0.9	46 ± 1	44.31 ± 0.01	48.9 ± 0.2	55.4 ± 0.2	55.83 ± 0.06	15.5 ± 0.5	27.2 ± 0.1
	H	4.6 ± 0.9	4.4 ± 0.4	5.4 ± 0.3	5.70 ± 0.02	6.99 ± 0.07	6.2 ± 0.4	1.2 ± 0.1	3.04 ± 0.01
	N	0.7 ± 0.4	1.3 ± 0.4	0.96 ± 0.01	1.3 ± 0.2	4.2 ± 0.1	2.65 ± 0.04	0 ± 0	2.71 ± 0.04
	S	0 ± 0	0 ± 0	0 ± 0	0 ± 0	0 ± 0	0 ± 0	0.21 ± 0.04	0.6 ± 0.1
	O ^b	52 ± 1	45 ± 1	48.8 ± 0.3	42.9 ± 0.3	30.1 ± 0.2	33.4 ± 0.4	27.7 ± 0.5	29.9 ± 0.2
	H/C	0.11 ± 0.02	0.10 ± 0.01	0.12 ± 0.01	0.117±0.001	0.126±0.001	0.11 ± 0.01	0.08 ± 0.01	0.112±0.001
	O/C	1.24 ± 0.04	0.97 ± 0.03	1.10 ± 0.01	0.878±0.007	0.543±0.004	0.60 ± 0.01	1.78 ± 0.07	1.110±0.008
HHV _{exp} (MJ kg ⁻¹)	18	20	19	21	24	27	2.8	9.3	

^aElemental (±standard deviation) and proximate analyses are presented on a dry basis.

^bEstimated by difference: O (%) = 100-C-H-N-S-Ash.

Note: [C]-carbon content; [H]-hydrogen content; [N]-nitrogen content; [S]-sulphur content; [O]-oxygen content.

3.3.2 Heat of combustion

The total energy released when the fuel is burned in air, including the latent heat contained in the water vapour, that could be potentially recoverable from a given biomass source is represented by the HHV. Table 3.2 presents the HHV of each biomass measured with a calorimeter bomb (HHV_{exp}). It can be easily observed that the agricultural biowastes have higher calorific values than the paper mill sludge (industrial biowastes). As described before, although both types of biowastes are cellulosic materials, they have quite different elemental and proximate composition, especially regarding the ash and volatile matter content, leading to different calorific values. When compared with fossil coals, almost all agricultural biowastes, especially PNS, PeS, GS and OW (Table 3.2), have equivalent HHV (20-30 MJ kg⁻¹) [26,27], making them highly competitive for combustion applications, such as fuel and power generation through the use of heat and catalysts [4].

Figure 3.2 shows the HHV calculated from the different correlations summarized in Table 3.1 and, for each case, the previously determined HHV_{exp} is represented together with a deviation limit of $\pm 10\%$. There are some correlations that satisfactorily estimate the HHV of the agricultural residues here presented, mostly those based on elemental and both elemental and proximate analyses. Correlations based only on proximate analysis (No. 7-11 in Table 3.1) overestimate the HHV in case of EB and underestimate the HHV in case of GS and OW. Jenkins (1980) [16] correlation based only on elemental analysis and Callejón-Ferre et al. (2011) [20] correlation based on both elemental and proximate analyses, mainly in volatile matter content (No. 2 and 15, respectively), are those that best estimated the value of all agricultural residues within the 10% limit of the HHV_{exp} . Contrarily, the correlations that better estimated the HHV of the primary and the biological paper mill sludge were IGT [22] and Channiwala et al. (2002) [14] (No. 12 and 14, respectively), which take into account elemental analysis and the ash content from proximate analysis. Disparities on the most adequate correlation to estimate HHV of agricultural and industrial biowastes here considered may be related with their different properties, as shown in Table 3.2. The application of correlations to estimate HHV could be useful to evaluate the calorific potential of a residue quickly and without recurring to calorimetric techniques.

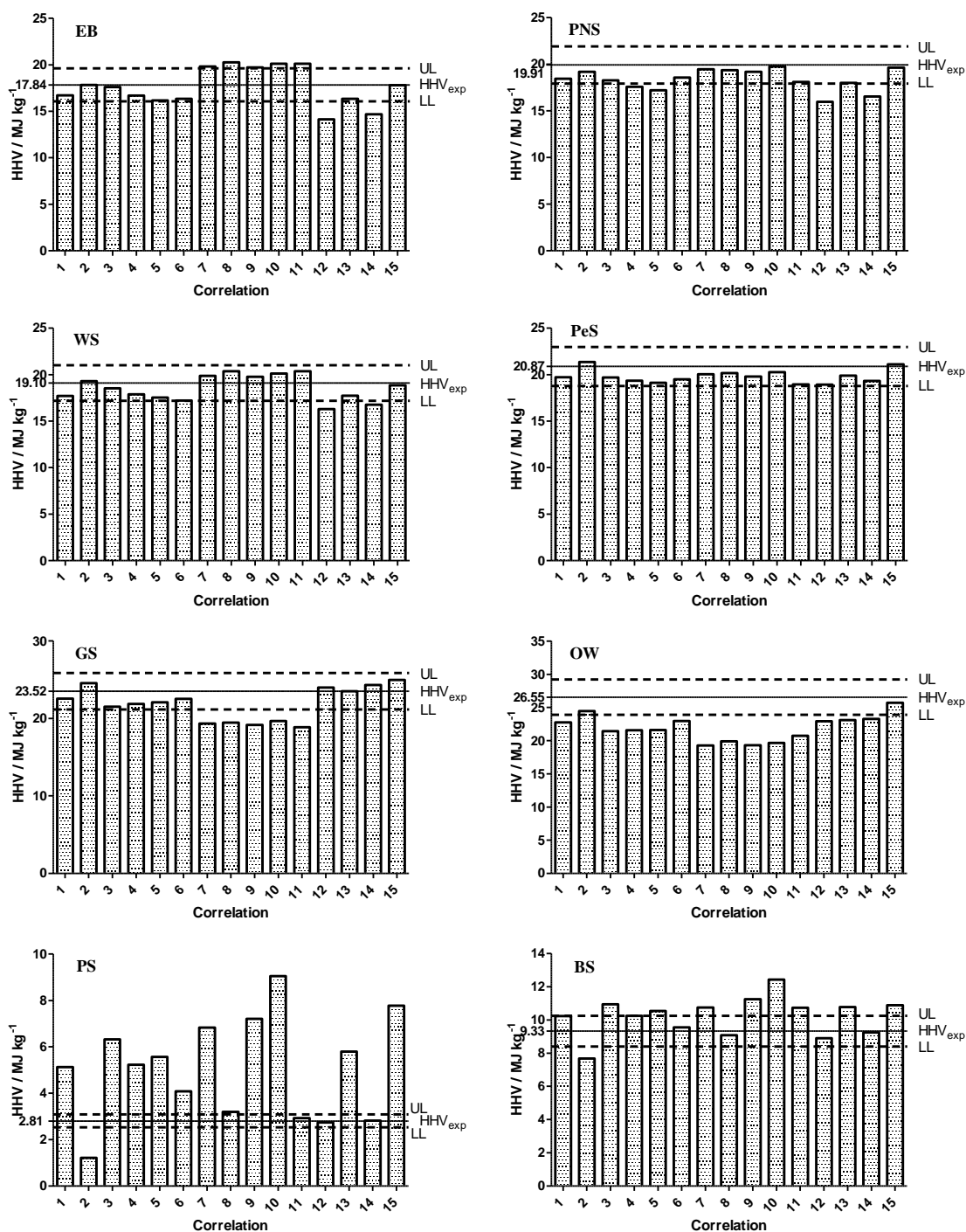


Figure 3.2 - Calculated and measured HHV for each material. UL - upper limit ($HHV_{exp} + 10\%$); LL - lower limit ($HHV_{exp} - 10\%$). Note that y-axis scale is not the same in all graphs to allow a better visualization of the results. Correlations No. 1-15 are listed in Table 3.1.

3.3.3 TG-MS results

The thermogravimetric (TG) and derivative thermogravimetric (DTG) curves obtained from the pyrolysis of each material, in the conditions described in section 3.2.2.4, are presented in Figure 3.3. In Table 3.3, the characteristic parameters of the pyrolysis profiles are shown. The TG curves corresponding to agricultural residues showed one weight loss, between 170 and 750 °C, due to hemicellulose and cellulose decomposition [28]. As it may be seen in Table 3.3 and in DTG curves (Figure 3.3), the pyrolysis yield (and also the ash free pyrolysis yield, as the ash content of these residues is very low) was about 20%, with a maximum weight loss rate between 30 and 48% min⁻¹ at about 400 °C. On the other hand, industrial bioresidues (PS and BS) had a distinct behaviour showing two clearly different weight loss steps: the first, between approximately 200 and 600 °C, with a maximum weight loss rate between 7 (PS) and 13% min⁻¹ (BS) approximately at 350-380 °C, corresponds to decomposition of the most thermo-labile fraction of organic matter, such as cellulose and hemicelluloses; and the second, between 600 and 955 °C, resulting from the decomposition of thermo-resistant organic matter along with decomposition of carbonates [29], with 20 (PS) and 16% min⁻¹ (BS) of maximum weight loss rate around 820-840 °C. In the case of industrial biowastes, the pyrolysis yield was 55% for PS and 40% for BS; however, due to their high ash content (Table 3.2), the effective yield (ash free pyrolysis yield) was much lower, as can be seen in Table 3.3. Despite that, the solid product resulting from the PS pyrolysis presented favourable properties to be used as adsorbent, as will be seen in the next Chapter 5.

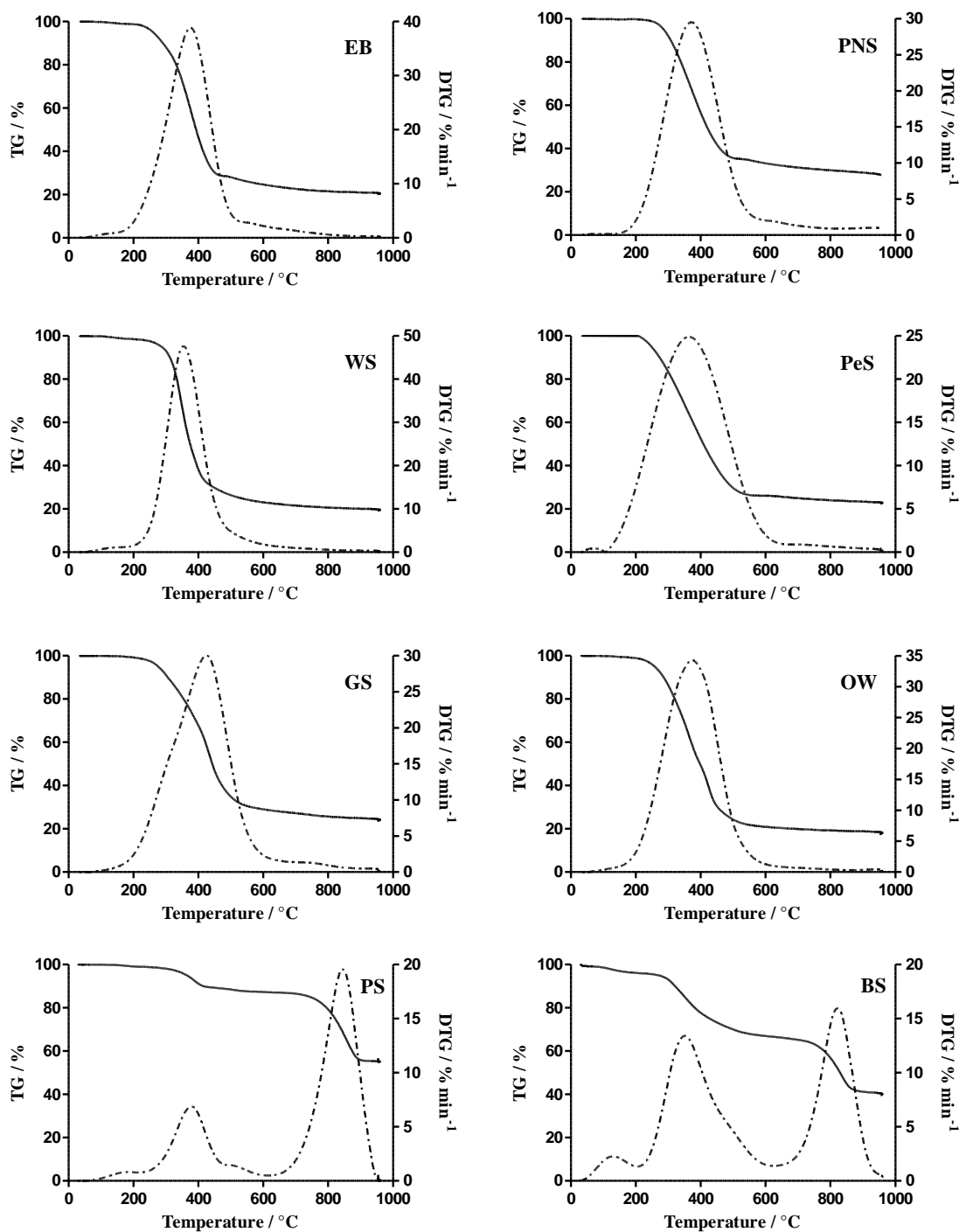


Figure 3.3 - Thermogravimetric (— TG) and derivative thermogravimetric (— • — DTG) curves corresponding to the pyrolysis of each material.

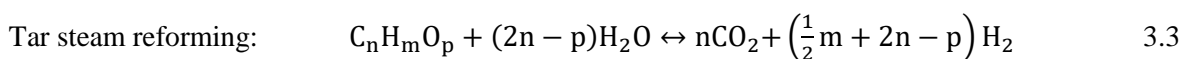
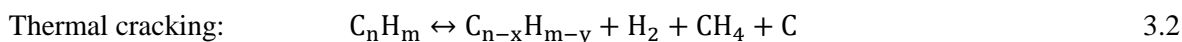
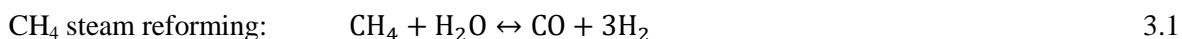
Table 3.3 - Characteristic parameters obtained from the TG and DTG curves corresponding to the agricultural and industrial wastes

	First Step of decomposition				Second Step of decomposition				r_p (%)	$r_{ash\ free}$ (%)
	$T_{i,1}$ (°C)	$T_{max,1}$ (°C)	$T_{f,1}$ (°C)	$DTG_{max,1}$ (% min ⁻¹)	$T_{i,2}$ (°C)	$T_{max,2}$ (°C)	$T_{f,2}$ (°C)	$DTG_{max,2}$ (% min ⁻¹)		
EB	192	376	680	39	-	-	-	-	20	19
PNS	226	371	679	30	-	-	-	-	28	24
WS	214	354	691	48	-	-	-	-	19	19
PeS	197	364	644	25	-	-	-	-	23	22
GS	190	425	751	30	-	-	-	-	24	21
OW	170	373	670	34	-	-	-	-	18	16
PS	258	379	548	7	684	844	954	20	55	0.30
BS	231	351	577	13	664	822	955	16	40	6

Note: T_i -initial thermal decomposition temperature; T_{max} -temperature of maximum rate of weight loss; T_f -final pyrolysis temperature detected as mass stabilization; DTG_{max} -maximum weight loss rate; r_p -pyrolysis yield; $r_{ash\ free}$ -ash free pyrolysis yield. The indexes 1 and 2 correspond to first and second steps of decomposition, respectively.

In order to obtain more complete information about the pyrolysis of each type of biomass, mainly regarding the emission of gaseous compounds, thermal/gas analysis was performed by coupling the TG analyser with mass spectrometer (TG-MS). This analysis provides the evolution of different volatile products which gives information on the chemical reactions occurred during the pyrolysis process. This study focused on the production of permanent gases such as H₂, CO, CO₂, some light hydrocarbons including CH₄, C₂H₂ and C₂H₆ and H₂O, which have been assigned to the *m/z* indicated in Table 3.4 [30]. For each of the *m/z* considered in this work, Figure 3.4 represents emissions throughout the temperature programmed pyrolysis of each waste. Also, integrated areas corresponding to the emission peak of each *m/z* for the different residues herein considered are given in Table 3.4.

The H₂ peaks (*m/z* 2) of all materials were detected in the last stages of thermal decomposition (maximum intensity at approximately 700 and 800 °C for industrial and agricultural biowastes, respectively) and may correspond to the condensation of aromatic structures or the decomposition of cellulose, hemicelluloses and lignin [30]. Moreover, some authors ascribed the production of H₂ through CH₄ consumption, by CH₄ steam reforming reactions (Eq. 3.1) or by secondary reactions such as thermal cracking (Eq. 3.2) or/and tar steam reforming (Eq. 3.3) [31].



CH₄ (*m/z* 16) was generated between 400 and 600 °C, mainly from agricultural residues, as shown in Figure 3.4, which is coincident with the weight loss showed by TG curves (Figure 3.3). Arenillas et al. (1999) [32] reported that the higher the volatile matter content, the more groups are likely to produce CH₄ during the pyrolysis processes. This is corroborated by the proximate analysis values (Table 3.2) and the integrated peak areas (Table 3.4), *i.e.*, the lower volatile matter content of the industrial residues resulted in a lower CH₄ production. The same conclusion could be taken for the remaining light hydrocarbons C₂H₂ and C₂H₆ (*m/z* 26 and 30, respectively), which are produced by the decomposition of the most thermo-labile fraction of organic matter, such as cellulose and hemicelluloses. Even so, BS presented a well-defined peak centred around 840 °C with *m/z* 16, which suggests that secondary reactions took place, namely tar cracking reactions, (Eq. 3.2 and Eq. 3.3), being CO₂, CH₄ and H₂ the main products of these reactions [30,31].

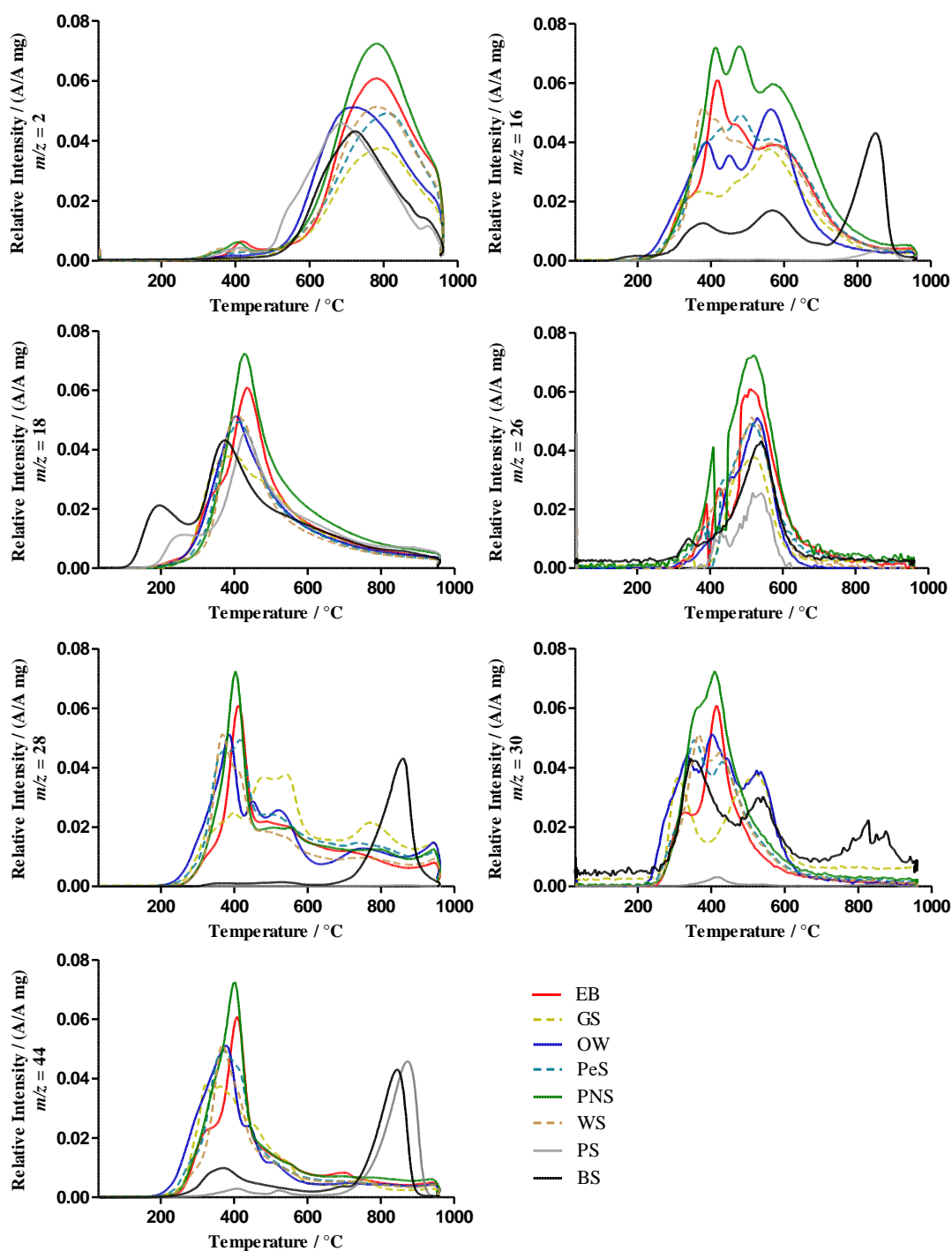


Figure 3.4 - Evolution curves of the gaseous products during pyrolysis process.

The evolution of H_2O (m/z 18) during pyrolysis process may arise from two different pathways (Figure 3.4) in the first one, the lowest temperature peak (more perceptible for PS and BS) reflected the moisture of the samples; in the second one, the peak at high temperature (between 300 and 600 °C) corresponds to the H_2O production by decomposition of oxygen-containing

groups, mainly OH groups. In this case, the oxygen content plays an important role in the H₂ and H₂O release, *i.e.*, the higher the oxygen content, the lower the H₂ emission, due to the pyrolytic formation of water in a broad range of temperature.

Oxygen content can also influence the formation of CO (*m/z* 28) by reaction with the most labile functional groups. It is important to note that *m/z* 28 may also be assigned to N₂ emission; however, due to the low content of the element N in the samples (Table 3.2), it was assumed that this corresponds to the CO emission. On the other hand, Huang et al. (2011) [30] reported that the H₂O and the char may interact to produce CO, according to Eq. 3.4:



which is the gasification of char with steam. They also ascribed the production of CO₂ (*m/z* 44) by self-gasification of biomass, following the Eq. 3.5:



These could be possible pathways to the CO and CO₂ emission at temperatures between 300 and 600 °C during the pyrolysis of the agricultural residues; however, PS and BS present well defined peaks (*m/z* 28 and 44) at about 840 °C, so, for this type of residues, the CO and CO₂ emission probably results from the decomposition of the carbonates at high temperatures [29].

Overall, the pyrolysis of agricultural biowastes resulted in more emissions of gaseous products when compared with industrial biowastes, mainly products containing the carbon element (CH₄, C₂H₂, CO and CO₂), as can be seen in Table 3.4, which could be used as fuel gas (*e.g.* syngas). Moreover, due to the low or null content of S element in the structure of all bioresidues (Table 3.2), it could be concluded that sulphur compounds, such as H₂S and SO₂, were not generated which is considered as an advantage when compared with fossil fuels.

Table 3.4 - Integrated peak areas of the gaseous compounds evolved during temperature programmed pyrolysis of each material

<i>m/z</i>	Assignment	Integrated peak areas ($\times 10^{-2}$ min mg ⁻¹)							
		EB	PNS	WS	PeS	GS	OW	PS	BS
2	H ₂ ⁺	24.2	27.5	21.2	20.0	15.1	21.7	16.9	15.4
16	CH ₄ ⁺	20.1	28.2	19.4	20.2	15.1	17.7	0.7	10.7
18	H ₂ O ⁺	16.1	19.1	13.1	13.8	14.1	15.0	15.7	16.4
26	C ₂ H ₂ ⁺	11.4	15.9	9.6	10.4	8.3	8.0	3.7	13.3
28	CO ⁺	14.4	16.8	14.1	18.6	20.1	17.8	0.1	5.7
30	C ₂ H ₆ ⁺	10.0	16.1	11.2	12.2	18.8	15.1	0.5	26.4
44	CO ₂ ⁺	12.4	14.7	10.8	12.4	11.2	12.4	6.3	7.2

3.4 Conclusions

All the materials considered in this work consist of lignocellulosic biomass; however, significant differences in their composition were noted, which affect their possible valorisation through combustion and pyrolysis. Agricultural residues had larger HHVs than those obtained for industrial residues, due to their high volatile matter content and low ash content. The calorific values of agricultural residues were very close to those usually obtained from fossil coals (20-30 MJ kg⁻¹), making them highly competitive for combustion applications, such as fuel and power generation. The solid products from the PS and BS pyrolysis have good properties to be used as adsorbents for possible applications as adsorbent in water remediation. Regarding the gaseous products, there was no formation of sulphur compounds in the pyrolysis of both agricultural and industrial biowastes, due to their low or null values of S element, which is considered as an advantage when compared with fossil fuels.

3.5 References

- [1] Ferreira, C.I.A., Calisto, V., Cuerda-Correa, E.M., Otero, M., Nadais, H. and Esteves, V.I., 2016, *Bioresource Technology*, 218, 918-925.
- [2] COM, 2013, Green Paper: A 2030 framework for climate and energy policies, COM(2013) 169 final, *European Commission*, Brussels.
- [3] COM, 2008, Green Paper: On the management of bio-waste in the European Union, COM(2008) 811 final, *Commission of the European Communities*, Brussels.
- [4] Brown, R.C., 2011, *Thermochemical Processing of Biomass*, John Wiley & Sons, Ltd, 1-12.
- [5] Götze, R., Boldrin, A., Scheutz, C. and Astrup, T.F., 2016, *Waste Management*, 49, 3-14.
- [6] Wu, L.M., Zhou, C.H., Tong, D.S. and Yu, W.H., 2014, *Bioenergy Research: Advances and Applications*, Elsevier, Amsterdam, 243-254.
- [7] Strezov, V. and Evans, T.J., 2014, *Biomass Processing Technologies*, CRC Press.
- [8] Stubenberger, G., Scharler, R., Zahirović, S. and Obernberger, I., 2008, *Fuel*, 87 (6), 793-806.
- [9] Kuppusamy, S., Thavamani, P., Megharaj, M., Venkateswarlu, K. and Naidu, R., 2016, *Environment International*, 87, 1-12.
- [10] Valenzuela, C. and Bernalte, A., 1985, *Boletín Geológico y Minero*, XCVI (I), 58-61.
- [11] ASTM D5373, Standard Test Methods for Instrumental Determination of Carbon, Hydrogen, and Nitrogen in Laboratory Samples of Coal C, H, N Coal & Coke, *ASTM International*, West Conshohocken, PA, 1993, www.astm.org.
- [12] ASTM D4239, Standard Test Method for Sulfur in the Analysis Sample of Coal and Coke Using High Temperature Tube Furnace Combustion Sulfur Coal & Coke, *ASTM International*, West Conshohocken, PA, 2014, www.astm.org.
- [13] AENOR, 2011. Biocombustibles sólidos. Determinación del poder calorífico. *Asociación Española de Normalización y Certificación*.
- [14] Channiwala, S.A. and Parikh, P.P., 2002, *Fuel*, 81 (8), 1051-1063.
- [15] Tillman, D.A., 1978, *Wood as an energy resource*, Academic Press, New York.
- [16] Jenkins, B.M., 1980, *Downdraft gasification characteristics of mayor California residue derived fuels*, University of California, Davis.

- [17] Jenkins, B.M. and Ebeling, J.M., 1985, *California Agriculture*, 39 (5/6), 14-16.
- [18] Sheng, C. and Azevedo, J.L.T., 2005, *Biomass and Bioenergy*, 28 (5), 499-507.
- [19] Yin, C.-Y., 2011, *Fuel*, 90 (3), 1128-1132.
- [20] Callejón-Ferre, A.J., Velázquez-Martí, B., López-Martínez, J.A. and Manzano-Agugliaro, F., 2011, *Renewable and Sustainable Energy Reviews*, 15 (2), 948-955.
- [21] Jiménez, L. and González, F., 1991, *Fuel*, 70 (8), 947-950.
- [22] Bridgwater, A.V., Double, J.M. and Earp, D.M., 1986, *ETSU Report*, UKAEA, Harwell, UK.
- [23] Grabosky, M. and Bain, R., 1981, Properties of biomass relevant to gasification, *Noyes Data Corporation*, New Jersey, 41-69.
- [24] Gräbner, M., 2014, Industrial Coal Gasification Technologies Covering Baseline and High-Ash Coal, *Wiley-VCH Verlag GmbH & Co. KGaA*, 25-106.
- [25] Butz, S., 2014, Energy and Agriculture: Science, Environment, and Solutions, *Cengage Learning*.
- [26] Frau, C., Ferrara, F., Orsini, A. and Pettinau, A., 2015, *Fuel*, 152, 138-145.
- [27] Ahmaruzzaman, M., 2008, *Bioresource Technology*, 99 (11), 5043-5050.
- [28] Ferreira, C.I.A., Calisto, V., Santos, S.M., Cuerda-Correa, E.M., Otero, M., Nadais, H. and Esteves, V.I., 2015, *Journal of Analytical and Applied Pyrolysis*, 112, 313-324.
- [29] Calisto, V., Ferreira, C.I.A., Santos, S.M., Gil, M.V., Otero, M. and Esteves, V.I., 2014, *Bioresource Technology*, 166 (0), 335-344.
- [30] Huang, Y.F., Kuan, W.H., Chiueh, P.T. and Lo, S.L., 2011, *Bioresource Technology*, 102 (3), 3527-3534.
- [31] Sanchez-Silva, L., López-González, D., Villaseñor, J., Sánchez, P. and Valverde, J.L., 2012, *Bioresource Technology*, 109, 163-172.
- [32] Arenillas, A., Rubiera, F. and Pis, J.J., 1999, *Journal of Analytical and Applied Pyrolysis*, 50 (1), 31-46.

Part III

Chapter 4

Application of pyrolysed agricultural biowastes as adsorbents for MS-222 removal from water

Chapter 5

Application of pyrolysed paper mill sludge as adsorbents for fish anaesthetics removal from water

Chapter 6

Study of the influence of operational conditions on the adsorption of MS-222 onto a biological paper mill sludge-based adsorbent

4 Application of pyrolysed agricultural biowastes as adsorbents for MS-222 removal from water

Tricaine methanesulfonate (MS-222) has been widely used in intensive aquaculture systems to control stress during handling and confinement operations. This compound is dissolved in the water tanks and, once it is present in the recirculating aquaculture systems, MS-222 can reach the environment by the discharge of contaminated effluents. This chapter presents the production of alternative adsorbents based on agricultural biowastes (Eucalyptus bark, peanut shells, walnut shells, peach stones, grape seeds and olive waste) for the removal of MS-222 from water. The starting materials and the resulting adsorbents were characterized by elemental and proximate analyses, total organic carbon, FTIR, ^{13}C and ^1H solid state NMR, and SEM. Also, specific surface area and porosity of biochars were determined. Batch kinetic and equilibrium experiments were performed to study the adsorption of MS-222 onto the produced adsorbents. The highest biochars adsorption capacity was obtained using peanut shells (34 mg g^{-1} predicted by the Langmuir-Freundlich model). The commercial activated carbon, used for comparison purposes, reaches 349 mg g^{-1} of maximum adsorption capacity, as predicted by the Langmuir model.

The work presented and discussed in this chapter resulted in the following publication:

[1] Ferreira C.I.A., Calisto V., Santos S.M., Cuerda-Correa E.M., Otero M., Nadais H., Esteves V.I. (2015) Application of pyrolysed agricultural biowastes as adsorbents for fish anaesthetic (MS-222) removal from water. *Journal of Analytical and Applied Pyrolysis*. 112, 313-324. DOI: 10.1016/j.jaap.2015.01.006

4.1 Contextualization

The intensive aquaculture practice imposes high risks on the welfare of fish, making it vulnerable to adverse impacts of disease and environmental conditions. Factors such as stress, water quality and disease caused by bacteria, fungi, parasites and viruses, highly contribute for the mortality rate of farmed fish. In this context, feed, medication and reproduction control are needed to gain an improved and effective production [2]. Tricaine methanesulfonate (MS-222) is the most widely used anaesthetic for several operations in aquaculture activity. This drug is administered by dissolving it directly into the water tank at the desired dosage. The recommended dosages are significantly different among species, *e.g.* varying between 25 mg L⁻¹ for Common carp and 480 mg L⁻¹ for Atlantic halibut, and the exposure times range from seconds or few minutes for high concentrations up to hours for low concentrations [3,4]. Although it is considered of low oral acute toxicity, the prolonged exposure to MS-222 may be fatal for the fish [5]. To the best of our knowledge no records about the degradability and persistence of such anaesthetic on the environment were found, albeit the chemical properties, particularly water solubility (100 g L⁻¹), point at its predominance on the aqueous phase.

The implementation of recirculating aquaculture systems (RASs) provides the opportunity to reduce water consumption and, at the same time, decrease the discharge of waste, especially organic pollutants, into the environment [6]. A typical RAS aims the removal of suspended solids and organic matter, mainly nitrogen-containing compounds; however, as far as we know, the removal of emerging pollutants, as fish anaesthetics, from water has not been considered yet in RASs and few studies have been made in this way. For example, Dawson et al. (1976) [7] tested the adsorption of MS-222, benzocaine and other fish toxicants onto activated carbon and the maximum adsorption capacity obtained was up to 64 mg g⁻¹ for MS-222, but the main drawback of activated carbons is their high price. As an alternative, biochars, which is a stable carbon-rich by-product synthesized through pyrolysis of biomass, may be used for water remediation [8]. Unlike activated carbons, in the production of biochars, the activation step may be avoided, making their production cheaper and environmentally friendlier. Moreover, as mentioned in Chapter 3, the thermal conversion of waste biomass into biochar produces bioenergy, which is considered an alternative energy with low fossil CO₂ emissions [9]. Herewith, biochars produced from the pyrolysis of different types of biowastes have been used for the adsorptive removal of pollutants in wastewater treatment, specifically for the removal of dyes [10-14], heavy metals and metalloids [15-20], and, more recently, emerging pollutants such as pharmaceutical compounds [21-23]. The

use of agricultural biowastes as precursors to biochars production has been considered attractive due to their world wide availability and low or null economic value.

In the present chapter, the adsorptive removal of the fish anaesthetic MS-222 from water was assessed using biochars produced from agricultural biowastes. *Eucalyptus* bark, grape seeds, peach stones, walnut shells, olive waste and peanut shells were used as starting materials. After pyrolysis (without employing any activating agent), the resulting materials were characterized by elemental and proximate analysis, total organic carbon, specific surface area (BET isotherms), mercury porosimetry, FTIR, NMR, and SEM. Then, MS-222 adsorption kinetic and equilibrium batch experiments were performed using the produced biochars.

4.2 Materials and methods

4.2.1 Adsorbent materials

4.2.1.1 Production of agricultural biowaste-based adsorbents

Agricultural biowastes, used as starting materials to produce the alternative adsorbents, were the same described in previous chapter (section 3.2.1.1). *Eucalyptus* bark (EB), grape seeds (GS), walnut shells (WS), peanut shells (PNS), peach stones (PeS) and olive waste (OW) were dried at room temperature for several days, followed by a 24 h period at 105 °C in an oven. Afterwards, EB, GS, PNS and OW were grinded with a blade mill, while WS and PeS with a mortar grinder, in order to obtain different grain sizes. Due to their particular physical characteristics, EB resulted in an extremely light net of fibrous material, impossible to sieve.

The starting materials were transferred into porcelain crucibles and pyrolysed using a muffle (Nüve furnace MF 106), under a N₂ flow. The heating rate was 10 °C min⁻¹ and the maximum temperature of pyrolysis was defined by thermogravimetric analysis (TGA) interpretation (see section 4.3.1). The pyrolysed material was maintained inside the muffle until the temperature reached room temperature under N₂ atmosphere. The effect of the pyrolysis residence time (τ_p) on the adsorption capacity was assessed, *i. e.*, each material was pyrolysed during 10 and 120 min and then their MS-222 adsorption capacity was determined under the same conditions (during 16 h of contact time), following the procedure described in section 4.2.5. According to the performances determined in these preliminary tests (shown in Appendix B), EB, PNS and WS were pyrolysed at 400 °C for 120 min (EB400-120, PNS400-120 and WS400-120, respectively); PeS was pyrolysed at 500 °C for 120 min (PeS500-120); GS and OW were pyrolysed at 500 °C for 10 min (GS500-10 and OW500-10, respectively). Then, all materials were sieved in order to

obtained powdered carbon (< 0.18 mm) and only these were physical and chemical characterized, as shown in Table 4.1.

Table 4.1 - Conditions of adsorbents production

Raw Material	T (°C)	τ_p (min)	Designation
EB	400	10	EB400-10
		120	EB400-120
PNS	400	10	PNS400-10
		120	PNS400-120
WS	400	10	WS400-10
		120	WS400-120
PeS	500	10	PeS500-10
		120	PeS500-120
GS	500	10	GS500-10
		120	GS500-120
OW	500	10	OW500-10
		120	OW500-120

Note: T - pyrolysis temperature; τ_p - pyrolysis residence time. Only materials in bold were characterized.

4.2.1.2 Commercial activated carbon

PULSORB WP270 (Powdered Activated Carbon - PAC) is a commercial activated carbon that were provided and recommended for this application by Chemviron Carbon and used in this work as reference carbon for comparison purposes.

4.2.2 Materials characterization

4.2.2.1 Thermogravimetric analysis (TGA)

Thermal characterization of starting materials was carried out by thermogravimetric analysis (TGA) and derivative thermogravimetric analysis (DTGA). Non-isothermal TG analysis was performed using a TAG analyser (Shimadzu TGA-50 instrument). The analyses were carried out under a $20 \text{ cm}^3 \text{ min}^{-1}$ N_2 flow at a heating rate of $10 \text{ }^\circ\text{C min}^{-1}$ from room temperature to 900-950 $^\circ\text{C}$. Approximately 10 mg of sample was used for each experiment. The weight loss (TG) and derivative curves (DTG) of the samples were represented as a function of temperature, to allow the selection of the pyrolysis temperatures. It is important to mention that this procedure is different from the procedure described in Chapter 3, section 3.2.2.4.

4.2.2.2 Proximate analysis

The proximate analyses were performed using a Setaram SETSYS Evolution-1750 thermal analyser and an experimental procedure proposed by Valenzuela et al. (1985) [24], as described in Chapter 3, section 3.2.2.1.

4.2.2.3 Elemental analysis

The acquisition of the elemental analysis data was performed in a LECO CHNS-932 elemental analyser as described in Chapter 3, section 3.2.2.2.

4.2.2.4 Total organic carbon (TOC)

Total carbon (TC) and inorganic carbon (IC) quantification were carried out in a TOC-VCPH Shimadzu analyser connected to a solid sample module SSM-5000A, on all starting and pyrolysed materials and reference activated carbon. The total organic carbon (TOC) was calculated by difference between TC and IC values. All analyses were performed in triplicate.

4.2.2.5 Fourier Transform Infra-red spectroscopy (FTIR)

FTIR spectra of all materials were performed in a Shimadzu-IRaffinity-1, using an attenuated total reflectance (ATR) module, with a N₂ purge. FTIR measurements were recorded between 600 and 4000 cm⁻¹, 4.0 of resolution, 128 scans and corrected against background and atmosphere.

4.2.2.6 ¹³C CP-MAS NMR and ¹H MAS NMR

All ¹³C CP-MAS NMR and ¹H MAS NMR spectra were acquired on Bruker Avance III 400 spectrometer operating at a B₀ field of 9.4 T. The ¹H and ¹³C Larmor frequencies were 400.1 and 100.6 MHz, respectively. All of the NMR experiments were performed at spinning rates in the range of 10–30 kHz. ¹H and ¹³C were referenced with respect to glycine (NH₃⁺ at 8.35 ppm and C=O at 176.03 ppm). NMR analysis was performed on all starting and pyrolysed materials mentioned above.

4.2.2.7 Physical Characterization

The physical characterization, comprising N₂ adsorption and porosimetry, was carried out on all the pyrolysed materials and PAC: The N₂ adsorption isotherms were acquired at -196 °C using a Quadrasorb Evo apparatus (Quantachrome Instruments). The samples were previously outgassed at 120 °C for 12 h. Mercury intrusion experiments were carried out in a Quantachrome PoreMaster mercury porosimeter. The computational program of the porosimeter used the values of

surface tension and contact angle of 0.480 N m^{-1} and 140° , respectively. The pore size distribution curves were obtained by differentiation of the curves of cumulative volume against pore radius. Macropore volume (V_{ma}) was considered to be the cumulative volume intruded at a pore radius equal to 250 \AA whereas the mesopore volume (V_{me}) was obtained as the difference between the cumulative volume intruded at a pore radius below 20 \AA and V_{ma} . Furthermore, the surface morphology of all starting and pyrolysed materials was observed by scanning electron microscopy (SEM) (Hitachi, SU-70, Japan) at 2 500, 10 000 and 30 000 \times magnification.

4.2.3 Fish anaesthetic

Adsorption tests were performed for the fish anaesthetic Tricaine methanesulfonate, commercially named Tricaine-S, (> 97%, TCI Europe) - MS-222. MS-222 solutions were prepared in ultra-pure water obtained from a Milli-Q Millipore system (Milli-Q plus 185). The MS-222 physico-chemical properties are summarized in Table 2.1 from Chapter 2.

4.2.4 Determination of the MS-222 concentration in water by micellar electrokinetic chromatography (MEKC)

MEKC analyses were performed using a Beckman P/ACE MDQ (Fullerton, CA, USA) instrument, equipped with an UV-Vis detection system, following the procedure described in Appendix C (section C.1.1.1). Aqueous samples and standard solutions were analyzed in triplicate. MS-222 calibration curve and parameters, including the limit of detection (LOD) and limit of quantification (LOQ), are also presented in Appendix C, section C.1.1.

4.2.5 Adsorption experiments

Adsorption experiments were performed in batch system, in polypropylene tubes, by contacting the adsorbent with MS-222 solutions, at a final adsorbent dose of: 50 g L^{-1} for GS500-10 and PeS500-120; 20 g L^{-1} for EB400-120, WS400-120 and OW500-10, and 10 g L^{-1} for PNS400-120. The same procedure was performed with PAC using an adsorbent dose of 0.5 g L^{-1} . Batch tests were carried out in an overhead shaker (Heidolph, Reax 2) at 90 rpm, inside a thermostatic incubator at $25 \text{ }^\circ\text{C}$. At the same time, control experiments were also performed, *i.e.*, the MS-222 solution was shaken under the same conditions but without the presence of the adsorbent. All adsorption tests were performed in triplicate. Before MS-222 adsorption experiments (kinetic and equilibrium studies) tests were performed to guarantee that biochars matrix did not affect the MEKC analyses.

To study the adsorption kinetics, a known MS-222 solution volume (initial concentration of 250 mg L^{-1}) was mixed with the defined amount of each pyrolysed material mentioned before. The study ended when adsorption equilibrium was attained; the sampling times varied from 5 to 7200 min, depending on the adsorbent. The remaining concentration of MS-222 in solution was quantified for each contact time by MEKC analysis. Kinetic data were fitted to pseudo-first order (Eq. 2.2) and pseudo-second order (Eq. 2.3) kinetic models and also to double exponential model (DEM) (Eq. 2.4) using GraphPad Prism 5 software (trial version). These models are described in Chapter 2, section 2.4.3.1.

Adsorption equilibrium experiments were carried out by varying the initial concentration of MS-222 from 50 up to 500 mg L^{-1} . This MS-222 concentration range includes all recommended dosages for fish administration [3], maintaining the adsorbent dosage previously defined. Adsorbents and MS-222 solutions were shaken until equilibrium, after which the MS-222 concentration remaining in solution was determined by MEKC analysis. Equilibrium data were fitted to three non-linear models frequently used to describe adsorption in solid/liquid systems, using GraphPad Prism 5 software: Langmuir model (Eq. 2.7), Freundlich model (Eq. 2.8) and the combination Langmuir-Freundlich (Eq. 2.9), previously described in Chapter 2, section 2.4.3.2.

4.3 Results and discussion

4.3.1 Agricultural biowastes pyrolysis

TG analyses were performed in order to choose the optimum pyrolysis temperature for each biowaste. From Figure 4.1 it can be observed that three distinct weight loss steps occur along the pyrolysis of these materials. The first weight loss, between 50 and $150 \text{ }^{\circ}\text{C}$, corresponds to dehydration of the biomass with a marginal weight loss. The second one, between 150 and $400 \text{ }^{\circ}\text{C}$ for EB, PNS and WS; or between 150 and $500 \text{ }^{\circ}\text{C}$ for PeS, GS and OW, corresponds to the main weight loss ($\sim 60\text{-}70\%$), due to hemicellulose and cellulose decomposition. The third zone is generically ascribed by several authors as lignin decomposition characterized by a slow weight loss ($\sim 10\text{-}30\%$), starting near $190 \text{ }^{\circ}\text{C}$ until $900 \text{ }^{\circ}\text{C}$ [25]. The pyrolysis temperature was selected according to the main weight loss zone in order to release the volatile matter, which might result on materials with highly developed carbonaceous structure, known as good for adsorption. So, EB, PNS and WS were pyrolysed at $400 \text{ }^{\circ}\text{C}$ and PeS, GS and OW were pyrolysed at $500 \text{ }^{\circ}\text{C}$.

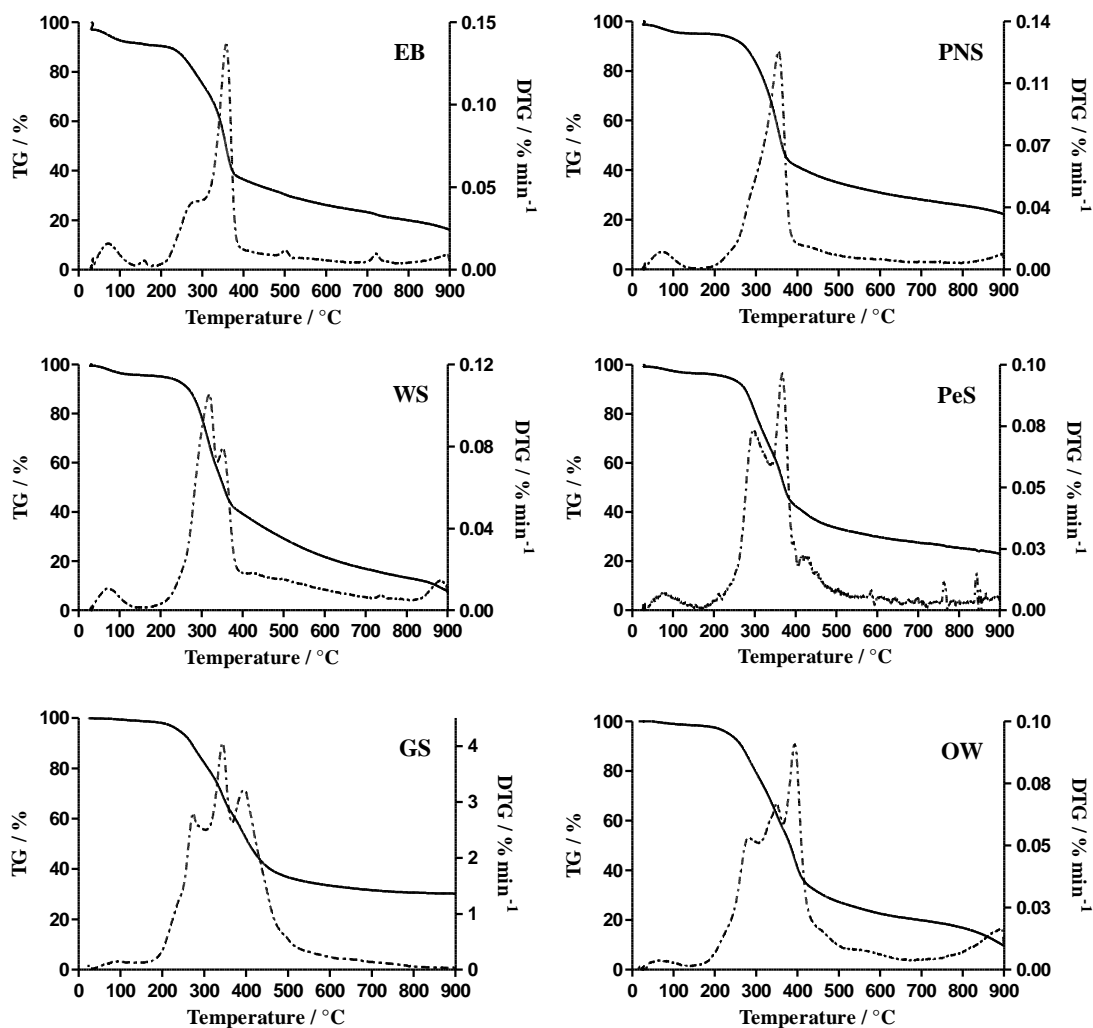


Figure 4.1 - Thermogravimetric (— TG) and derivative thermogravimetric (— • — DTG) curves corresponding to the pyrolysis of agricultural wastes.

Comparing the TG and DTG curves obtained in Chapter 3 with those herein obtained, the first zone (between 50 and 150 °C) was not noticeable perhaps due to the high heating rate used in TG analysis presented in Chapter 3 (80 °C min⁻¹); however, the main weight loss of each biowaste occurred at a similar range of temperatures with a maximum between 350 and 425 °C.

4.3.2 Adsorbents characterization

Table 4.2 summarizes the proximate and elemental analyses of starting and pyrolysed materials. As expected, after pyrolysis, the volatile matter decreases significantly while fixed carbon increases, in all materials. The evolution of the ratio between the volatile matter and fixed carbon is almost the same for all materials, varying between 0.2 and 0.7 after pyrolysis. The ash

content is much lower on starting materials, slightly increasing after pyrolysis with the exception of PNS. Low ash and high carbon content make these wastes good candidates for biochars' precursors. Concerning the elemental analysis, the notable increase of carbon content and the slight decrease of hydrogen content after pyrolysis suggest the occurrence of a satisfactory aromatization of these materials after pyrolysis. The TOC values listed in the Table 4.2 are consistent with elemental analysis while biochar's content in inorganic carbon appears to be negligible. As it may be seen in Table 4.2, WS400-120, PeS500-120 and OW500-10 show similar values of TOC. As a consequence of the increase on carbon content, the oxygen content decreases.

The FTIR spectra of the starting materials and the corresponding pyrolysed materials are presented in Figure 4.2. Concerning the raw materials there are some bands in common: the broad band between 3100 and 3600 cm^{-1} corresponds to phenols, alcohols and carboxylic groups (O-H stretching vibration) [26]; the narrow band around 2900 cm^{-1} is more evident in PNS, PeS, GS and OW and can be attributed to C-H_n stretching of cellulose and/or aliphatic chains [27]; the region from 1500 cm^{-1} up to 1620 cm^{-1} corresponds to aromatic linkages (aromatic and olefinic C=C vibrations) and C=O stretch vibrations from lignin [28]; the small band around 1220 cm^{-1} and the broad band between 1000 and 1050 cm^{-1} result from C-O-C and C-O-(H) stretching, respectively, present in luteolin, cellulose and hemicelluloses [26,28]. Additionally, PNS, PeS, GS and OW show a narrow band at 1750 cm^{-1} corresponding to C=O stretching vibrations present in esters, carboxylic and ketone groups; GS and OW reveal a small band at 1450 cm^{-1} resultant from bending vibration of CH₃ and CH₂ of aliphatic groups [27]. The biochars spectra show less absorption bands mainly due to the cellulose and hemicelluloses decomposition during pyrolysis. The aliphatic groups disappear and only some aromatic groups remain (between 1500 and 1620 cm^{-1}). For GS500-10 and OW500-10 spectra, a small band could be observed at 2900 cm^{-1} corresponding to C-H_n stretching of undecomposed fatty acids, probably due to the lower residence time during pyrolysis.

Table 4.2 - Chemical characterization of all starting and pyrolysed materials

Sample	EB	EB400-120	PNS	PNS400-120	WS	WS400-120	PeS	PeS500-120	GS	GS500-10	OW	OW500-10
<i>Proximate Analysis (wt%, db)^a</i>												
Moisture content	1.1	3.5	0.4	1.9	1.6	1.3	6.3	2.5	1.2	1.5	1.1	1.5
Volatile matter (VM)	80	32	73	32	81	28	76	16	76	38	82	30
Fixed carbon (FC)	20	64	23	65	19	68	23	80	21	53	16	64
Ash	0.8	3.9	3.7	3.3	0.5	3.5	1.2	4.3	3.3	8.7	1.9	6.2
VM/FC ^b	4.0	0.50	3.2	0.49	4.3	0.42	3.3	0.19	3.6	0.72	5.1	0.46
<i>Elemental Analysis (wt%, db)^a</i>												
C	42.0±0.9	67.4±0.7	46±1	66.1±0.8	44.31±0.01	70.5±0.4	48.9±0.2	78.2±0.6	55.4±0.2	64±1	55.83±0.06	70.6±0.7
H	4.6±0.9	3.6±0.2	4.4±0.4	3.4±0.3	5.4±0.3	3.76±0.04	5.70±0.02	3.3±0.2	6.99±0.07	3.0±0.1	6.2±0.4	4.5±0.2
N	0.7±0.4	0.66±0.01	1.3±0.4	1.76±0.07	0.96±0.01	1.77±0.02	1.3±0.2	2.09±0.01	4.2±0.1	3.1±0.1	2.65±0.04	3.9±0.1
S	0 ± 0	0±0	0±0	0±0	0±0	0±0	0±0	0±0	0±0	0±0	0±0	0±0
O ^c	52 ± 1	24.5±0.7	45±1	25.5±0.9	48.8±0.3	20.5±0.4	42.9±0.3	12.2±0.6	30.1±0.2	21±1	33.4±0.4	14.9±0.7
<i>Total organic carbon analysis (%)</i>												
TOC	41.7±0.1	66.87±0.03	45.5±0.3	65.3±0.1	47.2±0.4	70.4±0.3	49.9±0.3	76.6±0.3	54.3±0.6	64.8±0.5	53.6±0.2	70.2±0.3
IC	< LOQ ^d											

^aProximate and elemental analyses are presented on a dry basis (db).

^bRatio between the VM (volatile matter) and FC (fixed carbon) contents.

^cEstimated by difference: O (%) = 100-C-H-N-S-Ash.

^dLimit of quantification (LOQ)=0.104 mg IC.

Note: [C]-carbon content; [H]-hydrogen content; [N]-nitrogen content; [S]-sulphur content; [O]-oxygen content.

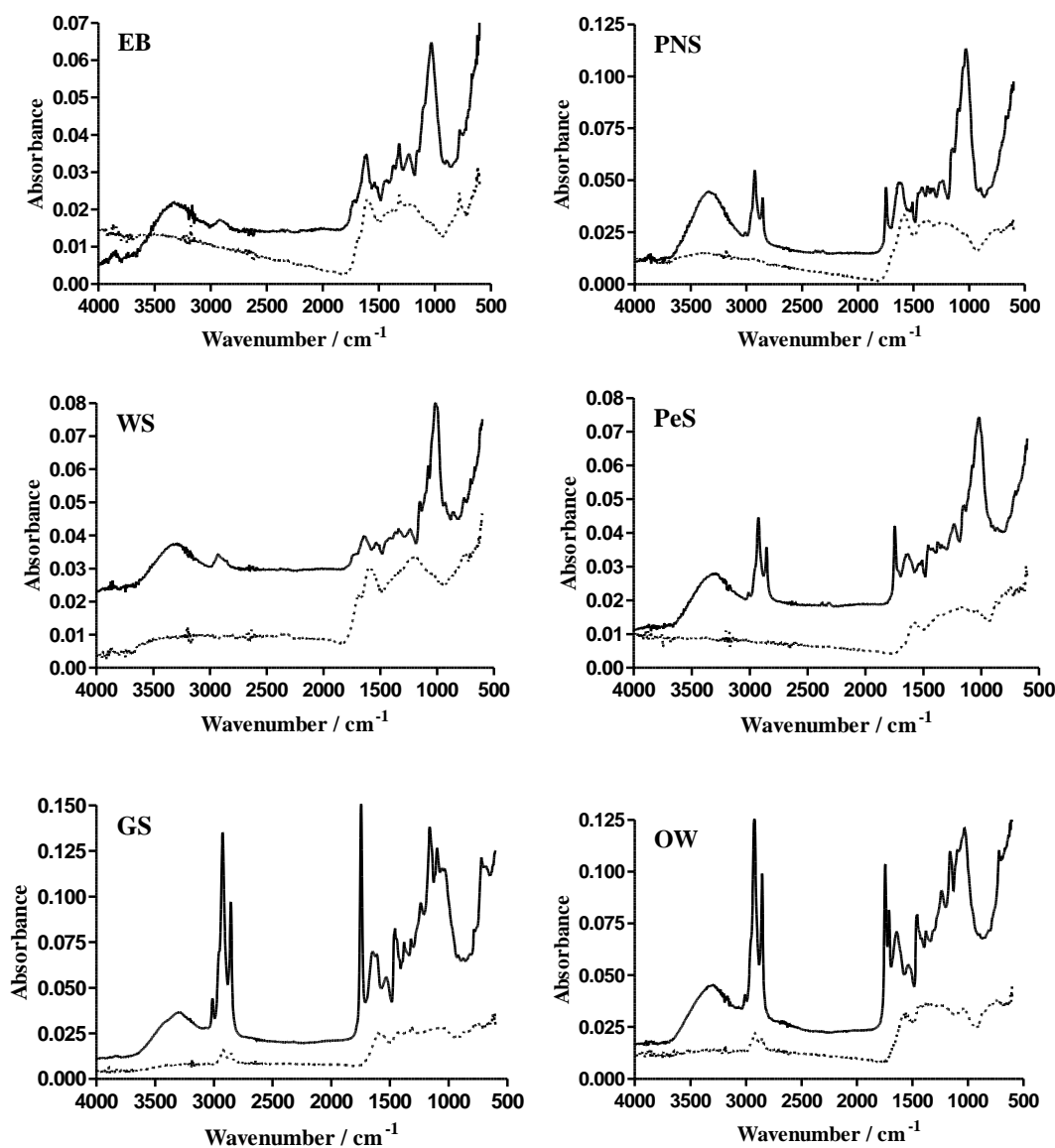


Figure 4.2 - FTIR spectra of starting biowaste materials (—), and their respective biochars (----).

The ^{13}C CPMAS solid state NMR spectra of biowastes used as starting materials and of the corresponding biochars are shown in Figure 4.3. ^{13}C NMR spectra of GS and OW reveal several peaks between 105 and 174 ppm (lignin's aromatic region) that could not be observed on the other raw materials: peak around 115 ppm on GS spectrum is assigned to C5 aromatic carbon of lignin guaiacyl; and region between 130 and 148 ppm on GS and OW spectra corresponding to C1,3,4,5 aromatic carbons of syringyl and C1,4 aromatic carbons of guaiacyl in lignin [29,30]. The signal at 174 ppm on GS, OW, PeS and PNS is assigned to carboxylic groups [28]. Notwithstanding the differences, several matching peaks are also observed in the spectra of these biowastes: at 22 ppm the peak is most likely assigned to CH_3 in acetyl groups of hemicelluloses; the peak at 55 ppm is

assigned to the methoxy groups of lignin; all biomass samples exhibit the strongest signal at 72 ppm, corresponding to C2,3,5 of cellulose; the 84 and 88 ppm peaks are assigned to C4 carbon of amorphous and crystalline cellulose, respectively; the peak at 105 ppm corresponds to C1 carbon of cellulose (anomeric carbon of sugars); and the resonances of C3 and C5 aromatic carbons of lignin syringyl are found around 154 ppm [27,29,30]. The most remarkable spectral feature after pyrolysis is the occurrence of a broad peak ranging from 100 ppm to 160 ppm corresponding to the aromatic groups from lignin, while peaks in the aliphatic region (between 50 and 100 ppm) disappear. EB400-120, PNS400-120, WS400-120 and PeS500-120 spectra have two neighbouring peaks around the broad peak due to the up and downfield shoulder of the signal. However, in all the above mentioned spectra, the high shielded region peak (between 10 and 50 ppm) is more intense than the low shielded region peak (between 200 and 250 ppm), indicating the presence of aliphatic CH₂ from lignin and/or aliphatic acids. Meanwhile, GS500-10 and OW500-10 spectra exhibit, additionally to the peak at 22 ppm, two extra peaks in the aliphatic region that could be assigned to aliphatic CH₂ from lignin and to the residual fatty acids still remaining after pyrolysis [29]. Moreover, the region between 5 and 40 ppm is attributed to methyl amines (CH₃-N) [28] and the strong resonance at around 22 ppm on GS500-10 and OW500-10 spectra confirm the presence of nitrogenous compounds observed on elemental analysis (see Table 4.2). Likewise to FTIR, ¹³C NMR analysis indicates that biowaste starting materials have, in fact, different chemical compositions; however, after pyrolysis, an enhancement of aromatization is observed in the corresponding biochars, *i.e.*, the total organic carbon content increased considerably (Table 4.2). Moreover, both FTIR and ¹³C NMR analyses show evidences of lipidic compounds on GS500-10 and OW500-10.

¹H MAS solid state RMN spectra of starting materials and their corresponding pyrolysed materials are represented in Figure 4.4. EB and WS spectra show a broad peak between -5 and 15 ppm, with a maximum around 4.4 ppm generally assigned to ether or/and alcohol protons of the cellulose structure. Yet a small peak at 1.2 ppm, linked to the broader peak can be observed, indicating the presence of alkyl protons from aliphatic acids (- (CH₂)_n-). The corresponding spectra of pyrolysed materials, EB400-120 and WS400-120, also show the same profile but bands seem broader than in the original materials spectra. These results suggest a high dispersion of the chemical environments of protons, both aliphatic and aromatic, once they include shielded and non-shielded regions. On the other materials (PNS, PeS, GS and OW) narrow peaks are observed, untypical of ¹H solid state NMR, compatible with the presence of liquids in the samples. The most evident peaks are found at 0.8 and 1.2 ppm and are attributable to -CH₂-CH₂-CH₃ and - (CH₂)_n- groups, respectively, from aliphatic acids. Peaks around 1.9 and 4.0 ppm are assigned to unsaturated fatty acids (-CH₂-CH=CH-) and triglycerides (-CH₂-OCOR) and the peak around 5.3

ppm corresponds to $-\text{CH}=\text{CH}-$ protons from unsaturated fatty acids [31,32]. After pyrolysis treatment, PNS400-120, GS500-10 and OW500-10 show a broad band between 0 and 8 ppm, implying dispersion of the protons on chemical environments, with a tendency to the shielded region, suggesting the presence of some aliphatic protons. PeS500-120 spectrum shows chemical shifts at 1.2, 1.9 and 5.3 ppm, corresponding to remaining aliphatic protons. Considering that both FTIR and ^{13}C NMR analyses pointed out the formation of aromatic material with little or no aliphatic groups, the remaining peaks at shielded regions may result from electron delocalization in aromatic structures promoting the existence of highly shielded protons.

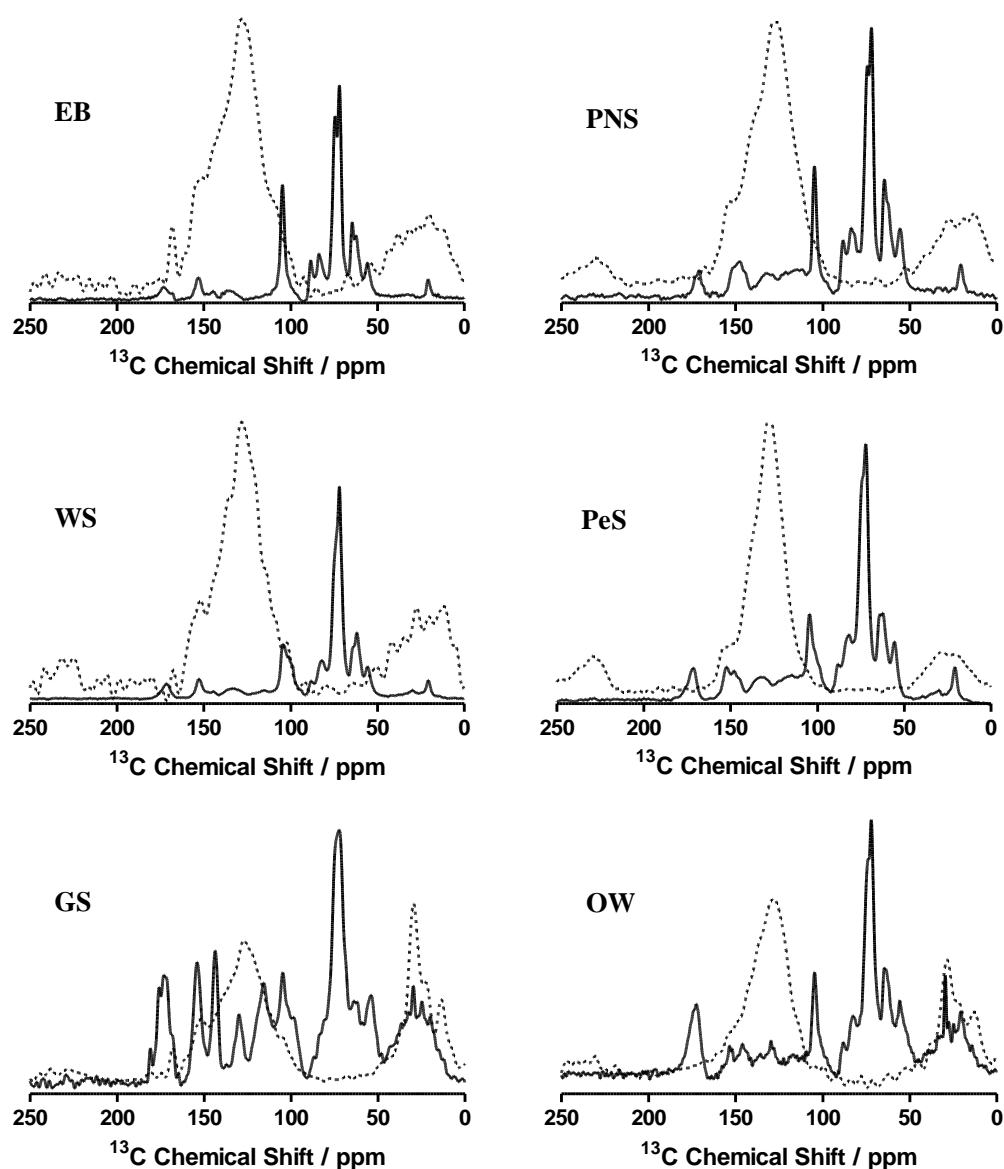


Figure 4.3 - ^{13}C CPMAS solid state NMR of starting materials (—) and respective biochar (----).

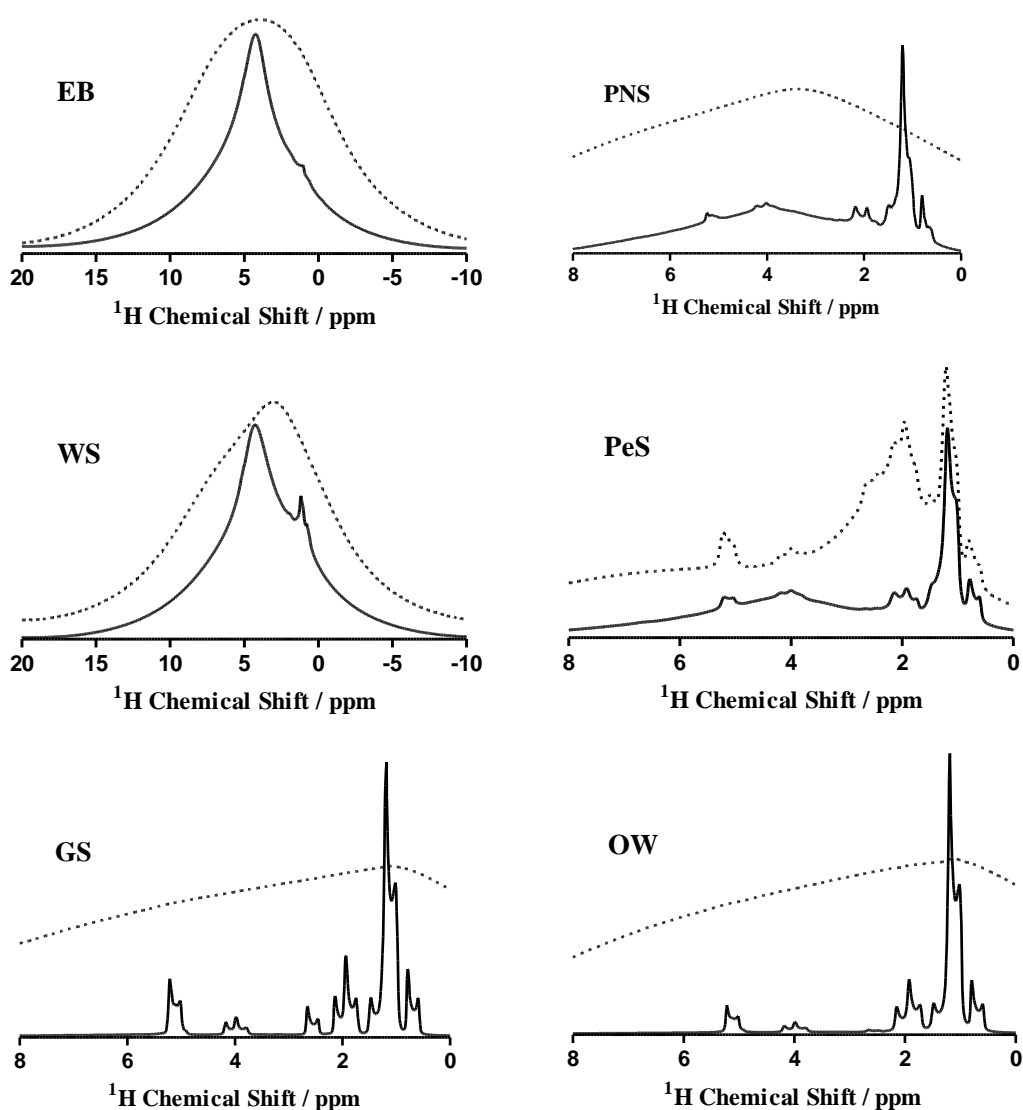


Figure 4.4 - ^1H MAS solid state NMR of starting materials (—) and respective biochar (----).

The textural data of the produced biochars and PAC are presented in Table 4.3. Biochars revealed low specific surface areas (ranging from 2 up to $11\text{ m}^2\text{ g}^{-1}$) with a negligible microporous development, in contrast to what was expected through chemical characterization (high organic carbon content and release of volatile matter and improvement of aromatic structure). Contrary, PAC presents high specific surface area and a highly microporous structure.

Table 4.3 - Textural characterization of the biochars

Sample	N ₂ adsorption at -196 °C			Hg porosimetry					
	S_{BET} (m ² g ⁻¹)	W_0 (cm ³ g ⁻¹)	Average pore radius (nm)	V_{me} (cm ³ g ⁻¹)	V_{ma} (cm ³ g ⁻¹)	Porosity (%)		ρ_{app} (g cm ⁻³)	τ
						Interparticle	Intraparticle		
PAC	1324	0.676	1.19	0.224	0.855	3.33	49.95	0.481	1.628
EB400-120	6	0.001	2.22	0.002	0.292	12.49	27.70	1.220	1.776
PNS400-120	5	0.002	1.87	0.090	0.420	8.92	37.60	0.903	1.704
WS400-120	11	0.002	1.69	0.060	0.367	13.42	26.72	0.926	1.776
PeS500-120	8	0.001	1.24	0.060	0.249	6.52	15.75	0.701	1.978
GS500-10	2	0.001	2.11	0.064	0.119	5.73	23.31	1.513	1.902
OW500-10	5	0.001	1.86	0.028	0.188	9.04	15.45	1.099	1.953

Note: S_{BET} - surface area; W_0 - total micropore volume; V_{me} - mesopore volume; V_{ma} - macropore volume; ρ_{app} - apparent density; τ - tortuosity

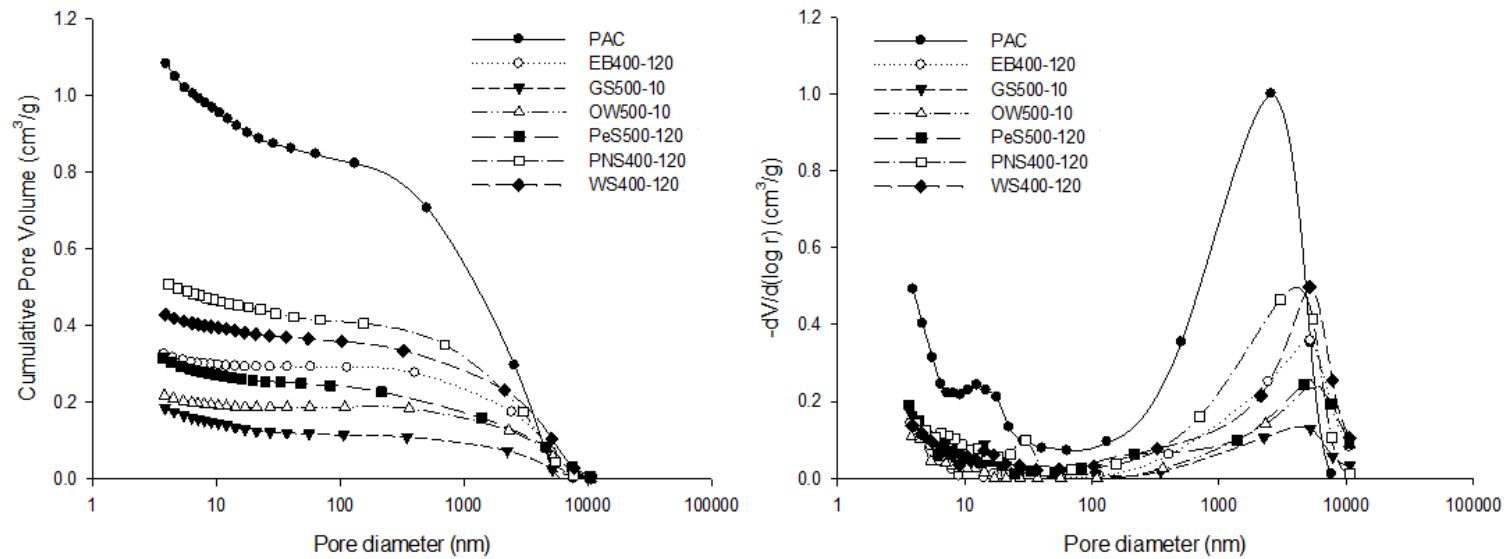


Figure 4.5 - Mercury intrusion curves (left) and corresponding pore size distributions (right) of biochars and PAC.

Figure 4.5 depicts the mercury intrusion curves (left) corresponding to the biochar samples and PAC. It is clearly perceptible that biochars exhibit a less developed meso- and macroporosity. The cumulative pore volume registered for all biochars is remarkably lower than that obtained for PAC along the whole operating interval. Furthermore, the PAC intrusion curve exhibits two steep tracts (5-50 nm and 500-8000 nm) that are clearly indicative of the presence of a well-developed porosity within these pore size intervals. The respective pore size distribution curves (Figure 4.5, right) corroborate these assertions. On the other hand, the textural parameters calculated from the mercury intrusion experiments are listed in Table 4.3. These data reveal that the biochar samples exhibit a moderate development of porosity in terms of wide mesopores and macropores. Intraparticle porosity is the most important contributor to the total porosity of the biochars, with interparticle porosity participating in a less remarkable manner. The tortuosity factor (τ) is closely related to the longer connecting path that is imposed by the occurrence of obstacles within the porous structure of solids. If the porous texture of the solid is attributable to the sole presence of nonintersecting cylindrical pores, the value of τ equals 2 whereas it progressively increases up to values close to 7 as the interconnection degree of the sample increases. From the values of tortuosity summarized in Table 4.3, it may be concluded that the porosity of biochars is constituted by isolated pores of cylindrical geometry.

Morphological characterization was performed by means of SEM analysis in order to assess the effect of pyrolysis on the texture of the materials. Figure 4.6 illustrates the electron micrographs (magnification of 2 500 \times , 10 000 \times and 30 000 \times) of wastes before and after pyrolysis. The starting materials exhibit an organized structure whilst after pyrolysis the destruction of such structure is observed. EB shows a long fiber-shape of cellulose with smooth surface and after pyrolysis at 400 $^{\circ}$ C for 120 min (EB400-120) an irregular surface can be identified most likely due to the destruction of the fiber. PNS, PeS, GS and OW revealed an irregular structure with smooth and homogeneous surface with absence of cracks and macropores; after pyrolysis these materials show a rough surface and crumbly texture with an overlap of layers. SEM micrograph of WS shows a well-developed network of channels and macropores while the pyrolysed material (WS400-120) holds large and irregular pores.

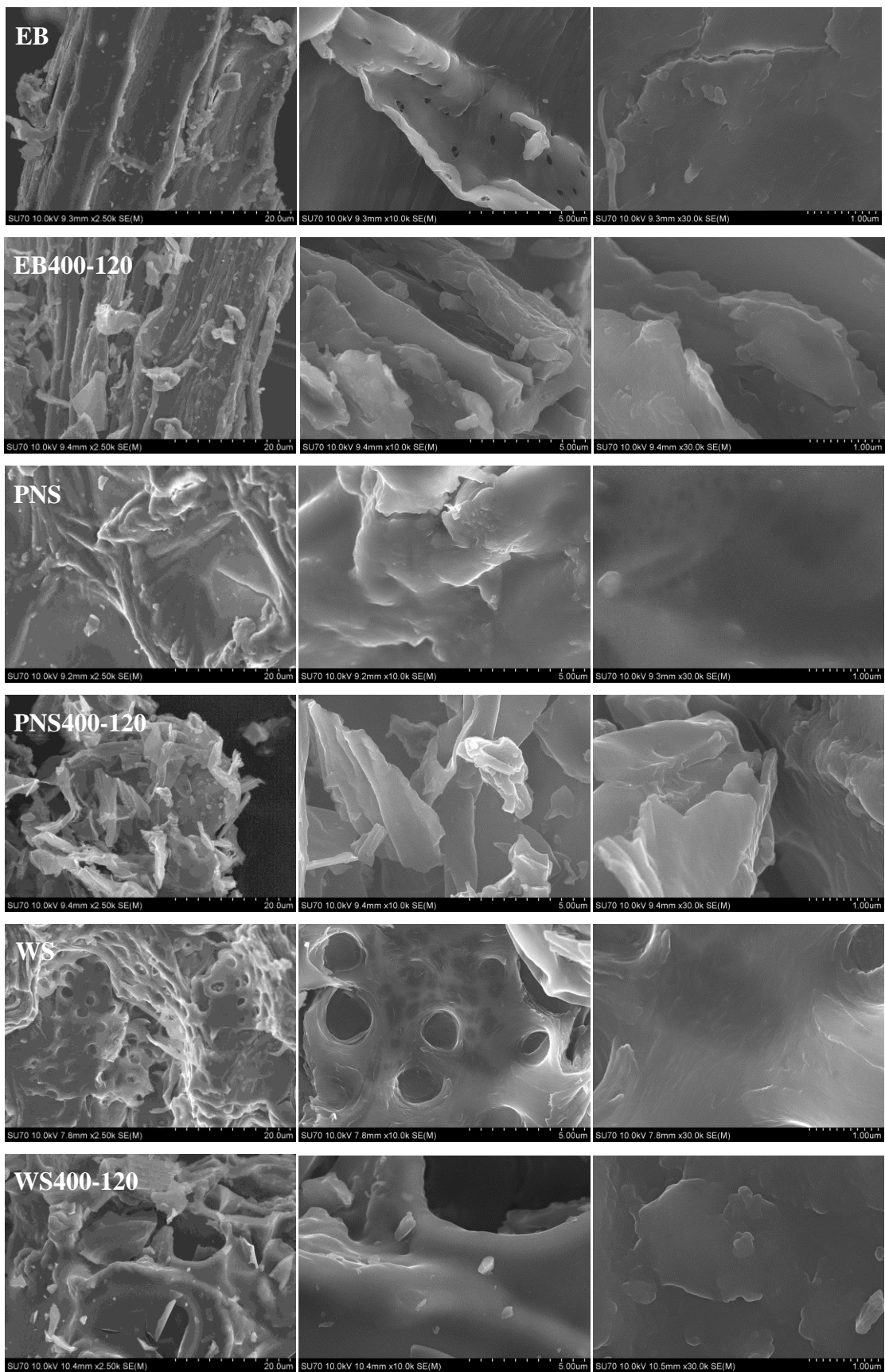


Figure 4.6 - SEM micrographs of starting and pyrolysed materials at 2 500 \times , 10 000 \times and 30 000 \times magnification (from left to right).

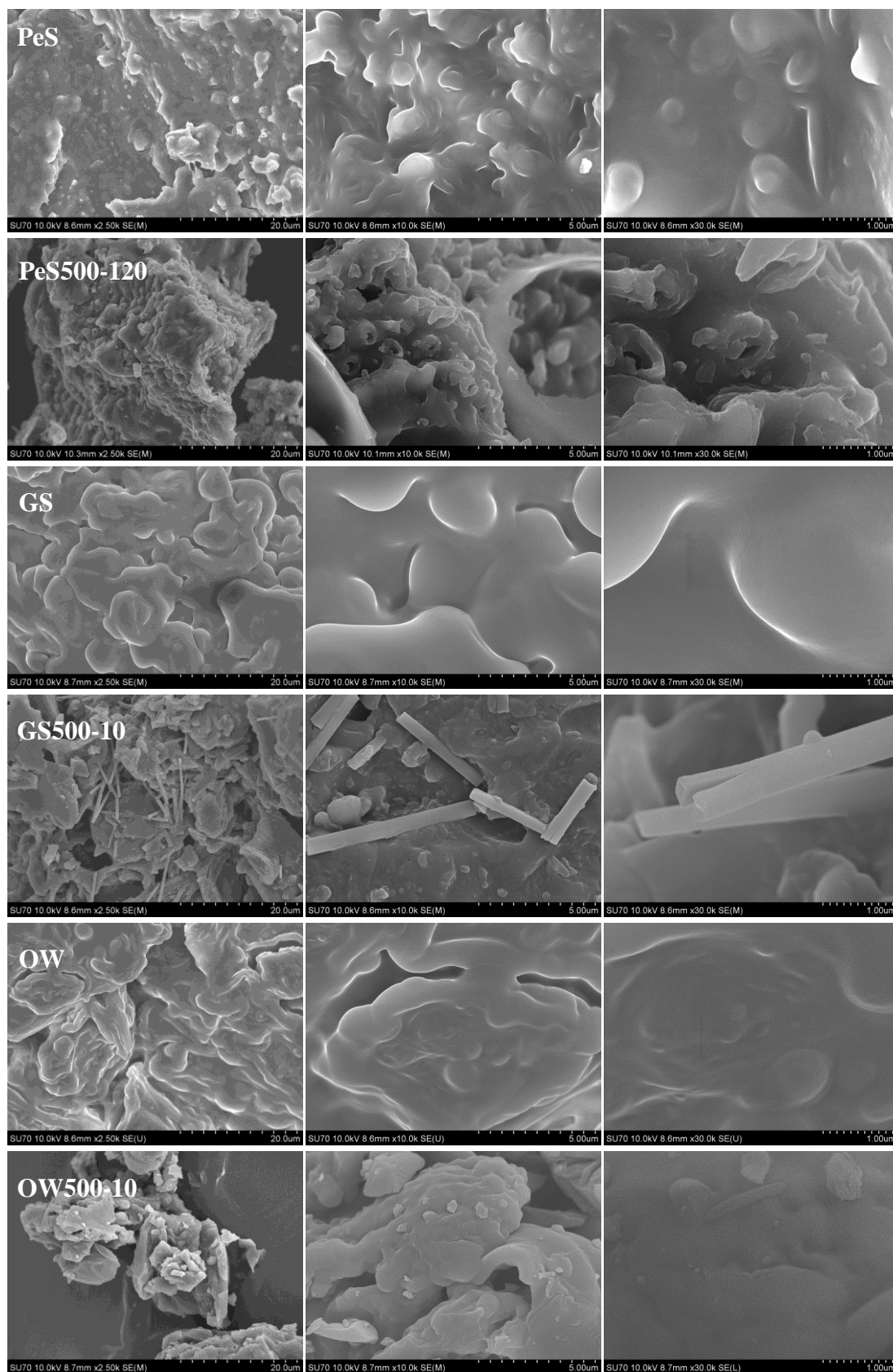


Figure 4.6 (continuation) - SEM micrographs of starting and pyrolysed materials at 2 500 \times , 10 000 \times and 30 000 \times magnification (from left to right).

4.3.3 Adsorption results

Figure 4.7 shows the adsorption kinetics of MS-222 onto the produced biochars and PAC and the fittings of the kinetic models to the experimental data as described in section 2.4.3.1. Table 4.4 lists the adsorption rate constants fitted to pseudo-first order, pseudo-second order and double exponential kinetic models and coefficients of determination, r^2 . The adsorption time until equilibrium varies significantly depending on the adsorbent. Among all adsorbents, the fastest kinetic was obtained for PAC, attaining the equilibrium after 60 min; on the other hand, kinetics of the biochars produced in this work are much slower. The slow adsorption kinetics of MS-222 onto biochars may be caused by their low surface area presented. Furthermore, mainly for kinetics of produced adsorbents, two kinetic steps are distinguishable: during the first step, a rapid MS-222 uptake takes place and might involve external and internal diffusion; subsequently, a slow step prevails which may correspond to intraparticle diffusion. In this sense, double exponential model, mostly used for metal adsorption kinetics [33], was used to fit the experimental data; compared to the pseudo-first and pseudo-second order models, this model had a higher coefficient of determination. Values of diffusion rate, k , suggest that EB400-120, PNS400-120, WS400-120 and GS500-10 have similar adsorption kinetics, controlled by intraparticle diffusion ($k_i < k_e$); on the other hand, OW500-10 and PAC kinetics are controlled by external diffusion ($k_e < k_i$). In the case of PeS500-120, the ambiguous determination of k_e indicates that the kinetic of the MS-222 adsorption onto PeS500-120 is controlled by intraparticle diffusion. This conclusion is more perceptible by the calculation of the adsorption rate, using Eq. 2.5, over the time for both the external diffusion and the intraparticle diffusion steps. The resulting rates *versus* time are represented in Figure 4.8. These representations allow to easily observe which step prevails over the time for each adsorbent and, as it may be seen, it is confirmed that the adsorption kinetics of MS-222 onto OW500-10 and PAC are mainly controlled by external diffusion ($r_e > r_i$). The double exponential model is used to describe a two-step adsorption mechanism controlled by diffusion which, according to Wilczak et al. (1993) [33], may suggest two different types of adsorption sites.

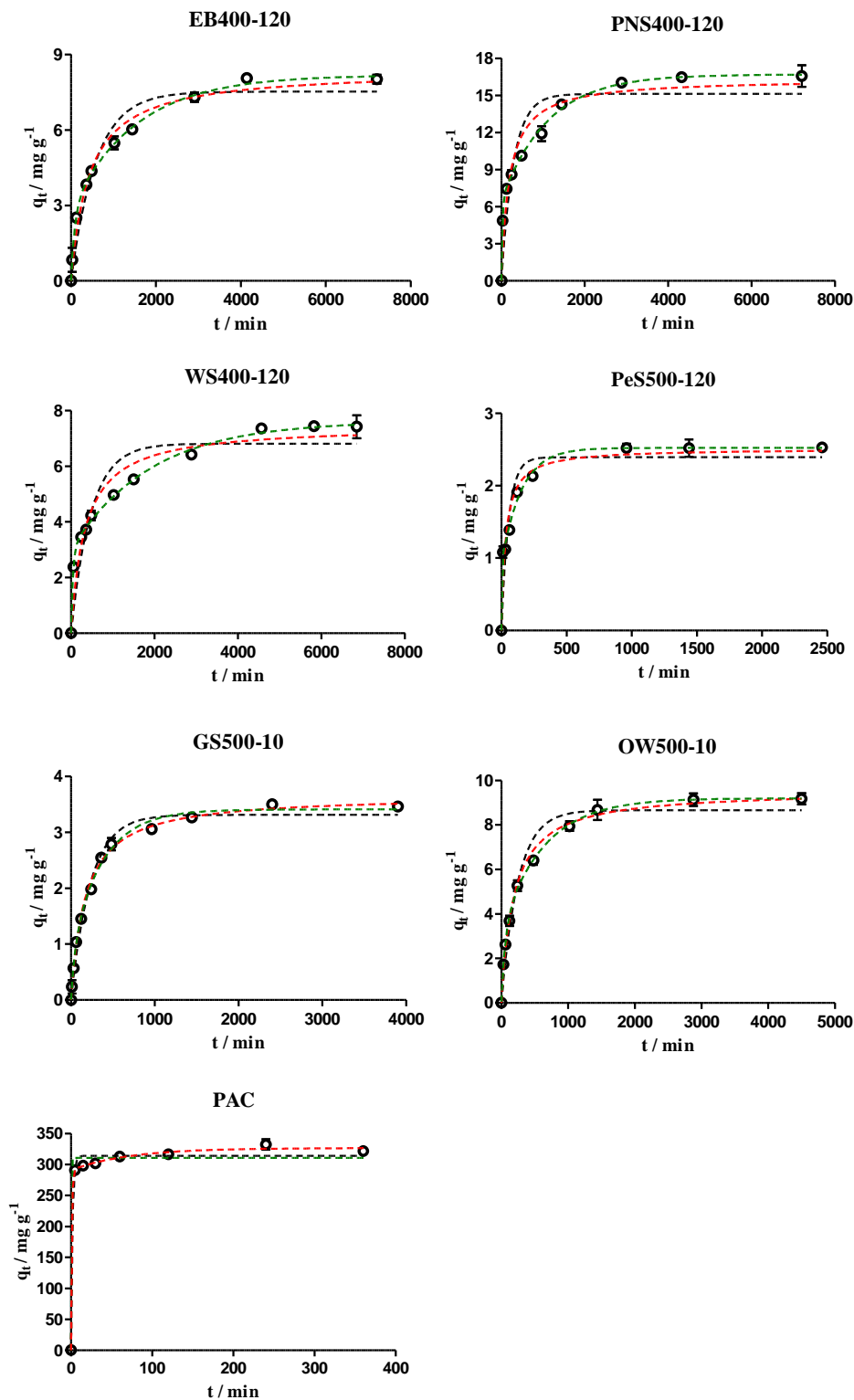


Figure 4.7 - Experimental and predicted kinetic curves for the adsorption of MS-222 in water using produced biochars and PAC. The experimental data (o) were fitted to pseudo-first order (---), pseudo-second order (---) and double exponential (---) kinetic models. Each experimental point (\pm standard deviation) is the average of three replicates. Note that x and y -axis scales are not the same in all graphs to allow a better visualization of the result.

Table 4.4 - Fitting parameters of pseudo-first order and pseudo-second order and double exponential kinetic models to the experimental data

Kinetic Parameters		EB400-120	PNS400-120	WS400-120	PeS500-120	GS50000-10	OW500-10	PAC
Pseudo-1 st order	k_1 (min ⁻¹)	0.0017±0.0003	0.0034 ± 0.0009	0.0021 ± 0.0005	0.018 ± 0.005	0.0043 ± 0.0004	0.0040 ± 0.0006	0.5 ± 0.1
	q_e (mg g ⁻¹)	7.5 ± 0.4	15 ± 1	6.8 ± 0.4	2.4 ± 0.2	3.31 ± 0.08	8.7 ± 0.3	314 ± 5
	r^2	0.9530	0.8774	0.8864	0.8880	0.9854	0.9688	0.9907
Pseudo-2 nd order	k_2 (g mg ⁻¹ min ⁻¹)	0.00028±0.00005	0.00032±0.00009	0.0004 ± 0.0001	0.012 ± 0.003	0.0016 ± 0.0001	0.00056±0.00005	(7.0 ± 0.5)×10 ⁹
	q_e (mg g ⁻¹)	8.4 ± 0.3	16.3 ± 0.8	7.5 ± 0.4	2.5 ± 0.1	3.67 ± 0.05	9.6 ± 0.2	311 ± 6
	r^2	0.9844	0.9432	0.9474	0.9448	0.9966	0.9941	0.9853
Double Exponential	D_e (mg L ⁻¹)	58 ± 5	65 ± 4	60 ± 4	46 ± 12	44 ± 21	118 ± 7	18 ± 4
	k_e (min ⁻¹)	0.011 ± 0.002	0.041 ± 0.007	0.022 ± 0.004	-	0.02 ± 0.01	0.0016 ± 0.0002	0.014 ± 0.008
	D_i (mg L ⁻¹)	106 ± 5	102 ± 3	92 ± 3	80 ± 12	126 ± 20	65 ± 8	145 ± 5
	k_i (min ⁻¹)	0.00065±0.00007	0.00090±0.00008	0.00053±0.00006	0.007 ± 0.02	0.0026 ± 0.0006	0.016 ± 0.003	1.0 ± 0.7
	q_e (mg g ⁻¹)	8.2 ± 0.1	16.7 ± 0.2	7.6 ± 0.1	2.52 ± 0.05	3.41 ± 0.07	9.2 ± 0.1	327 ± 5
	r^2	0.9986	0.9985	0.9978	0.9948	0.9990	0.9990	0.9990

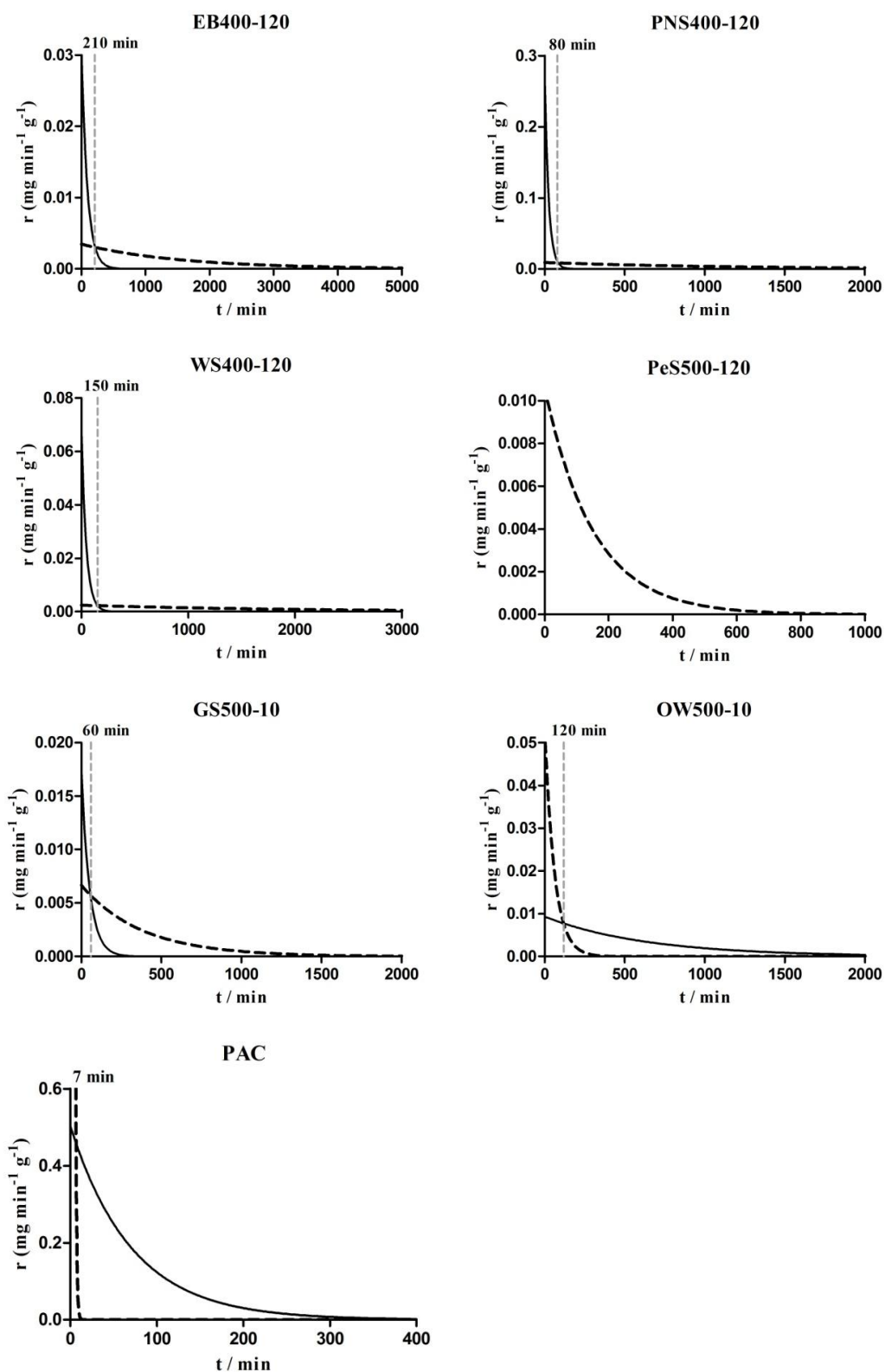


Figure 4.8 - Adsorption rate profile for the external diffusion step (— r_e) and intraparticle diffusion step (--- r_i) from double exponential kinetic model. Vertical line indicates the prevalent step change.

Figure 4.9 shows the equilibrium isotherms of MS-222 adsorption onto the adsorbents here considered together with fittings to the equilibrium models described in section 2.4.3.2. The fitting results, *i.e.*, equilibrium parameters and the coefficient of determination, r^2 , are shown in Table 4.5. In general, Langmuir-Freundlich combination appears to be a suitable mathematical model to describe the equilibrium data. However, the experimental results of the adsorption of MS-222 onto GS500-10 and PAC could not be fitted to this model in an adequate manner. In fact, no *plateau* is observed on GS500-10 isotherm. In this case, Freundlich isotherm fits better, suggesting GS500-10 as an adsorbent with heterogeneous surface. Concerning PAC isotherm, the use of the Langmuir model provided a better fit and the maximum adsorption capacity predicted was 349 mg g⁻¹. Among the isotherms that better fit to the Langmuir-Freundlich combined model, PNS400-120 showed the highest maximum adsorption capacity, 34 mg g⁻¹, followed by EB400-120 and OW500-10 with 22 and 18 mg g⁻¹, respectively. In comparison to PAC, the maximum adsorption capacity estimated for PNS400-120 is one order of magnitude lower; however considering the surface area of both adsorbents (S_{BET} of PNS400-120 is three orders of magnitude lower than that of PAC) PNS400-120 is apparently a more efficient adsorbent than that expected by physical characterization. This result suggests that adsorption capacity may not be directly correlated with the surface area and microporous structure: *e.g.*, WS400-120 has the highest surface area among all the produced biochars but its adsorption capacity is about two times lower than PNS400-120 capacity.

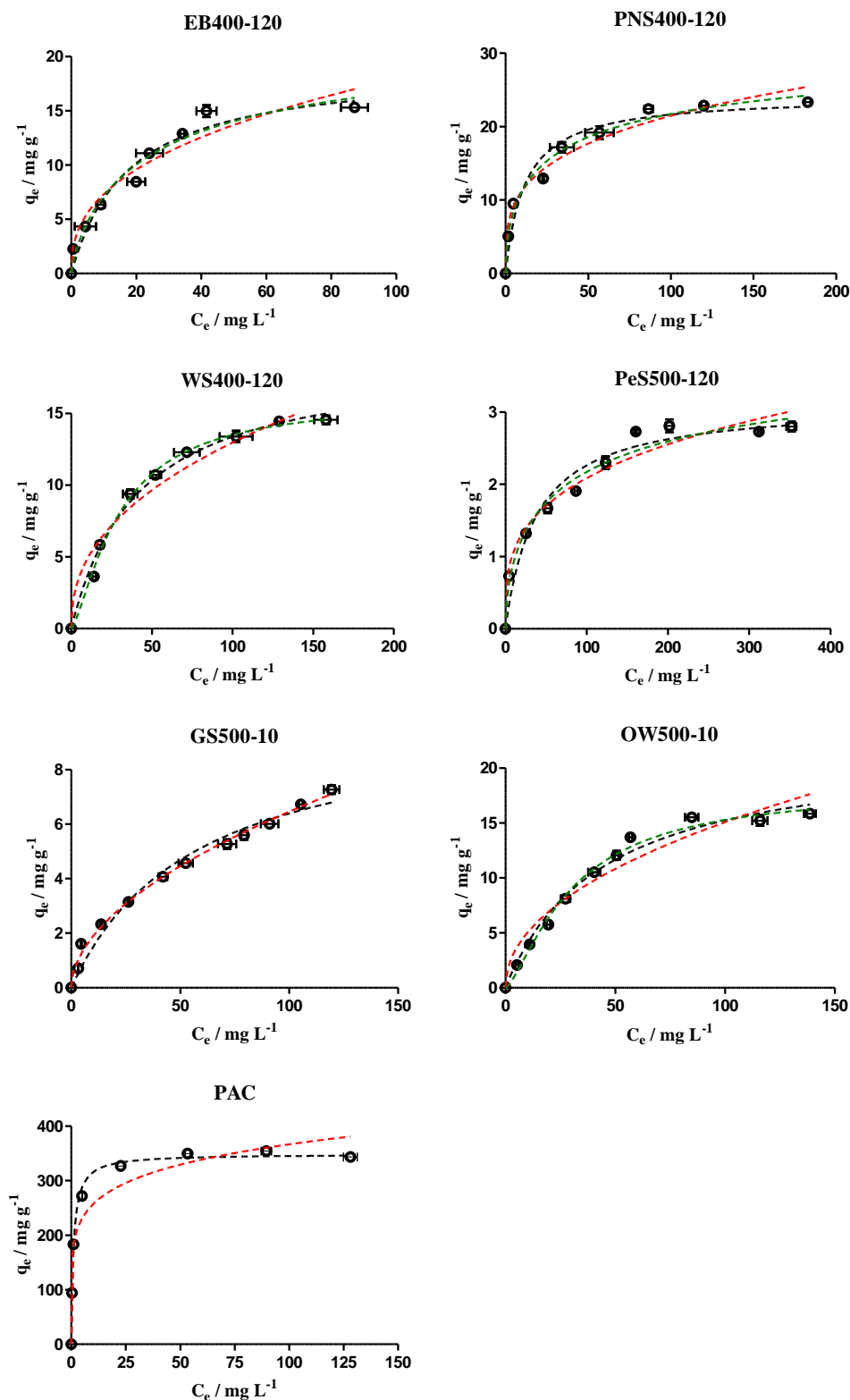


Figure 4.9 - Experimental and predicted isotherms for the adsorption of MS-222 in water using biochars and PAC. The experimental data (o) were fitted to Langmuir (---), Freundlich (---) and Langmuir-Freundlich (-.-) equilibrium models. Each experimental point (\pm standard deviation) is the average of three replicates. Note that x and y -axis scales are not the same in all graphs to allow a better visualization of the results.

Table 4.5 - Fitting parameters of Langmuir, Freundlich and Langmuir-Freundlich equilibrium models to the experimental data

Equilibrium Parameters		EB400-120	PNS400-120	WS400-120	PeS500-120	GS500-10	OW500-10	PAC
Langmuir	$q_{m,L}$ (mg g ⁻¹)	19 ± 2	24 ± 1	19.0 ± 0.9	3.1 ± 0.2	10 ± 1	22 ± 1	349 ± 5
	K_L (L mg ⁻¹)	0.06 ± 0.01	0.09 ± 0.02	0.024 ± 0.003	0.026 ± 0.007	0.017 ± 0.004	0.023 ± 0.003	0.94 ± 0.08
	r^2	0.9648	0.9597	0.9904	0.9608	0.9763	0.9832	0.9961
Freundlich	K_F (mg g ⁻¹ (mg L ⁻¹) ^{-N_F})	3.0 ± 0.6	5.9 ± 0.8	1.8 ± 0.4	0.5 ± 0.1	0.55 ± 0.05	1.7 ± 0.4	180 ± 22
	N_F	2.6 ± 0.4	3.6 ± 0.4	2.3 ± 0.3	3.4 ± 0.4	1.87 ± 0.07	2.1 ± 0.3	6 ± 2
	r^2	0.9503	0.9729	0.9602	0.9661	0.9947	0.9419	0.9329
Langmuir-Freundlich	$q_{m,LF}$ (mg g ⁻¹)	22 ± 7	34 ± 8	16.0 ± 0.8	4 ± 1		18 ± 1	
	K_{LF} (L ^{1/N_{LF}} mg ^{-1/N_{LF}})	0.07 ± 0.03	0.14 ± 0.03	0.009 ± 0.004	0.07 ± 0.02	Not converged	0.008 ± 0.004	Not converged
	N_{LF}	1.3 ± 0.4	1.8 ± 0.4	0.72 ± 0.08	1.7 ± 0.5		0.71 ± 0.09	
	r^2	0.9673	0.9858	0.9956	0.9770		0.9907	

4.4 Conclusions

The chemical characterization of the agricultural biowastes herein considered showed low ash and high carbon contents, indicating them as good candidates for biochars' precursors. In fact, the pyrolysis of these biowastes resulted in a high release of volatile matter, an improvement of aromatic structure and an increase of the total organic carbon content up to 76.6%, which is characteristic of a good adsorbent. However, the physical characterization of the produced biochars was not as promising as expected through chemical characterization, *i.e.*, low specific surface areas were obtained (from 2 to 11 m² g⁻¹) with a negligible microporous development. Regarding the adsorption results, all the biochars were able to adsorb MS-222 from water, even though this anaesthetic has a great affinity for the aqueous phase. In general, the Langmuir-Freundlich isotherm model fits well biochars equilibrium data and Langmuir model fits PAC isotherm. Among biochars, PNS400-120 showed the maximum MS-222 adsorption capacity (34 mg g⁻¹); however, its adsorption capacity is ten times lower than that of PAC.

4.5 References

- [1] Ferreira, C.I.A., Calisto, V., Santos, S.M., Cuerda-Correa, E.M., Otero, M., Nadais, H. and Esteves, V.I., 2015, *Journal of Analytical and Applied Pyrolysis*, 112, 313-324.
- [2] Sapkota, A., Sapkota, A.R., Kucharski, M., Burke, J., McKenzie, S., Walker, P. and Lawrence, R., 2008, *Environment International*, 34 (8), 1215-1226.
- [3] Ross, L.G. and Ross, B., 2008, *Anaesthetic and Sedative Techniques for Aquatic Animals*, Blackwell Publishing Ltd, Oxford, UK.
- [4] Topic Popovic, N., Strunjak-Perovic, I., Coz-Rakovac, R., Barisic, J., Jadan, M., Persin Berakovic, A. and Sauerborn Klobucar, R., 2012, *Journal of Applied Ichthyology*, 28 (4), 553-564.
- [5] Marking, L.L., 1967, Toxicity of MS-222 to Selected Fishes, *U.S. Department of Interior, Fish and Wildlife Service*.
- [6] Martins, C.I.M., Eding, E.H., Verdegem, M.C.J., Heinsbroek, L.T.N., Schneider, O., Blancheton, J.P., d'Orbcastel, E.R. and Verreth, J.A.J., 2010, *Aquacultural Engineering*, 43 (3), 83-93.
- [7] Dawson, V.K., Marking, L.L. and Bills, T.D., 1976, *Transactions of the American Fisheries Society*, 105 (1), 119-123.
- [8] Ahmad, M., Rajapaksha, A.U., Lim, J.E., Zhang, M., Bolan, N., Mohan, D., Vithanage, M., Lee, S.S. and Ok, Y.S., 2014, *Chemosphere*, 99 (0), 19-33.
- [9] Bolan, N.S., Thangarajan, R., Seshadri, B., Jena, U., Das, K.C., Wang, H. and Naidu, R., 2013, *Bioresource Technology*, 135 (0), 578-587.
- [10] Qiu, Y., Zheng, Z., Zhou, Z. and Sheng, G.D., 2009, *Bioresource Technology*, 100 (21), 5348-5351.
- [11] Xu, R.-k., Xiao, S.-c., Yuan, J.-h. and Zhao, A.-z., 2011, *Bioresource Technology*, 102 (22), 10293-10298.
- [12] Uras-Postma, Ü., Carrier, M. and Knoetze, J., 2014, *Journal of Analytical and Applied Pyrolysis*, 107 (0), 123-132.

- [13] Carrier, M., Hardie, A.G., Uras, Ü., Görgens, J. and Knoetze, J., 2012, *Journal of Analytical and Applied Pyrolysis*, 96 (0), 24-32.
- [14] Ates, F. and Un, U.T., 2013, *Journal of Analytical and Applied Pyrolysis*, 103 (0), 159-166.
- [15] Mohan, D., Rajput, S., Singh, V.K., Steele, P.H. and Pittman Jr, C.U., 2011, *Journal of Hazardous Materials*, 188 (1-3), 319-333.
- [16] Tong, X.-j., Li, J.-y., Yuan, J.-h. and Xu, R.-k., 2011, *Chemical Engineering Journal*, 172 (2-3), 828-834.
- [17] Lima, I.M., Boateng, A.A. and Klasson, K.T., 2010, *Journal of Chemical Technology & Biotechnology*, 85 (11), 1515-1521.
- [18] Lu, H., Zhang, W., Yang, Y., Huang, X., Wang, S. and Qiu, R., 2012, *Water Research*, 46 (3), 854-862.
- [19] Agrafioti, E., Bouras, G., Kalderis, D. and Diamadopoulos, E., 2013, *Journal of Analytical and Applied Pyrolysis*, 101 (0), 72-78.
- [20] Liu, H., Liang, S., Gao, J., Ngo, H.H., Guo, W., Guo, Z. and Li, Y., 2014, *Journal of Analytical and Applied Pyrolysis*, 107 (0), 336-341.
- [21] Yao, Y., Gao, B., Chen, H., Jiang, L., Inyang, M., Zimmerman, A.R., Cao, X., Yang, L., Xue, Y. and Li, H., 2012, *Journal of Hazardous Materials*, 209-210 (0), 408-413.
- [22] Teixidó, M., Pignatello, J.J., Beltrán, J.L., Granados, M. and Peccia, J., 2011, *Environmental Science & Technology*, 45 (23), 10020-10027.
- [23] Liu, P., Liu, W.-J., Jiang, H., Chen, J.-J., Li, W.-W. and Yu, H.-Q., 2012, *Bioresource Technology*, 121 (0), 235-240.
- [24] Valenzuela, C. and Bernalte, A., 1985, *Boletín Geológico y Minero*, XCVI (I), 58-61.
- [25] Açıklın, K., 2011, *Journal of Thermal Analysis and Calorimetry*, 105 (1), 145-150.
- [26] Li, J. and Zhang, W., 2013, *Desalination and Water Treatment*, 51 (28-30), 5831-5839.
- [27] Hajjouji, H.E., Bailly, J.R., Winterton, P., Merlina, G., Revel, J.C. and Hafidi, M., 2008, *Bioresource Technology*, 99 (11), 4958-4965.
- [28] Apaydın-Varol, E. and Pütün, A.E., 2012, *Journal of Analytical and Applied Pyrolysis*, 98 (0), 29-36.
- [29] Link, S., Arvelakis, S., Spliethoff, H., De Waard, P. and Samoson, A., 2008, *Energy & Fuels*, 22 (5), 3523-3530.
- [30] Lima, M., Lavorente, G., da Silva, H., Bragatto, J., Rezende, C., Bernardinelli, O., deAzevedo, E., Gomez, L., McQueen-Mason, S., Labate, C. and Polikarpov, I., 2013, *Biotechnology for Biofuels*, 6 (1), 75.
- [31] Dais, P. and Hatzakis, E., 2013, *Analytica Chimica Acta*, 765 (0), 1-27.
- [32] Hanganu, A., Todașcă, M.-C., Chira, N.-A., Maganu, M. and Roșca, S., 2012, *Food Chemistry*, 134 (4), 2453-2458.
- [33] Wilczak, A. and Keinath, T.M., 1993, *Water Environment Research*, 65 (3), 238-244.

5 Application of pyrolysed paper mill sludge as adsorbents for fish anaesthetics removal from water

The production of alternative adsorbents from paper mill sludge may be an interesting solution for the management of such waste. In this work, two types of adsorbents were produced by pyrolysis of primary and biological paper mill sludge at different temperatures and residence times. All starting and produced materials were fully characterized by elemental and proximate analyses, total organic carbon, FTIR, ¹³C and ¹H solid state NMR, SEM, N₂ isotherms, PZC and Boehm's titration. Finally, selected adsorbents were tested for the removal of three widely used fish anaesthetics (tricaine methanesulfonate, benzocaine and 2-phenoxyethanol) from water and compared with a commercial activated carbon. The use of commercial activated carbon resulted in maximum adsorption capacities of 631, 435 and 289 mg g⁻¹ for tricaine, benzocaine and 2-phenoxyethanol, respectively (obtained by the fitting of Langmuir-Freundlich model), which are between 4 and 8 times higher than those determined for the alternative adsorbents. Even so, the obtained results point to the promissory utilization of these waste-based adsorbents in recirculating aquaculture systems.

The work presented and discussed in this chapter resulted in the following publications:

- [1] Calisto V., Ferreira C.I.A., Santos, S.M., Gil, M.V., Otero M., Esteves V.I. (2014), Production of adsorbents by pyrolysis of paper mill sludge and application on the removal of citalopram from water. *Bioresource Technology*, 166, 335-344. DOI: 10.1016/j.biortech.2014.05.047
- [2] Ferreira C.I.A., Calisto V., Otero M., Nadais H., Esteves V.I. (2016), Comparative adsorption evaluation of biochars from paper mill sludge with commercial activated carbon for the removal of fish anaesthetics from water in Recirculating Aquaculture Systems. *Aquacultural Engineering*, 74, 76-83. DOI: 10.1016/j.aquaeng.2016.06.003

5.1 Contextualization

Paper mill sludge is produced in the order of eleven million tons per year only by European mills [3]. The use of pulp and paper industry sub-products is quite dependable on the legislation applied in each country; however, in general, main applications include energy recovery, disposal on landfills and composting. In recent years, and considering that environmental legislation is increasingly stringent, the pulp and paper industry has been facing some challenges with respect to the management of the resulting wastes. The Confederation of European Paper Industries (CEPI) itself supports a complete ban of landfilling and incineration in the European Union in agreement with the Waste Framework Directive (2008/98/EC) [4]. Hence, from a sustainable point of view, it is necessary to develop innovative handling strategies that maximize recovery of useful materials and/or energy and that also allow the minimization of such wastes [5,6]. Since that these residues are derived from natural resources (wood) and are a result of controlled and well known processes, their use as raw materials in other industries has been increasing, such as heat insulation material, paper and wood adhesive, dried mixture for use as pesticides or fertilizers carriers in agriculture and as building materials (cement, brick and tile manufacturing) [7-9]. Also, given the carbonaceous nature of paper mill sludge, their conversion into adsorbents (activated or non-activated carbons) has been proposed by several authors for the adsorption of heavy metals [10], dyes [11], phenolic compounds [12] and pharmaceuticals [13,14] from contaminated waters.

In the last chapter, the potential use of agricultural biowaste-based adsorbents for the removal of tricaine methanesulfonate (MS-222) from water was evaluated and compared with a commercial one. On the other hand, the present chapter describes the production of alternative adsorbents by pyrolysis, using primary (PS) and biological (BS) paper mill sludge whose management is challenging. In this context, pyrolysis temperature and residence time were assessed and, further, an acidic washing of the waste-based carbons was performed. All these materials were characterized chemical and physically. The main goal is to obtain an adsorbent with high adsorption capacity using cheap and environmentally friendly production methods (without employing chemical or physical activation) and, simultaneously, to propose a new way to valorise this industrial sub-product. The two most promising adsorbents were applied on the removal of three different fish anaesthetics, MS-222, benzocaine and 2-phenoxyethanol (2-PE), from water. Also, the comparison of the adsorptive performance of these alternative materials with that of a commercial powdered activated carbon (PAC) was aimed.

5.2 Materials and methods

5.2.1 Adsorbent materials

5.2.1.1 Production of paper mill sludge-based adsorbents

Paper mill sludge, used as starting materials to produce the alternative adsorbents, were the same described in previous Chapter 3 (section 3.2.1.2). PS and BS were dried at room temperature for several days, followed by a 24 h period at 105 °C in an oven. PS was ground with a blade mill, while BS was grinded with a mortar grinder, in order to obtain different grain sizes. Due to their particular physical characteristics, PS resulted in an extremely light net of fibrous material, impossible to sieve.

The starting materials were transferred into porcelain crucibles and pyrolysed using a muffle (Nüve furnace MF 106), under a N₂ flow. The heating rate was 10 °C min⁻¹ and the maximum temperature of pyrolysis was defined by thermogravimetric analysis (TGA) interpretation (see section 5.3.1). After the pyrolysis, the material was maintained inside the muffle until the temperature reached room temperature; the N₂ stream was continuously applied during the cooling step. The pyrolysis temperature and residence time were varied in order to evaluate the influence of those parameters in the characteristics of the material. Accordingly, PS and BS were pyrolysed at 315 °C for 150 min (PS315-150 and BS315-150), at 600 °C for 10 min (PS600-10 and BS600-10), at 800 °C for 10 min (PS800-10 and BS800-10). Ultimately, PS and BS were pyrolysed at 800 °C for 150 min (PS800-150 and BS800-150).

Only PS800-150 and BS800-150 were washed with HCl 1.2 M followed by distilled water until neutral pH, for removal of ashes and other inorganic matter. After washing, pyrolysed and washed PS and BS were dried in an oven for 24 h at 105 °C, originating PSC and BSC, respectively. Due to its fibrous structure, PSC resulted in a powdered carbon, while BSC was sieved and separated by particle size: < 0.18 mm (BSC-a); between 0.18 and 0.5 mm (BSC-b); between 0.5 and 1 mm (BSC-c), and between 1 and 2 mm (BSC-d). In Table 5.1 are summarized the conditions of adsorbents production and are indicated which ones were characterized.

Table 5.1 - Conditions of adsorbents production (T -pyrolysis temperature; τ_p -pyrolysis residence time)

Raw Material	T (°C)	τ_p (min)	Washing	Particle size (mm)	Designation
PS	315	150	-	Powder	PS315-150
	600	10	-		PS600-10
	800	10	-		PS800-10
	800	150	-		PS800-150
	800	150	HCl 1.2 M		PSC
BS	315	150	-	< 0.18	BS315-150
	600	10	-	0.18-0.50	BS600-10
	800	10	-	0.18-0.50	BS800-10
	800	150	-	< 2.0	BS800-150
	800	150	HCl 1.2 M	< 0.18	BSC-a
		150		0.18-0.50	BSC-b
		150		0.50-1.0	BSC-c
150		1.0-2.0		BSC-d	

Note: T - pyrolysis temperature; τ_p - pyrolysis residence time. Only materials in bold were characterized.

5.2.1.2 Commercial activated carbon

PULSORB WP270 (Powdered Activated Carbon - PAC) is a commercial activated carbon that were provided and recommended for this application by Chemviron Carbon and used in this work as reference carbon for comparison purposes.

5.2.2 Materials characterization

5.2.2.1 Characterization of paper mill sludge before and after pyrolysis

Thermal characterization of PS and BS was carried out by TGA and DTGA. Non-isothermal TG analysis was performed using a TAG analyser (Setaram Instrumentation, TAG24, France). The analyses were carried out under a $50 \text{ cm}^3 \text{ min}^{-1}$ N_2 flow at a heating rate of $10 \text{ }^\circ\text{C min}^{-1}$ from room temperature to $1000 \text{ }^\circ\text{C}$. Approximately 5 mg of sample was used for each experiment. The TG and DTG curves of the samples were represented as a function of temperature, to allow the selection of the pyrolysis temperatures. It is important to mention that this procedure is different from the procedure described in Chapter 3, section 3.2.2.4.

The proximate and elemental analyses were applied to PS, BS and all the pyrolysed materials. Proximate analysis was conducted in a TGA-601 automatic analyser (LECO, model TGA601, Spain). Standard methods were employed to determine the moisture (UNE 32002) [15], volatile matter (UNE 32019) [16] and ash contents (UNE 32004) [17]. The fixed carbon content corresponds to the weight lost during the determination of ash content (at a dry basis). Elemental

analysis, involving the determination of the sample content in C, H, N, S and O, was performed in a CHNS-932 analyzer (LECO, model CHNS-932, Spain). The oxygen content was calculated by difference. The results were corrected considering the water content of the samples (presented at a dry basis).

TC, IC and TOC quantification, FTIR spectra and NMR spectra (^{13}C CP-MAS NMR and ^1H MAS NMR) were performed to all starting and pyrolysed paper mill sludge according to the procedure described in Chapter 4, sections 4.2.2.4, 4.2.2.5 and 4.2.2.6, respectively.

The physical characterization, comprising porosimetry and N_2 adsorption, was carried out only to pyrolysed paper mill sludge. The apparent density (ρ_{app}) was determined with mercury at 0.1 MPa in a mercury porosimeter (Micromeritics, Autopore IV 9500, USA). The textural properties were studied by physical adsorption of N_2 at $-196\text{ }^\circ\text{C}$ on an ASAP 2420 apparatus (Micromeritics, ASAP 2420, USA). The samples were outgassed overnight at $100\text{ }^\circ\text{C}$ under vacuum prior to adsorption measurements. The S_{BET} was calculated from the Brunauer–Emmett–Teller equation [18] in the relative pressure range 0.01–0.1. The total pore volume (V_p) was estimated from the amount of nitrogen adsorbed at a relative pressure of 0.99. The total volume of micropores (W_0) was determined by applying the Dubinin–Radushkevich equation [19] to the lower relative pressure zone of the N_2 adsorption isotherm. The average micropore width (L) was calculated by means of the Stoeckli–Ballerini equation [20]. The average pore diameter (D_p) was calculated as $D=2 V_p/S_{BET}$. Furthermore, the surface morphology of PS, BS, PS800-10, PS800-150 and BS800-10 was observed by SEM (Hitachi, SU-70, Japan) at 3 000, 10 000 and 30 000 \times magnification.

5.2.2.2 Characterization of pyrolysed and washed paper mill sludge and PAC

The proximate analysis of PSC, BSC-b and PAC was performed using a Setaram SETSYS Evolution-1750 thermal analyser. Briefly, 15-20 mg of sample was placed in an alumina crucible and heated, under N_2 atmosphere (heating rate of $10\text{ }^\circ\text{C min}^{-1}$) from room temperature up to $105\text{ }^\circ\text{C}$. The sample was kept at $105\text{ }^\circ\text{C}$ until total stabilization of the weight (approximately 30 min). Next, temperature was increased from 105 to $950\text{ }^\circ\text{C}$ ($10\text{ }^\circ\text{C min}^{-1}$), keeping the sample at $950\text{ }^\circ\text{C}$ until total stabilization of the weight (approximately 30 min); finally, at $950\text{ }^\circ\text{C}$, the carrier gas was automatically switched to air and the sample was maintained at $950\text{ }^\circ\text{C}$ until total stabilization of the weight. The weight loss observed around $105\text{ }^\circ\text{C}$ is attributed to moisture; the weight loss registered from the end of this first step up to the switching of the carrier gas corresponds to the volatile matter. The weight loss comprised between the introduction of the air flow and the stabilization of the weight is attributed to the fixed carbon content. The final residue corresponds to the ash content of the sample.

The elemental analysis of PSC, BSC-b and PAC was performed in a LECO TruSpec CHNS Micro analyser, using sulfamethazine as calibration standard. The oxygen content was calculated by difference. The results were corrected considering the water content of the samples (presented at a dry basis). Each analysis was performed in triplicate.

The quantification of functional groups present on the adsorbents surface (PSC, BSC-b and PAC) was performed by the Boehm's method [21]. Accordingly, each adsorbent was added to 0.05 M NaOH (99.3%, José Manuel Gomes dos Santos, Portugal), 0.05 M NaHCO₃ (>99.5%, Fluka), 0.05 M Na₂CO₃ (>99.5%, Panreac) or 0.05 M HCl (37%, Panreac) solutions into polypropylene tubes at a final concentration of 10 g L⁻¹, under N₂ atmosphere. The mixture was stirred in an overhead shaker (Heidolph, Reax 2) at 200 rpm, inside a thermostatic incubator at 25 °C for 24 h. Subsequently, the supernatants were filtered and 15 mL of each one were titrated with standardized 0.1 M HCl or 0.1 M NaOH solutions in order to quantify the total acid and basic functional groups, respectively. In addition, the different acidic groups on the adsorbents surface were determined assuming that NaOH neutralizes carboxylic, phenolic and lactone groups, Na₂CO₃ neutralizes carboxylic and lactone groups and NaHCO₃ neutralizes carboxylic groups. The amount of basic groups was calculated from the amount of HCl that reacts with the adsorbent. Note that NaOH and HCl solutions were standardized with C₈H₅KO₄ (99.8%, Panreac) and Na₂CO₃ solutions, respectively, for the determination of their exact concentration.

The point of zero charge (PZC) of each adsorbent was obtained according to the procedure described by Souza et al. (2014) [22]. Accordingly, the highest dosage of PSC, BSC-b and PAC used in the adsorption experiments (6, 5 and 1.5 g L⁻¹, respectively) was shaken with 0.1 M NaCl (> 99.5%, Panreac) solutions in polypropylene tubes at different initial pH (pH_i) ranging from 2 to 11. The pH was adjusted using 1 M and 0.1 M of NaOH or HCl solutions. After equilibration for 24 h, the final pH was measured (pH_f). The PZC value (pH_{PZC}) corresponds to the pH at which pH_i and pH_f coincided, which was determined by plotting the ΔpH vs. pH_i (the PZC corresponds to pH value where the curve crosses the x -axis).

The N₂ adsorption isotherms were obtained at 77 K using a Micromeritics Instrument, Gemini VII 2380 to determinate the S_{BET} , W_0 and V_p of PSC, BSC (all particle sizes) and PAC. The samples were previously outgassed at 120 °C for 12 h.

5.2.3 Fish anaesthetics

Adsorption tests were performed for three fish anaesthetics: Tricaine methanesulfonate (> 97%, TCI Europe) - MS-222; Ethyl 4-Aminobenzoate (> 99%, TCI Europe) - Benzocaine, and 2-Phenoxyethanol (> 98.5%, TCI Europe) - 2-PE. All anaesthetic solutions were prepared in ultra-

pure water obtained from a Milli-Q Millipore system (Milli-Q plus 185) and buffered using 10^{-2} M of NaHCO_3 to pH 7-7.5, according to the recommended by Ross et al. (2008) [23]. The anaesthetics physico-chemical properties are summarized in Table 2.1 from Chapter 2.

5.2.4 Determination of the anaesthetics concentration in water by MEKC

MEKC analyses were performed using a Beckman P/ACE MDQ (Fullerton, CA, USA) instrument, equipped with an UV-Vis detection system, following the procedure described in Appendix C (section C.1.1.1). Detection of benzocaine, MS-222 and 2-PE were monitored at 200, 220 and 230 nm, respectively. Aqueous samples and standard solutions were analyzed in triplicate. MS-222, benzocaine and 2-PE calibration curves and parameters, including the limit of detection (LOD) and limit of quantification (LOQ), are also presented in Appendix C, sections C.1.1, C.1.2 and C.1.3, respectively.

5.2.5 Adsorption experiments

Kinetic and equilibrium adsorption experiments were performed in batch systems aiming to study the removal of the three fish anaesthetics from water onto the pyrolysed and washed adsorbents (PSC and BSC-b) and PAC. With this purpose, single solutions with a known initial concentration of MS-222, benzocaine and 2-PE in ultrapure water were buffered to pH 7-7.5 using 1×10^{-2} M NaHCO_3 . Then, known masses of each of adsorbent were placed in contact with the corresponding anaesthetic solution in polypropylene tubes in the dosage listed in Table 5.2. Batch tests were carried out in an overhead shaker at 90 rpm, inside a thermostatic incubator at 18 °C (the ideal temperature for the intensive production of several fish species in Europe [24]). At the same time, anaesthetic solutions were shaken under identical conditions but without any adsorbent (control experiments). All adsorption tests were performed in triplicate. Before the adsorption experiments it was verified that fish anaesthetics were not adsorbed onto the polypropylene tubes used as test vessels and that the adsorbent matrixes did not affect the MEKC analyses.

Table 5.2 - Dosage of each adsorbent used in adsorption experiments

Anaesthetic solution	Adsorbent Dosage (g L^{-1})		
	PSC	BSC-b	PAC
MS-222	2.0	2.0	0.50
Benzocaine	1.0	1.0	0.15
2-PE	6.0	5.0	1.5

In order to obtain the equilibrium contact time, adsorption kinetics studies were performed with each anaesthetic using the produced biochars and PAC. The initial concentration of each anaesthetic was chosen according to the recommended dosage for the majority of fish species: 250 mg L⁻¹ of MS-222; 100 mg L⁻¹ of benzocaine, and 0.5 cm³ L⁻¹ (555 mg L⁻¹) of 2-PE [23]. For each anaesthetic, tubes containing the referred initial concentration together with the corresponding adsorbent were placed in the incubator and started to be shaken. Then, throughout the kinetic study, which ended when the adsorption equilibrium was attained, tubes corresponding to a defined time were periodically removed from the shaker (between 5 and 500 min). Next, for each tube, the concentration of the anaesthetics remaining in solution was determined by MEKC analysis. Kinetic data were fitted to pseudo-first order (Eq. 2.2) and pseudo-second order (Eq. 2.3) kinetic models and also to double exponential model (DEM) (Eq. 2.4) using GraphPad Prism 5 software (trial version). These models are described in Chapter 2, section 2.4.3.1.

After determining the equilibrium time for each adsorbent-anaesthetic system, adsorption equilibrium experiments were carried out by using different initial concentrations of each anaesthetic. The range of anaesthetics concentration included all the recommended dosages for fish administration; thus, initial concentration of MS-222 varied between 100 and 500 mg L⁻¹; between 25 and 200 mg L⁻¹ for benzocaine and between 0.3 and 1.3 cm³ L⁻¹ (333 and 1443 mg L⁻¹) for 2-PE [23]. Tubes containing the adsorbent and fish anaesthetic solutions were shaken until equilibrium and then, the anaesthetics concentration remaining in solution was determined by MEKC analysis. Equilibrium data were fitted to the three non-linear models described in Chapter 2, section 2.4.3.2: Langmuir (Eq. 2.7), Freundlich (Eq. 2.8) and the Langmuir-Freundlich (Eq. 2.9) models.

5.3 Results and discussion

5.3.1 Paper mill sludge pyrolysis

The thermogravimetric results, presented in Figure 5.1, show that PS and BS have a distinct behaviour: PS has two main mass losses corresponding to DTG peaks at approximately 335 °C (decomposition of the most thermo-labile fraction of organic matter) and at 755 °C (possibly the decomposition of the most thermo-resistant organic matter and carbonates); BS has four significant weight losses corresponding to DTG peaks at 50 and 310 °C (water evaporation and decomposition of organic matter) and 720 and 950 °C (decomposition of thermo-resistant organic matter along with decomposition of carbonates). The PS major weight loss corresponds to the peak at 755 °C while the major weight loss of BS occurs during the decomposition of organic matter at 310 °C. In addition, PS and BS also differ in the total weight loss which is approximately

42 and 74% at 900 °C, respectively. In general, the pyrolysis yield varied from 58% at 315 °C to 34% at 800 °C for both sludges.

In order to understand the effect of pyrolysis temperature on the adsorbent's characteristics, three temperatures were selected: 315, 600 and 800 °C (during 10 or/and 150 min). Despite the differences observed in the thermogravimetric analyses, the chosen temperatures were used for both PS and BS to allow a direct comparison of the produced adsorbents.

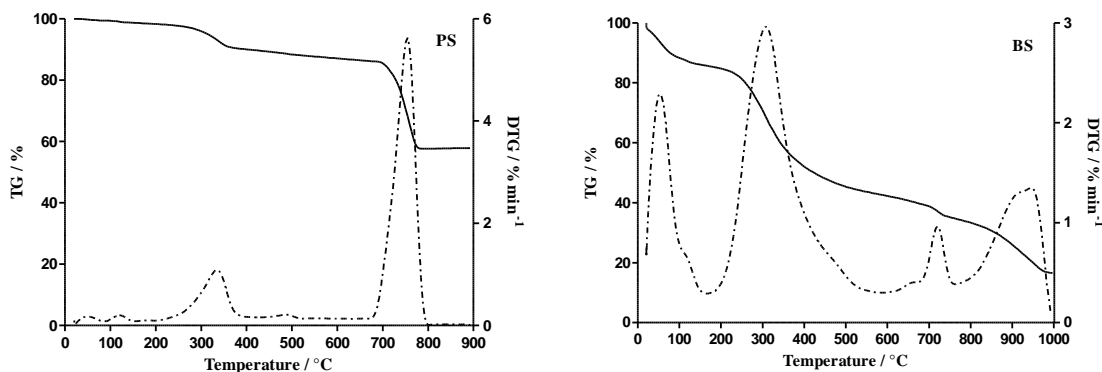


Figure 5.1 - Thermogravimetric (— TG) and derivative thermogravimetric (— • — DTG) curves for PS and BS.

5.3.2 Characterization of paper mill sludge before and after pyrolysis

The proximate and elemental analyses of PS, BS and all the resulting biochars are summarized in Table 5.3. The results revealed that PS and BS have a very distinct chemical composition which is then reflected in the composition of the pyrolysed sludge. PS possesses more than twice the amount of ashes of BS. However, with increasing pyrolysis temperature, the percentage of ash does not increase significantly for PS but doubles in the case of BS (for BS800-10); consequently, the several PS800 and BS800 biochars have similar percentages of ash, approximately between 50 and 60%. As expected, the percentage of volatile matter decreases significantly with increasing pyrolysis temperature; nevertheless, BS suffers a much more accentuated release of volatile matter during pyrolysis (reducing 4 times the volatile percentage from the starting material to BS800-10) while the release of volatiles for PS is only significant for PS800-150. The same conclusion is valid for the fixed carbon content: PS and BS have very similar percentages but the increase of its percentage after pyrolysis is much more evident for the BS. Following the evolution of the ratio between the volatile matter and fixed carbon percentages, it is possible to conclude that this ratio evolved more favorably for the BS adsorbents, decreasing from 6.0 to 0.5, indicating good volatile matter release and the increase of non-volatile carbon which are two factors that positively contribute for the formation of a carbon rich and highly porous

adsorbent. Concerning the elemental analysis, the results point out that PS has lower carbon content than BS which also results in lower carbon content materials after the pyrolysis. Both PS and BS have a very significant content in oxygen (in the case of PS it corresponds to twice the carbon percentage). The oxygen percentage suffers a constant decrease with increasing pyrolysis temperature; this fact is much more obvious for the BS pyrolysis remaining only 2% of oxygen for BS800-10 which is in good agreement with a more accentuated release of volatiles with the loss of oxygen functional groups. Moreover, a reduction in the hydrogen content is also observed which is consistent with the increase of the aromaticity of the produced biochar.

The values of total organic carbon presented in Table 5.3 are in accordance with the elemental analysis: BS has a higher content of TOC than PS. These results allow concluding that BS content in IC is negligible while in the case of PS it accounts for fifty percent of the total carbon. The PS percentage in IC is significantly reduced after pyrolysis resulting in PS related adsorbents with approximately 2 to 6% of IC.

Table 5.3 - Chemical characterization of PS, BS and pyrolysed sludge

Sample	PS	PS315-150	PS600-10	PS800-10	PS800-150	BS	BS315-150	BS600-10	BS800-10
<i>Proximate analysis (wt.%, db)^a</i>									
Moisture content	1.57	3.73	2.30	3.15	3.16	16.8	4.14	4.95	5.56
Volatile Matter	36.1	35.7	35.4	31.4	20.8	64.4	47.8	27.2	16.9
Fixed Carbon	8.60	18.5	17.5	18.1	18.0	10.8	19.9	27.2	32.9
Ash	55.3	45.8	47.1	50.5	61.3	24.8	32.3	45.6	50.2
VM/FC ^b	4.20	1.93	2.02	1.74	1.16	5.99	2.40	1.00	0.51
<i>Elemental analysis (wt.%, db)^a</i>									
C	14.8	30.8	30.7	28.8	27.1	39.1	43.6	39.2	42.1
H	1.26	2.14	0.96	0.47	0.82	4.68	3.73	1.63	0.70
N	0.40	0.43	0.32	0.33	0.33	6.00	6.30	4.38	3.10
S	0.29	0.50	0.56	0.60	0.82	2.10	1.93	2.19	2.27
O ^c	27.9	20.3	20.4	19.3	9.73	23.3	12.2	6.99	1.68
<i>Total organic carbon analysis (%)</i>									
TOC	8±1	nd	23.2±0.4	27±1	24.9±0.4	30.8±0.1	41.9±0.4	30.4±0.1	40.8±0.1
IC	8.4±0.1	nd	5.6±0.1	5.6±0.2	2.2±0.3	0.34±0.02	< LOQ ^d	1.75±0.08	0.15±0.02

^aProximate and elemental analyses are presented on a dry basis (db).

^bRatio between the VM (volatile matter) and FC (fixed carbon).

^cEstimated by difference: O (%) = 100-C-H-N-S-Ash.

^dLimit of quantification (LOQ)=0.104 mg IC.

Note: [C]-carbon content; [H]-hydrogen content; [N]-nitrogen content; [S]-sulphur content; [O]-oxygen content; nd- not determined.

The FTIR spectra of PS, BS and pyrolysed materials are presented in Figure 5.2. The spectrum of PS presents several typical bands of cellulose [25]. The broad band between 3200 and 3600 cm^{-1} can be attributed to O-H stretching from hydroxyl groups of cellulose and water; bands at 1110 and 1160 cm^{-1} correspond to the cellulosic ethers (C-O-C bonds) and the small band at 1055 cm^{-1} results from C-OH stretch of primary alcohols and carbohydrates [26]. The narrow band at 1315 cm^{-1} can be attributed to alcohols O-H stretch [25] or to aromatic ring stretches. Around 1630 cm^{-1} it is possible to identify the characteristic deformation band of water OH groups; however, this band might also be due to carbonyl groups of hemicelluloses. No other characteristic peaks of hemicelluloses or lignin are evident indicating that, if present in PS, these natural polymers occur in relatively small amounts. Finally, the broad band at 1415 cm^{-1} combined with a very sharp band at 870 cm^{-1} is characteristic of carbonates [26]. Despite approximately 50% of the PS carbon content being inorganic carbon (Table 5.3), which is in agreement with the presence of carbonates, these two peaks remain present in the FTIR spectrum of PS after pyrolysis at 800 °C, temperature at which carbonates should have already suffered degradation. For this reason, these peaks might also be attributed to the functional groups of the most thermo-resistant fraction of PS organic matter. In the FTIR spectra of the pyrolysed PS (PS315-150, PS600-10, PS800-10 and PS800-150), the typical bands of cellulose gradually disappear with the increase of pyrolysis temperature. In fact, PS800-10 and PS800-150 only have bands at 870 and 1415 cm^{-1} showing that, at this temperature, there was a considerable degradation of the main functional groups of PS. Concerning the BS spectrum, it is possible to observe several bands which were identified in PS as cellulose characteristic, such as the band at 1110 cm^{-1} and the broad band between approximately 3100 and 3600 cm^{-1} . Nevertheless, some of the bands found in PS are absent and, simultaneously, the presence of absorption at 1015, 1220 and 1530 cm^{-1} could be indicative of aromatic groups. However, the clear identification of the provenience of these absorption bands is difficult: for instance, 1530 cm^{-1} can be a typical absorption band of lignin or could be attributed to amide groups of cellular proteins from the microorganisms present in the biological sludge reactor. Absorption at 1220 cm^{-1} could also be tentatively attributed to phenol C-O stretch or to aryl-O stretch in aromatic ethers [26]. Similarly to PS, the two peaks at 870 and 1415 cm^{-1} are clearly visible, though, in this case, the relative intensity of those peaks towards the organic functional groups is much lower (contrarily to PS). The disappearance of the functional groups with the pyrolysis is also observed and, in BS800-10, there are no perceptible bands.

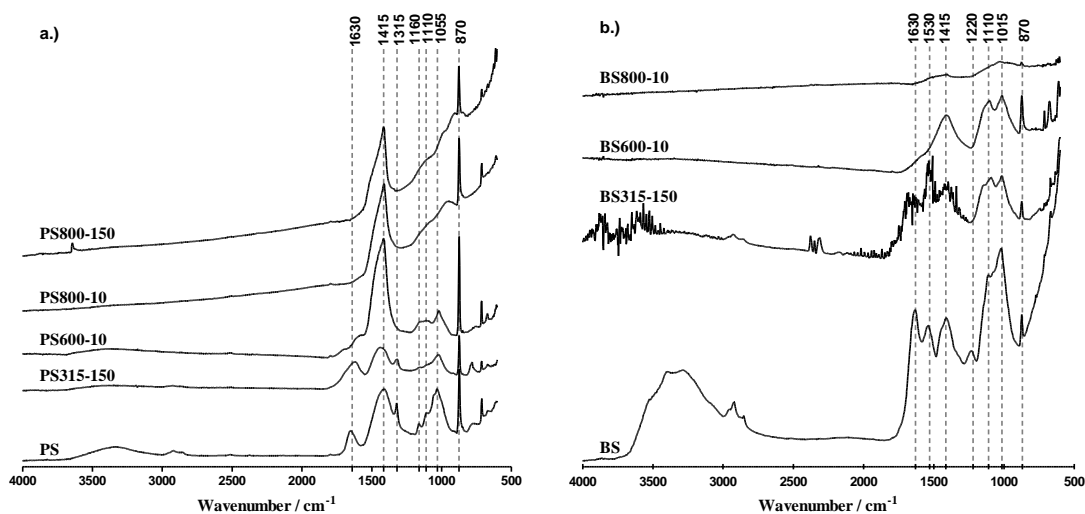


Figure 5.2 - FTIR spectra of a.) primary sludge (PS) and b.) biological sludge (BS) before and after pyrolysis at different temperatures and residence times.

^{13}C CPMAS solid state NMR spectra of PS, BS and the pyrolysed adsorbents are presented in Figure 5.3 a.) and b.). The PS spectrum strongly resembles the published spectrum of cellulose, leading to the same conclusions as those taken from FTIR analysis [27]. The peak at 65 ppm is due to cellulose carbon C6, the doublet at 72 and 75 ppm corresponds to carbons C2, C3 and C5, signals at 89 and 83 ppm are due to carbon C4 and finally the signal at 105 ppm can be assigned to C1. Moreover, the spectrum also indicates the presence of little or no lignin due to the absence of a peak at 56 ppm attributed to lignin methoxyl groups and the absence of signal in the aromatic region. Also, the inexistence of a shoulder in the peak at 105 ppm (hemicellulose carbons of xylose, mannose and arabinose) and the absence of signals at 22 and 174 ppm (methyl and carbonyl carbons of acetate groups) could be an indication that PS does not have hemicelluloses [28]. After pyrolysis, the most clear difference is the emergence of a wide band in the aromatic region (between 110 and 160 ppm) and the disappearance of the cellulose typical peaks (first, partially at 315 °C and then completely at 600 and 800 °C), showing that the pyrolysis resulted, as expected, in the increase of the aromaticity of the structure along with major functional group losses. Similarly to FTIR, ^{13}C NMR analysis also evidenced clear differences between PS and BS. The BS spectrum does not resemble that of pure cellulose, despite having some of the typical peaks (such as 72 and 105 ppm). The appearance of several peaks in the high shielded region (20, 24, 30, 33 and 40 ppm) is also observable and can be derived from alkyl carbons which resulted from cellulose degradation by microorganisms during the biological treatment. There are a number of peaks that can be indicative of the presence of lignin (such as 56, 105, 130 and 137 ppm) [29] and a dominant peak centered at 175 ppm which points out to the presence of carboxylic and/or carbonyl groups. The occurrence of lignin typical peaks in BS and not in PS could be explained by the

resistance of lignin to biodegradation (increasing its concentration during the biological treatment) and by the easiness of biodegradability of cellulose by microorganisms. Similarly to PS, BS peaks gradually disappear with pyrolysis increasing temperatures with the simultaneous emergence of a wide band in the aromatic region that fully dominates the spectra of BS600-10 and BS800-10.

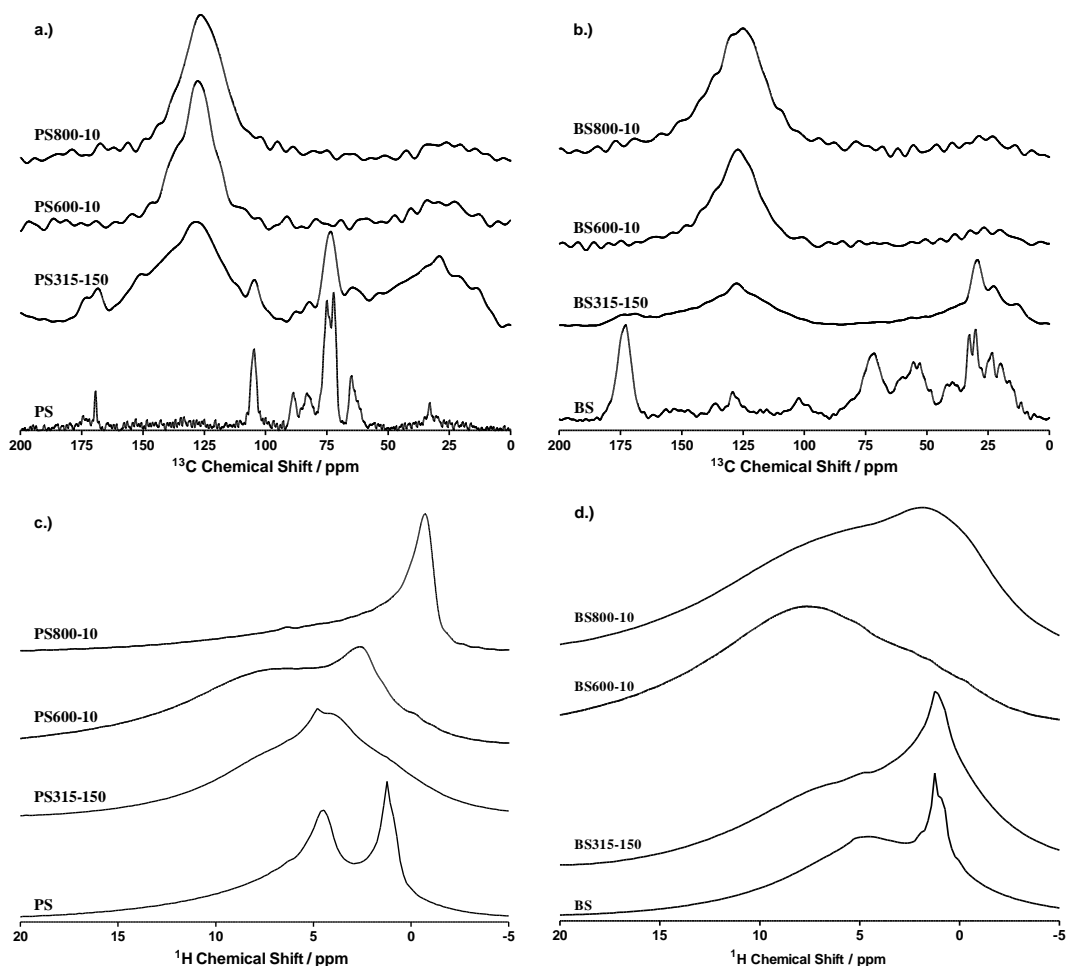


Figure 5.3 - ^{13}C CPMAS and ^1H MAS solid state NMR of primary sludge (a.) and c.), respectively) and biological sludge (b.) and d.), respectively) before and after pyrolysis.

The ^1H MAS solid state NMR spectra of the raw sludge and produced adsorbents are shown in Figure 5.3 c.) and d.). The results are consistent with the conclusions taken from the ^{13}C CPMAS NMR spectra. PS presents two broad peaks centered at 1.2 and 4.4 ppm which might correspond to alkyl protons and ether/alcohol protons of the cellulose, respectively. With the increase of pyrolysis temperature (PS315-150 and PS600-10) these bands are replaced for broader bands shifted towards the aromatic region of the spectra. Finally, PS800-10 presents a narrower band than the previous adsorbents centered at -0.6 ppm. Taking into account that FTIR and ^{13}C CPMAS NMR point out to the formation of an aromatic material with little or no aliphatic groups,

the occurrence of this peak might result from highly shielded protons due to very intense aromatic electronic currents in a highly aromatic structure. The same conclusions can be applied to BS and corresponding adsorbents. The main difference relies on BS800 spectrum that presents an even broader band, including shielded and non-shielded regions, probably caused by a considerable dispersion of the protons chemical environments in the produced material.

The results of the physical characterization of the pyrolysed sludge are detailed in Table 5.4. Despite knowing, from the elemental analysis, that the pyrolysis of BS resulted in the largest release of volatiles, physical characterization indicates that PS related biochars developed a more porous surface. The apparent density of PS biochars is around 0.5 g cm^{-3} , while BS biochars have a very high apparent density, suggesting low pore formation. Concerning the specific surface area (S_{BET}), there is a steep increase of this parameter for PS biochars with the increase of pyrolysis temperature, reaching $209 \text{ m}^2 \text{ g}^{-1}$ for PS800-150 (which is a very satisfactory value for a pyrolysed non-activated carbon), while BS adsorbents' surface area did not evolved significantly. The total pore and micropore volumes are also much higher for PS pyrolysed sludge as well as the average micropore width which is 1.02 nm for PS800-150. The same conclusions can be taken from the average pore diameter: it reduces considerably with the increase of pyrolysis temperature of PS, reaching 1.26 nm for PS800-150, compatible with a microporous structure and again very close to that of the commercial carbon. On the other hand, biological sludge-based carbons did not significantly developed micropores: their characterization is consistent with a mesoporous material. Overall, the physical characterization of the produced adsorbents indicates that the pyrolysis of PS results in the most interesting characteristics: low apparent density, high surface area and higher total pore and micropore volumes. These results also show that the residence time of 150 min (PS800-150) in comparison with 10 min (PS800-10) resulted in an adsorbent that should have the most promising adsorption capacity.

Table 5.4 - Physical characterization of the pyrolysed sludge

Sample	N ₂ adsorption at -196 °C					Hg porosimetry
	S_{BET} (m ² g ⁻¹)	V_p (cm ³ g ⁻¹)	W_θ (cm ³ g ⁻¹)	L (nm)	D_p (nm)	ρ_{app} (g cm ⁻³)
PS315-150	3.43	0.02	0.0014	-	9.82	0.50
PS600-10	94.4	0.06	0.0390	-	1.37	0.50
PS800-10	121	0.08	0.0470	0.88	1.41	0.51
PS800-150	209	0.13	0.0780	1.02	1.26	0.52
BS315-150	0.77	0.0043	0.0003	-	11.15	0.83
BS600-10	1.01	0.0053	0.0004	-	10.54	1.34
BS800-10	10.8	0.020	0.0014	-	3.69	0.99

Note: S_{BET} -surface area; V_p -total pore volume; W_θ -total micropore volume; L -average micropore width; D_p -average pore diameter.

The morphological characterization of the PS, BS and adsorbents produced at 800 °C (chosen due to their higher surface areas) was evaluated by SEM (PS and BS micrographs are shown in Figure 5.4). All the samples were visualized at 3 000, 10 000 and 30 000× magnification to allow a direct comparison of different detail levels between them. PS micrographs show long and homogeneous cellulose fibers with a relatively smooth surface. After pyrolysis at 800 °C for 10 and 150 min (PS800-10 and PS800-150) it is clearly observed a high fragmentation of those fibers and an enormous increase in the roughness of the surface. When comparing the micrographs taken at 10 000 and 30 000 × magnifications (on the right), the increase on surface area is evidently shown; this fact is particularly clear for PS800-150 where the existence of several layers of adsorbent and pores can be easily observed. These results fully support the conclusions taken from the remaining characterization techniques, showing a very satisfactory increase in the surface area and development of a porous adsorbent. The micrographs of BS and BS800-10 evidence that, despite the formation of a roughest surface after pyrolysis, BS are in the form of unevenly organized large aggregates (see the scale at 3 000× magnification micrograph in comparison with PS) which should be the main reason for the low surface areas obtained in the physical characterization.

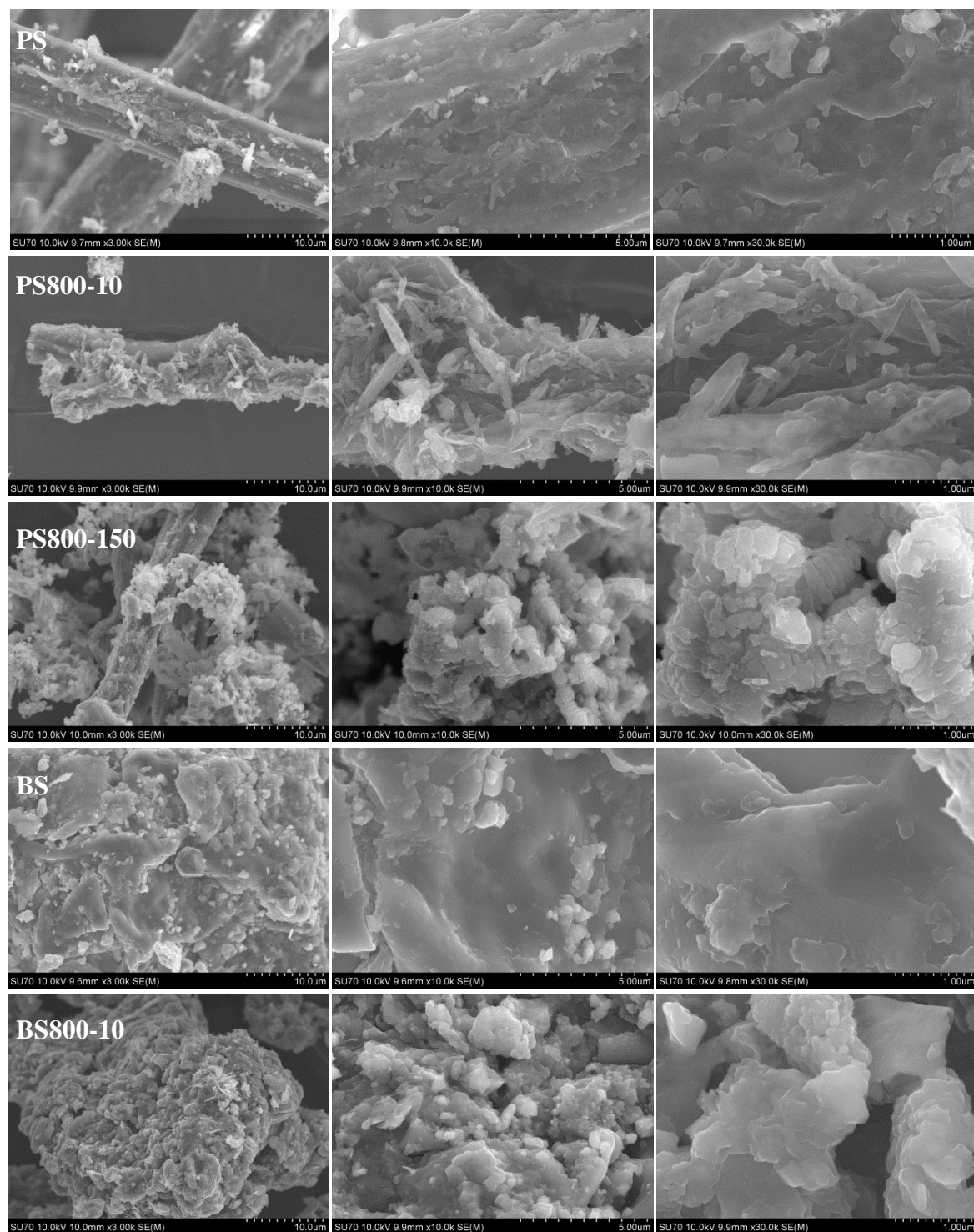


Figure 5.4 - SEM micrographs of PS, PS800-10, PS800-150, BS and BS800-10 (from top to bottom) at 3 000, 10 000 and 30 000 \times magnifications (from left to right).

In a collaborative work [1], PS and BS pyrolysed materials were applied as adsorbents on the removal of citalopram, a human antidepressant, from water. In general, all the produced adsorbents were capable to remove citalopram in a very short time of equilibrium; however, their adsorption capacities did not compete with those obtained using a commercial activated carbon. It

was observed that the BS adsorbents did not present advantageous characteristics for the removal of this pharmaceutical from contaminated waters, contrarily to PS adsorbents that shown a reasonable adsorption capacity. The increase of the pyrolysis temperature resulted in adsorbents with better adsorption capacity (5 times more adsorption for the highest temperature). The effect of the residence time at 800 °C (PS800-10 and PS800-150) was also tested and the highest residence time doubled the adsorption capacity. The best results were obtained for the adsorbent with highest surface area and microporous volume (PS800-150) and not for the adsorbents with the highest organic carbon content and the most efficient volatiles release (as it is the case of the BS related adsorbents) [1].

Taking into consideration all the results obtained in the removal of citalopram onto pyrolysed PS and BS, which can be consulted in detailed in Calisto et al. (2014) [1], and in order to improve the performance of these adsorbents, in the context of the work presented in this thesis, the pyrolysis temperature and residence time were uniformed for both sludge and, likely PS800-150, BS was also pyrolysed at 800 °C during 150 min (BS800-150). However, it was observed the increase of ash content with pyrolysis temperature and residence time in PS and BS materials and several studies have reported that the presence of ash and inorganic matter (including carbonates) could negatively influence the adsorption [13,30]. So, in order to rinse ashes and inorganic matter from the surface of these produced biochars, an acidic wash was performed, resulting in new adsorbent materials, named PSC and BSC, respectively. Physicochemical characterization of PSC and BSC is presented and discussed in the next section.

5.3.3 Characterization of pyrolysed and washed paper mill sludge and PAC

As it can be seen by proximate analysis results, presented in Table 5.5, and compared with those shown in Table 5.3, PSC ash content is about two times lower than the respective pyrolysed material (PS800-150). Although BS800-150 was not characterized, after the acidic wash, BSC slightly decreased the ash content when compared with BS800-10 (from 50 to 42%). In general, moisture content, volatile matter and fixed carbon increased for PSC, while for BSC only volatile matter was increased. On the other hand, PAC has highly volatile matter content and almost no fixed carbon.

The elemental analysis of PAC, PSC and BSC is presented on a dry basis in Table 5.5. PSC has significantly higher amount of elemental carbon and lower amount of elemental oxygen than that of its raw material and PS800-150 (Table 5.3). BSC has nearly the same elemental carbon and hydrogen contents as the other BS pyrolysed (mainly BS800-10), as shown in Table 5.3. Also, it can be observed that the elemental nitrogen and sulphur decreased after acidic wash, while

elemental oxygen content increased. Comparing PSC and BSC with PAC, the latter has the highest elemental carbon and oxygen contents which are consequence of the lowest ash content.

Table 5.5 - Proximate and elemental analyses of PSC, BSC and PAC

Sample	PAC	PSC	BSC
<i>Proximate analysis (wt. %, db)^a</i>			
Moisture content	8.13	9.04	5.35
Volatile matter	90.4	68.5	28.1
Fixed carbon	0.01	31.6	29.9
Ash	9.58	28.7	42.0
<i>Elemental analysis (wt. %, db)^a</i>			
C	82.0±0.4	67±1	49±3
H	0.6±0.1	1.1±0.3	1.06±0.09
N	0.28±0.01	0.30±0.01	2.49±0.09
S	0.72±0.03	1.29±0.02	0.92±0.04
O ^b	6.9±0.4	2±1	5±3

^aProximate and elemental analyses are presented on a dry basis (db).

^bEstimated by difference: O (%) = 100-C-H-N-S-Ash.

Note: [C]-carbon content; [H]-hydrogen content; [N]-nitrogen content; [S]-sulphur content; [O]-oxygen content

The FTIR results (Figure 5.5) evidence that the spectra of PSC and BSC did not present any bands, as well as PAC, which is typical of activated carbons. This result, together with elemental analysis, suggests that both adsorbents have few functional groups in its surface.

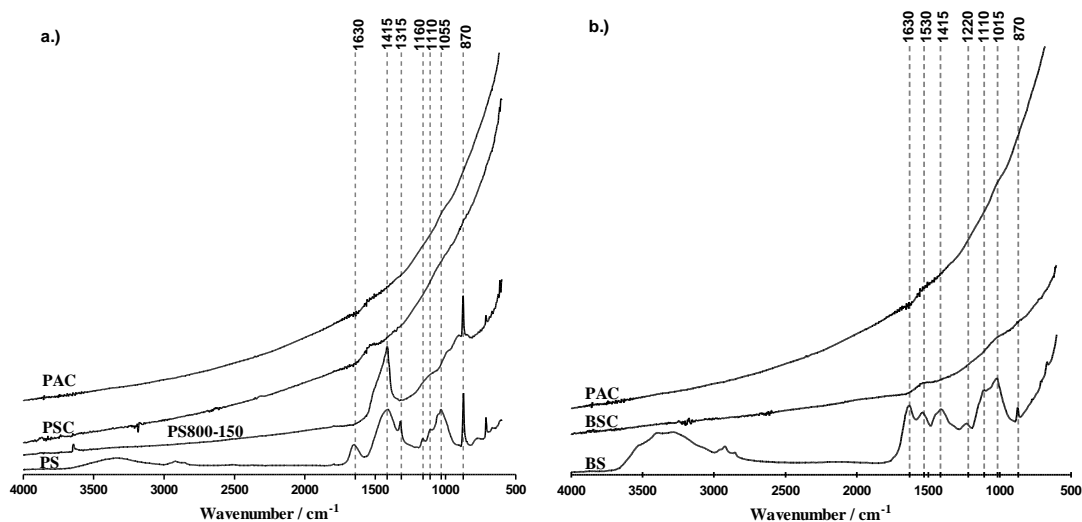


Figure 5.5 - FTIR spectra of PS, BS and pyrolysed and washed sludge (a.) and b.), respectively).

Results from the Boehm's titration of acid and basic functional groups are depicted in Table 5.6 together with PZC values. Concerning the amount of acidic groups, only the carboxylic groups were measurable (*i.e.*, amount of lactone and phenol groups are negligible) and the quantity of carboxylic groups are almost the same for the three adsorbents. Regarding the amount of basic groups, differences between carbons are more perceptible: BSC is the material with highest quantity of basic groups, $4.2 \pm 0.5 \text{ mmol g}^{-1}$, followed by PSC and PAC with $1.3 \pm 0.1 \text{ mmol g}^{-1}$ and $0.6 \pm 0.1 \text{ mmol g}^{-1}$, respectively. Analysing the PZC values, they indicate different net surface charges between the carbons. Under the conditions adopted in the adsorption studies, pH 7-7.5, PAC and BSC have a net positive charge ($\text{PZC} > \text{pH}$) while PSC has a neutral surface charge since its $\text{PZC} \approx \text{pH}$ 7-7.5. These results corroborate with those obtained from Boehm's titration, mainly for BSC where the quantity of basic groups is higher than the acidic groups.

Concerning the S_{BET} , determined from the N_2 adsorption isotherms, PAC has the highest surface area ($1109 \text{ m}^2 \text{ g}^{-1}$). Regarding PSC and BSC-a (powdered materials), whose production did not involve activation, the surface areas are only 3 to 4 times lower than PAC, as can be seen in Table 5.6. As discussed in section 5.3.2, when PS is used as starting material, it was observed a significant increase of S_{BET} with the increase of pyrolysis temperature and time of residence (Table 5.4). A further increase of surface area from 209 up to $414 \text{ m}^2 \text{ g}^{-1}$ and, consequently, an increase of micropore volume, were obtained by the single acidic wash step. Thus, the acidic washing significantly improved the surface area of the pyrolysed PS by the removal of inorganic matter (mainly carbonates in PS) and ashes and the associated unclogging of pores. The same conclusion could be taken for BSC, which S_{BET} increased up to $291 \text{ m}^2 \text{ g}^{-1}$ after acidic wash. Regarding the change of physical properties related with BSC particle size, as expected S_{BET} decreases with particle size increases, as well as V_p and W_0 . As mentioned in Chapter 2, the use of powdered adsorbents has advantages concerning the adsorption capacity and the kinetic of adsorption; however, in real continuous flow process, granulated adsorbents have more advantages. In this sense, the effect of the BSC particle size in the adsorption of MS-222 is assessed in the next Chapter 6. In the present chapter, PSC (powdered) and BSC-b (granulated) were used in the adsorption of the three most used fish anaesthetics (MS-222, benzocaine and 2-PE).

Table 5.6 - Physico-chemical properties of pyrolysed and washed materials

Sample	N ₂ adsorption at -196 °C			Boehm Titration ^a				PZC
	S_{BET} (m ² g ⁻¹)	V_p (cm ³ g ⁻¹)	W_0 (cm ³ g ⁻¹)	Acidic Groups (mmol g ⁻¹)			Basic Groups (mmol g ⁻¹)	
				Carboxylic	Lactone	Phenol		
PAC	1109	0.637	0.187	1.0±0.1	0	0	0.6±0.1	8.7
PSC	414	0.275	0.0949	1.18±0.05	0	0	1.3±0.1	7.0
BSC-a	291	0.269	0.0386	-	-	-	-	-
BSC-b	258	0.247	0.0388	1.6±0.3	0	0	4.2±0.5	10.4
BSC-c	140	0.146	0.0179	-	-	-	-	-
BSC-d	72	0.080	0.0064	-	-	-	-	-

^aEach value (±standard deviation) is the average of three replicates.

Note: S_{BET} - surface area; V_p - total pore volume; W_0 - total micropore volume; PZC - Point of zero charge

BSC-a: <0.18 mm; -b: 0.18-0.5 mm; -c: 0.5-1.0 mm; -d: 1.0-2.0 mm

5.3.4 Adsorption results

Figure 5.6 shows the adsorption kinetics of the three fish anaesthetics onto the produced adsorbents (PSC, BSC-b) and PAC and the fittings of the kinetic models to the experimental data. Table 5.7 lists the adsorption rate constants of the pseudo-first order, pseudo-second order and double exponential kinetic models fittings and their respective coefficients of determination, r^2 . In general, the adsorption equilibrium was rapidly attained: adsorption equilibrium using PAC was reached after 60 to 120 min for all anaesthetics; equilibrium times using biochars were slightly higher (between 120 and 240 min, depending on the anaesthetic). Globally, the DEM model was the one giving the best fittings, as it may be inferred by r^2 values in Table 5.7. The application of this model to the experimental data provided some interesting conclusions: values of diffusion rate, k , suggest that the adsorption is controlled by external diffusion ($k_e < k_i$); but for the initial conditions (Eq. 2.6) the adsorption rate of the intraparticle diffusion is significantly higher than the external diffusion ($r_{i,0} > r_{e,0}$) in all adsorption experiments. This fact suggests the occurrence of a rapid adsorption when the molecules reach the intraparticle sites, being the external or interparticle diffusion the rate limiting step. Contrarily, as mentioned in last Chapter 4 (section 4.3.3), in general, the MS-222 adsorption onto agricultural biowaste-based adsorbents is controlled by intraparticle diffusion and, thus, their adsorption kinetics are much slower than onto PSC, BSC-b and PAC.

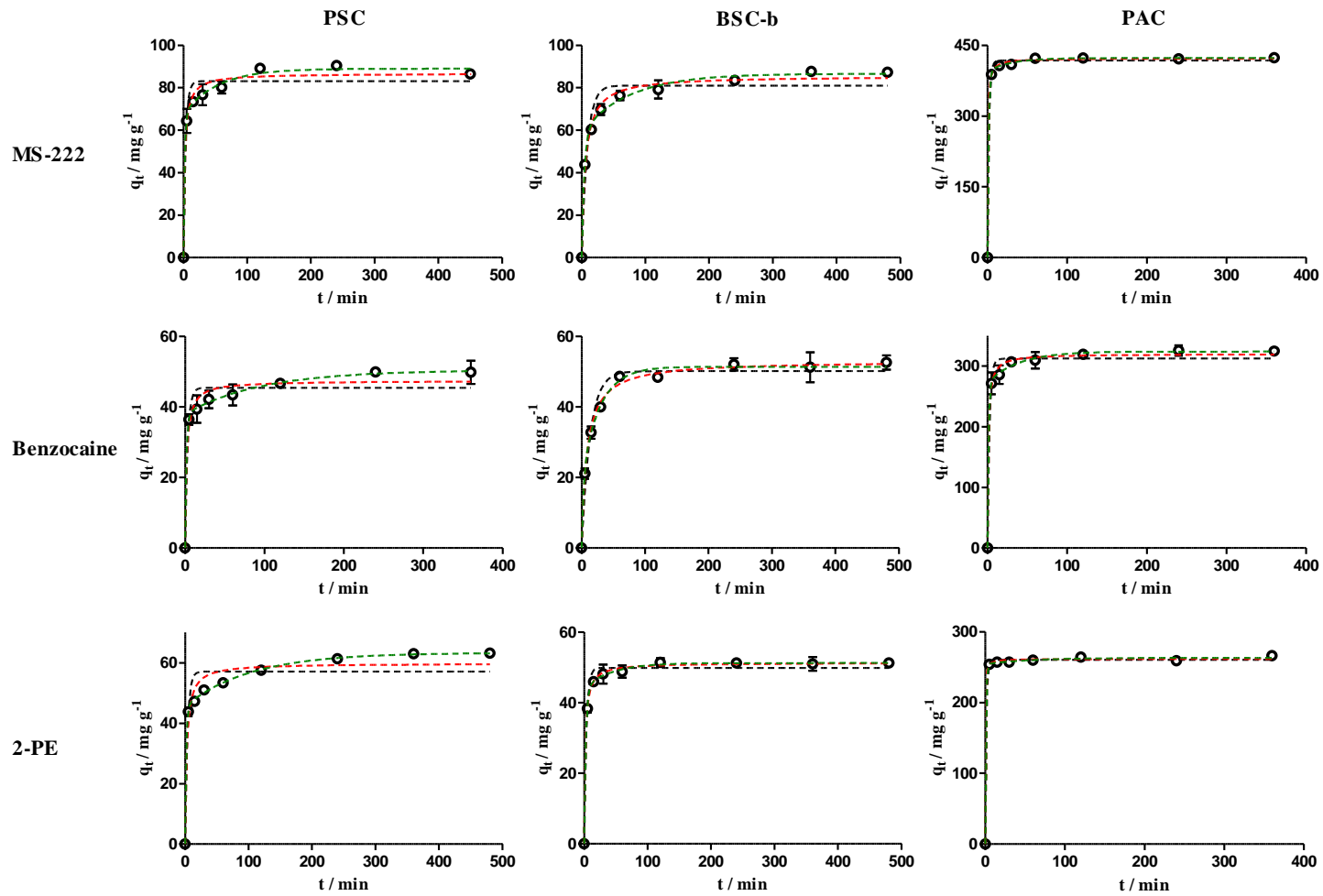


Figure 5.6 - Experimental data and predicted kinetic curves for the adsorption of three fish anaesthetics in water using the produced adsorbents and PAC. The experimental data (o) of PAC, PSC and BSC-b were fitted to pseudo-first order (---), pseudo-second order (---) and double exponential (---) kinetic models. Each experimental point (\pm standard deviation) is the average of three replicates. Note that x and y -axis scales are not the same in all graphs to allow a better visualization of the results.

Table 5.7 - Fitting parameters of pseudo-first and pseudo-second order kinetic models and double exponential model to the experimental data

		MS-222			Benzocaine			2-PE		
Kinetic Parameters		PSC	BSC-b	PAC	PSC	BSC-b	PAC	PSC	BSC-b	PAC
Pseudo-1 st order	k_1 (min ⁻¹)	0.28±0.06	0.11±0.02	0.52±0.05	0.31±0.08	0.07±0.01	0.40±0.07	0.26±0.08	0.28±0.03	0.7±0.1
	q_e (mg g ⁻¹)	83±3	81±3	418±3	45±2	50±1	312±6	57±2	49.9±0.7	261±1
	r^2	0.9635	0.9529	0.9983	0.9522	0.9733	0.9871	0.9285	0.9899	0.9988
Pseudo-2 nd order	k_2 (g mg ⁻¹ min ⁻¹)	0.006±0.001	0.0021±0.0003	0.0051±0.0006	0.011±0.003	0.0022±0.0002	0.0030±0.0006	0.007±0.002	0.011±0.007	0.021±0.008
	q_e (mg g ⁻¹)	87±2	86±1	422±2	47±1	53.1±0.7	320±4	60±2	51.3±0.2	262±1
	r^2	0.9862	0.9920	0.9996	0.9785	0.9952	0.9959	0.9686	0.9991	0.9992
Double Exponential (DEM)	D_e (mg L ⁻¹)	43±9	55±8	14±5	12.5±0.9	31±6	8±2	106±4	35±6	13±8
	k_e (min ⁻¹)	0.019±0.009	0.013±0.004	0.03±0.02	0.010±0.002	0.035±0.009	0.03±0.01	0.0097±0.0001	0.023±0.007	0.02±0.02
	$r_{e,0}$ (mg g ⁻¹ min ⁻¹)	0.4±0.2	0.4±0.1	0.9±0.5	0.13±0.03	1.1±0.4	1.4±0.6	0.1±0.1	0.2±0.1	0.1±0.1
	D_i (mg L ⁻¹)	135±11	119±10	198±5	38±1	20±6	41±2	274±6	221±7	382±9
	k_i (min ⁻¹)	0.5±0.2	0.24±0.04	0.7±0.1	0.57±0.09	0.3±0.2	0.7±0.3	0.56±0.06	0.38 ±0.03	1.0±0.7
	$r_{i,0}$ (mg g ⁻¹ min ⁻¹)	35±12	14±3	278±47	22±4	7±4	200±81	26±4	17±2	259±173
	q_e (mg g ⁻¹)	89±2	87±2	423±2	50.5±0.8	51.4±0.8	324±3	63.3±0.6	51.3±0.3	263±2
	r^2	0.9970	0.9965	0.9998	0.9993	0.9962	0.9991	0.9995	0.9995	0.9995

Figure 5.7 shows the equilibrium data of anaesthetics adsorption onto the adsorbents used in this work together with the fittings to the equilibrium models. As may it be seen in Figure 5.7, the three adsorbents here used were able to efficiently remove the considered anaesthetics from solution. The shape of the adsorption isotherms of the anaesthetics onto the adsorbents revealed that the process is favourable, which means that the adsorbents are efficient not only in removing high but also low concentrations of the contaminant. When comparing the adsorbents performance, Figure 5.7 evidences that PAC displayed larger adsorption capacities for the three anaesthetics than both the biochars here produced. With respect to the biochars, their performance was similar for MS-222 and benzocaine while PSC displayed larger 2-PE adsorption capacity than BSC-b. In order to support this information, Table 5.8 shows fitting parameters to Langmuir, Freundlich and Langmuir-Freundlich isothermal models and their coefficient of determination, r^2 . In general, the Langmuir-Freundlich model has the highest coefficient being these fitting parameters the ones selected for the following analysis. The first aspect that stands out is the PAC performance, *i.e.*, the maximum adsorption capacities obtained were between 4 and 8 times higher than that for produced biochars: 631, 435 and 289 mg g⁻¹ for MS-222, benzocaine and 2-PE, respectively (removal percentages above 98%). These results suggest that the surface area and carbonaceous structure play an important role in the performance of the adsorbents, since, as could be observed in Table 5.6, PAC has the highest value of S_{BET} , which is about 3 and 4 times higher than that for PSC and BSC-b, respectively. Besides S_{BET} , another important characteristic to take into account is the charge of the adsorbents surface and the charge of each anaesthetic molecule. Under the conditions adopted in the adsorption studies, pH 7-7.5, the three anaesthetics here considered are in the neutral form (see pK_a values in Table 2.1). Moreover, in this pH range, the PAC and the BSC-b surfaces are positively charged while PSC has a neutral net charge (see PZC values in Table 5.6). The fact that BSC-b and PAC have a positive net charge could induce van der Waals forces (dipole-induced dipole interactions) with the anaesthetics; *i.e.*, forces between the positively charged basic groups of these adsorbents (permanent dipole) and a corresponding induced dipole in the anaesthetic molecules. On the other hand, the salt used to buffer the anaesthetic solutions (NaHCO₃) could interact with the positively charged groups of the adsorbents by electrostatic interactions, forming an electric double layer and allowing the salt to mediate the interaction between the carbon and the anaesthetic.

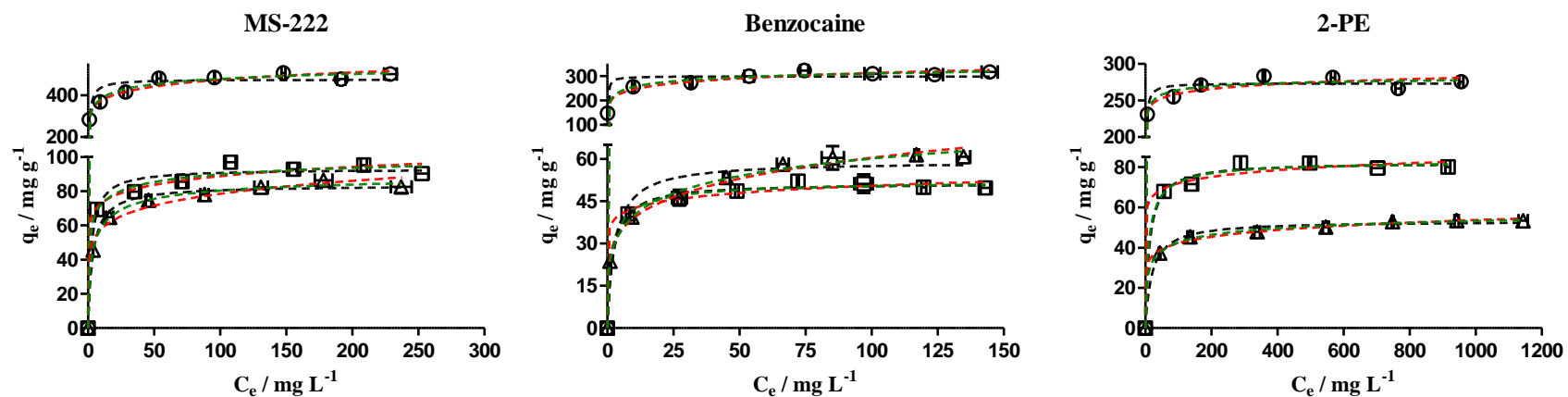


Figure 5.7 - Experimental and predicted isotherms for the adsorption of the MS-222, benzocaine and 2-PE in water using produced biochars and PAC. The experimental data of PAC (o), PSC (\square) and BSC-b (Δ) were fitted to Langmuir (---), Freundlich (---) and Langmuir-Freundlich (-.-) equilibrium models. Each experimental point (\pm standard deviation) is the average of three replicates. Note that y-axis scales are not the same in all graphs to allow a better visualization of the results.

Table 5.8 - Fitting parameters of Langmuir, Freundlich and Langmuir-Freundlich equilibrium models to the experimental data

		MS-222			Benzocaine			2-PE		
Equilibrium Parameters		PSC	BSC-b	PAC	PSC	BSC-b	PAC	PSC	BSC-b	PAC
Langmuir	$q_{m,L}$ (mg g ⁻¹)	93±2	83±2	475±15	51.4±0.7	59±3	299±8	82±2	53.2±0.8	274±4
	K_L (L mg ⁻¹)	0.4±0.1	0.28±0.04	1.1±0.4	0.45±0.08	0.4±0.1	7±2	0.08±0.02	0.050±0.007	0.8±0.2
	r^2	0.9831	0.9910	0.9571	0.9955	0.9471	0.9659	0.9939	0.9943	0.9930
Freundlich	K_F (mg g ⁻¹ (mg L ⁻¹) ^{-1/NF})	60±5	43±3	296±15	36±2	25±1	193±8	54±6	26±1	220±10
	N_F	12±2	8±1	10±1	13±3	5.3±0.4	9.6±0.9	16±5	9.5±0.8	28±6
	r^2	0.9867	0.9851	0.9865	0.9921	0.9927	0.9900	0.9907	0.9967	0.9934
Langmuir-Freundlich	$q_{m,LF}$ (mg g ⁻¹)	109±29	92±4	631±124	53±3	107±30	435±103	83±6	63±7	289±28
	K_{LF} (L ^{1/NLF} mg ^{-1/NLF})	0.8±0.2	0.44±0.06	0.8±0.2	0.7±0.5	0.27±0.09	0.8±0.4	0.14±0.03	0.31±0.09	2.0±0.6
	N_{LF}	3±2	1.7±0.3	3±1	1.3±0.7	3.0±0.6	4±1	1.2±0.9	2.4±0.8	3±2
	r^2	0.9889	0.9973	0.9914	0.9958	0.9958	0.9938	0.9940	0.9983	0.9950

Comparing the adsorption results presented in this chapter with the literature studies mentioned in the Chapter 2 using activated carbon to adsorb MS-222 and benzocaine from water (adsorption capacities up to 64 mg g^{-1}) [31] and in the Chapter 4 using agricultural waste-based adsorbents to adsorb MS-222 (adsorption capacity of 34 mg g^{-1} using pyrolysed peanut shell as adsorbent), both PAC and industrial waste-based adsorbents herein studied have higher adsorption capacities. Also, comparing the biological treatment in an upflow anaerobic sludge blanket reactor (96.4% of efficiency in 154 days) [32] and photo-Fenton process (62% of efficiency in 1.5 min) [33] for the removal of 2-PE, with both biochars and PAC herein tested, these last have the best relation between adsorption efficiency and removal time. The obtained results point to the promissory utilization of paper mill sludge-based adsorbents as alternative materials for the recycling of water in RASs, rather the agricultural biowaste-based ones, produced and tested in Chapter 4. Among the industrial waste-based adsorbents, BSC was chosen for the following experiments, given that it is more versatile for real continuous flow processes, *i.e.*, it can be produced in powdered or granulated form. In this context, studies have been performed in order to evaluate the effect of its particle size, as well as the effect of temperature, salinity, aquaculture water matrix and the effect of competitive adsorption, and the results will be presented in next Chapter 6.

5.4 Conclusions

Physical and chemical characterization of the adsorbents revealed that pyrolysis effectively resulted in the disappearance of PS and BS main functional groups, generating highly aromatic structures. However, contrarily to BS, only PS resulted in the production of a microporous biochar with high surface area, *i.e.*, there was a steep increase of S_{BET} for PS biochars with the increase of pyrolysis temperature, reaching $209 \text{ m}^2 \text{ g}^{-1}$ for PS800-150 (which is a very satisfactory value for a pyrolysed non-activated carbon), while BS adsorbents' surface area did not evolved significantly, reaching only $10 \text{ m}^2 \text{ g}^{-1}$ for BS800-10. After the acidic wash performed to PS800-150 and BS800-150, the S_{BET} increased up to 414 and $291 \text{ m}^2 \text{ g}^{-1}$ in the case of PSC and BSC, respectively, and, consequently, the micropore volume increased for both adsorbents. These last two adsorbents were tested in the adsorption of three fish anaesthetics from water and compared with the commercial activated carbon.

Despite the different concentration range of utilization of the considered anaesthetics and, consequently, their respective different concentrations found in the RASs, adsorption seems to be an excellent option for their removal from water. The use of powdered activated carbon resulted in highest adsorption capacities, between 289 and 631 mg g^{-1} . On the other hand, adsorbents produced

from primary and biological paper mill sludge displayed removal capacities in the range 53-109 mg g⁻¹ and 63-107 mg g⁻¹, respectively. Considering that, contrarily to commercial activated carbons, the production process of these adsorbents avoids the utilization of activating chemicals and, also, allows the recovery of energy from wastes, it may be considered an environmentally friendly process. For this reason, and allied to the good results obtained for the removal of fish anaesthetics in batch system, the use of paper mill sludge-based adsorbents may be an alternative choice to be used in RASs and will be tested in real continuous flow processes, such as fixed-bed column reactors, in laboratory and semi-pilot scales, in the next chapters.

5.5 References

- [1] Calisto, V., Ferreira, C.I.A., Santos, S.M., Gil, M.V., Otero, M. and Esteves, V.I., 2014, *Bioresource Technology*, 166 (0), 335-344.
- [2] Ferreira, C.I.A., Calisto, V., Otero, M., Nadais, H. and Esteves, V.I., 2016, *Aquacultural Engineering*, 74, 76-83.
- [3] Monte, M.C., Fuente, E., Blanco, A. and Negro, C., 2009, *Waste Management*, 29 (1), 293-308.
- [4] EC, 2008, Directive 2008/98/EC of European Parliament and of the Council of 19 November 2008 on waste and repealing certain Directives, *Official Journal of the European Union*.
- [5] Stoica, A., Sandberg, M. and Holby, O., 2009, *Bioresource Technology*, 100 (14), 3497-3505.
- [6] CEPI, <http://www.cepi-sustainability.eu/forestry>, last accessed in August 2016.
- [7] Likon, M. and Trebše, P., 2012, Industrial Waste, *InTech*.
- [8] Pervaiz, M. and Sain, M., 2015, *CLEAN – Soil, Air, Water*, 43 (6), 919-926.
- [9] Buruberri, L.H., Seabra, M.P. and Labrincha, J.A., 2015, *Journal of Hazardous Materials*, 286, 252-260.
- [10] Battaglia, A., Calace, N., Nardi, E., Petronio, B.M. and Pietroletti, M., 2003, *Microchemical Journal*, 75 (2), 97-102.
- [11] Auta, M. and Hameed, B.H., 2014, *Journal of Industrial and Engineering Chemistry*, 20 (3), 830-840.
- [12] Masomi, M., Ghoreyshi, A.A., Najafpour, G.D. and Mohamed, A.R.B., 2015, *Desalination and Water Treatment*, 55 (6), 1453-1466.
- [13] Jaria, G., Calisto, V., Gil, M.V., Otero, M. and Esteves, V.I., 2015, *Journal of Colloid and Interface Science*, 448 (0), 32-40.
- [14] Coimbra, R.N., Calisto, V., Ferreira, C.I.A., Esteves, V.I. and Otero, M., 2015, *Arabian Journal of Chemistry*.
- [15] AENOR, 1995. Solid mineral fuels. Determination of moisture in the analysis sample. *Asociación Española de Normalización y Certificación*.
- [16] AENOR, 1985. Hard coal and coke. Determination of volatile matter content. *Asociación Española de Normalización y Certificación*.
- [17] AENOR, 1984. Solid mineral fuels. Determination of ash. *Asociación Española de Normalización y Certificación*.
- [18] Brunauer, S., Emmett, P.H. and Teller, E., 1938, *Journal of the American Chemical Society*, 60 (2), 309-319.
- [19] Dubinin, M.M., 1966, *Chemistry and Physics of Carbon*, Marcel Dekker Inc., New York, p. 51-120.
- [20] Stoeckli, F. and Ballerini, L., 1991, *Fuel*, 70 (4), 557-559.

- [21] Boehm, H.P., 1966, *Advances in Catalysis*, Academic Press, p. 179-274.
- [22] Souza, C., Majuste, D. and Ciminelli, V.S.T., 2014, *Hydrometallurgy*, 142 (0), 1-11.
- [23] Ross, L.G. and Ross, B., 2008, *Anaesthetic and Sedative Techniques for Aquatic Animals*, Blackwell Publishing Ltd, Oxford, UK.
- [24] FAO, <http://www.fao.org/fishery/culturedspecies/search/en>, last accessed in January 2016.
- [25] Méndez, A., Fidalgo, J.M., Guerrero, F. and Gascó, G., 2009, *Journal of Analytical and Applied Pyrolysis*, 86 (1), 66-73.
- [26] Coates, J., 2000, *Interpretation of infrared spectra – a practical approach*, John Wiley & Sons Ltd., Chichester.
- [27] McBrierty, V.J. and Packer, K.J., 2006, *Nuclear Magnetic Resonance in Solid Polymers*, Cambridge University Press, New York.
- [28] Jackson, M.J. and Line, M.A., 1997, *Journal of Agricultural and Food Chemistry*, 45 (6), 2354-2358.
- [29] Beyer, L., Fründ, R. and Mueller, K., 1997, *Science of The Total Environment*, 197 (1), 127-137.
- [30] Nevskaiia, D.M., Sepulveda-Escribano, A. and Guerrero-Ruiz, A., 2001, *Physical Chemistry Chemical Physics*, 3 (3), 463-468.
- [31] Dawson, V.K., Marking, L.L. and Bills, T.D., 1976, *Transactions of the American Fisheries Society*, 105 (1), 119-123.
- [32] Puyol, D., Monsalvo, V.M., Mohedano, A.F., Sanz, J.L. and Rodriguez, J.J., 2011, *Journal of Hazardous Materials*, 185 (2-3), 1059-1065.
- [33] Real, F.J., Benitez, F.J., Acero, J.L., Roldan, G. and Casas, F., 2012, *Industrial & Engineering Chemistry Research*, 51 (50), 16209-16215.

6 Study of the influence of operational conditions on the adsorption of MS-222 onto biological paper mill sludge-based adsorbent

In the present chapter, the implementation of the adsorption process in the RASs is proposed by using pyrolysed biological paper mill sludge as adsorbent, to remove MS-222 from aquaculture wastewater. Adsorption experiments were performed under extreme operating conditions, simulating those corresponding to different farmed fish species: temperature (from 8 to 30 °C), salinity (from 0.8 to 35‰) and presence of organic and inorganic matter in the aquaculture wastewater. Furthermore, the MS-222 adsorption from a real aquaculture effluent was compared with that from ultrapure water. Under the studied conditions, the performance of the produced adsorbent remained mostly the same, removing satisfactorily MS-222 from water. Therefore, it may be concluded that the produced adsorbent can be employed in intensive aquaculture wastewater treatment with the same performance independently of the farmed fish species.

The work presented and discussed in this chapter resulted in the following publication:

[1] Ferreira C.I.A., Calisto V., Otero M., Nadais H., Esteves V.I. (2017), Removal of tricaine methanesulfonate from aquaculture wastewater by adsorption onto pyrolysed paper mill sludge. *Chemosphere*, 168, 139-146. DOI: 10.1016/j.chemosphere.2016.10.045

6.1 Contextualization

Tricaine methanesulfonate (MS-222) is the most widely used fish anaesthetic and the only one approved by the U.S. Food and Drug Administration (FDA) [2]. The recommended dosages are significantly different among species, varying between 25 and 480 mg L⁻¹, and the exposure times range from seconds or few minutes for high concentrations up to hours for low concentrations [3]. The MS-222 in solution may reduce pH by 0.5–1.0 units and low pH has been described as being irritant to fish [4]. So, to prevent this effect, the administered anaesthetic solutions should be buffered using sodium bicarbonate or Tris-buffer at pH 7.0-7.5 [3]. Apart from pH, other operational conditions of intensive aquaculture systems have to be considered and controlled, such as temperature, salinity, oxygen and the density of the water column. These conditions are essentially dependent on the fish species.

Although numerous factors need to be taken into account for a high-quality indoor fish rearing, water quality is one of the most important conditions for the success of fish cultures. The implementation of recirculating aquaculture systems (RASs) in intensive fish culture systems allows cleaning the water for reuse through fish culture tanks, maintaining the water quality. As mentioned in Chapter 2, within the several water treatment processes presented, the adsorption using activated carbons has been pointed as a very interesting and efficient process, mainly in the removal of organic contaminants, such as pharmaceuticals; however, the high price of activated carbons is their main limitation for the implementation of this process in RASs (see section 2.4.1). Throughout this work, waste-based adsorbents were produced aiming at the removal of fish anaesthetics from water as an alternative to the commercial activated carbons. Paper mill sludge-based adsorbents seem to be promising to their application in RASs and also with the advantage that allow for the thermal valorisation of a waste from the paper industry. However, the RASs processes have to take into account the particular conditions of fish production, *i.e.*, any water treatment process applied in this context should not be affected by operating conditions such as temperature, salinity and/or dissolved organic matter.

In this chapter, the adsorptive removal of the fish anaesthetic MS-222 from water by biological paper mill sludge-based adsorbents was evaluated under operating conditions normally used in aquaculture systems, namely temperature, salinity and organic/inorganic matter content. Also, MS-222 adsorption kinetic and equilibrium experiments were performed using aquaculture wastewater as aqueous matrix provided by a local producer of common sole in an intensive aquaculture system. For comparison purposes, a commercial activated carbon was tested in the same conditions.

6.2 Materials and methods

6.2.1 Adsorbent materials

In this chapter, the tested adsorbents were the pyrolysed and washed biological paper mill sludge (BSC), produced and characterized in previous Chapter 5. In a first approach, the four BSC particle sizes were tested (BSC-a: <0.18 mm; BSC-b: 0.18-0.5 mm; BSC-c: 0.5-1.0 mm and BSC-d: 1.0-2.0 mm) to assess the influence of BSC particle size on the MS-222 adsorption, and then one size was chosen for the further experiments. Since those adsorbents are granulated carbons, a commercial granulated activated carbon (GAC) DARCO 12×20 (particle size between 0.8 and 1 mm), provided and recommended by Norit for this specific application, was used as reference carbon for comparison purposes. This commercial GAC has $619 \text{ m}^2 \text{ g}^{-1}$ of specific surface area and a total micropore volume of $0.106 \text{ cm}^3 \text{ g}^{-1}$ (determined following the procedure described in Chapter 5, section 5.2.2.2).

6.2.2 Fish anaesthetics

Adsorption tests were performed for the fish anaesthetic tricaine methanesulfonate (> 97%, TCI Europe) - MS-222. Anaesthetic solutions were prepared in ultra-pure water obtained from a Milli-Q Millipore system (Milli-Q plus 185), buffered using 10^{-2} M of NaHCO_3 (> 99.5%, Fluka) to pH 7-7.5 as recommended by Ross et al. (2008) [3], and in aquaculture wastewater. The MS-222 physico-chemical properties are summarized in Chapter 2, Table 2.1.

6.2.3 Determination of the MS-222 concentration in water by MEKC

MEKC analyses were performed using a Beckman P/ACE MDQ (Fullerton, CA, USA) instrument, equipped with an UV-Vis detection system, following the procedure described in Appendix C (section C.1.1.1). Aqueous samples and standard solutions were analysed in triplicate. MS-222 calibration curve and parameters, including the limit of detection (LOD) and limit of quantification (LOQ), are also presented in Appendix C, section C.1.1.

6.2.4 Adsorption experiments

Adsorption experiments were performed in batch system, in 15 mL polypropylene tubes, by shaking the adsorbent with MS-222 solutions. Batch tests were carried out in an overhead shaker (Heidolph, Reax 2) at 90 rpm, inside a thermostatic incubator at different temperatures (as described in the following subsections). Conditions, such as adsorbent particle size, temperature, salinity and organic matter content were tested. At the same time, control experiments were also

performed, *i.e.*, the MS-222 solution was shaken under the same conditions but without the presence of the adsorbent, and it was verified that MS-222 was not adsorbed on polypropylene tubes. All the adsorption tests were performed in triplicate and the remaining concentration of MS-222 in solution after contacting with the adsorbent was determined by MEKC analysis.

Kinetic data were fitted to pseudo-first order (Eq. 2.2) and pseudo-second order (Eq. 2.3) kinetic models, using GraphPad Prism 5 software (trial version). These models are described in Chapter 2, section 2.4.3.1. Equilibrium data were fitted to the non-linear models, Langmuir (Eq. 2.7), Freundlich (Eq. 2.8) and Langmuir-Freundlich (Eq. 2.9) models, described in Chapter 2, section 2.4.3.2.

6.2.4.1 Influence of the adsorbent particle size

In order to evaluate the influence of particle size on the adsorption of MS-222 onto BSC, kinetic studies were performed using the different particle sizes listed in section 6.2.1. MS-222 solutions with initial concentration of 250 mg L^{-1} (the average concentration administered to farmed fish) were buffered using 10^{-2} M of NaHCO_3 to pH 7-7.5 and mixed with 2 g L^{-1} of each adsorbent. Batch tests were carried out at a constant shaking (90 rpm) and constant temperature ($18 \text{ }^\circ\text{C}$), between 5 and 480 min.

6.2.4.2 Influence of the temperature

Operating water temperature depends on the farmed fish species, as mentioned in Chapter 2. Thus, in order to evaluate the adsorption performance over the range of the most commonly used temperatures, kinetic studies were performed at different temperatures. MS-222 solutions (buffered using 10^{-2} M of NaHCO_3 to pH 7-7.5) were mixed with 2 g L^{-1} of BSC-b at 8, 18 and $30 \text{ }^\circ\text{C}$. Batch tests were carried out between 5 and 480 min at a constant shaking (90 rpm).

Also, in order to determinate the thermodynamic parameters, adsorption equilibrium experiments were performed. Solutions containing from 100 up to 450 mg L^{-1} MS-222 were mixed with 2 g L^{-1} of BSC-b and were shaken at a constant rotation (90 rpm) until equilibrium. These experiments were also carried out at three different temperatures: 8, 18 and $30 \text{ }^\circ\text{C}$. The equilibrium data were fitted to Langmuir model and the thermodynamic parameters, ΔG° , ΔH° and ΔS° , were determined, as described in Chapter 2, section 2.4.3.3.

6.2.4.3 Influence of the salinity

Salinity of water in intensive aquaculture is another factor that depends on the cultured aquatic species; so it is also important to evaluate the adsorption at different salt concentrations. Buffered MS-222 solution using 10^{-2} M of NaHCO_3 (pH 7-7.5) has a salinity of 0.8‰; MS-222

solutions with higher salinities (20 and 35‰) were prepared using a commercial sea salt (Tropic Marin®). This salt possesses buffering capacity at pH 7, so pH adjustment was not required. Kinetic studies were performed mixing 2 g L⁻¹ of BSC-b with each MS-222 solution (0.8, 20 and 35‰), for 5 to 480 min, at constant shaking (90 rpm) and constant temperature (18 °C).

6.2.4.4 Aquaculture wastewater

In order to recreate the real conditions, mainly the organic matter nature and concentration, adsorption experiments were performed using an effluent from a national fish producer as aqueous matrix. This aquaculture farm produces common sole in intensive system and has a RAS implemented that allows reutilizing approximately 95% of water. The production works at 18-19 °C, 20-21‰ of salinity and pH 7-7.5, which allows comparing the results here obtained with the results obtained under simulated conditions. Aquaculture wastewater was collected after the biological treatment (secondary wastewater treatment) and before the ozonation process (tertiary wastewater treatment) and was then filtered by using a glass microfiber filter of 2 µm (GF/C Whatman®), to remove the suspended solids. The filtered aquaculture wastewater was stored in glass bottles, in the dark, and used within 3 days. Total carbon (TC) and inorganic carbon (IC) quantification were carried out by TOC-VCPH Shimadzu analyser. Dissolved organic carbon (DOC) was estimated by difference between TC and IC contents of the filtrate.

Using the aquaculture wastewater as aqueous matrix (salinity 20‰), adsorption kinetic and equilibrium experiments were performed with BSC-b and DARCO 12×20 adsorbents. To study the adsorption kinetics, a defined amount of adsorbent (2 g L⁻¹ of BSC-b and 0.5 g L⁻¹ of DARCO 12×20) was mixed with aquaculture wastewater spiked with MS-222 (final concentration of 250 mg L⁻¹) at constant shaking (90 rpm), temperature (18 °C) and pH 7-7.5 (pH adjustment was not required). Sampling times varied from 5 min to 480 min for BSC-b and 15 min to 960 min for DARCO 12×20. In parallel and under identical operating conditions, the aquaculture effluent (without MS-222 spiking) was mixed with either BSC-b or DARCO 12×20 adsorbents and DOC and IC were monitored at each sampling time in order to evaluate the organic and/or inorganic matter adsorption onto the carbons. These experiments were performed in order to assess the possibility of competitive adsorption between the MS-222 molecules and the organic and/or inorganic matter. Also, the possibility of the MS-222 adsorption onto dissolved organic matter (DOM) presented in aquaculture wastewater was considered. For that purpose, in parallel to all adsorption experiments using aquaculture effluent as matrix, MS-222 solutions were shaken under the same conditions but without any adsorbent. These control experiments were analysed by MEKC after the equilibrium time was reached (480 min for BSC and 960 min for DARCO 12×20) and compared with MS-222 standards, prepared in ultra-pure water.

Adsorption equilibrium experiments were carried out under constant shaking velocity (90 rpm) and constant temperature (18 °C). Using the adsorbent dosage defined in the kinetic studies, the equilibrium isotherm was determined by varying the initial concentration of MS-222 from 100 up to 500 mg L⁻¹ in aquaculture wastewater matrix. This MS-222 concentration range includes all recommended dosages for fish administration [3].

6.3 Results and discussion

6.3.1 Influence of particle size

Kinetic adsorption tests were performed in order to evaluate the influence of BSC particle size on MS-222 adsorption. Experimental kinetic curves are shown in Figure 6.1 a.) and the fitting parameters of pseudo-first order and pseudo-second order kinetic models are presented in Table 6.1. The results showed that adsorbent particle size plays an important role in the adsorption process. At equilibrium, under these experimental conditions, the adsorbed MS-222 onto < 0.18 mm and 0.18-0.5 mm was almost the same, and two and three times higher than onto 0.5-1 mm and 1-2 mm particles, respectively. Moreover, it could be observed from Figure 6.1 a.) that the equilibrium was attained between 2 and 4 h for all the particle sizes tested; however, analysing the fitting parameters from Table 6.1, the kinetic constants (k_1 and k_2) decrease with the increase of particle size. The explanation for these results is in the adsorbent surface structure: decreasing the grain size of BSC implies that a higher external surface area is exposed to the bulk solution and then more sites are available to the adsorption of MS-222. In fact, Table 5.6 (Chapter 5) shows that BSC-a and BSC-b, which presented approximately the same adsorption kinetic curves, have almost the same specific surface area and micropore volume. BSC-c and BSC-d have lower surface area and micropore volume and the adsorption rate and the adsorbed MS-222 at the equilibrium are also proportionally lower.

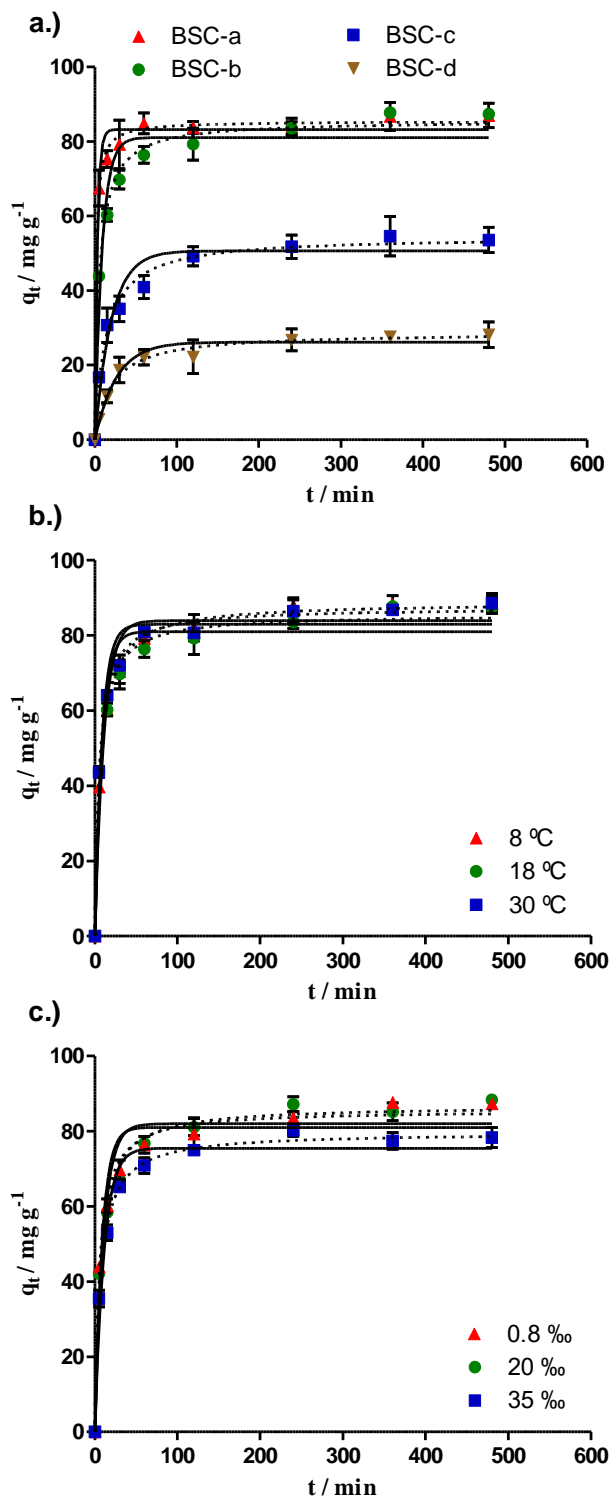


Figure 6.1 - Experimental kinetic curves for the adsorption of MS-222 in aqueous solution testing the effect of a.) BSC particle size; b.) temperature (BSC-b), and c.) salinity (BSC-b) on adsorption capacity. The experimental data were fitted to pseudo-first order (—) and pseudo-second order (---) kinetic models. Each experimental point (\pm standard deviation) is the average of three replicates.

Table 6.1 - Fitting parameters of pseudo-first order and pseudo-second order kinetic models to the experimental data for different particle size of BSC

	Particle size	BSC-a	BSC-b	BSC-c	BSC-d
Pseudo-1 st order	k_1 (min ⁻¹)	0.32±0.05	0.11±0.02	0.050±0.009	0.038±0.006
	q_e (mg g ⁻¹)	83±1	81±3	51±2	26.2±0.9
	r^2	0.9838	0.9529	0.9486	0.9713
Pseudo-2 nd order	k_2 (g mg ⁻¹ min ⁻¹)	0.008±0.001	0.0021±0.0003	0.0013±0.0002	0.0017±0.0003
	q_e (mg g ⁻¹)	85.4±0.8	86±1	55±1	28.8±0.8
	r^2	0.9962	0.9920	0.9887	0.9886

The use of granulated adsorbents in a real continuous flow process has more advantages than powdered adsorbents, in terms of equipment maintenance and adsorbent regeneration. In this context, BSC-b is a granulated material and presents better results than BSC-c and BSC-d, so BSC-b will be used in the subsequent studies.

6.3.2 Influence of the temperature

Three temperatures (8, 18 and 30 °C) from the range used in the intensive production of several aquatic species were tested in order to evaluate their effect in MS-222 adsorption onto BSC-b. Figure 6.1 b.) shows the kinetic adsorption curves and the fitting of the kinetic models to the experimental data. Table 6.2 lists the adsorption rate constants of the pseudo-first order and pseudo-second order kinetic models fittings and these results suggest that, between 8 and 30 °C, the equilibrium time was not significantly affected by the temperature, as well as the maximum quantity of MS-222 adsorbed, $q_{m,L}$, as show the Figure 6.2 a.) and Table 6.3. So, in general, BSC-b has the same behaviour on the removal of MS-222 by adsorption for the temperature range here considered which means that it can be employed with the same performance independently of the temperature conditions of farmed fish species.

Table 6.2 - Fitting parameters of pseudo-first and pseudo-second order kinetic models to the experimental data for different temperatures for BSC-b

Temperature		8 °C	18 °C	30 °C
Pseudo-1 st order	k_1 (min ⁻¹)	0.09±0.01	0.11±0.02	0.12±0.02
	q_e (mg g ⁻¹)	84±3	81±3	83±2
	r^2	0.9670	0.9529	0.9693
Pseudo-2 nd order	k_2 (g mg ⁻¹ min ⁻¹)	0.0016±0.0001	0.0021±0.0003	0.0021±0.0002
	q_e (mg g ⁻¹)	88.8±0.8	86±1	87.4±0.9
	r^2	0.9974	0.9920	0.9968

The thermodynamic parameters calculated through the Van't Hoff plot (Eq. 2.12) shown in Figure 6.2 b.) are presented in Table 6.3. The values of ΔG° suggest that the adsorption of MS-222 onto BSC-b is a non-spontaneous process at standard state conditions ($\Delta G^\circ > 0$). The negative value of ΔH° reflects an exothermic adsorption, *i.e.*, the adsorbate-adsorbent bond is stronger than that of adsorbate-water [5]. Moreover, the negative value of ΔS° states that MS-222 molecules were orderly adsorbed on the surface of the BSC-b.

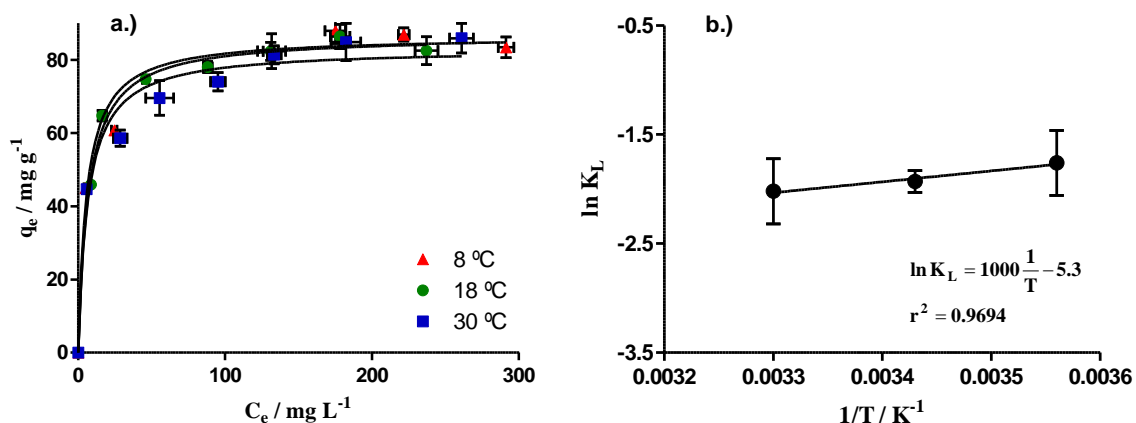


Figure 6.2 - a.) Experimental isotherms for the adsorption of MS-222 in aqueous solution at different temperatures and the fitting of the Langmuir model to the experimental data; b.) Variation of $\ln K_L$ with temperature for the adsorption of MS-222 onto BSC-b (Van't Hoff plot).

Table 6.3 - Fitting parameters of Langmuir model and thermodynamic parameters for the adsorption of MS-222 onto BSC-b

Temperature (°C)	Langmuir Model			Thermodynamic Parameters		
	K_L (L mg ⁻¹)	$q_{m,L}$ (mg g ⁻¹)	r^2	ΔG° (kJ mol ⁻¹)	ΔH° (kJ mol ⁻¹)	ΔS° (kJ mol ⁻¹ K ⁻¹)
8	0.17 ± 0.05	84 ± 3	0.9587	4.1		
18	0.15 ± 0.02	87 ± 2	0.9936	4.7	-8.3	-0.044
30	0.13 ± 0.04	85 ± 3	0.9582	5.1		

6.3.3 Influence of the salinity

The influence of water salinity in MS-222 adsorption onto BSC-b was assessed for the range of salt concentrations comprising the concentrations found in freshwater and saltwater (0.8, 20 and 35‰). The kinetic adsorption curves and respective fitting to pseudo-first order and pseudo-second order models are shown in Figure 6.1 c.). Table 6.4 presents the fitting parameters of kinetic models and the results showed that the adsorption rate constant, k_1 or k_2 , was not affected significantly by the salinity; however the quantity of MS-222 adsorbed at the equilibrium was slightly lower for 35‰ of salinity.

Table 6.4 - Fitting parameters of pseudo-first order and pseudo-second order kinetic models to the experimental data for different solution salinities for BSC-b

Salinity		0.8‰	20‰	35‰
Pseudo-1 st order	k_1 (min ⁻¹)	0.11±0.02	0.10±0.02	0.09±0.01
	q_e (mg g ⁻¹)	81±3	82±3	75±2
	r^2	0.9529	0.9479	0.9728
Pseudo-2 nd order	k_2 (g mg ⁻¹ min ⁻¹)	0.0021±0.0003	0.0018±0.0002	0.0018±0.0001
	q_e (mg g ⁻¹)	86±1	87±2	79.7±0.8
	r^2	0.9920	0.9909	0.9973

6.3.4 Aquaculture wastewater

Adsorption experiments with aquaculture wastewater were carried out in order to evaluate the performance of BSC-b for the removal of MS-222 in a real situation of temperature, salinity and, essentially, organic matter. Figure 6.3 shows the kinetic adsorption curves, using BSC-b and, for comparison purposes, DARCO 12×20, and the application of the kinetic models to the experimental data. Table 6.5 lists the adsorption rate constants of the pseudo-first order and pseudo-second order kinetic models fittings and coefficients of determination of each fitting, r^2 . In general, both experimental kinetic curves are well described by pseudo-second order model with highest coefficient r^2 . From Figure 6.3, it could be observed that adsorption equilibrium was more rapidly attained for BSC-b (between 4 and 6 h) than for DARCO 12×20 (about 10 h). In fact, analysing the adsorption rate constants of pseudo-second order, k_2 , presented on Table 6.5, BSC-b had a quite higher adsorption rate. Despite the higher quantity of MS-222 adsorbed at the equilibrium using DARCO 12×20 comparing with the BSC-b, it is important to note that, up to 1 h of contact time, the adsorption capacity was the same for both sludge-based and commercial carbons (about 70 mg g⁻¹).

Regarding the presence of organic and inorganic matter, the collected aquaculture wastewater contained $4.3 \pm 1.3 \text{ mg L}^{-1}$ of DOC and $43.1 \pm 0.5 \text{ mg L}^{-1}$ of IC. After contacting this effluent (without MS-222 spiking) with both carbons, in the same dosage used in adsorption experiments, the results of DOC and IC contents remaining in aqueous phase were constant over the experiment, *i.e.*, organic and inorganic matter remaining in the collected aquaculture wastewater were not adsorbed by the adsorbents during the time interval needed to attain the MS-222 adsorption equilibrium. Thus, it may be assumed that organic and inorganic matter does not compete with the anaesthetic MS-222 for the adsorption sites onto the carbons, for the studied contact time (480 min for BSC-b and 960 min for DARCO 12×20). Some other studies have been reported that many hours are needed and sometimes several days to the establishment of the adsorption equilibrium between DOM and activated carbons (*e.g.*, 24 h, 14 days and 21 days were reported by Shi et al. (2014) [6], Cheng et al. (2005) [7] and Schreiber et al. (2005) [8], respectively); so, once again, the lower time of equilibrium herein obtained for BSC-b is an advantage to avoid the DOM competitive adsorption.

Concerning the possibility to occur adsorption of MS-222 onto DOM contained in aquaculture wastewater, the results from the control experiments (described in section 6.2.4.4) showed that no significant variation was observed in the MS-222 concentration after 960 min in contact with aquaculture wastewater (variations under 4%, for concentrations between 100 and 500 mg L^{-1}), comparing with MS-222 standard solutions prepared in ultra-pure water. In this sense, it can be assumed that no adsorption of MS-222 onto aquaculture wastewater DOM occurred. Also, comparing the results obtained for the MS-222 adsorption onto BSC-b using aquaculture wastewater (Figure 6.3 and Table 6.5) with those obtained with ultra-pure water as matrix (Figure 6.1 c.) and Table 6.4, for 20‰ of salinity), the adsorption rate and the quantity of MS-222 adsorbed at the equilibrium were not affected significantly by the presence of organic and inorganic matter.

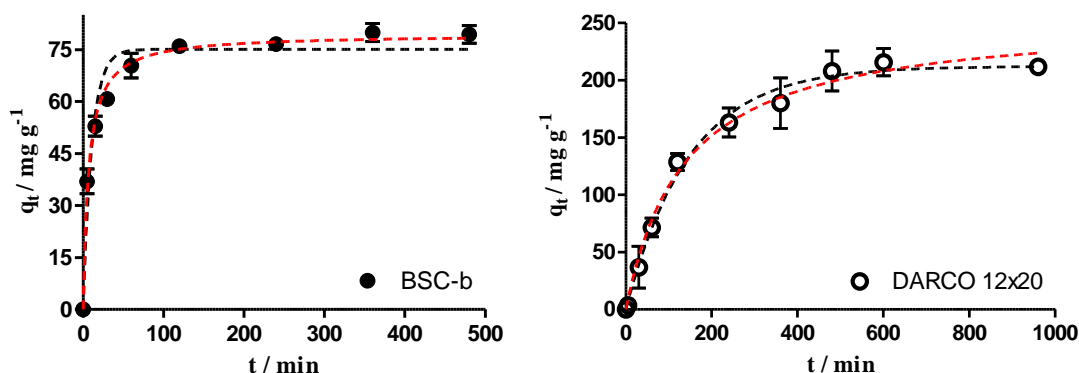


Figure 6.3 - Experimental and predicted kinetic curves for the adsorption of MS-222 in aquaculture wastewater matrix using BSC-b (left) and DARCO 12×20 (right). The experimental data were fitted to pseudo-first order (---) and pseudo-second order (-.-) kinetic models. Each experimental point (\pm standard deviation) is the average of three replicates. Note that x and y -axis scales are not the same in both graphs to allow a better visualization of the results.

Table 6.5 - Fitting parameters of pseudo-first and pseudo-second order kinetic models and of Langmuir, Freundlich and Langmuir-Freundlich equilibrium models to the experimental data

		BSC-b	DARCO 12×20
<i>Kinetic Adsorption Models</i>			
Pseudo-1st order	k_1 (min^{-1})	0.09±0.02	0.0067±0.0005
	q_e (mg g^{-1})	75±3	212±5
	r^2	0.9546	0.9936
Pseudo-2nd order	k_2 ($\text{g mg}^{-1} \text{min}^{-1}$)	0.0018±0.0002	0.000028±0.000005
	q_e (mg g^{-1})	79±1	256±9
	r^2	0.9934	0.9919
<i>Equilibrium Adsorption Models</i>			
Langmuir	$q_{m,L}$ (mg g^{-1})	95±3	306±14
	K_L (L mg^{-1})	0.5±0.2	0.026±0.005
	r^2	0.9514	0.9800
Freundlich	K_F ($\text{mg g}^{-1} (\text{mg L}^{-1})^{-N_F}$)	49±3	58±7
	N_F	7.4±0.6	3.6±0.3
	r^2	0.9903	0.9896
Langmuir-Freundlich	$q_{m,LF}$ (mg g^{-1})	149±43	581±467
	K_{LF} ($\text{L}^{1/N_{LF}} \text{mg}^{-1/N_{LF}}$)	0.4±0.1	0.07±0.03
	N_{LF}	3±1	2±1
	r^2	0.9934	0.9907

Figure 6.4 shows the equilibrium isotherms of MS-222 adsorption onto the BSC-b and DARCO 12×20 together with the fittings to the equilibrium models. Fitting parameters to Langmuir, Freundlich and Langmuir-Freundlich isothermal models and the coefficient of determination, r^2 , are shown in Table 6.5. In general, equilibrium experimental data are described by Freundlich and Langmuir-Freundlich models with satisfactory coefficients of determination. However, the errors associated to the estimated Langmuir-Freundlich parameters are high, mainly in the DARCO 12×20 case, which implies the lack of physical significance of these values; so, the Freundlich fitting parameters were selected for the subsequent analysis. Results showed that the process is favourable ($N_F > 1$) using both adsorbents, which means that the adsorbents are efficient in removing high and low concentrations of the contaminant. Yet, the experimental BSC-b isotherm showed a quite well defined plateau for MS-222 initial concentrations higher than 300 mg L^{-1} , where the maximum capacity is reached. When comparing the adsorption coefficient obtained using BSC-b and DARCO 12×20 (49 ± 3 and $58 \pm 7 \text{ mg g}^{-1} (\text{mg L}^{-1})^{-NF}$, respectively), the last one is only slightly higher than the produced carbon.

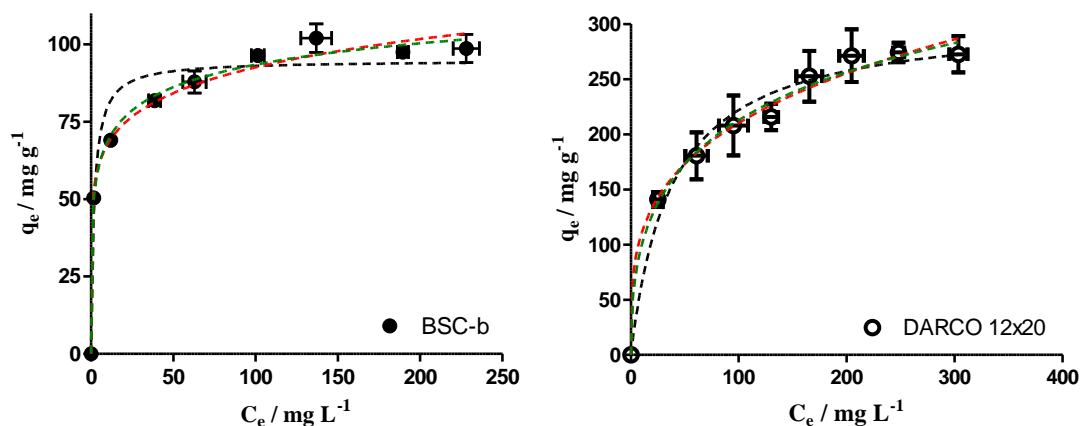


Figure 6.4 - Experimental and predicted isotherms for the adsorption of MS-222 in aquaculture wastewater matrix using BSC-b (left) and DARCO 12×20 (right). The experimental data were fitted to Langmuir (---), Freundlich (---) and Langmuir-Freundlich (---) equilibrium models. Each experimental point (\pm standard deviation) is the average of three replicates. Note that x and y -axis scales are not the same in both graphs to allow a better visualization of the results.

6.4 Conclusions

The biological paper mill sludge-based adsorbent (BSC) was able to remove MS-222 both from ultra-pure water and from aquaculture wastewater, under very different operating conditions. The adsorbent particle size was shown to be an important feature for adsorption purposes and, in this study, the smallest sizes of BSC particle (<0.18 mm and 0.18-0.5 mm) produced better results of adsorption. On the other hand, varying operating conditions such as temperature (8 to 30 °C) and salinity (0.8 to 35‰) did not affect the MS-222 adsorption using BSC-b, making this adsorbent versatile for a possible implementation on RASs. Also, it was proved that the presence of organic and inorganic matter in aquaculture effluents did not interfere with the adsorption of MS-222 onto BSC-b. The adsorption rate constant of pseudo-second order kinetic model fitting using BSC-b was $0.0018 \text{ g mg}^{-1} \text{ min}^{-1}$, which is higher than the obtained using DARCO 12×20 ($0.000028 \text{ g mg}^{-1} \text{ min}^{-1}$), while the equilibrium adsorption coefficient using BSC-b, predicted by Freundlich model, was lower than using DARCO 12×20. Resuming, for salty aquaculture wastewaters, BSC-b showed a lower adsorption capacity but a quite larger adsorption rate when compared with a commercial activated carbon; therefore, at short contact times ($\leq 1 \text{ h}$) the capacities of both materials are comparable. Since BSC-b was proved to be a quite efficient adsorbent to be used for the removal of MS-222 from intensive aquaculture wastewater in batch system; in the next chapters, the adsorption process in continuous system will be tested by using fixed-bed column reactors packed with BSC-b, as well as the variables that can affect this operation mode.

6.5 References

- [1] Ferreira, C.I.A., Calisto, V., Otero, M., Nadais, H. and Esteves, V.I., 2017, *Chemosphere*, 168, 139-146.
- [2] FDA, 2011, Fish and Fishery Products Hazards and Controls Guidance, *U.S. Department of Health and Human Services; Food and Drug Administration; Center for Food Safety and Applied Nutrition*.
- [3] Ross, L.G. and Ross, B., 2008, Anaesthetic and Sedative Techniques for Aquatic Animals, *Blackwell Publishing Ltd*, Oxford, UK.
- [4] Palmer, L.M. and Mensinger, A.F., 2004, *Journal of Neurophysiology*, 92 (2), 1034-1041.
- [5] Masterton, W., Hurley, C. and Neth, E., 2011, Chemistry: Principles and Reactions, *Cengage Learning*.
- [6] Shi, B., Fang, L., Li, Z. and Wang, D., 2014, *CLEAN – Soil, Air, Water*, 42 (10), 1363-1369.
- [7] Cheng, W., Dastgheib, S.A. and Karanfil, T., 2005, *Water Research*, 39 (11), 2281-2290.
- [8] Schreiber, B., Brinkmann, T., Schmalz, V. and Worch, E., 2005, *Water Research*, 39 (15), 3449-3456.

Part IV

Chapter 7

Fixed-bed adsorption of MS-222 and 2-phenoxyethanol onto biological paper mill sludge-based adsorbent

Chapter 8

Chemical and thermal regeneration of biological paper mill sludge-based adsorbent

7 Fixed-bed adsorption of MS-222 and 2-phenoxyethanol onto biological paper mill sludge-based adsorbent

This chapter reports the removal of tricaine methanesulfonate (MS-222) and 2-phenoxyethanol (2-PE) from water in a fixed-bed column packed with pyrolysed paper mill sludge (BSC-b) for application in recirculating aquaculture systems. The influence of feed flow rate, influent concentration and bed depth was analysed and different mathematical models were fitted to the experimental data. The results showed that, using synthetic solutions of MS-222, a bed adsorption capacity of 125 mg g^{-1} was obtained under a flow rate of 4.4 mL min^{-1} , 4.5 cm bed depth and an initial concentration of 400 mg L^{-1} of MS-222. The performance of the continuous adsorption in a BSC-b packed column using real aquaculture wastewater as matrix, was not significantly affected. Then, scale-up was carried out and the bed depth service time (BDST) model was applied and provided good predictions. Concerning 2-PE fixed-bed experiments, the highest bed adsorption capacity of 104 mg g^{-1} and volume treated of 286 mL were obtained under a flow rate of 4.4 mL min^{-1} , with $0.3 \text{ cm}^3 \text{ L}^{-1}$ of 2-PE with 13 cm bed depth. In this case, Yoon-Nelson and Dose-Response models fitting are recommended. On the other hand, the application of BDST model in the prediction of 2-PE scale-up adsorption experiment was not as good as expected.

Part of the work presented and discussed in this chapter resulted in the following publication:

Ferreira C.I.A., Calisto V., Otero M., Nadais H., Esteves V.I., 2017, Fixed-bed adsorption of Tricaine Methanesulfonate onto pyrolysed paper mill sludge. *Aquacultural Engineering*. DOI: 10.1016/j.aquaeng.2017.02.006.

7.1 Contextualization

A typical RAS consists of primary treatment (sedimentation and/or filtration to remove mostly suspended solid waste), biological treatment (to convert the ammonia and nitrite into nitrate through nitrification in aerobic biological filters) and tertiary treatment processes such as oxygenation, ozonation and UV radiation aimed at removing organic matter, mainly nitrogen-containing compounds, and disinfection [1-3]. As referred in the previous chapters, carbon filters, mostly fixed-bed activated carbon columns, may be also used in addition to biological filters as a polishing stage to remove persistent nonbiodegradable organic materials [4]. However, despite their high efficiency, the main drawback of activated carbons is the high price [5] so their expense is a main reason for activated carbon filters not being typically found in food-fish production systems [4]. All over this thesis, it was evaluated the removal of MS-222, benzocaine and 2-PE from water by adsorption onto adsorbents produced by the pyrolysis of different wastes and promising results were obtained with the paper mill sludge-based adsorbents. It was also proved that the temperature, salinity and the presence of organic and inorganic matter did not interfere with the adsorption of MS-222 onto the biological paper mill sludge-based carbon. These studies have been carried out under batch operation conditions; however, fixed-bed systems hold some advantages over batch-type reactors for water treatment [6] and are more frequently used in the aquaculture industry [4].

In this context, the aim of this study was the evaluation of the fixed-bed adsorption of MS-222 and 2-PE from water, using biological paper mill sludge-based adsorbent. For this purpose, the influence of important design parameters (feed flow rate, influent concentration and bed depth) was analysed and different mathematical models were fitted to the experimental data. In view of application in RASs, an experiment using real effluent from aquaculture was performed and compared with those using synthetic effluent.

7.2 Materials and methods

7.2.1 Adsorbent materials

In this chapter, the adsorbent tested was the pyrolysed and washed biological paper mill sludge with particle size between 0.18 and 0.5 mm (BSC-b), produced and characterized in Chapter 5.

7.2.2 Fish anaesthetics

Adsorption tests were performed for the fish anaesthetics tricaine methanesulfonate, commercially named Tricaine-S, (>97%, TCI Europe) - MS-222 and 2-phenoxyethanol (>98.5%, TCI Europe) – 2-PE. Anaesthetic solutions were buffered using 10^{-2} M of NaHCO_3 to pH 7-7.5, according to the recommended by Ross et al. (2008) [7]. The anaesthetics physico-chemical properties are summarized in Chapter 2, Table 2.1.

7.2.3 Determination of the MS-222 and 2-PE concentrations in water by MEKC

MEKC analyses were performed using a Beckman P/ACE MDQ (Fullerton, CA, USA) instrument, equipped with a UV-Vis detection system, following the procedure described in Appendix C (section C.1.1.1). Detection of MS-222 and 2-PE were monitored at 220 and 230 nm, respectively. Aqueous samples and standard solutions were analysed in triplicate. MS-222 and 2-PE calibration curves and parameters, including the limit of detection (LOD) and limit of quantification (LOQ), are also presented in Appendix C, sections C.1.1 and C.1.3, respectively.

7.2.4 Fixed-bed column adsorption experiments

Fixed-bed column experiments were conducted in a 1 cm diameter and 13 cm length glass column (CHROMAFLEX[®]). A thermostatic recirculating bath (ThermoScientific HAAKE A10) maintained the temperature constant, at 18 °C, by circulating water through an acrylic jacket surrounding the column body. A flow adapter, with a 20 µm porosity HDPE bed support, was attached to the top of the column. The column was packed with BSC-b (1.0, 2.0 and 2.5 g) resulting in different bed depths ($Z = 4.5, 9.0$ and 13.0 cm, respectively). As represented in Figure 7.1, synthetic influent solutions ($C_i = 100, 250$ and 400 mg L^{-1} of MS-222 and $C_i = 0.3, 0.8$ and 1.3 cm³ L^{-1} of 2-PE, in ultra-pure water) were pumped up flow by a peristaltic pump (Gilson Minipuls 3) with different flow rates ($Q = 1.2, 2.1, 4.4$ mL min^{-1}). Effluent samples were collected by a programmable fraction collector (Gilson FC 203B Fraction Collector), filtered through 0.22 µm Simplepure PVDF filters, and analysed for the concentration of MS-222 and 2-PE by MEKC.

In order to recreate the real conditions, a fixed-bed experiment was performed by spiking MS-222 into an effluent from a national fish producer as aqueous matrix ($Q=4.4$ mL min^{-1} , $C_i=250$ mg L^{-1} and $Z=4.5$ cm). This aquaculture farm produces fishes in intensive system and has a RAS implemented that allows reutilizing approximately 95% of water. The collected aquaculture

wastewater, used in MS-222 adsorption experiments, contained $27 \pm 3 \text{ mg L}^{-1}$ of dissolved organic carbon (DOC), $46 \pm 2 \text{ mg L}^{-1}$ of inorganic carbon (IC), 20-21% of salinity and pH 7-7.5.

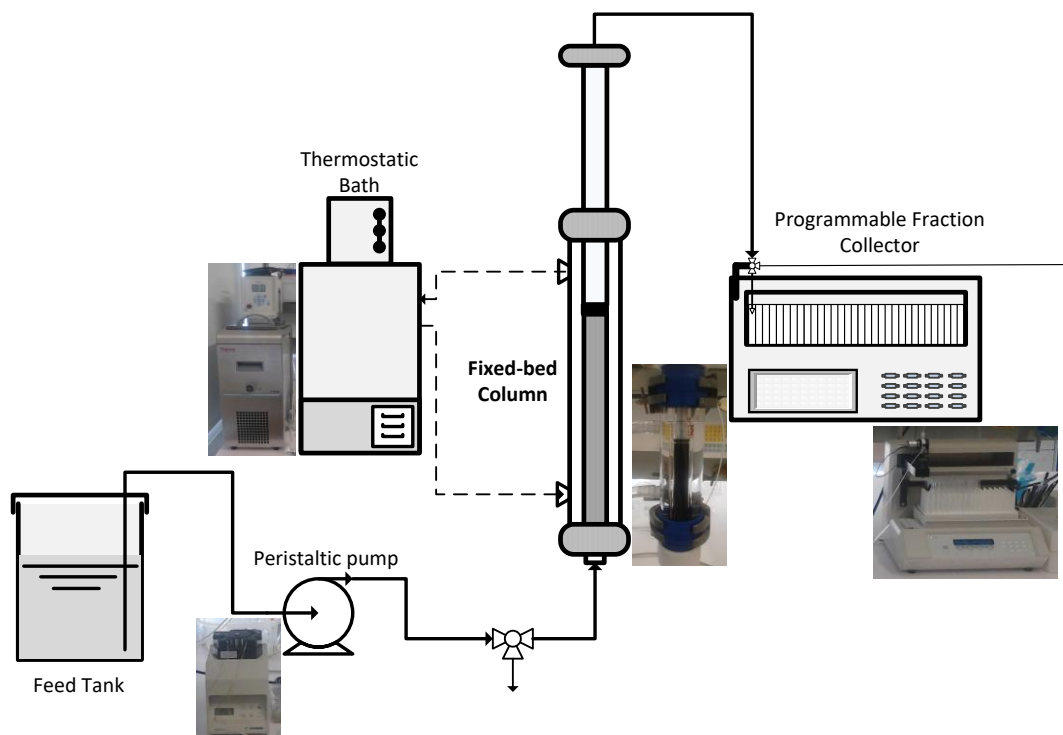


Figure 7.1 - Schematic diagram of the experimental setup for fixed-bed column experiments.

A scale-up experiment was performed using the same experimental setup, with a 2.5 cm diameter and 50 cm length glass column (13/219 POBEL). This column was packed with 55 g of BSC-b (corresponding to a bed depth of 35 cm) and a solution of MS-222 (250 mg L^{-1}) was passed through the column at a flow rate of 12 mL min^{-1} . The scale-up experiment was performed in the same conditions but passing through the column a solution of 2-PE ($0.3 \text{ cm}^3 \text{ L}^{-1}$).

7.2.4.1 Fixed-bed column data analysis and modelling

In order to evaluate the adsorption of MS-222 and 2-PE in a BSC-b packed column under different operating conditions, breakthrough curves were obtained by expressing C/C_i as a function of operation time (t , in min), where C and C_i (mg L^{-1}) are the effluent and influent concentration, respectively. From a practical point of view, the breakthrough point allows determining the volume of effluent treated (V_b). Usually, this point is settled according to the target quality of the final effluent; however, in the case of MS-222 and 2-PE there is not yet a maximum limit established of discharge into the environment. So, the breakthrough point was considered as the point where effluent concentration reaches about 10% of the influent concentration ($C/C_i \approx 0.1$). The time corresponding to this point is the breakthrough time (t_b). When the effluent concentration reaches

95% of the influent concentration, it is considered the saturation point (corresponding to a saturation time (t_s)). The total bed capacity, *i.e.*, the total mass of solute adsorbed by the adsorbent at t_s , q_s (mg g^{-1}), can be calculated using the Eq. 2.14, as described in Chapter 2, section 2.4.4.1.

Several simple mathematical models have been proposed to predict the dynamic behaviour of fixed-bed columns and estimate the adsorption kinetic coefficients. The models developed by Thomas [8] (Eq. 2.17), Clark [9] (Eq. 2.18), Yoon-Nelson [10] (Eq. 2.19) and Dose-Response [11] (Eq.2.20) were fitted to the experimental breakthrough curves using GraphPad Prism 5 software. The description of each of these models is presented in Chapter 2, section 2.4.4.1. For the scale-up, the bed depth service time (BDST) model [12] (Eq. 2.21), which establishes a relationship between the bed depth, Z (cm), and the operation time, was used on the basis of previously obtained results. This model is entirely described in Chapter 2, section 2.4.4.2.

7.3 Results and discussion

7.3.1 Fixed-bed adsorption of MS-222

7.3.1.1 Effect of the flow rate, influent concentration and bed depth

Breakthrough curves at different flow rates are presented in Figure 7.2 a.) (keeping $C_i=250 \text{ mg L}^{-1}$ and $Z=4.5 \text{ cm}$). The results show that the saturation time (t_s) decreases with the increase of the flow rate, and, consequently, reduces the volume of treated effluent until breakthrough point (V_b), mainly between 1.2 and 2.1 mL min^{-1} , as can be seen in Table 7.1. This fact is due to the decrease of the contact time between the MS-222 molecules and the BSC-b particles at higher flow rates when compared with 1.2 mL min^{-1} . However, between flow rate 2.1 and 4.4 mL min^{-1} , the volume treated until the breakthrough point is almost the same, varying only 5%. Therefore, under the operation conditions herein considered, the use of 4.4 mL min^{-1} of flow rate may be more advantageous (same volume treated in less time). Concerning the total adsorption capacity of the bed, there are no differences between the different flow rates tested (differences under 2%). Comparing these values (102-104 mg g^{-1}) with the ones obtained in batch system, presented in Chapter 5, section 5.3.4 (83±2 mg g^{-1} , estimated by Langmuir model, $r^2=0.9910$), BSC-b might have a slightly better performance in continuous system.

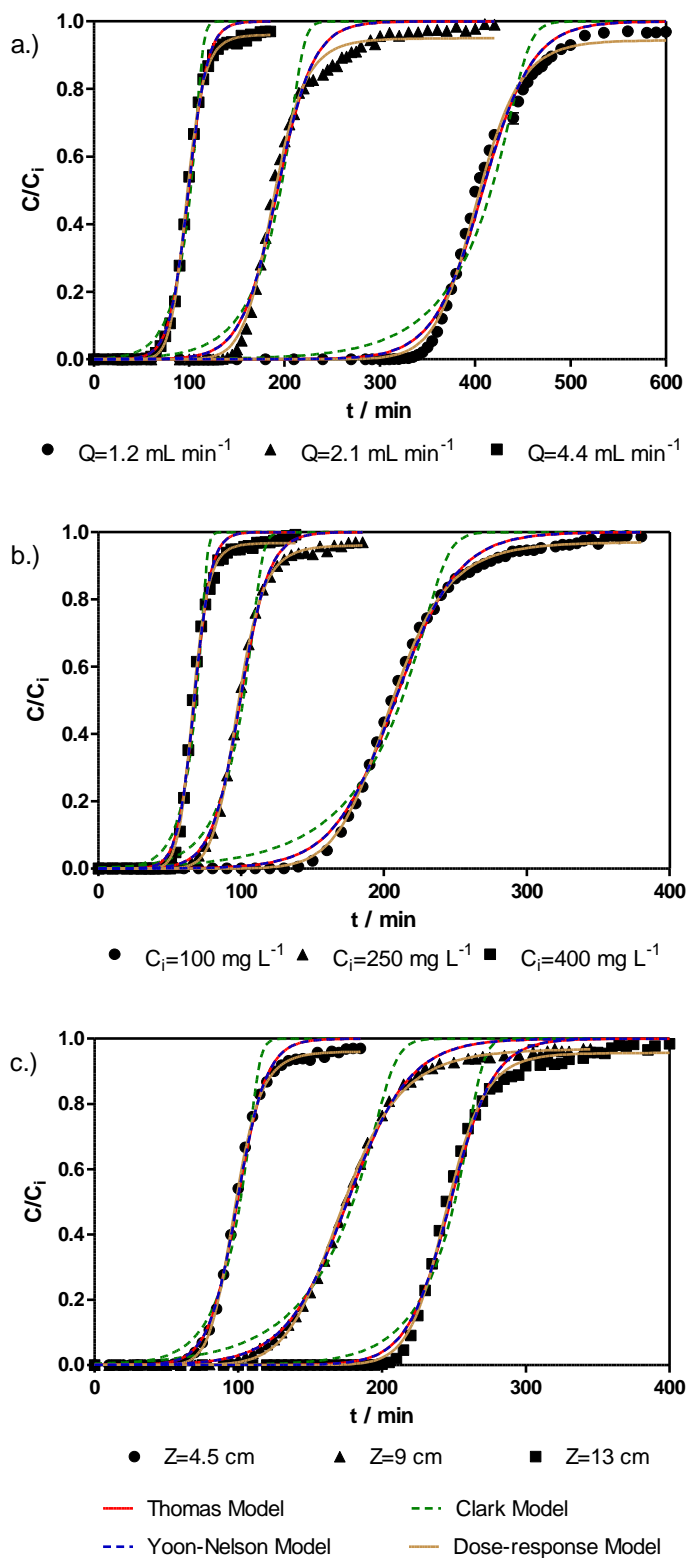


Figure 7.2 - Breakthrough curves for MS-222 adsorption onto BSC-b at different a.) flow rate ($C_i=250 \text{ mg L}^{-1}$ and $Z=4.5 \text{ cm}$); b.) influent concentration ($Q=4.4 \text{ mL min}^{-1}$ and $Z=4.5 \text{ cm}$), and c.) bed depth ($Q=4.4 \text{ mL min}^{-1}$ and $C_i=250 \text{ mg L}^{-1}$). The experimental data were fitted to Thomas, Clark, Yoon-Nelson and Dose-Response models.

The effect of the variation of MS-222 influent concentration, while keeping the other parameters constant ($Q=4.4 \text{ mL min}^{-1}$; $Z=4.5 \text{ cm}$), is shown in Figure 7.2 b.). The first point that stands out is the shape of the breakthrough curves: for lower values of influent concentration, the adsorption occurs slowly, so the curve is less steep; for increased influent concentrations, the steepness of the slope increases, attaining bed saturation in less time. This increase in adsorption rate of MS-222 onto BSC-b for higher influent concentrations is associated with the relative concentration gradients, *i.e.*, higher concentration gradient at high influent concentration of MS-222 provides higher driving force for the transfer process to overcome the mass transfer resistance. In this case, the mass transfer zone is small and the adsorption process is mostly controlled by intraparticle diffusion, as several authors reported [13-15]. From Table 7.1, it can be seen that higher influent concentrations reduce both the treated volume and the saturation time, while total adsorption capacity increases.

The breakthrough curves obtained for MS-222 adsorption onto different bed depths of BSC-b ($Z=4.5$; 9.0 and 13.0 cm) are illustrated in Figure 7.2 c.), at constant flow rate and influent concentration ($Q=4.4 \text{ mL min}^{-1}$; $C_i=250 \text{ mg L}^{-1}$). The results show that both breakthrough and saturation times increased as bed depth increased, and consequently the volume of treated effluent increased significantly (Table 7.1). The increase in the breakthrough time is related to the larger mass of adsorbent and to the longer distance it takes the mass transfer zone to move from the entrance to the exit of the bed when its depth is increased. On the other hand, the bed adsorption capacity varies only 4% for the different depths investigated.

Table 7.1 - Data from breakthrough curves for the fixed-bed adsorption of MS-222 (solutions in ultra-pure water) onto BSC-b at different flow rates, Q ($C_i=250 \text{ mg L}^{-1}$ and $Z=4.5 \text{ cm}$); influent concentrations, C_i ($Q=4.4 \text{ mL min}^{-1}$ and $Z=4.5 \text{ cm}$); bed depths, Z ($Q=4.4 \text{ mL min}^{-1}$ and $C_i=250 \text{ mg L}^{-1}$); and also using aquaculture wastewater as matrix ($Q=4.4 \text{ mL min}^{-1}$; $C_i=250 \text{ mg L}^{-1}$; $Z=4.5 \text{ cm}$)

	t_b (min)	V_b (ml)	$t_{50\%}$ (min)	t_s (min)	q_s (mg g ⁻¹)
Q (ml min⁻¹)					
1.2	365	438	400	515	104
2.1	165	347	188	290	102
4.4	80	352	99	155	102
C_i (mg L⁻¹)					
100	170	748	205	310	87
250	80	352	99	155	102
400	57	251	66	93	125
Z (cm)					
4.5	80	352	99	155	102
9	130	572	175	285	98
13	223	968	245	345	102
Aquaculture Wastewater	70	308	100	125	108

7.3.1.2 Breakthrough curves data modelling

To describe the column breakthrough curves obtained at different flow rates, influent concentrations and bed depths, the models presented in Chapter 2, section 2.4.4.1 were used. The experimental and theoretical breakthrough curves are shown in Figure 7.2 and the model parameters obtained from the corresponding fittings are presented in Table 7.2. Among the considered models, the one by Clark was the less appropriate to describe the experimental data, with coefficients of determination, r^2 , below 0.986 and predicted breakthrough times with a deviation higher than 18% from experimental data. Then, the Thomas and the Yoon-Nelson models better fitted the experimental data and are apparently coincident (Figure 7.2), both with similar coefficients of determination (Table 7.2). Both models predict the adsorption rate constant and, in general, they follow the same trend, *i.e.*, adsorption rate increased with increasing flow rate and decreased with increasing bed depth. The discordance between the models is for the variation of influent concentration, for which according to the Thomas model the adsorption rate was not significantly affected, while according to the Yoon-Nelson model the adsorption rate increased with the increase of influent concentration, as already observed by experimental data, in section

7.3.1.1. Thomas model allows calculating the maximum adsorption capacity of the bed, q_{Th} , and the fitted values (Table 7.2) are in accordance with q_s shown in Table 7.1, with less than 5% of deviation. Yoon-Nelson model predicts the time necessary to reach 50% of the influent concentration, $t_{50\%}$, and the fitted values are close to the experimental ones (Table 7.2), with less than 2% of deviation. So, the breakthrough curves predicted by either the Thomas or the Yoon-Nelson models showed reasonably good agreement with the experimental results, with some deviations at the beginning and at the end of the curves.

For all the conditions examined, the Dose-Response model was the most adequate to describe the experimental data, with the highest coefficients of determination, all above 0.996 (Table 7.2). From Figure 7.2, it is easily observed that the use of this model minimizes the errors presented by the other models considered in this work. The normalized concentration at saturation time (C_s/C_i) and $t_{50\%}$ were predicted by Dose-Response model (Table 7.2) with less than 2 and 1% of deviation from the experimental values (Table 7.1), respectively. This model has been widely applied for modelling continuous fixed-bed adsorption of inorganic pollutants, such as heavy metals [16,17], as well as for organic pollutants, such as pharmaceuticals [18].

7.3.1.3 *Aquaculture wastewater*

The continuous experiment using aquaculture wastewater was carried out in order to evaluate the performance of a column packed with BSC-b for the removal of MS-222 in a real situation of salinity and, essentially, organic and inorganic matter. Breakthrough curves using synthetic and real matrices are presented in Figure 7.3 a.) for the same conditions of flow rate, influent concentration and bed depth ($Q=4.4 \text{ mL min}^{-1}$; $C_i=250 \text{ mg L}^{-1}$; $Z=4.5 \text{ cm}$). Both results are quite similar, although the wastewater breakthrough curve is less steeped in the beginning, increasing slightly the slope at the end of the curve and, consequently, attaining the bed saturation earlier (as can be seen in Table 7.1). However, Table 7.1 also shows that other experimental parameters do not diverge significantly: time and volume at breakthrough point have differences of 13% between matrices, while bed adsorption capacities differ only 6%.

Table 7.2 - Thomas, Clark, Yoon-Nelson and Dose-Response model parameters at different flow rate ($C_i=250 \text{ mg L}^{-1}$ and $Z=4.5 \text{ cm}$), influent concentrations ($Q=4.4 \text{ mL min}^{-1}$ and $Z=4.5 \text{ cm}$) and bed depths ($Q=4.4 \text{ mL min}^{-1}$ and $C_i=250 \text{ mg L}^{-1}$) to MS-222 fixed-bed column adsorption

Parameters	$Q \text{ (mL min}^{-1}\text{)}$			$C_i \text{ (mg L}^{-1}\text{)}$			$Z \text{ (cm)}$			
	1.2	2.1	4.4	100	250	400	4.5	9	13	
Thomas	$k_{Th} \text{ (mL min}^{-1} \text{ mg}^{-1}\text{)}$	0.167±0.007	0.22±0.01	0.40±0.02	0.49±0.01	0.40±0.02	0.40±0.02	0.40±0.02	0.185±0.005	0.28±0.01
	$q_{Th} \text{ (mg g}^{-1}\text{)}$	102.8±0.3	99.0±0.6	107.5±0.5	85.6±0.3	107.5±0.5	124.0±0.6	107.5±0.5	96.4±0.4	106.2±0.3
	r^2	0.9911	0.9869	0.9961	0.9959	0.9961	0.9955	0.9961	0.9967	0.9943
Clark	$k_C \text{ (min}^{-1}\text{)}$	0.1246±0.0007	0.203±0.002	0.362±0.003	0.155±0.001	0.362±0.003	0.618±0.004	0.362±0.003	0.169±0.001	0.249±0.001
	$t_b \text{ (min)}$	435	207	108	227	108	72	108	194	260
	r^2	0.9636	0.9665	0.9862	0.9807	0.9862	0.9848	0.9862	0.9845	0.9832
Yoon-Nelson	$k_{YN} \text{ (min}^{-1}\text{)}$	0.038±0.001	0.053±0.003	0.099±0.004	0.046±0.001	0.099±0.004	0.170±0.008	0.099±0.004	0.046±0.001	0.067±0.003
	$t_{50\%} \text{ (min)}$	408±1	193±1	99.3±0.5	207.8±0.7	99.3±0.5	67.1±0.3	99.3±0.5	176.0±0.6	247.6±0.7
	r^2	0.9911	0.9869	0.9961	0.9959	0.9961	0.9955	0.9961	0.9967	0.9943
Dose-Response	C_s/C_i	0.944±0.008	0.950±0.006	0.962±0.002	0.971±0.002	0.962±0.002	0.967±0.003	0.962±0.002	0.970±0.003	0.956±0.004
	$t_{50\%} \text{ (min)}$	402.3±0.9	188.6±0.7	97.7±0.2	204.7±0.3	97.7±0.2	66.2±0.1	97.7±0.2	172.6±0.3	245.1±0.4
	α	17.8±0.6	11.5±0.4	10.8±0.2	10.4±0.1	10.8±0.2	12.3±0.3	10.8±0.2	8.5±0.1	18.4±0.5
	r^2	0.9964	0.9961	0.9997	0.9995	0.9997	0.9992	0.9997	0.9994	0.9985

The experimental and theoretical breakthrough curves using aquaculture wastewater as matrix are shown in Figure 7.3 b.) and, for comparison proposes, the model parameters obtained from the corresponding fittings to both matrices are presented in Table 7.3. All models fit the experimental wastewater breakthrough curve, with r^2 higher than 0.99. Comparing the predicted parameters of both matrices, the adsorption rate parameters are slightly lower using the real matrix, which is a consequence of the lower steepness in the beginning of the curve possibly caused by an initial competition between the organic and/or inorganic matter and MS-222 molecules for the adsorption sites onto BSC. However, as mentioned above, the bed adsorption capacity experimentally obtained was not affected by the presence of organic and inorganic matter. Moreover, regarding the predicted q_{Th} , t_b and $t_{50\%}$ parameters, there are no differences between both synthetic and real matrices, with variations under 2% (see Table 7.3). Thus, it may be assumed that the presence of organic and inorganic matter in solution does not affect the performance of MS-222 continuous adsorption in a BSC-b packed column, which is in accordance with the results obtained in batch system (Chapter 6).

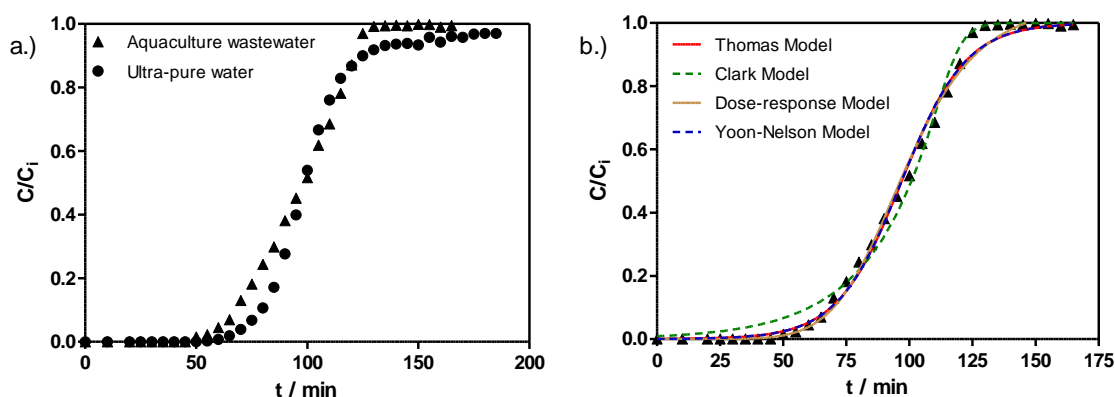


Figure 7.3 - Breakthrough curves for adsorption of MS-222 onto BSC-b a.) in ultra-pure water and aquaculture wastewater, b.) in aquaculture wastewater fitted to Thomas, Clark, Yoon-Nelson and Dose-Response models ($Q=4.4 \text{ mL min}^{-1}$; $C_i=250 \text{ mg L}^{-1}$; $Z=4.5 \text{ cm}$).

Table 7.3 - Thomas, Clark, Yoon-Nelson and Dose-Response model parameters for different matrices

Model	Parameters	Ultra-pure water	Aquaculture wastewater
		$Q=4.4 \text{ mL min}^{-1}; C_i=250 \text{ mg L}^{-1}; Z=4.5 \text{ cm}$	
Thomas	k_{Th} ($\text{mL min}^{-1} \text{ mg}^{-1}$)	0.40±0.02	0.30±0.01
	q_{Th} (mg g^{-1})	107.5±0.5	109.1±0.6
	r^2	0.9961	0.9960
Clark	k_C (min^{-1})	0.362±0.003	0.25±0.01
	t_b (min)	108	110
	r^2	0.9862	0.9936
Yoon-Nelson	k_{YN} (min^{-1})	0.099±0.004	0.078±0.003
	$t_{50\%}$ (min)	99.3±0.5	97.0±0.5
	r^2	0.9961	0.9960
Dose-Response	C_s/C_i	0.962±0.002	1.07±0.02
	$t_{50\%}$ (min)	97.7±0.2	98±1
	α	10.8±0.2	6.7±0.4
	r^2	0.9997	0.9954

7.3.1.4 Scale-up

Figure 7.4 shows the iso-concentration lines for MS-222 retained in the fixed-bed at 10, 50 and 90% of breakthrough points for the three bed depths considered, as presented in Figure 7.2 c.). Table 7.4 gives the slopes and intercepts of the fitted lines, which correspond to a and b respectively, according to Eq. 2.22. Also, Table 7.4 depicts BDST model parameters, N_0 and k_{BDST} , which were calculated from Eq. 2.23 and Eq. 2.24. It may be observed that N_0 increased with increasing of breakthrough point, as for the increase of the slope, and the k_{BDST} decreased with increasing breakthrough point. However, the line for 50% of breakthrough does not pass through the origin, $b \neq 0$, which has been reported by some authors with the existence of more than one rate-limiting step [19, 20]. In fact, in previous Chapter 5, section 5.3.4, the adsorption kinetics of MS-222 onto BSC-b and other two adsorbents revealed the presence of two steps: for initial conditions, adsorption was controlled by intraparticle diffusion and then, when the molecules reach the intraparticle sites, the external diffusion becomes the rate limiting step.

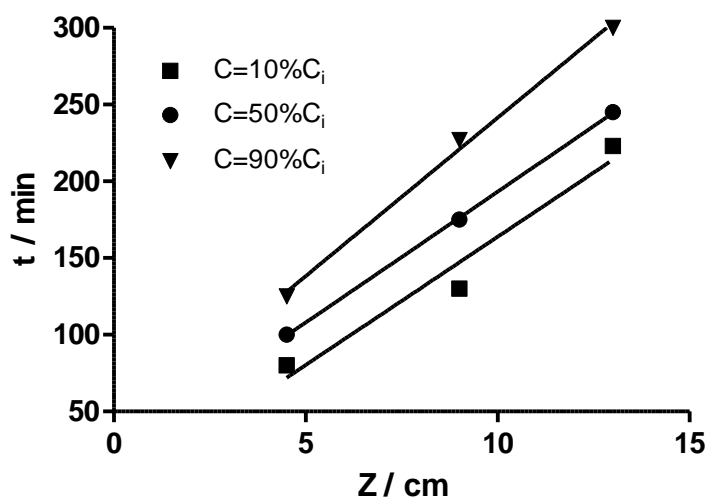


Figure 7.4 - MS-222 iso-concentration lines for breakthrough points of 10, 50 and 90% and for bed depths of 4.5, 9 and 13 cm ($C_i=250 \text{ mg L}^{-1}$; $Q=4.4 \text{ mL min}^{-1}$; $v=5.6 \text{ cm min}^{-1}$).

Table 7.4 - Predicted parameters for the BDST model at $Q=4.4 \text{ mL min}^{-1}$ to MS-222 fixed-bed column scale-up

C/C_i	$a \text{ (min cm}^{-1}\text{)}$	$b \text{ (min)}$	$N_0 \text{ (mg mL}^{-1}\text{)}$	$k_{BDST} \text{ (mL mg}^{-1} \text{ min}^{-1}\text{)}$	r^2
0.10	16.7	2.89	22.9	3.10	0.9588
0.50	17.1	-22.7	23.4	0	0.9998
0.90	20.6	-35.1	28.4	0.255	0.9962

For the scale-up experiment, flow rate and both the internal diameter and bed depth of the fixed-bed column were increased up to 12 mL min^{-1} , 2.5 cm and 35 cm, respectively. Under these conditions, $v = 2.4 \text{ cm min}^{-1}$ and a new BDST model parameter, a' , was calculated recurring to Eq.2.25. Meanwhile, the intercept, b' , remained the same as for the unchanged initial concentration (C_i). Predicted and experimental breakthrough curves are represented in Figure 7.5 while Table 7.5 depicts the experimental and calculated times from BDST model for the breakthrough points considered (10, 50 and 90%). As can be observed in Figure 7.5, the BDST model satisfactorily predicted experimental scale-up results, with a maximum deviation of 11% , which occurred for $C/C_i=0.7$. Thus, one can conclude that BDST model provides good prediction of breakthrough curves at different conditions.

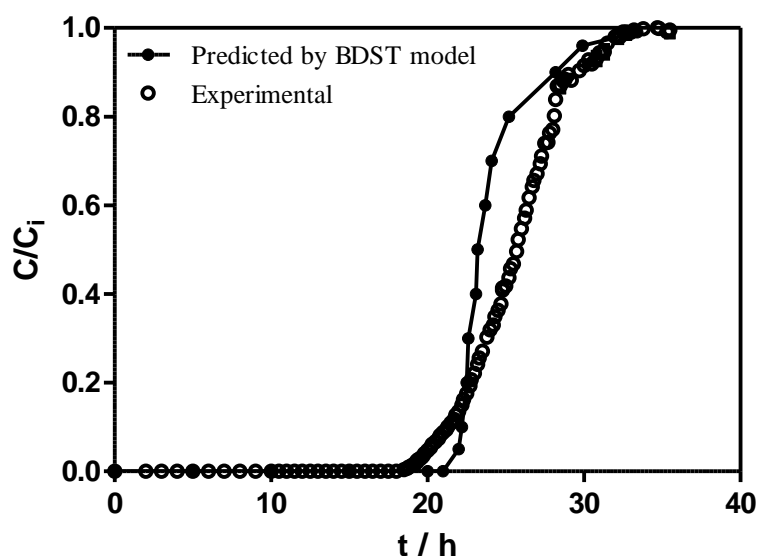


Figure 7.5 - BDST model predicted and experimental breakthrough curves of MS-222 fixed-bed column scale-up experiment ($C_i=250 \text{ mg L}^{-1}$; $Z=35 \text{ cm}$; $Q=12 \text{ mL min}^{-1}$; $v=2.4 \text{ cm min}^{-1}$).

Table 7.5 - Predicted breakthrough times based on the BDST model parameters for MS-222 fixed-bed column scale-up at $v=2.4 \text{ cm min}^{-1}$

C/C_i	$a' (\text{min cm}^{-1})$	$b' (\text{min})$	$t_{cal} (\text{h})$	$t_{exp} (\text{h})$	Error (%)
0.10	38.1	2.89	22.2	21.3	4
0.50	39.1	-22.7	23.2	25.7	10
0.90	47.3	-35.1	28.2	29.7	5

7.3.2 Fixed-bed adsorption of 2-PE

7.3.2.1 Effect of the flow rate, influent concentration and bed depth

Breakthrough curves of fixed-bed adsorption of 2-PE onto BSC-b at different flow rates are presented in Figure 7.6 a.) (keeping $C_i=0.3 \text{ cm}^3 \text{ L}^{-1}$ and $Z=4.5 \text{ cm}$). The results show the same trend that those obtained with MS-222, *i.e.*, the saturation time (t_s) and breakthrough time (t_b) decrease with the increase of the flow rate, and, consequently, reduce the volume of treated effluent until breakthrough point (V_b). This is more noticeable between 1.2 and 2.1 mL min^{-1} , where there is a more evident increase of treated volume, as can be seen in Table 7.6. Once again, the increase of the flow rate causes the decrease of the contact time between the 2-PE molecules and the BSC-b particles. Nevertheless, between flow rate 2.1 and 4.4 mL min^{-1} , the decrease of volume treated until the breakthrough point is negligible. For that reason, under the operation conditions here

considered, the use of 4.4 mL min^{-1} of flow rate may be more advantageous (almost the same volume treated in less time). Concerning the total adsorption capacity of the bed, interesting results were obtained: between 1.2 and 2.1 mL min^{-1} , the bed capacity was almost the same; however, increasing the flow rate to 4.4 mL min^{-1} , the bed capacity increased from 35 to 41 mg g^{-1} , corresponding to about 16% (Table 7.6). Comparing these values with the ones obtained in batch system, shown in Chapter 5, section 5.3.4 ($53.2 \pm 0.8 \text{ mg g}^{-1}$, estimated by Langmuir model, $r^2=0.9943$), the performance of BSC-b in continuous system was not as attractive as in batch system.

The effect of the 2-PE influent concentration, while keeping the other parameters constant ($Q=4.4 \text{ mL min}^{-1}$; $Z=4.5 \text{ cm}$), is shown in Figure 7.6 b.). As already observed in MS-222 breakthrough curves, for lower influent concentrations, the adsorption occurs slowly, so the curve is less steep. On the other hand, increasing the influent concentration to 0.8 and $1.3 \text{ cm}^3 \text{ L}^{-1}$, the steepness of the slope increases and these curves are very close to each other. In these cases, the breakthrough and the saturation points are reached earlier (Table 7.6). The reason for the increase in adsorption rate of 2-PE onto BSC-b for higher influent concentrations was discussed in previous section 7.3.1.1. About the total bed adsorption capacity, it can be observed in Table 7.6 that higher influent concentrations increase the adsorption capacity to values near to those obtain in batch system experiments (Chapter 5, section 5.3.4).

Lastly, the breakthrough curves obtained for 2-PE adsorption onto different bed depths of BSC-b ($Z=4.5$; 9.0 and 13.0 cm) are illustrated in Figure 7.6 c.), at constant flow rate and influent concentration ($Q=4.4 \text{ mL min}^{-1}$; $C_i=0.3 \text{ cm}^3 \text{ L}^{-1}$). As also observed in MS-222 fixed-bed adsorption results, both breakthrough and saturation times increased as bed depth increased, and consequently the volume of treated effluent increased significantly (Table 7.6). A progressively decrease of the steepness of the slope with the increase of the bed depth is observed in Figure 7.6 c.), which is a consequence of the longer distance it takes the mass transfer zone to move from the entrance to the exit of the bed when its depth is increased. The BSC-b bed adsorption capacity to 2-PE slightly decreases when bed depth increases, which may be also a consequence of the broad mass transfer zone formed when the bed depth is higher.

In Chapter 5 (section 5.3.4), the Table 5.7 shows higher values of adsorption rate constants to the adsorption of 2-PE onto BSC-b in batch system than that to MS-222. This may be the reason for the variation on the BSC-b bed adsorption to 2-PE with the flow rate, influent concentration and bed depth variation.

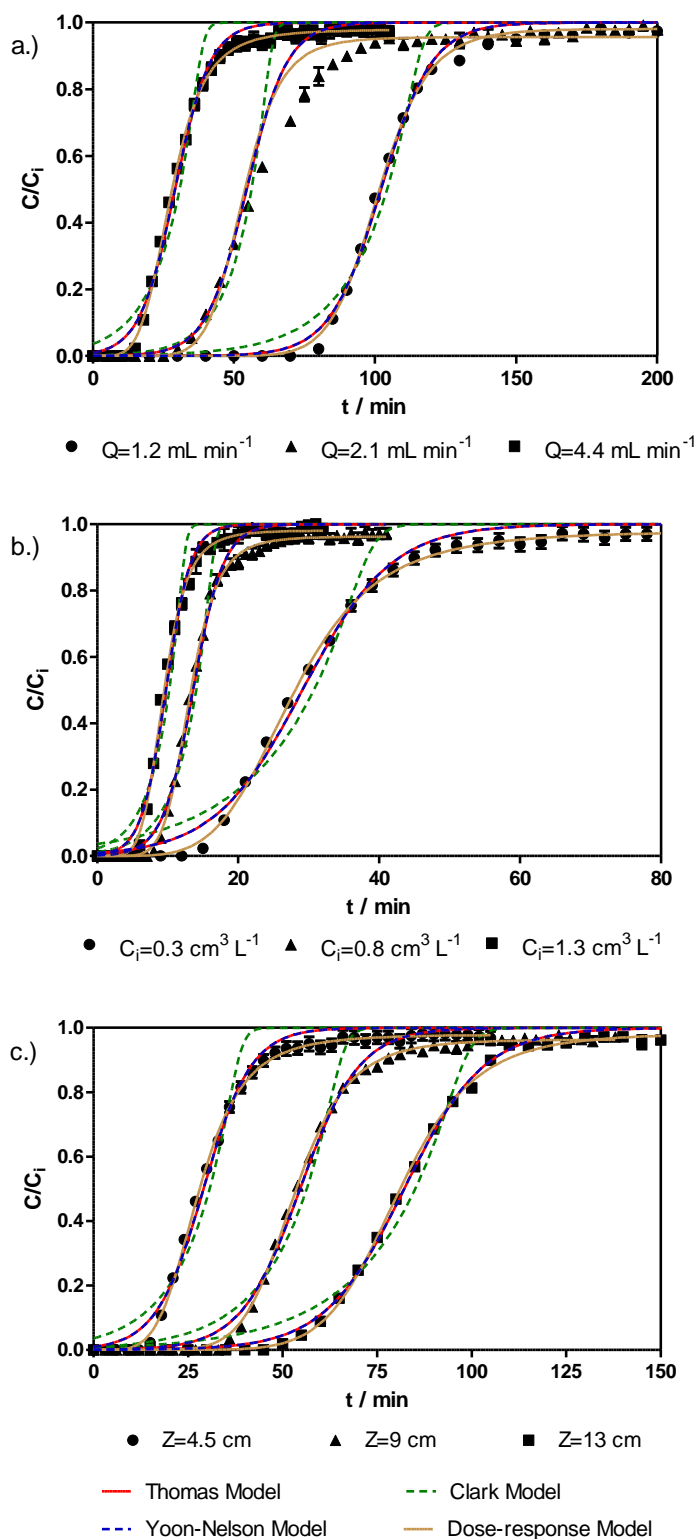


Figure 7.6 - Breakthrough curves for 2-PE adsorption onto BSC-b at different a.) flow rate ($C_i=0.3 \text{ cm}^3 \text{ L}^{-1}$ and $Z=4.5 \text{ cm}$); b.) influent concentration ($Q=4.4 \text{ mL min}^{-1}$ and $Z=4.5 \text{ cm}$), and c.) bed depth ($Q=4.4 \text{ mL min}^{-1}$ and $C_i=0.3 \text{ cm}^3 \text{ L}^{-1}$). The experimental data were fitted to Thomas, Clark, Yoon-Nelson and Dose-Response models.

Table 7.6 - Column data from breakthrough curves for the fixed-bed adsorption of 2-PE (solutions in ultra-pure water) onto BSC-b at different flow rates ($C_i=0.3 \text{ cm}^3 \text{ L}^{-1}$ and $Z=4.5 \text{ cm}$), influent concentrations ($Q=4.4 \text{ mL min}^{-1}$ and $Z=4.5 \text{ cm}$) and bed depths ($Q=4.4 \text{ mL min}^{-1}$ and $C_i=0.3 \text{ cm}^3 \text{ L}^{-1}$)

	t_b (min)	V_b (ml)	$t_{50\%}$ (min)	t_s (min)	q_s (mg g ⁻¹)
Q (ml min⁻¹)					
1.2	85	102	102	160	34
2.1	40	84	60	105	35
4.4	18	79	30	66	41
C_i (cm³ L⁻¹)					
0.3	18	79	30	66	41
0.8	10	44	14	28	49
1.3	7	31	10	19	52
Z (cm)					
4.5	18	79	30	66	41
9	42	185	54	102	37
13	65	286	80	130	35

7.3.2.2 Breakthrough curves data modelling

Thomas, Clark, Yoon-Nelson and Dose-Response models were used to fit the experimental 2-PE breakthrough curves, obtained at different flow rates, influent concentrations and bed depths, which are shown in Figure 7.6. The corresponding fitting parameters are presented in Table 7.7. Observing the Figure 7.6, it is easily concluded that the Clark model is the less appropriate model to describe the experimental 2-PE breakthrough curve data, presenting the lowest coefficient of determination values, r^2 , and, also, higher deviation from experimental data (Table 7.7). Similarly to MS-222 breakthrough curves fittings, Thomas and Yoon-Nelson models applied to 2-PE experimental breakthrough curves seem to be coincident, although their adsorption rate constants do not follow the same trend concerning to the variation of flow rate and influent concentration. Thomas rate constant slightly increases from 0.38 to 0.48 min⁻¹ and 0.48 to 0.53 min⁻¹ with the increase of flow rate and influent concentration, respectively, and then decrease to higher influent concentration and maintaining constant to higher flow rate. Moreover, the bed adsorption capacity values predicted by Thomas model, q_{Th} , are distant from the experimental ones, with deviation up to 65%. On the other hand, the Yoon-Nelson model is the simplest model applied to fixed-bed adsorption and is considered the less valuable to obtain process variables and to predict adsorption under distinct conditions [21]. However, in this case, Yoon-Nelson model predicts the time

necessary to reach 50% of the influent concentration, $t_{50\%}$, with less than 4% of deviation from the experimental values. In addition, the Yoon-Nelson rate constants have a logical trend, also as previously obtained for MS-222 fixed-bed adsorption, *i.e.*, the adsorption rate constant increases significantly with flow rate and influent concentration increase and decreases with bed depth increase. So, the breakthrough curves predicted by the Yoon-Nelson model showed reasonably good agreement with the experimental results. Once again, the Dose-Response model was, in general, the most appropriate to describe the experimental data, with coefficients of determination above 0.998, except to the breakthrough curve of 2.1 mL min^{-1} flow rate (Table 7.7). The normalized concentration at saturation time (C_s/C_i) was well predicted by Dose-Response model with less than 3% of deviation from the experimental values. However, the prediction of the parameter $t_{50\%}$ was not as good as that obtained with Yoon-Nelson model, having deviations up to 7.2%. In conclusion, for this adsorbent-adsorbate system in fixed-bed adsorption experiments, the application of both Yoon-Nelson and Dose-Response models is advised in order to obtain the most correct values of $t_{50\%}$ and C_s/C_i parameters and, also, to obtain information about the adsorption rate, k_{YN} .

Table 7.7 - Thomas, Clark, Yoon-Nelson and Dose-Response model parameters at different flow rate ($C_i=0.3 \text{ cm}^3 \text{ L}^{-1}$ and $Z=4.5 \text{ cm}$), influent concentrations ($Q=4.4 \text{ mL min}^{-1}$ and $Z=4.5 \text{ cm}$) and bed depths ($Q=4.4 \text{ mL min}^{-1}$ and $C_i=0.3 \text{ cm}^3 \text{ L}^{-1}$) to 2-PE fixed-bed column adsorption

Parameters	$Q \text{ (mL min}^{-1}\text{)}$			$C_i \text{ (cm}^3 \text{ L}^{-1}\text{)}$			$Z \text{ (cm)}$			
	1.2	2.1	4.4	0.3	0.8	1.3	4.5	9	13	
Thomas	$k_{Th} \text{ (mL min}^{-1} \text{ mg}^{-1}\text{)}$	0.38±0.02	0.48±0.08	0.48±0.02	0.48±0.02	0.53±0.03	0.41±0.02	0.48±0.02	0.41±0.02	0.32±0.01
	$q_{Th} \text{ (mg g}^{-1}\text{)}$	33.5±0.1	31.6±0.8	42.2±0.5	42.2±0.5	50.7±0.5	56.6±0.7	42.2±0.5	35.7±0.3	36.5±0.2
	r^2	0.9965	0.9416	0.9922	0.9922	0.9912	0.9928	0.9922	0.9932	0.9977
Clark	$k_C \text{ (min}^{-1}\text{)}$	0.488±0.003	0.83±0.01	0.73±0.07	0.73±0.07	2.28±0.03	2.6±0.3	0.73±0.07	0.613±0.007	0.424±0.004
	$t_b \text{ (min)}$	112	61	36	36	16	12	36	62	94
	r^2	0.9885	0.9464	0.9736	0.9736	0.9766	0.9746	0.9736	0.9782	0.9869
Yoon-Nelson	$k_{YN} \text{ (min}^{-1}\text{)}$	0.111±0.005	0.14±0.02	0.159±0.008	0.159±0.008	0.46±0.03	0.57±0.03	0.159±0.008	0.128±0.006	0.095±0.003
	$t_{50\%} \text{ (min)}$	102.2±0.4	55±1	29.1±0.4	29.1±0.4	13.6±0.1	9.7±0.1	29.1±0.4	54.6±0.4	82.2±0.4
	r^2	0.9965	0.9416	0.9922	0.9922	0.9912	0.9928	0.9922	0.9932	0.9977
Dose-Response	C_s/C_i	0.981±0.003	0.96±0.02	0.979±0.003	0.979±0.003	0.963±0.003	0.981±0.004	0.979±0.003	0.964±0.002	0.981±0.004
	$t_{50\%} \text{ (min)}$	101.2±0.2	53±1	27.8±0.1	27.8±0.1	13.1±0.1	9.42±0.05	27.8±0.1	53.1±0.1	80.7±0.2
	α	11.5±0.3	8±1	4.70±0.09	4.70±0.09	6.7±0.1	5.6±0.2	4.70±0.09	7.5±0.1	8.0±0.2
	r^2	0.9988	0.9509	0.9992	0.9992	0.9992	0.9986	0.9992	0.9995	0.9993

7.3.2.3 Scale-up

In Figure 7.7 is presented the iso-concentration lines for 2-PE retained in the fixed-bed at 10, 50 and 90% of breakthrough points for the three bed depths considered in section 7.3.2.1. Table 7.8 gives the slopes and intercepts of the fitted lines, which correspond to a and b respectively, and BDST model parameters, N_0 and k_{BDST} . It may be observed that N_0 increased with increasing of breakthrough point, as for the increase of the slope, and the k_{BDST} decreased with increasing breakthrough point. Contrarily to the results shown in section 7.3.1.4, the line for 50% of breakthrough nearly passes through the origin, $b \approx 0$. This has been reported by some authors as a demonstration of the reliability of the BDST model [20,22].

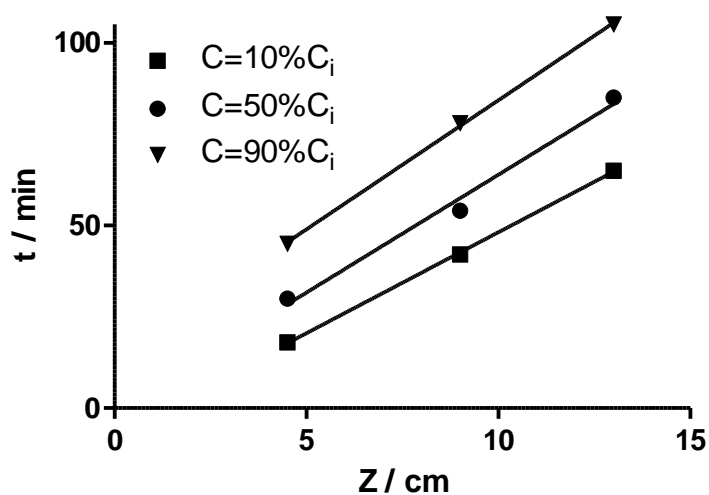


Figure 7.7 - 2-PE iso-concentration lines for breakthrough points of 10, 50 and 90% and for bed depths of 4.5, 9 and 13 cm ($C_i=0.3 \text{ cm}^3 \text{ L}^{-1}$; $Q=4.4 \text{ mL min}^{-1}$; $v=5.6 \text{ cm min}^{-1}$).

Table 7.8 - Predicted parameters for the BDST model at $Q=4.4 \text{ mL min}^{-1}$ to 2-PE fixed-bed column scale-up

C/C_i	$a \text{ (min cm}^{-1}\text{)}$	$b \text{ (min)}$	$N_0 \text{ (mg mL}^{-1}\text{)}$	$k_{BDST} \text{ (mL mg}^{-1} \text{ min}^{-1}\text{)}$	r^2
0.10	5.53	7.14	9.69	0.983	0.9995
0.50	6.45	0.62	11.3	0	0.9885
0.90	7.06	-13.6	12.4	0.516	0.9994

In order to confirm the applicability of the BDST model, a scale-up experiment was performed increasing the flow rate and both internal diameter and bed depth of the fixed-bed column up to 12 mL min^{-1} , 2.5 cm and 35 cm, respectively. New BDST parameter a' was calculated recurring to Eq. 2.25, while the intercept, b' , remained the same as for the unchanged initial concentration (C_i). In Table 7.9 are presented the new BDST model parameters and the experimental and calculated times from BDST model for the breakthrough points considered (10, 50 and 90%). The respective predicted and experimental breakthrough curves are shown in Figure 7.8. The first point that stands up is the under-estimated breakthrough curve by BDST model, with deviations between 19 ($C/C_i=0.5$) and 35% ($C/C_i=0.05$ and $C/C_i=0.98$). So, it can be concluded that, in the case of 2-PE fixed-bed adsorption experiments, the BDST model is not so good as in the case of MS-222 to predict a scale-up even the conditions of the model have been accomplished.

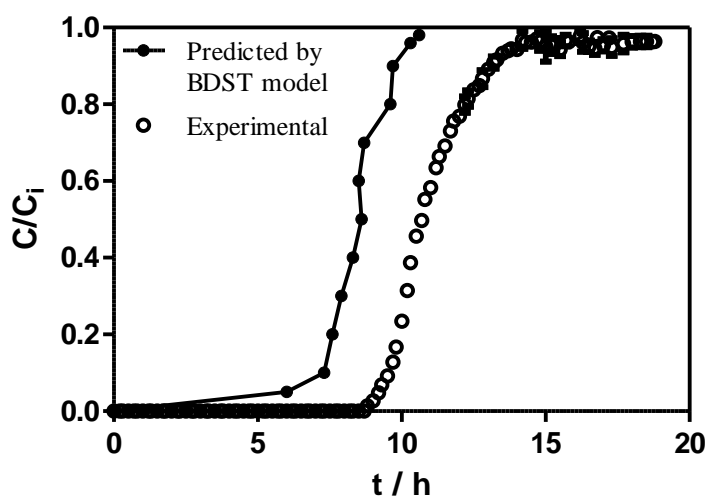


Figure 7.8 - BDST model predicted and experimental breakthrough curves of 2-PE fixed-bed column scale-up experiment ($C_i=0.3 \text{ cm}^3 \text{ L}^{-1}$; $Z=35 \text{ cm}$; $Q=12 \text{ mL min}^{-1}$; $v=2.4 \text{ cm min}^{-1}$).

Table 7.9 - Predicted breakthrough times based on the BDST model parameters for 2-PE fixed-bed column scale-up at $v=2.4 \text{ cm min}^{-1}$

C/C_i	$a' \text{ (min cm}^{-1}\text{)}$	$b' \text{ (min)}$	$t_{cal} \text{ (h)}$	$t_{exp} \text{ (h)}$	Error (%)
0.10	12.7	7.14	7.27	9.67	25
0.50	14.8	0.62	8.61	10.7	19
0.90	16.2	-13.6	9.67	13.2	27

7.4 Conclusions

Continuous adsorption experiments of MS-222 onto BSC-b revealed that decreasing flow rate and influent concentration resulted in larger volume of effluent treated at breakthrough time; additionally, the highest volume treated (968 mL) was obtained for the highest bed depth (13 cm). Furthermore, a maximum bed adsorption capacity of 125 mg g^{-1} was obtained under a flow rate of 4.4 mL min^{-1} , with 400 mg L^{-1} of MS-222 in 4.5 cm bed depth. It was demonstrated that, in general, fixed-bed column data can be adequately described by the Dose-Response model with less than 2% of deviation from the experimental values. Also, the performance of the continuous adsorption in a BSC-b packed column using real aquaculture wastewater as matrix was not affected significantly by the presence of organic (high DOC content) and inorganic matter, which is a great advantage for the possible application of BSC as adsorbent in RASs. On the other hand, the application of BDST model resulted in an excellent prediction of scale-up experiments, with an error of less than 11% compared with experimental data.

Regarding the continuous adsorption experiments of 2-PE onto BSC-b, the decrease of flow rate and influent concentration resulted in an increase of volume of effluent treated at breakthrough time and, also, increase with the increase of bed depth. The highest volume treated (286 mL) was obtained for the highest bed depth, 13 cm, and flow rate of 4.4 mL min^{-1} and influent concentration of $0.3 \text{ cm}^3 \text{ L}^{-1}$. However, when comparing the bed adsorption capacities values, the performance of BSC-b in continuous system was not as attractive as in batch system. For the fixed-bed adsorption experiments of 2-PE onto BSC-b, the application of both Yoon-Nelson and Dose-Response models is recommended in order to obtain the most correct values of $t_{50\%}$, C_s/C_i and adsorption rate. Finally, the application of BDST model in the prediction of 2-PE scale-up adsorption experiment was not as good as expected.

7.5 References

- [1] Martins, C.I.M., Eding, E.H., Verdegem, M.C.J., Heinsbroek, L.T.N., Schneider, O., Blancheton, J.P., d'Orbcastel, E.R. and Verreth, J.A.J., 2010, *Aquacultural Engineering*, 43 (3), 83-93.
- [2] Miller, D. and Semmens, K., 2002, *Aquaculture Information Series*, AQ02-1.
- [3] Summerfelt, S.T., Sharrer, M.J., Tsukuda, S.M. and Gearheart, M., 2009, *Aquacultural Engineering*, 40 (1), 17-27.
- [4] Lawson, T.B., 1995, Fundamentals of aquacultural engineering, 1st ed., *Chapman & Hall*, New York, USA.
- [5] Robinson, T., McMullan, G., Marchant, R. and Nigam, P., 2001, *Bioresource Technology*, 77 (3), 247-255.
- [6] McKay, G., 1995, Use of Adsorbents for the Removal of Pollutants from Wastewater, 1st ed., *CRC Press*, New York, USA.

- [7] Ross, L.G. and Ross, B., 2008, *Anaesthetic and Sedative Techniques for Aquatic Animals*, Blackwell Publishing Ltd, Oxford, UK.
- [8] Thomas, H.C., 1944, *Journal of the American Chemical Society*, 66 (10), 1664-1666.
- [9] Clark, R.M., 1987, *Environmental Science & Technology*, 21 (6), 573-580.
- [10] Yoon, Y.H. and Nelson, J.H., 1984, *American Industrial Hygiene Association Journal*, 45 (8), 509-516.
- [11] Yan, G., Viraraghavan, T. and Chen, M., 2001, *Adsorption Science & Technology*, 19 (1), 25-43.
- [12] Hutchins, R.A., 1973, *Chemical Engineering Journal*, 20, 133-138.
- [13] Tan, I.A.W., Ahmad, A.L. and Hameed, B.H., 2008, *Desalination*, 225 (1-3), 13-28.
- [14] Salman, J.M., Njoku, V.O. and Hameed, B.H., 2011, *Chemical Engineering Journal*, 174 (1), 33-40.
- [15] Canteli, A.M.D., Carpiné, D., Scheer, A.d.P., Mafra, M.R. and Igarashi-Mafra, L., 2014, *LWT - Food Science and Technology*, 59 (2, Part 1), 1025-1032.
- [16] Singh, A., Kumar, D. and Gaur, J.P., 2012, *Water Research*, 46 (3), 779-788.
- [17] Calero, M., Hernáinz, F., Blázquez, G., Tenorio, G. and Martín-Lara, M.A., 2009, *Journal of Hazardous Materials*, 171 (1-3), 886-893.
- [18] Katsigiannis, A., Noutsopoulos, C., Mantziaras, J. and Gioldasi, M., 2015, *Chemical Engineering Journal*, 280, 49-57.
- [19] El Qada, E.N., Allen, S.J. and Walker, G.M., 2006, *Industrial & Engineering Chemistry Research*, 45 (17), 6044-6049.
- [20] Cortés-Martínez, R., Solache-Ríos, M., Martínez-Miranda, V. and Alfaro-Cuevas, R., 2008, *Water, Air, and Soil Pollution*, 196 (1), 199-210.
- [21] Xu, Z., Cai, J.-g. and Pan, B.-c., 2013, *Journal of Zhejiang University SCIENCE A*, 14 (3), 155-176.
- [22] Netpradit, S., Thiravetyan, P. and Towprayoon, S., 2004, *Water Research*, 38 (1), 71-78.

8 Chemical and thermal regeneration of biological paper mill sludge-based adsorbent

In the present chapter, the regeneration of biological paper mill sludge-based carbon saturated with tricaine methanesulfonate (MS-222) was assessed by chemical and thermal regeneration methods. Water, NaOH and HCl solutions were used as chemical regeneration agents by passing them through a fixed-bed column packed with the exhausted carbon. From the chemical regenerations, the elution with 500 mL of an acidic solution of HCl 1 M resulted in the best MS-222 recovery efficiency, 56%; however, the high volume of eluent used makes this technique less attractive. The thermal regeneration was performed in a single pyrolysis step and the adsorption capacity of the fixed-bed was assessed for three cycles of regeneration-saturation. The thermal regeneration of the exhausted carbon revealed satisfactory results for one cycle reusability after saturation; however, considering the nature of its precursor, the use of new biological sludge-based carbon could be more interesting than its regeneration, functioning also as an additional option for the management of such wastes.

Part of the work presented and discussed in this chapter resulted in the following publication:

Ferreira C.I.A., Calisto V., Otero M., Nadais H., Esteves V.I., 2017, Fixed-bed adsorption of Tricaine Methanesulfonate onto pyrolysed paper mill sludge. *Aquacultural Engineering*. DOI: 10.1016/j.aquaeng.2017.02.006.

8.1 Contextualization

The adsorption process using activated carbons (ACs) as adsorbent is widely applied to the treatment of industrial water effluents in order to meet environmental legislations. The excellent ACs properties, namely the large surface area and high micropore volume are the key for their high removal efficiencies. During the adsorption process, the progressive accumulation of pollutants adsorbed occurs on the surface of the adsorbent, leading to a gradual reduction of its adsorption capacity until adsorption is no longer possible. Considering that the main disadvantage of ACs is the high price, the substitution of the exhausted AC for new AC in the end of each cycle is, nowadays, impracticable. In this sense, the saturated adsorbent can be reused after an appropriate regeneration step. The main goal of this extra-step is to remove the adsorbed pollutant molecules, by their degradation or desorption, recovering the original adsorption capacity of the adsorbent [1,2]. Several studies have been performed to develop new techniques of AC regeneration, such as, biological regeneration [3,4], electrochemical regeneration [5,6], extraction with supercritical fluids [7,8] and microwave-assisted regeneration [9,10]; however, the conventional techniques are still the most applied and are based on chemical and thermal methods. Chemical regeneration consists of desorption of adsorbed molecules by elution, using solvents or any other solution that modifies the adsorption equilibrium. This technique may be operated *in situ* and the adsorbent loss is less or null [11]. On the other hand, thermal regeneration consists of heating the exhausted adsorbent (CO₂, steam and/or inert atmosphere) to provide the amount of energy necessary to remove the retained adsorbate. In this case, the adsorbed molecules can suffer thermal desorption and/or degradation. The main drawbacks of thermal regeneration are the *ex situ* operation and the lost of adsorbent weight by attrition and burnoff [12]; however, until now, this is the most efficient regeneration technique, with efficiencies above 97% [13,14].

In this chapter, the regeneration of biological sludge-based adsorbent (BSC-b) saturated with MS-222 was tested by chemical and thermal methodologies. The chemical regeneration agents used were water, NaOH 0.1 and 1 M and HCl 1 M, and the elution occurred passing them through a fixed-bed column packed with exhausted BSC-b. Recovery efficiencies of MS-222 were determined for each eluent. The thermal regeneration was carried out by a single step of pyrolysis, in N₂ atmosphere, and three cycles of regeneration-saturation were performed. In this case, the bed adsorption capacity in each cycle was evaluated.

8.2 Materials and methods

8.2.1 Adsorbent materials

In this chapter, the adsorbent tested was the pyrolysed and washed biological paper mill sludge with particle size between 0.18 and 0.5 mm (BSC-b), produced and characterized in previous Chapter 5.

8.2.2 Fish anaesthetics

Adsorption tests were performed for the fish anaesthetic tricaine methanesulfonate (> 97%, TCI Europe) - MS-222. Anaesthetic solutions were prepared in ultra-pure water obtained from a Milli-Q Millipore system (Milli-Q plus 185), buffered using 10^{-2} M of NaHCO_3 to pH 7-7.5 as recommended by Ross et al. (2008) [15]. The MS-222 physico-chemical properties are summarized in Chapter 2, Table 2.1.

8.2.3 Determination of the MS-222 concentration

8.2.3.1 *In water matrix*

MEKC analyses were performed using a Beckman P/ACE MDQ (Fullerton, CA, USA) instrument, equipped with an UV-Vis detection system, following the procedure described in Appendix C (section C.1.1.1). Aqueous samples and standard solutions were analyzed in triplicate. MS-222 calibration curve and parameters, including the limit of detection (LOD) and limit of quantification (LOQ), are also presented in Appendix C, section C.1.1.

8.2.3.2 *In NaOH matrix*

For the quantification of MS-222 in NaOH matrix, capillary zone electrophoresis (CZE) analyses were performed using the same equipment from previous section 8.2.3.1 and following the procedure described in Appendix C (section C.1.1.2). Aqueous samples and standard solutions were analyzed in triplicate. MS-222 calibration curve and parameters in NaOH matrix, including the limit of detection (LOD) and limit of quantification (LOQ), are also presented in Appendix C, section C.1.1.

8.2.3.3 *In HCl matrix*

For the quantification of MS-222 in HCl matrix, MEKC analyses were performed using same equipment from previous section 8.2.3.1 and following the procedure described in Appendix

C (section C.1.1.3). Aqueous samples and standard solutions were analyzed in triplicate. MS-222 calibration curve and parameters in NaOH matrix, including the limit of detection (LOD) and limit of quantification (LOQ), are also presented in Appendix C, section C.1.1.

8.2.4 Chemical regeneration

The saturation of the BSC-b, for the further chemical regeneration tests, was performed in a fixed-bed column packed with 1 g of BSC-b ($Z=4.5$ cm) by passing a 400 mg L^{-1} of MS-222 solution at a flow rate of 4.4 mL min^{-1} , until BSC-b saturation (more details in Chapter 7, section 7.2.4). Then, the BSC-b chemical regeneration was carried out by passing through the saturated bed, at a flow rate of 2.1 mL min^{-1} , 500 mL of an eluent solution that will desorb the MS-222. In this work, in order to avoid the use of organic solvents, three low-cost and more environmentally friendly eluents were chosen: water, NaOH 0.1 and 1 M, and HCl 1 M. Throughout the chemical regeneration, effluent samples were collected by a programmable fraction collector (Gilson FC 203B Fraction Collector), filtered through $0.22 \mu\text{m}$ Simplepure PVDF filters, and analyzed for the concentration of MS-222 by MEKC. It is important to mention that the MEKC analytical method is different and is dependent on the eluent used.

In each experiment, adsorption breakthrough curves were obtained in order to calculate the total mass of MS-222 adsorbed in BSC-b, m_{adsorbed} :

$$m_{\text{adsorbed}} = q_s m \quad 8.1$$

where q_s is the total bed capacity, determined by Eq. 2.14 (Chapter 2, section 2.4.4.1), and m is the adsorbent weight.

Desorption kinetic curves were obtained by plotting the effluent concentration (*i.e.*, the MS-222 concentration in the eluent solution), C (mg L^{-1}), versus time, t (min). The quantity of MS-222 desorbed corresponds to the area under the curve, so the mass of MS-222 desorbed by each eluent solution, m_{desorbed} , is determined by the follow equation:

$$m_{\text{desorbed}} = \frac{Q}{1000} A_u = \frac{Q}{1000} \int_{t=0}^{t=t_f} C dt \quad 8.2$$

where Q (mL min^{-1}) is the flow rate of eluent, A_u (mg min L^{-1}) is the area under the curve and t_f (min) the final time of desorption experiment. The area under each curve was obtained using GraphPad Prism 5 software.

The MS-222 recovery efficiency of the chemical regeneration using the different eluent solutions, RE (%), may be calculated by:

$$RE (\%) = \frac{m_{\text{desorbed}}}{m_{\text{adsorbed}}} 100\% \quad 8.3$$

8.2.5 Thermal regeneration

The saturation of the BSC-b was performed in a fixed-bed column packed with 2.5 g of BSC-b ($Z=13.0$ cm) by passing a 250 mg L^{-1} of MS-222 solution at a flow rate of 4.4 mL min^{-1} , until BSC-b saturation. Then, the saturated BSC-b was removed from the column and dried in an oven at $105 \text{ }^\circ\text{C}$ overnight. The BSC-b regeneration was carried out by pyrolysis using a muffle (Nüve furnace MF 106), under N_2 saturated atmosphere, at a heating rate of $10 \text{ }^\circ\text{C min}^{-1}$ up to $600 \text{ }^\circ\text{C}$, which was kept during 90 min. The maximum temperature of $600 \text{ }^\circ\text{C}$ was chosen to guarantee thermal desorption/degradation of MS-222, as can be seen by the results of thermogravimetric analysis (TGA) performed to MS-222 presented in Figure 8.1.

TGA of MS-222 was carried out by thermogravimetric analysis (TGA) and derivative thermogravimetric analysis (DTGA). Non-isothermal TG analysis was performed using a TAG analyser (Shimadzu TGA-50 instrument). The analysis was carried out under a $20 \text{ cm}^3 \text{ min}^{-1}$ N_2 flow at a heating rate of $10 \text{ }^\circ\text{C min}^{-1}$ from room temperature to $950 \text{ }^\circ\text{C}$. Approximately 20 mg of sample was used. The weight loss (TG) and derivative (DTG) curves of MS-222 were represented as a function of temperature, to allow the knowledge of MS-222 degradation temperatures.

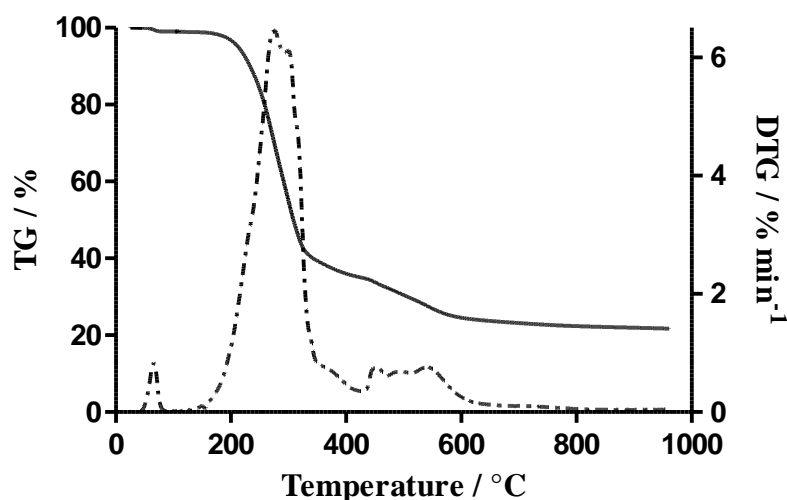


Figure 8.1 - Thermogravimetric (— TG) and derivative thermogravimetric (--- DTG) curves of MS-222.

After regeneration, the fixed-bed experiment was repeated under identical operational conditions ($Z=13$ cm, $C_i= 250 \text{ mg L}^{-1}$, $Q=4.4 \text{ mL min}^{-1}$), and the whole process (saturation-regeneration) was repeated up to three cycles. Breakthrough curves were drawn for each cycle of saturation-regeneration and the experimental parameters of breakthrough time and volume, saturation time and bed adsorption capacity were determined.

Specific surface area (S_{BET}) and total micropore volume (W_0) were determined by N_2 adsorption isotherms for saturated and regenerated BSC-b in cycle 1. These analyses were acquired at 77 K using a Micromeritics Instrument, Gemini VII 2380. The samples were previously outgassed at 120 °C for 12 h.

8.3 Results and discussion

8.3.1 Chemical regeneration

Figure 8.2 shows desorption kinetic curves of MS-222 using the eluents considered in this work with the respective MS-222 recovery efficiency, RE . According to the RE results, the use of NaOH and HCl yields a 40 and 52% increase, respectively, in the RE with respect to water. The maximum RE achieved was for the HCl 1 M chemical regeneration, with 56%. The better regeneration performance of the HCl solution can be explained by the following mechanisms acting together: in this acidic condition ($pH \approx 0$), MS-222 is in cationic form ($pK_a = 3.6$) and its solubility in water is higher; also, in HCl solutions, both the surface of BSC-b ($pH_{PZC} = 10.4$) and adsorbed MS-222 are protonated and, because of electrostatic repulsions between MS-222 and BSC-b surface groups, MS-222 is desorbed.

The RE values obtained for these chemical regeneration agents were good, taking into account that they are not organic solvents (reported by several authors as the most efficient eluents for AC chemical regeneration); however, the volume of eluent used to obtain such RE was high (500 mL) and it is, approximately, the same volume of contaminated effluent needed to reach the saturation of the BSC-b bed. Despite the chemical regeneration advantages, such as the *in situ* operation and the low or no loss of adsorbent during the regenerative process, the volume of eluent required makes this process less attractive.

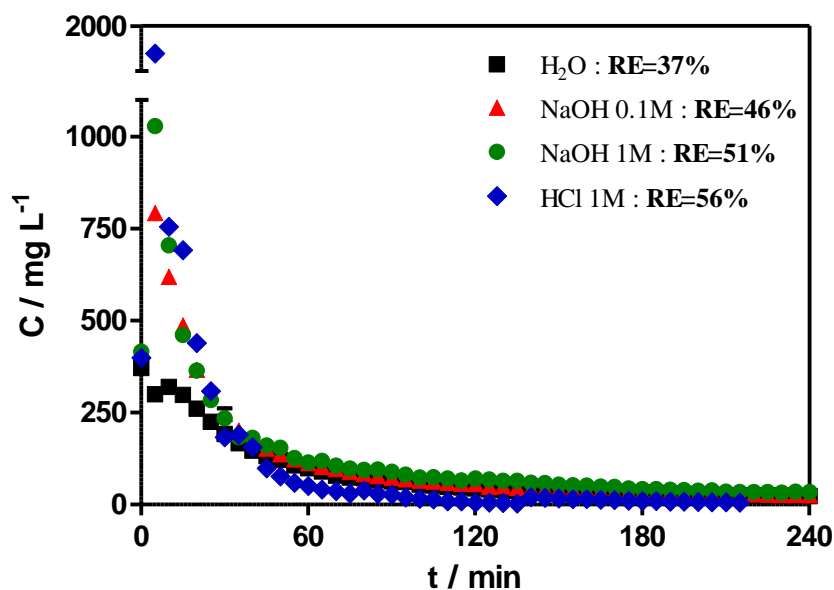


Figure 8.2 – MS-222 desorption kinetic curves using different chemical agents of regeneration and respective recovery efficiency.

8.3.2 Thermal regeneration

Breakthrough curves after thermal regeneration of exhausted BSC-b are presented in Figure 8.3 for three consecutive cycles. It is clearly observed in Table 8.1 that t_b and, consequently, the volume of effluent treated at breakthrough, V_b , decreased 11, 34 and 48% at the first, second and third cycles, respectively. This may be related to the decrease of adsorption capacity of the regenerated BSC-b and/or to the loss of BSC-b during the thermal regeneration process, due to BSC-b oxidation and attrition, which resulted in weight losses of about 20%. However, the time of saturation, t_s , and the bed adsorption capacity, q_s , were slightly higher for the first regeneration cycle. For this first cycle of BSC saturation-regeneration, N_2 adsorption isotherms were performed and the results are presented in Table 8.2. An obvious decrease of S_{BET} can be observed after BSC-b saturation with MS-222, while the total micropore volume analysis was inconclusive. During the BSC regeneration, the thermal desorption of the adsorbed MS-222 molecules may occur, together with some MS-222 degradation and, consequently, the S_{BET} increased significantly, without, however, attaining the original surface area. Therefore, BSC-b regeneration and reusability for the adsorption of MS-222 could be considered for one cycle, after which its performance decreases significantly.

Notwithstanding, regeneration costs must be carefully addressed in view of the economic efficiency of the whole adsorption process. In this sense, considering the nature of the BSC-b precursor (waste produced at very large scale all over the world by pulp and paper mills) and its

production process (without applying any chemical or physical activation procedure), obtaining new BSC-b could be more interesting than its regeneration. In fact, alternative adsorbents, such as those from waste products, are typically not regenerated but the exhausted materials are disposed of by landfill or incineration [16].

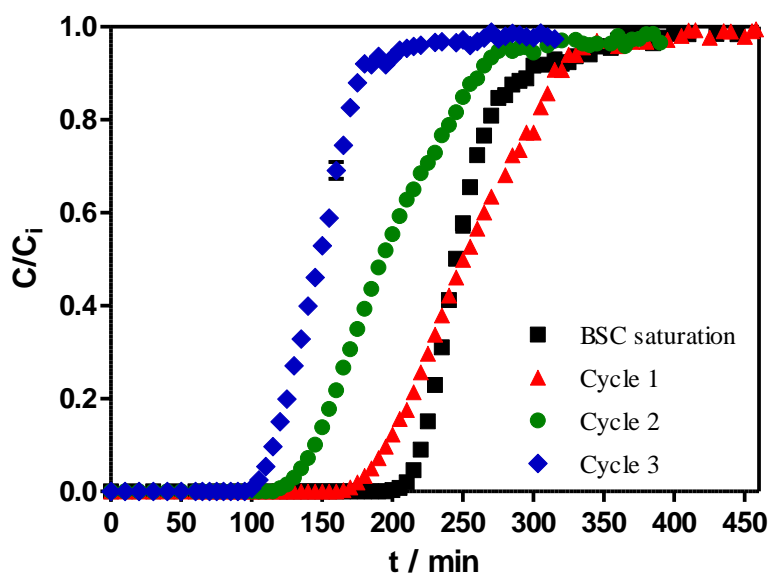


Figure 8.3 - Breakthrough curves for saturation of BSC-b with MS-222 and subsequent cycles of regeneration-adsorption ($Q=4.4 \text{ mL min}^{-1}$; $C_i=250 \text{ mg L}^{-1}$; $Z=13 \text{ cm}$).

Table 8.1 - Column data obtained from BSC-b saturation and subsequent regeneration-adsorption cycles ($Q=4.4 \text{ mL min}^{-1}$; $C_i=250 \text{ mg L}^{-1}$; $Z=13 \text{ cm}$)

	t_b (min)	V_b (ml)	$t_{50\%}$ (min)	t_s (min)	q_s (mg g ⁻¹)
BSC-b saturation	223	968	245	345	102
Cycle 1	195	858	250	360	124
Cycle 2	145	638	195	355	100
Cycle 3	115	506	150	230	80

Table 8.2 - Physical and chemical properties of BSC-b before and after saturation and after regeneration

Sample	BSC-b	BSC-b saturated (cycle 1)	BSC-b regenerated (cycle 1)
N_2 adsorption	S_{BET} (m ² g ⁻¹)	258	98.6
	W_0 (cm ³ g ⁻¹)	0.039	-

Note: S_{BET} - specific surface area; W_0 - total micropore volume

8.4 Conclusions

The chemical regeneration experiments, using low-cost and more environmentally friendly solutions as eluents, showed that the acidic solution of HCl 1 M resulted in the best MS-222 recovery efficiency (56%); however, the volume of the chemical regeneration agent necessary to attain such efficiency is high, making this regeneration technique less attractive. The thermal regeneration process carried out with the exhausted BSC-b provided good results for its reusability only for one cycle ($q_s=124 \text{ mg g}^{-1}$); its performance decreased significantly in the subsequent cycles ($q_s=80 \text{ mg g}^{-1}$ in the third cycle). In conclusion, considering the nature of its precursor, the use of new BSC-b could be more interesting than its regeneration, functioning also as an additional option for the management of such wastes.

8.5 References

- [1] Salvador, F., Martin-Sanchez, N., Sanchez-Hernandez, R., Sanchez-Montero, M.J. and Izquierdo, C., 2015, *Microporous and Mesoporous Materials*, 202, 259-276.
- [2] Salvador, F., Martin-Sanchez, N., Sanchez-Hernandez, R., Sanchez-Montero, M.J. and Izquierdo, C., 2015, *Microporous and Mesoporous Materials*, 202, 277-296.
- [3] Coelho, C., Oliveira, A.S., Pereira, M.F.R. and Nunes, O.C., 2006, *Journal of Hazardous Materials*, 138 (2), 343-349.
- [4] Toh, R.-H., Lim, P.-E., Seng, C.-E. and Adnan, R., 2013, *Bioresource Technology*, 143, 265-274.
- [5] Narbaitz, R.M. and Karimi-Jashni, A., 2012, *Chemical Engineering Journal*, 197, 414-423.
- [6] Asghar, H.M.A., Hussain, S.N., Roberts, E.P.L. and Brown, N.W., 2013, *Korean Journal of Chemical Engineering*, 30 (7), 1415-1422.
- [7] Salvador, F., Martin-Sanchez, N., Sanchez-Montero, M.J., Montero, J. and Izquierdo, C., 2013, *The Journal of Supercritical Fluids*, 74, 1-7.
- [8] Carmona, M., Garcia, M.T., Carnicer, Á., Madrid, M. and Rodríguez, J.F., 2014, *Journal of Chemical Technology & Biotechnology*, 89 (11), 1660-1667.
- [9] Pan, R.R., Fan, F.L., Li, Y. and Jin, X.J., 2016, *RSC Advances*, 6 (39), 32960-32966.
- [10] Mao, H., Zhou, D., Hashisho, Z., Wang, S., Chen, H. and Wang, H., 2015, *Journal of Industrial and Engineering Chemistry*, 21, 516-525.
- [11] Guo, D., Shi, Q., He, B. and Yuan, X., 2011, *Journal of Hazardous Materials*, 186 (2-3), 1788-1793.
- [12] Berenguer, R., Marco-Lozar, J.P., Quijada, C., Cazorla-Amorós, D. and Morallón, E., 2010, *Energy & Fuels*, 24 (6), 3366-3372.
- [13] CalgonCarbon, <http://www.calgoncarbon.com/reactivation-services/>, last accessed in August 2016.
- [14] Carbot, <http://www.cabotcorp.com/solutions/products-plus/activated-carbon/reactivation-services>, last accessed in August 2016.
- [15] Ross, L.G. and Ross, B., 2008, *Anaesthetic and Sedative Techniques for Aquatic Animals*, Blackwell Publishing Ltd, Oxford, UK.
- [16] Worch, E., 2012, *Adsorption Technology in Water Treatment, Fundamentals, Processes, and Modeling*, 1st ed., Walter de Gruyter GmbH & Co. KG, Berlin, Germany.

Part V

Chapter 9

Final remarks

9 Final remarks

This final chapter presents the most important results and conclusions reported throughout this thesis. Some suggestions for future work are also presented.

9.1 Conclusions

In the first part of this thesis an exhaustive survey was performed about the use of therapeutic agents in intensive aquaculture systems, mainly fish anaesthetics, and, due to their toxicological effects at long-exposure for both fish and human, it was concluded that it is important to ensure the water quality for recycling and/or for discharge in the environment. So, water treatment processes should be implemented in order to prevent the release of these pollutants in the environment. Based on the literature review, the adsorption process using activated carbons has been proposed, in addition to biological filters, as tertiary treatment or polishing stage in RASs to remove ozone and persistent nonbiodegradable organic compounds, such as pharmaceuticals. However, activated carbons are expensive materials and this is a main reason for activated carbon filters not being typically found in food-fish production. In this context, the main objective of the work of this thesis was the production of alternative adsorbents, using as precursors agricultural or industrial biowastes, for the removal of fish anaesthetics from water in the recirculating aquaculture systems (RASs).

The comparative valorisation of agricultural (*Eucalyptus* bark, grape seeds, peach stones, walnut shells, olive waste and peanut shells) and industrial (primary and biological paper mill sludge) biowastes by two thermochemical conversion techniques, combustion and pyrolysis, was assessed in the second part of this work. The results showed that agricultural biowastes possessed larger calorific values than those obtained for industrial residues and very close to those usually obtained from fossil coals ($\text{HHVs}=20\text{-}30 \text{ MJ kg}^{-1}$), making them highly competitive for combustion applications, such as fuel and power generation. On the other hand, it was concluded that the solid products from the primary and biological paper mill sludge pyrolysis have promising properties to be used as adsorbents for possible applications as adsorbent in water remediation.

In the third part of this thesis, the production of alternative adsorbents, using as precursors the agricultural and industrial biowastes, by pyrolysis was reported, as well as the characterization of the respective materials and their application on the adsorption of fish anaesthetics in batch system. Regarding the production of the biowaste-based adsorbents, the pyrolysis of both agricultural and industrial wastes resulted in an enhanced aromaticity of the samples, an increase of the total organic carbon content and release of volatile matter. However, in contrast to what was expected, biochars resulting from pyrolysis of agricultural biowastes revealed low specific surface areas (S_{BET} ranging from 2 up to $11 \text{ m}^2 \text{ g}^{-1}$) with a negligible microporous development. The pyrolysis of biological paper mill sludge (BS) resulted in the largest release of volatiles compared with the primary paper mill sludge (PS), but the physical characterization indicates that PS related biochars developed a more porous surface. The apparent density of PS adsorbents is around

0.5 g cm⁻³, while BS biochars have high apparent density (between 0.83 and 1.34 g cm⁻³), suggesting low pore formation. Concerning the S_{BET} , there is a steep increase of this parameter for PS biochars with the increase of pyrolysis temperature, reaching 209 m² g⁻¹ for PS800-150 (which is a quite good value for a pyrolysed non-activated carbon), while BS adsorbents' surface area did not evolved significantly, reaching only 10 m² g⁻¹ for BS800-10. The acidic washing performed to PS800-150 and BS800-150 significantly improved the biochars characteristics: surface area increased up to 414 and 291 m² g⁻¹ in the case of pyrolysed and washed primary paper mill sludge (PSC) and pyrolysed and washed biological paper mill sludge (BSC), respectively, and, consequently, the micropore volume increased for both adsorbents. Concerning the adsorption results using the produced adsorbents based on agricultural wastes, all of them were able to adsorb MS-222 from water, even though this anaesthetic has high affinity for the aqueous phase. Comparing the agricultural biowaste-based adsorbents, pyrolysed peanut shells (PNS400-120) showed the best MS-222 adsorption capacity (34 mg g⁻¹, predicted by Langmuir-Freundlich model), which is still ten times lower than that of the commercial powdered activated carbon (PAC), used as a reference material. On the other hand, PSC and BSC obtained better adsorptive results: MS-222 maximum adsorption capacities of 109 and 92 mg g⁻¹ were obtained using PSC and BSC, respectively (predicted by Langmuir-Freundlich model). These two produced adsorbents were also tested in the adsorption of two more fish anaesthetics, benzocaine and 2-phenoxyethanol (2-PE), and maximum adsorption capacities of 53 and 83 mg g⁻¹, respectively, were obtained using PSC and 107 and 63 mg g⁻¹, respectively, were obtained using BSC. In comparison, PAC resulted in between 4 and 8 times higher maximum adsorption capacities than that of these biochars. Notwithstanding, the achieved results are very promising taking into account that no chemical or physical activation was employed for the production of PSC and BSC.

The subsequent adsorption studies were performed using BSC adsorbent due to the possibility of obtaining different particle sizes (not possible with PS-derived materials), which is an advantage in a real continuous flow process using fixed-bed columns. In this sense, the effect of the adsorbent particle size in the adsorption of MS-222 from water was assessed and the results showed that the smallest sizes of BSC particle (BSC-a and BSC-b corresponding to <0.18 mm and 0.18-0.5 mm, respectively) produced better adsorptive capacities. On the other hand, varying operating conditions such as temperature (8 to 30 °C) and salinity (0.8 to 35‰) did not affect the MS-222 adsorption using BSC-b, making this adsorbent versatile for a possible implementation on RASs. Also, it was verified that the presence of organic and inorganic matter in aquaculture effluents did not interfere with the adsorption of MS-222 onto the biological sludge-based carbon. Comparing these results with a commercial granulated activated carbon (GAC), BSC-b showed a

lower adsorption capacity but faster adsorption kinetics. Yet, it is worth noting that at short contact times (≤ 1 h) the capacities of both materials are comparable.

In the fourth part of this thesis and the last one presenting experimental results, the adsorption of MS-222 and 2-PE in continuous system, using fixed-bed columns packed with BSC-b, was presented and, also, the chemical and thermal regeneration of the exhausted BSC-b with MS-222 was reported. Continuous adsorption results of MS-222 onto BSC-b revealed that decreasing flow rate and influent concentration resulted in larger volume of treated effluent at the breakthrough time. The highest treated volume (968 mL) was obtained for the highest bed depth (13 cm, corresponding to a 2.5 g of BSC-b). However, the maximum bed adsorption capacity (125 mg g^{-1}) was obtained under a flow rate of 4.4 mL min^{-1} , with 400 mg L^{-1} of MS-222 in 4.5 cm bed depth (1.0 g of BSC-b). It was demonstrated that, in general, the data can be adequately described by the Dose-Response model with less than 2% of deviation from the experimental values. Once again, but now in continuous adsorption system, it was concluded that the performance of BSC-b using real aquaculture wastewater as matrix was not affected significantly, by the presence of organic and inorganic matter, which is an important advantage for the possible application of BSC as adsorbent in RASs. Regarding the continuous adsorption results of 2-PE onto BSC-b, the decrease of flow rate and influent concentration resulted in an increase of volume of treated effluent at the breakthrough time, which also increases with the increase of bed depth. The highest treated volume (286 mL) and maximum bed adsorption capacity (104 mg g^{-1}) were obtained for the highest bed depth, 13 cm, at flow rate of 4.4 mL min^{-1} and influent concentration of $0.3 \text{ cm}^3 \text{ L}^{-1}$. In this case, the application of both Yoon-Nelson and Dose-Response models is recommended in order to obtain the most correct parameters. The application of bed depth service time (BDST) model resulted in an excellent prediction of MS-222 scale-up adsorption experiments, with an error of less than 11% compared with experimental data, while the prediction of 2-PE scale-up was not as good as expected. Finally, the chemical regeneration of the saturated BSC-b, using as eluent an acidic solution of HCl 1 M, resulted in 56% of MS-222 recovery efficiency; however, the volume of the chemical regeneration agent necessary to attain such efficiency is high (500 mL), making this regeneration technique less attractive. On the other hand, the thermal regeneration provided good results for BSC-b reusability only for one cycle, without losing adsorption capacity for MS-222, decreasing significantly in the subsequent cycles.

Overall, PS and BS are residues produced in large scale by paper and pulp industry, constituting a massive environmental and sustainable challenge for this industry. Thus, the cost associated to the precursor of these alternative adsorbents is null with the additional benefit of eliminating managing costs of the referred residues. Also, contrarily to commercial activated carbons, the production process used avoids the utilization of activating chemicals and allows the

recovery of energy from wastes, and thus it may be considered an environmentally friendly process. For these reasons, and allied to the good results obtained for the removal of fish anaesthetics, the use of paper mill sludge-based adsorbents may be an alternative choice to be used in RASs.

9.2 Future work

The main conclusions pointed out the promising use of the paper mill sludge as precursor of the production of new adsorbents. Despite the good adsorption results obtained using primary paper mill sludge-based adsorbent, the fact that it is a powdered material led to its exclusion from the fixed-bed column studies. As suggestion for future work, it would be interesting to test its pelletization, by physical compression or agglomeration, using an agglomeration chemical agent, in order to obtain different particle sizes and finally use it in fixed-bed column experiments. Alternatively, the produced powdered material could be tested in another reactor configuration, such as continuous stirred tank reactor. Also, as future work suggestion, the improving of the biochars surface (*i.e.*, increase in the specific surface area and micropore volume) by means of chemical or physical activation or functionalization processes would be useful to achieve higher adsorption capacities.

Regarding the implementation of such alternative adsorbents in RASs, an economic evaluation should be performed in order to effectively compare the advantages of these carbons with the commercial activated carbons. Also, it would be interesting to evaluate if the implementation of filters using these adsorbents in RASs are more profitable than other tertiary treatment processes. The implementation of BSC filters also depends on the aquacultures operation mode. Some aquaculture facilities administered the anaesthetic directly in the fish's tanks, but most facilities make up the recommended drug concentration in a separate container and transfer the fish into that container. In this last case, the adsorption process can be implemented as a supplementary technique to treat small volumes of contaminated water. However, if the contaminated water is released to the recirculation system, the concentration of the anaesthetic becomes unknown and the challenge is higher if the adsorption process has to operate continuously, involving the treatment of high volumes of water on a daily basis.

Also, the end-of-life of the saturated adsorbents should be carefully analysed. If their destination is the incineration, the emission of gases should be analysed and the gaseous products must be identified. On the other hand, if their destination is the landfill disposal, leaching studies should be performed and the resultant leachate must be also analysed for noxious compounds.

Finally, in order to quantify the potential environmental impacts and critical life stages associated with the production process of paper mill sludge-based adsorbents, a life cycle assessment (LCA) should be performed.

Appendix

A Anaesthetics properties

A.1 Absorbance spectra

The spectra of MS-222, benzocaine and 2-PE were obtained using a UV-Vis Shimadzu spectrophotometer and an optical path length of 1 cm. The resulting spectra are depicted in Figures A.1 to A.3.

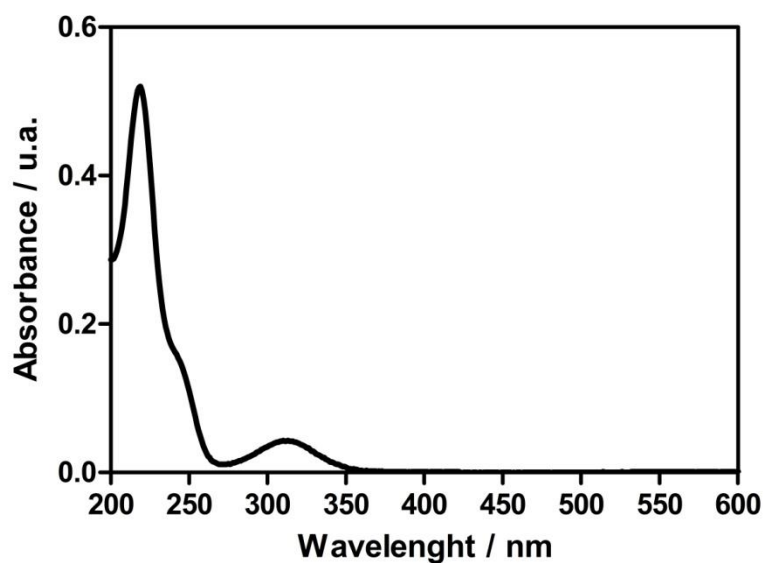


Figure A.1 - Absorbance spectrum of MS-222 ($C=5 \text{ mg L}^{-1}$).

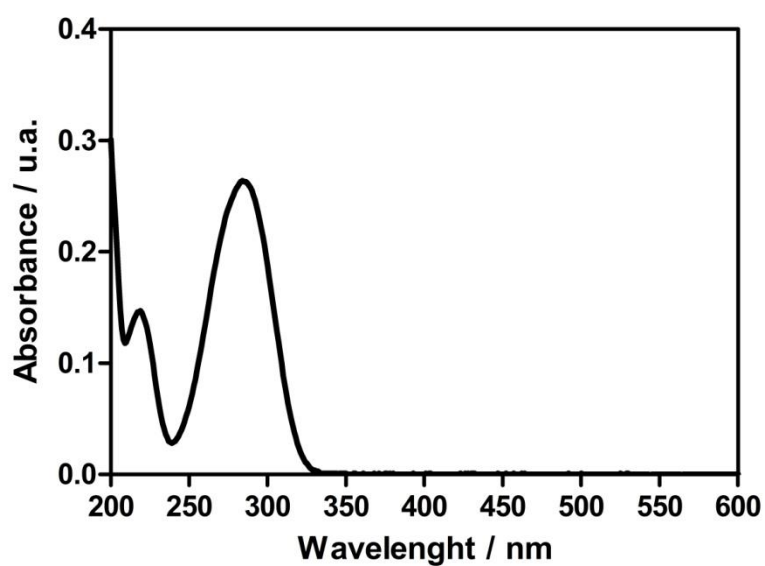


Figure A.2 - Absorbance spectrum of benzocaine ($C=2.5 \text{ mg L}^{-1}$).

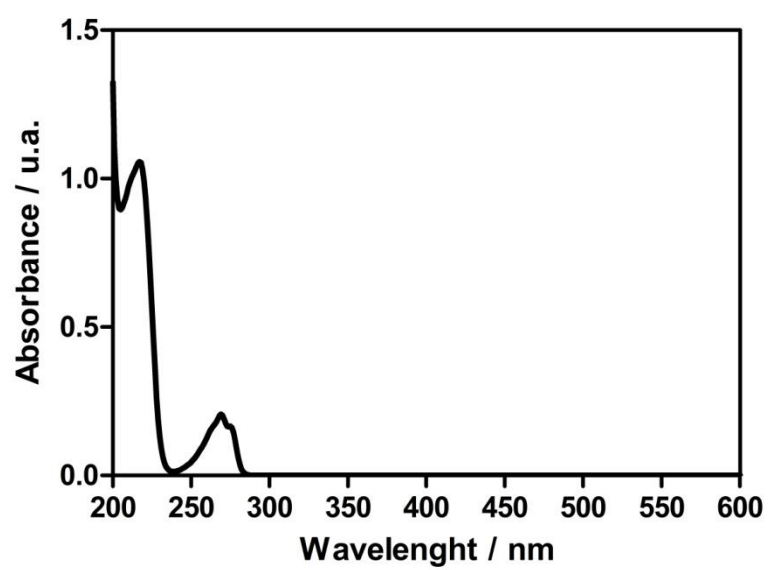


Figure A.3 - Absorbance spectrum of 2-PE ($C=0.2 \text{ cm}^3 \text{ L}^{-1}$).

B Preliminary adsorption experiments

B.1 Effect of the pyrolysis residence time on the adsorption capacity

The effect of the pyrolysis residence time on the adsorption capacity was assessed by contacting each biochar, pyrolysed during 10 and 120 min, with 250 mg L⁻¹ of MS-222 solution ($C_{MS-222, t=0h}$), in polypropylene tubes, during 16 h of contact time, in the same conditions. The remaining MS-222 in solution after 16 h of agitation ($C_{MS-222, t=16h}$) was quantified for each contact time by MEKC analysis (as described in Appendix C, section C.1.1.1). The adsorption percentage for each case was calculated by:

$$\% \text{ Adsorption} = \frac{C_{MS-222, t=0h} - C_{MS-222, t=16h}}{C_{MS-222, t=0h}} 100\% \quad \text{B.1}$$

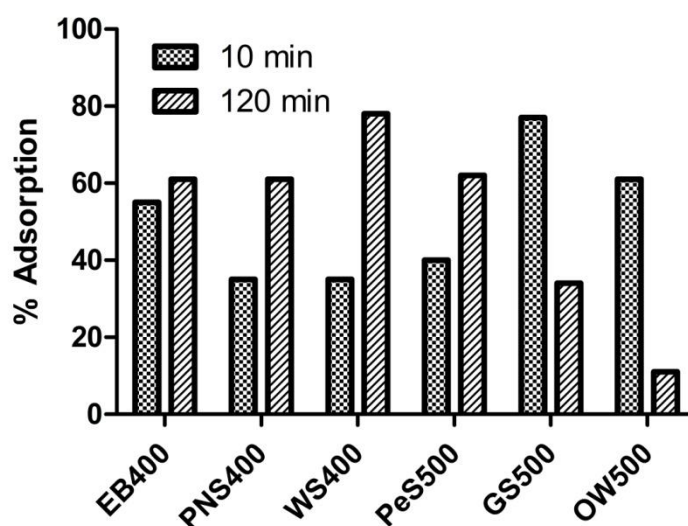


Figure B.1 - Adsorption percentages for biochars pyrolysed during 10 and 120 min.

According to Figure B.1, EB, PNS, WS and PeS obtained the highest adsorption percentage when pyrolysed during 120 min, while GS and OW obtained better adsorption percentage when pyrolysed during 10 min.

C Capillary electrophoresis (CE)

C.1 CE calibration curves

The quantification of the anaesthetics used in this work was performed by capillary electrophoresis, using micellar electrokinetic chromatography (MEKC) or capillary zone electrophoresis (CZE) methods. Internal standard (IS) was spiked in all samples and standard solutions in order to control the variations of injection volumes. For new capillaries, new calibration curves were obtained. The anaesthetic standards were analysed in triplicate with the conditions described in the following sections.

The calibration curve is the graphical representation of the ratio between the anaesthetic and IS peak areas (*e.g.*, A_{MS-222}/A_{IS}) versus the correspondent anaesthetic concentration, (C , mg L^{-1}). The equation of the regression curve is given by [1]:

$$y = a + bx \quad \text{C.1}$$

where y is the ratio between the area under the curve of anaesthetic and IS, a is the intercept on the y -axis, b (L mg^{-1}) is the slope of the curve and x (mg L^{-1}) is the concentration of the anaesthetic solution. The errors of the slope, S_b , and the intercept, S_a , of the linear regression were calculated by:

$$S_b = \frac{S_{y/x}}{\sqrt{\sum_i (x_i - \bar{x})^2}} \quad \text{C.2}$$

$$S_a = S_{y/x} \sqrt{\frac{\sum_i x_i^2}{n \sum_i (x_i - \bar{x})^2}} \quad \text{C.3}$$

where $S_{y/x}$ is a estimative of the random errors in the y -direction, calculated by the following equation:

$$S_{y/x} = \sqrt{\frac{\sum_i (y_i - \hat{y}_i)^2}{n-2}} \quad \text{C.4}$$

The limit of detection (LOD) and the limit of quantification (LOQ) were calculated according to:

$$\text{LOD: } y_{LOD} = a + bx_{LOD} \quad \text{where} \quad y_{LOD} = b + 3S_b \quad \text{C.5}$$

$$\text{LOQ: } y_{LOQ} = a + bx_{LOQ} \quad \text{where} \quad y_{LOQ} = b + 10S_b \quad \text{C.6}$$

C.1.1 Quantification of MS-222

C.1.1.1 *in water*

All the adsorption experiments using MS-222 solutions prepared in water or water buffered with 10^{-2} M of NaHCO_3 were followed by MEKC analysis. The MEKC analyses were performed using a Beckman P/ACE MDQ (Fullerton, CA, USA) instrument, equipped with an UV-Vis detection system. A dynamically coated silica capillary was used as described by Calisto et al. (2011) [2]. For capillary coating, solutions of 0.5% (w/v) hexadimethrine bromide (polybrene, $\geq 95\%$, Sigma Aldrich) in 0.5 M NaCl ($\geq 99.5\%$, Fluka) and 1 M NaOH (99.3%, José Manuel Gomes dos Santos, Portugal) were used. Time of injection of aqueous samples and standard solutions were 4 s at 0.5 psi of pressure and the electrophoretic separation was performed in direct polarity mode with a positive power supply of 22 kV maintaining the capillary temperature at 30 °C. Detection of MS-222 was monitored at 220 nm. The separation buffer consisted on 20 mM of sodium tetraborate (Borax, Riedel-de Haën) and 30 mM of sodium dodecylsulphate (SDS, 99%, for electrophoresis, Sigma Aldrich), pH 9.2. Also, 3-ethoxy-4-hydroxybenzaldehyd (Ethylvanilin, 99%, Sigma Aldrich) was used as internal standard, spiked in all samples and standard solutions at a final concentration of 33.4 mg L^{-1} . Capillary washing between runs consisted of 1 min of ultra-pure water followed by 2 min of separation buffer. Samples were filtered through $0.22 \mu\text{m}$ Simplepure PVDF filters prior to analysis.

A range of standards were prepared by dilution with ultra-pure water of 1 g L^{-1} stock solution to obtain the MS-222 calibration curves, with the concentrations: 2.5, 10, 20, 30, 40 and 50 mg L^{-1} . An example of calibration curve for MS-222 quantification is shown in Figure C.1, while the calibration and uncertainty parameters of this method are presented in Table C.1.

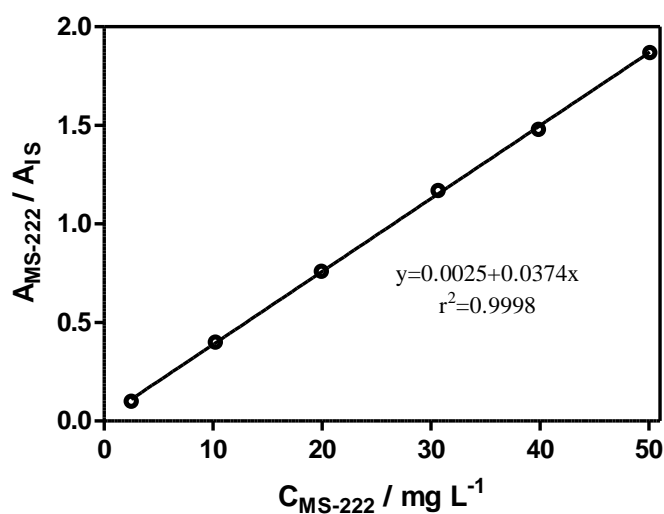


Figure C.1 - CE calibration curve for MS-222 in water solution. Each point (\pm standard deviation) is the average of three replicates.

C.1.1.2 *in NaOH*

All the adsorption experiments using MS-222 solutions prepared in NaOH matrix were followed by CZE analyses. These analyses were performed using the same equipment from previous section C.1.1.1. In this sense, a non-coated silica capillary (50 cm×75 µm i.d.) was used after its proper conditioning. The capillary conditioning consisted of 30 min of NaOH 1 M (20 psi), followed by 2 min of H₂O (20 psi) and 20 min of buffer (120 mM sodium cholate and 20 mM sodium tetraborate) Time of injection of aqueous samples and standard solutions in NaOH matrix were 7 s at 0.5 psi and the electrophoretic separation was performed in direct polarity mode with a positive power supply of 18 kV maintaining the capillary temperature at 50 °C. Detection of MS-222 was monitored at 220 nm. The separation buffer consisted on 120 mM of sodium cholate hydrate (98%, Sigma Aldrich) and 20 mM of sodium dodecylsulphate (SDS, 99%, for electrophoresis, Sigma Aldrich). Also, 3-ethoxy-4-hydroxybenzaldehyd (Ethylvanilin, 99%, Sigma Aldrich) was used as internal standard, spiked in all samples and standard solutions at a final concentration of 33.4 mg L⁻¹. Capillary washing between runs consisted of 1 min of ultra-pure water followed by 2 min of separation buffer. Samples were filtered through 0.22 µm Simplepure PVDF filters prior to analysis.

A range of standards were prepared by dilution with NaOH (0.1 or 1 M) of 1 g L⁻¹ stock solution to obtain the MS-222 calibration curves, with the concentrations: 2.5, 10, 20, 30 and 40 mg L⁻¹. An example of calibration curve for MS-222 quantification is shown in Figure C.2, while the calibration and uncertainty parameters of this method are presented in Table C.1.

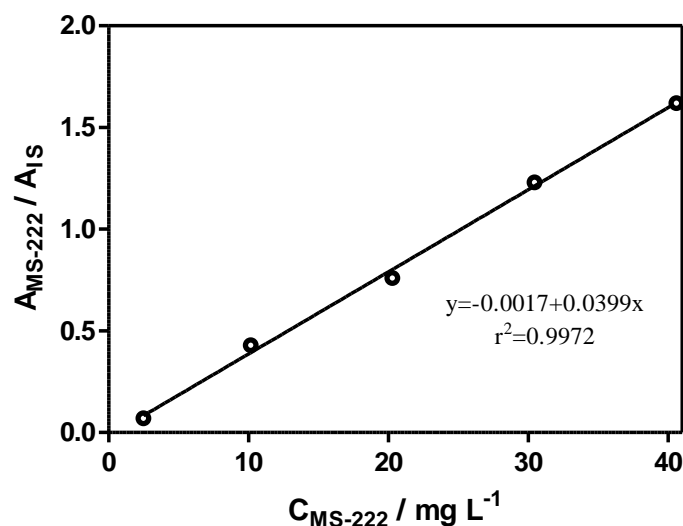


Figure C.2 - CE calibration curve for MS-222 in NaOH solution. Each point (\pm standard deviation) is the average of three replicates.

C.1.1.3 in HCl

All the adsorption experiments using MS-222 solutions prepared in HCl matrix were followed by MEKC analysis. The analyses were performed using the same equipment from previous section C.1.1.1. A dynamically coated silica capillary was used as described by Calisto et al. (2011) [2]. For capillary coating, solutions of 0.5% (w/v) hexadimethrine bromide (polybrene, $\geq 95\%$, Sigma Aldrich) in 0.5 M NaCl ($\geq 99.5\%$, Fluka) and 1 M NaOH (99.3%, José Manuel Gomes dos Santos, Portugal) were used. Time of injection of aqueous samples and standard solutions were 4 s at 0.5 psi of pressure and the electrophoretic separation was performed in direct polarity mode with a positive power supply of 8 kV for 10 min, and the temperature of the capillary maintained at 25 °C. Detection of MS-222 was monitored at 220 nm. The separation buffer consisted on 5 mM of sodium tetraborate (Borax, Riedel-de Haën) and 20 mM of sodium dodecylsulphate (SDS, 99%, for electrophoresis, Sigma Aldrich), pH 9.2. Also, 3-ethoxy-4-hydroxybenzaldehyd (Ethylvanilin, 99%, Sigma Aldrich) was used as internal standard, spiked in all samples and standard solutions at a final concentration of 33.4 mg L⁻¹. Capillary washing between runs consisted of 1 min of ultra-pure water followed by 2 min of separation buffer. Samples were filtered through 0.22 μm Simplepure PVDF filters prior to analysis.

A range of standards were prepared by dilution with HCl (1 M) of 1 g L⁻¹ stock solution to obtain the MS-222 calibration curves, with the concentrations: 10, 20, 30, 40 and 50 mg L⁻¹. An example of calibration curve for MS-222 concentration quantification is shown in Figure C.3, while the calibration and uncertainty parameters of this method are presented in Table C.1.

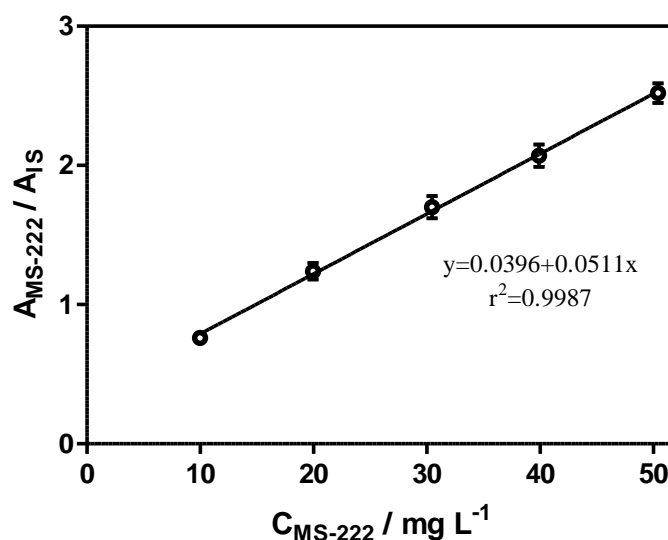


Figure C.3 - CE calibration curve for MS-222 in HCl solution. Each point (\pm standard deviation) is the average of three replicates.

Table C.1 - Calibration parameters of MS-222 calibration curves in different matrices

MS-222	Matrix		
	water	NaOH	HCl
$a \pm S_a$	0.003±0.002	-0.002±0.004	0.04±0.03
$b \pm S_a$ (L mg ⁻¹)	0.0373±0.0001	0.0399±0.0003	0.051±0.002
r^2	0.9998	0.9972	0.9987
LOD (mg L ⁻¹)	0.156	0.320	1.767
LOQ (mg L ⁻¹)	0.521	1.067	5.890

C.1.2 Benzocaine

All the adsorption experiments using benzocaine solutions prepared in water or water buffered with 10⁻² M of NaHCO₃ were followed by MEKC analysis. The MEKC analyses were performed using the same equipment and following the same procedure described in previous section C.1.1.1. The detection of benzocaine was monitored at 200 nm.

A range of standards were prepared by dilution with ultra-pure water of 500 mg L⁻¹ stock solution to obtain the benzocaine calibration curves, with the concentrations: 2.5, 5, 7.5, 10, 12.5, 15, 17.5 and 20 mg L⁻¹. An example of calibration curve for benzocaine concentration quantification is shown in Figure C.4, while the calibration and uncertainty parameters of this method are presented in Table C.2.

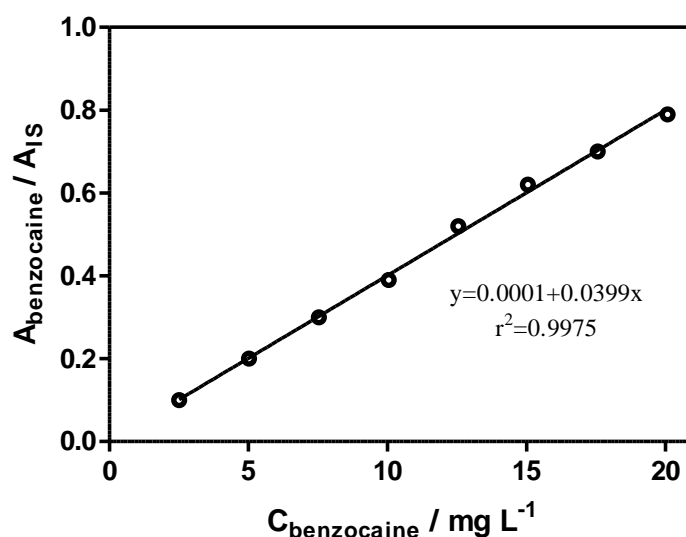


Figure C.4 - CE calibration curve for benzocaine. Each point (\pm standard deviation) is the average of three replicates.

Table C.2 - Calibration parameters of benzocaine calibration curve

	Benzocaine
a ± S_a	0.0001±0.001
b ± S_a (L mg⁻¹)	0.0399±0.0002
r²	0.9975
LOD (mg L⁻¹)	0.098
LOQ (mg L⁻¹)	0.325

C.1.3 2-phenoxyethanol

All the adsorption experiments using 2-phenoxyethanol solutions prepared in water or water buffered with 10⁻² M of NaHCO₃ were followed by MEKC analysis. The MEKC analyses were performed using the same equipment and following the same procedure described in previous section C.1.1.1. The detection of 2-phenoxyethanol was monitored at 230 nm.

A range of standards were prepared by dilution with ultra-pure water of 5 cm³ L⁻¹ (555 mg L⁻¹) stock solution to obtain the 2-phenoxyethanol calibration curves, with the concentrations: 0.025, 0.050, 0.075, 0.100, 0.125, 0.150, 0.175, and 0.200 cm³ L⁻¹ (27.8, 55.5, 83.3, 111, 139, 167, 194 and 222 mg L⁻¹, respectively). An example of calibration curve for 2-phenoxyethanol quantification is shown in Figure C.5, while the calibration and uncertainty parameters of this method are presented in Table C.3.

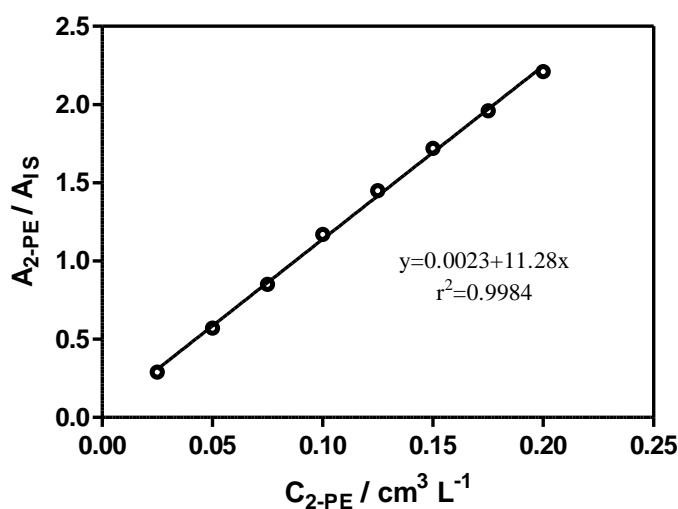


Figure C.5 - CE calibration curve for 2-phenoxyethanol. Each point (±standard deviation) is the average of three replicates.

Table C.3 - Calibration parameters of 2-phenoxyethanol calibration curve

	2-phenoxyethanol
a ± S_a	0.002±0.003
b ± S_a (L cm⁻³)	11.28±0.05
r²	0.9984
LOD (cm³ L⁻¹)	0.0008
LOQ (cm³ L⁻¹)	0.0028

C.2 References

- [1] Miller, J.N. and Miller, J.C., 2010, *Statistics and Chemometrics for Analytical Chemistry*, Prentice Hall/Pearson.
- [2] Calisto, V., Domingues, M.R.M., Erny, G.L. and Esteves, V.I., 2011, *Water Research*, 45 (3), 1095-1104.